

Sampling-Based Nuclear Data Uncertainty Quantification for Continuous Energy Monte Carlo Codes

THÈSE N° 6598 (2015)

PRÉSENTÉE LE 8 MAI 2015

À LA FACULTÉ DES SCIENCES DE BASE

LABORATOIRE DE PHYSIQUE DES RÉACTEURS ET DE COMPORTEMENT DES SYSTÈMES

PROGRAMME DOCTORAL EN ENERGIE

ÉCOLE POLYTECHNIQUE FÉDÉRALE DE LAUSANNE

POUR L'OBTENTION DU GRADE DE DOCTEUR ÈS SCIENCES

PAR

Ting ZHU

acceptée sur proposition du jury:

Prof. S. Haussener, présidente du jury
Prof. A. Pautz, Dr A. Vasiliev, directeurs de thèse
Dr J. Gulliford, rapporteur
Prof. L. Rivkin, rapporteur
Dr W. Zwermann, rapporteur



ÉCOLE POLYTECHNIQUE
FÉDÉRALE DE LAUSANNE

Suisse
2015

Acknowledgements

The present doctoral research was conducted at the Laboratory for Reactor Physics and Systems Behaviour (LRS) at the Paul Scherrer Institut (PSI) and of the Doctoral School in Energy of the Swiss Federal Institute of Technology Lausanne (EPFL), with the financial support of *swissnuclear* (the nuclear energy section of *swisselectric*).

This thesis would not have been possible without the academic contributions and personal support of many amazing individuals.

- Prof. Andreas Pautz and Dr. Alexander Vasiliev, my thesis directors have been the most supportive throughout the thesis work. I am very thankful for the freedom and trust they have bestowed on me and allowed me to explore scientific topics even outside of the original PhD project proposal. Given their busy schedules, they often fulfilled my last-minute requests for which I could never thank them enough!
- It was an honour to have Dr. Winfried Zwermann, Dr. Jim Gulliford and Prof. Leonid Rivkin on my thesis committee. Their interest and the time spent on reviewing my thesis are highly appreciated.
- Dr. Stefano Tarantola of the Ispra JRC was instrumental in helping me understand global sensitivity analysis and apply it in the PhD work. I have benefited greatly through our collaboration.
- The entire LRS team has created the most positive working environment a PhD student could ever ask for. Thanks to Mr. Martin Zimmermann with the conception of the PhD project proposal, emeritus Prof. Rakesh Chawla and group leader Mr. Hakim Ferroukhi for offering me the PhD position in 2011, Dr. Konstantin Mikityuk for acting as my interim thesis co-director, Ruth Ringele and Philippe Jacquemoud for being the kindest and most helpful with my administrative and computer-related requests.
- Sharing the same office with Olivier Leray has led to many funny moments which I will cherish. I am also happy that I could finally understand his French (60% of the time) after almost two years.
- Mathieu Hursin, Gregory Perret and Dimitri Rochman have been most generous with their time whenever I have scientific or career-related questions. Their good humour is so infectious!

-
- My present and past hiking buddies: Marco Pecchia, Damar Wicaksono, Vladimir Brankov, Raoul Happy-Ngayam, Younsuk Yun, Carl Adamsson. Thank you for the unforgettable experiences in the Swiss Alps.
 - I feel extremely lucky to have befriended Sarah Steimer, Gwen Pascua and Manasa Sridhar at PSI whose perseverance and optimism I admire a lot.
 - Special thanks to my Chinese friends in Switzerland and in Europe who can always build a strong community anywhere in the world.
 - To the Fritz's families, it has been a privilege knowing you all. Thanks a million for taking such good care of me!

Finally, I am forever grateful to my parents and Ben Schmidt who experienced the ups and downs of my PhD journey with me even across the Atlantic ocean.

Villigen, 19 April 2015

Ting ZHU

Abstract

Research on the uncertainty of nuclear data is motivated by practical necessity. Nuclear data uncertainties can propagate through nuclear system simulations into operation and safety related parameters. The tolerance for uncertainties in nuclear reactor design and operation can affect the economic efficiency of nuclear power, and essentially its sustainability.

The goal of the present PhD research is to establish a methodology of nuclear data uncertainty quantification (NDUQ) for MCNPX, the continuous-energy Monte-Carlo (M-C) code. The high fidelity (continuous-energy treatment and flexible geometry modelling) of MCNPX makes it the choice of routine criticality safety calculations at PSI/LRS, but also raises challenges for NDUQ by conventional sensitivity/uncertainty (S/U) methods. For example, only recently in 2011, the capability of calculating continuous energy k_{eff} sensitivity to nuclear data was demonstrated in certain M-C codes by using the method of iterated fission probability.

The methodology developed during this PhD research is fundamentally different from the conventional S/U approach: nuclear data are treated as random variables and sampled in accordance to presumed probability distributions. When sampled nuclear data are used in repeated model calculations, the output variance is attributed to the collective uncertainties of nuclear data. The NUSS (Nuclear data Uncertainty Stochastic Sampling) tool is based on this sampling approach and implemented to work with MCNPX's ACE format of nuclear data, which also gives NUSS compatibility with MCNP and SERPENT M-C codes. In contrast, multigroup uncertainties are used for the sampling of ACE-formatted pointwise-energy nuclear data in a groupwise manner due to the more limited quantity and quality of nuclear data uncertainties. Conveniently, the usage of multigroup nuclear data uncertainties allows consistent comparison between NUSS and other methods (both S/U and sampling-based) that employ the same nuclear data uncertainty format.

The first stage of NUSS development focuses on applying simple random sampling (SRS) algorithm for uncertainty quantification. The effect of combining multigroup and ACE format on the propagated nuclear data uncertainties is assessed. It is found that the number of energy groups has minor impact on the precision of k_{eff} uncertainty as long as the group structure reflects the neutron flux spectrum. Successful verification of the NUSS tool for propagating nuclear data uncertainties through MCNPX and quantifying MCNPX output parameter uncertainties is obtained.

The second stage of NUSS development is motivated by the need for an efficient sensitivity analysis methodology based on global sampling and coupled with MCNPX. For complex systems, the computing time for obtaining a breakdown of total uncertainty contributions by individual inputs becomes prohibitive when many MCNPX runs are required. The capability of determining simultaneously the total uncertainty and individual nuclear data uncertainty contributions is thus researched and implemented into the NUSS-RF tool. It is based on the Random Balance Design algorithm and is validated by three mathematical test cases for both linear and nonlinear models and correlated inputs. NUSS-RF is then applied to demonstrate the efficient decomposition of total uncertainty by individual nuclear data. However an attempt to decompose total uncertainty into individual contributions using the conventional S/U method shows different decomposition results when the inputs are correlated.

The investigation and findings of this PhD work are valuable because of the introduction of global sensitivity analysis into the existing repertoire of nuclear data uncertainty quantification methods. The NUSS tool is expected to be useful for expanding the types of MCNPX-related applications, such as an upgrade to the current PSI criticality safety assessment methodology for Swiss application, for which nuclear data uncertainty contributions can be quantified.

Keywords: nuclear data, nuclear data covariance, ACE format, continuous-energy MCNPX, criticality safety, k_{eff} sensitivity, stochastic sampling, Fourier Amplitude Sensitivity Testing, Random Balance Design, global sensitivity analysis.

Résumé

La recherche concernant les incertitudes des données nucléaires est une nécessité pratique. La propagation des incertitudes sur les données nucléaires au travers des simulations impactent les paramètres de sûreté. La tolérance pour les incertitudes lors de la conception et l'opération des réacteurs nucléaires affecte la rentabilité et donc la durabilité de l'énergie nucléaire.

Le but de cette thèse est l'établissement d'une méthodologie pour la propagation des incertitudes dues aux données nucléaires et la quantification de leurs impacts pour le code Monte-Carlo MCNPX. Le traitement à énergie continue et la modélisation flexible de la géométrie en fait un code de choix pour les calculs de sûreté-criticité au PSI/LRS, mais également un défi pour la quantification des incertitudes dues aux données nucléaires par des méthodes conventionnelles d'analyse de sensibilité et de quantification d'incertitudes (S/U). Ce n'est que récemment, en 2011, que la capacité de calculer la sensibilité du k_{eff} aux données nucléaires n'a été implémentée qu'à certains codes Monte-Carlo.

La méthodologie développée dans ce travail est fondamentalement différente des approches conventionnelles de S/U : les données nucléaires sont traitées comme des variables aléatoires et échantillonnées selon une distribution multivariée normal. Afin d'assurer la compatibilité avec MCNPX, le code NUSS (Nuclear data Uncertainty Stochastic Sampling) fonctionne avec des fichiers de données nucléaires au format ACE. Cependant, des incertitudes multi-groupe sont utilisées pour l'échantillonnage de données nucléaires ponctuelles en énergie au format ACE, car la quantité et la qualité des incertitudes des données nucléaires sont relativement limités. Ainsi, l'utilisation d'incertitudes de données nucléaires multi-groupe permet une comparaison cohérente entre NUSS et les autres méthodes employant le même format d'incertitude des données nucléaires.

La première étape du développement de NUSS se concentre sur l'application d'un algorithme de "simple random sampling" (SRS). L'effet de combiner un format multi-groupe avec le format ACE sur la propagation des incertitudes sur les données nucléaires est estimé. Il est montré que le nombre de groupe énergétique a un impact mineur sur la précision de l'incertitude du k_{eff} tant que la mise en groupe reflète le spectre neutronique. La vérification de la propagation des incertitudes à travers MCNPX par NUSS et la quantification des incertitudes sur le paramètre de sortie de MCNPX sont obtenus.

La seconde partie du développement est motivée par le besoin d'une méthodologie efficace d'analyse de sensibilité basé sur un échantillonnage global et couplé avec MCNPX. Dans le cas de systèmes complexes, la décomposition de l'incertitude totale du paramètre de sortie par NUSS-SRS n'est plus rentable (temps de calcul). La capacité de déterminer simultanément l'incertitude totale et les contributions individuelles provenant des données nucléaires, basée sur un algorithme de type "Random Balance Design", a ainsi été implémentée dans l'outil NUSS-RF. Cette capacité a été validée par trois tests analytiques utilisant des modèles linéaires et non-linéaires et des variables d'entrée corrélées. NUSS-RF est ensuite utilisé pour démontrer l'efficacité de la décomposition de l'incertitude totale selon les données nucléaires perturbées. Par opposition, une tentative de décomposition de l'incertitude totale en contributions individuelles utilisant une méthode conventionnelle de S/U résulte en une décomposition différente lorsque les variables d'entrée sont corrélées.

Les recherches et les implémentations de ce travail de thèse sont de grande valeur de par l'introduction de l'analyse globale de sensibilité dans le répertoire des méthodes de quantification de l'incertitude des données nucléaires. L'outil NUSS est attendu à être extrêmement utile pour élargir les applications de MCNPX pour lesquelles l'incertitude due aux données nucléaires d'une réponse peut être quantifiée.

Mots clés : données nucléaires, covariance des données nucléaires, format ACE, Monte-Carlo à énergie continue, MCNP(X), sûreté-criticité, sensibilité du k_{eff} , échantillonnage stochastique, Fourier Amplitude Sensitivity Testing, Random Balance Design, sensibilité globale.

Outline

Acknowledgements	iii
Abstract	v
Résumé	vii
Outline	1
1 Quantifying nuclear data uncertainty	1
1.1 Background and context	1
1.2 Nuclear data	3
1.3 Nuclear data uncertainty	7
1.4 Propagating nuclear data uncertainty by deterministic method	9
1.5 Propagating nuclear data uncertainty by stochastic methods	11
1.6 Contribution of PhD on NDUQ by SS for MCNPX	15
1.6.1 Mixing of continuous-energy and multigroup	15
1.6.2 Stochastic sampling with MCNPX	16
1.6.3 Sensitivity from stochastic sampling	17
2 Building NUSS-SRS for ACE-formatted nuclear data	19
2.1 MCNP(X) and ACE-formatted nuclear data	19
2.2 NJOY and the generation of groupwise covariances	25
2.3 NUSS-SRS implementation	28
2.3.1 Assumption and limitation	28
2.3.2 MATLAB programs for modifying nuclear data	30
2.3.3 Link to MCNPX on MERLIN	36
2.3.4 Output analysis methods	37
3 Evaluating NUSS-SRS against existing methods and its applications	41
3.1 NUSS Direct perturbation versus MCNPX PERT CARD	41
3.2 NUSS-SRS versus TSUNAMI	44
3.3 NUSS-SRS versus TMC	47
3.4 Energy-group-structure effect in NUSS-SRS	53
3.5 Sensitivity analysis with NUSS-SRS	57
3.6 UAM Pincell application by NUSS-SRS	60

Outline

3.7	UACSA application by NUSS-SRS	63
4	Introducing variance-based global sensitivity analysis	71
4.1	Motivation for global sensitivity analysis	71
4.2	Variance decomposition by global sensitivity analysis	72
4.3	Theory of FAST for uncorrelated inputs	74
4.4	RBD for correlated inputs	78
4.5	Variance decomposition by Sandwich Rule	81
5	Implementing NUSS-RF and its applications	85
5.1	Introducing NUSS-RF	85
5.2	Verification by analytical functions	86
5.3	Application for small correlation: Jezebel and Godiva	94
5.4	Application for large correlation: PB2-HZP	101
6	Conclusion and future work	107
6.1	Chapterwise summary	107
6.2	Contribution summary and future work	110
6.3	Concluding remarks	115
	Appendix	117
A	Derivations	117
A1	Sandwich Rule	117
A2	Differential Operator Sampling	118
A3	First-order Adjoint Perturbation Method	119
A4	Decomposition of Covariance Matrix	121
A5	Covariance of Samples from Simple Random Sampling	124
A6	Nuclear Data Variances in Different Energy Groups	125
A7	Derivation of Squared of Pearson Correlation Coefficient	127
A8	Fourier Transform and Parseval's Theorem	127
A9	Power Spectrum and Variance Calculation in MATLAB	129
A10	Additive Model with Multivariate Normal Distribution	131
A11	Higher-Order Sensitivity Coefficient and Variance	135
B	Supplementary Tables and Figures	136
B1	xmdir File	136
B2	Explanation of NXS and JXS Arrays	136
B3	NJOY Input File Example	137
B4	Energy Boundaries for SCALE 238-group and 44-group	137
	Bibliography	148
	Curriculum Vitae	149

1 Quantifying nuclear data uncertainty

1.1 Background and context

The demand for more accurate and precise prediction of the behaviour of a fission system is always increasing. Only by satisfying such a demand, can we have greater confidence in our current understanding of the governing equations which are used to describe the system behaviour. This in turn will allow us to study more advanced systems or conditions (such as in transient or accident) where the integrity of the system must be maintained. An increase of accuracy and precision also means the allowance for reduced conservatism for the benefit of greater economic efficiency without compromising safety. However, what limits the accuracy and precision are uncertainties that can come from diverse sources and at various stages of the system calculation.

Uncertainties in nuclear data and their propagation through a fission system are the subjects of this work. Historically, nuclear data measurements started with using neutrons to probe nuclear structures given its neutrality and the ability to penetrate into the charged nucleus. During experiments, uncertainties of both systematic (or epistemic) and random (or aleatoric) nature can affect the nuclear data measurement results. For example, the resolution of measurement equipment gives rise to the energy dependency of nuclear data measurement; correlations between nuclear data also exist when their values are derived from the same background normalization of experimentally measured values. As the quality of nuclear data and their associated uncertainties are continuously improved by new mathematical and experimental methods, nuclear data uncertainty analysis in addition to the standard neutronics calculations is not only possible, but also becoming an expected step in the standard practice.

The quantitative knowledge of the amount of uncertainty due to nuclear data gives rise to new approaches in different applications. For example, in Criticality Safety Assessment (CSA), uncertainties in the discrepancy between calculated and experimental k_{eff} values (called the k_{eff} bias [1]) will be explained partially by the uncertainty contribution from nuclear data. Consequently, the administrative safety margin (e.g. 5000 pcm) which is imposed to cover unknown sources of uncertainty as a conservative measure might be relaxed if the uncertainty

Chapter 1. Quantifying nuclear data uncertainty

contribution of nuclear data is quantifiable. In another application, the Burn-up Credit methodology is to account for (i.e. give credit to) the reactivity decrease in depleted nuclear fuel due to the reduction of fissile nuclides content, the accumulation of fission products and absorbing minor actinides. By propagating nuclear data uncertainty throughout criticality, depletion and decay calculations, the final prediction of isotopic compositions of the nuclear fuel can be evaluated with uncertainties contributed by nuclear data. Hence, by quantifying uncertainties, the conventional practice of CSA can have a more rigorous and best-estimate approach, steering away from the excessive conservatism in the past.

The efforts for nuclear data uncertainty quantification are reflected in recent OECD/NEA/NSC working party activities. Since 2005, the Expert Group on Uncertainty Analysis in Modelling (UAM-LWR) has concentrated on defining sources of uncertainties and on benchmarking different uncertainty quantification methodologies for Light Water Reactor (LWR) applications. Nuclear data uncertainties were first tackled in the Phase I (Neutronics) of UAM-LWR activities by participants from the U.S.A, France and Switzerland etc. The exercises in Phase I involved examining the propagation of nuclear data uncertainties into the derivation of few-group cross sections and steady-state neutronics calculations with confidence bounds. Phase II focused on the core-level uncertainty propagation and Phase III is for the system-level where the several sources of uncertainties including nuclear data are propagated through neutronics and thermal-hydraulics core performances. Similarly, the Expert Group on Uncertainty Analysis for Criticality Safety Assessment (UACSA) was established in 2007 to address sensitivity and uncertainty for criticality calculations. Phase I of UACSA collects different validation methods of criticality safety from various countries, taking into consideration the uncertainty in criticality codes due to nuclear data uncertainties [2].

Locally at the Paul Scherrer Institut, major activities related to the propagation and quantification of uncertainties in the applications of Criticality Safety Assessment and Burn-up Credit are on-going and perhaps even emphasized due to the political decision to phase out nuclear power in Switzerland after the Fukushima accident in March 2011. For example, fuel rod design/technological parameter uncertainties were propagated [3] using the GRS SUSA code for burnup calculations in the deterministic code CASMO. Since then, the capability of nuclear data uncertainty quantification for CASMO has been developed into a powerful platform called SHARKX [4] and it has been applied in the UAM-LWR activities for more general LWR-type applications. On the other hand, the Monte Carlo-based MCNP(X) code is the validated, routine tool for CSA applications at PSI, given its accurate geometric modelling capability and continuous energy treatment. So far, PSI has participated in the UACSA Phase I and II activities which demonstrated PSI's CSA validation methodology and examined k_{eff} confidence bounds in consideration of manufacturing parameter uncertainties respectively. Naturally, the uncertainty quantification for nuclear data in continuous-energy MCNP(X) is of great interest, for the on-going development of PSI's CSA methodology.

Both criticality safety assessment and burnup credit validation methodologies are highly relevant applications in which nuclear data uncertainty plays an important role. The nature

of these applications dictates the type of nuclear data and neutronics code that are most suitable. In the next few sections, the origin and organization of nuclear data and their uncertainties are explained, followed by the survey of current available methods for nuclear data uncertainty quantification. They shall provide the background information for this PhD thesis on the development of a computational tool to propagate uncertainties of evaluated, general-purpose continuous-energy nuclear data through MCNPX and the analysis of the uncertainties of MCNPX outputs.

1.2 Nuclear data

The probability of an incoming neutron to collide and interact with a target nucleus is known as the “cross section”. For example, fission reaction and inelastic scattering of neutrons can be denoted by the incoming (n for neutron) and outgoing particles, i.e. (n, f) and (n, n’) respectively. In a laboratory environment, time-of-flight experiments can be performed where a beam of neutrons is fired at a target sample of nuclide of interest. From the path length (L) and time (t) that the neutron takes to travel, its energy can be calculated as

$$E = \frac{mv^2}{2} = \frac{mL^2}{2t^2} \quad (1.1)$$

The ratio of outgoing and incoming neutron beam intensities (I_o , I_i) after neutrons pass through the sample of thickness D without interacting is:

$$\frac{I_i}{I_o} = e^{-DN\sigma_t} \quad (1.2)$$

where N (in particles/cm³) is the material density and σ_t is the total microscopic cross section, i.e. the probability of all possible reactions between the neutrons and the material. The unit of microscopic cross section is commonly cm² or barn (where 1 barn=10⁻²⁴cm²). Macroscopic cross section (in cm⁻¹) is defined as $N\sigma$, and is the probability of reaction per unit path length traversed per unit incident neutron. Total cross section is a sum of partial cross sections which can occur depending on the incident neutron energies and characterized by the products of specific reactions (e.g. gamma rays, secondary particles). Similarly, through time-of-flight measurements, the angle and energy distributions of the outgoing particles can be obtained. Collectively, cross sections and other quantities such as fission neutron yield ($\bar{\nu}$), fission neutron spectrum (χ), angular and energy distributions of outgoing particles upon interactions and so forth are known as “nuclear data”. Experimental results and bibliographic information of nuclear data can be found in EXFOR [5] and CINDA[6] databases respectively.

For practical nuclear applications, experimentally measured nuclear data are, however, not suitable to be used directly. Fig. 1.1 illustrates how sparse the experimental measurements can be with the example of ¹H(n, elastic) cross section. To fill in the missing data, theoretical nuclear models are relied upon heavily. The so-called “evaluated nuclear data” are shown as the solid line in Fig. 1.1, as a result of combining experimental measurements, theoretical nuclear

Chapter 1. Quantifying nuclear data uncertainty

models, and statistical analysis (when multiple experimental measurements are available for the same quantity of interest). Evaluated nuclear data reflect the best representation of the true cross sections [7]. They are organized into the “ENDF-6” format [8] which is highly-ordered and computer readable. Inside the ENDF-6 formatted nuclear data files, nuclear data are available from incident neutron energy of 10^{-5} eV to 20 MeV (or sometimes even 200 MeV) with precisely defined interpolation laws between energy points. National laboratories and international organization around the world generate and maintain their own nuclear data libraries, shown in Table 1.1. It is worthwhile to mention that, the OECD/NEA Data Bank compiles a “High Priority Request List” [9] for the purpose of planning and guiding nuclear data experiment activities and nuclear model theory evaluation, in order to meet the nuclear data users’ most urgent needs given the limited resources in facility and time.

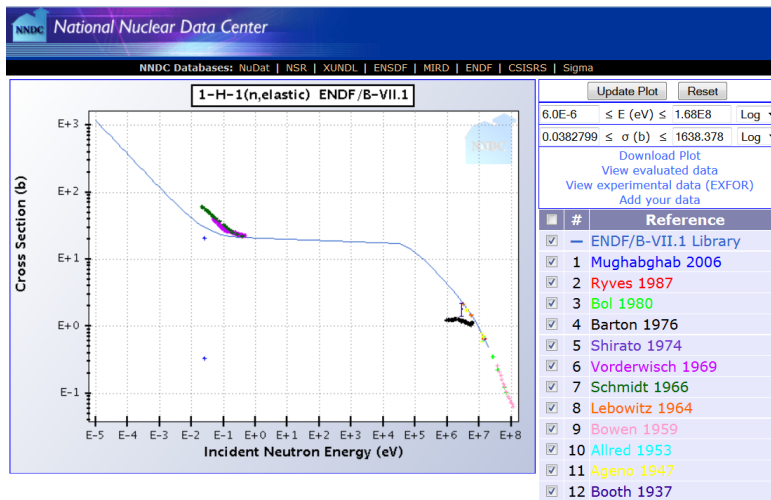


Figure 1.1: The evaluated data (solid line) of $^1\text{H}(n, \text{elastic})$ taken from the ENDF/B-VII.1 library are plotted over the experimental measurements.

Organizer	Library	Released in
Europe OECD/NEA	JEFF-3.2	2014
Netherland NRG	TENDL-2014	2014
USA BNL	ENDF/B-VII.1	2011
Japan	JENDL-4.0	2011
China	CENDL-3.1	2011
Russia	BROND-2.2	1992

Table 1.1: Major general purpose libraries, all use ENDF-6 format for the evaluated nuclear data files.

Given their comprehensive content, the general-purpose ENDF-6 files can be too “heavy” to manipulate. Processing codes such as NJOY [10] can extract the necessary data and introduce problem-dependent adjustments such as Doppler broadening, calculation of group-averaged constants etc. NJOY can also generate a specific format called ACE (A Compact ENDF) for the continuous-energy Monte Carlo-based code MCNPX. In this case, the reconstruction of

the pointwise cross sections in ACE format from the ENDF-6 format is performed by NJOY's RECONR module (more details in Chapter 2.2). Then, Doppler-broadening by the BROADR module adds temperature dependence to the cross sections and the PURR module prepares probability tables [11] for the unresolved resonances of the cross sections.

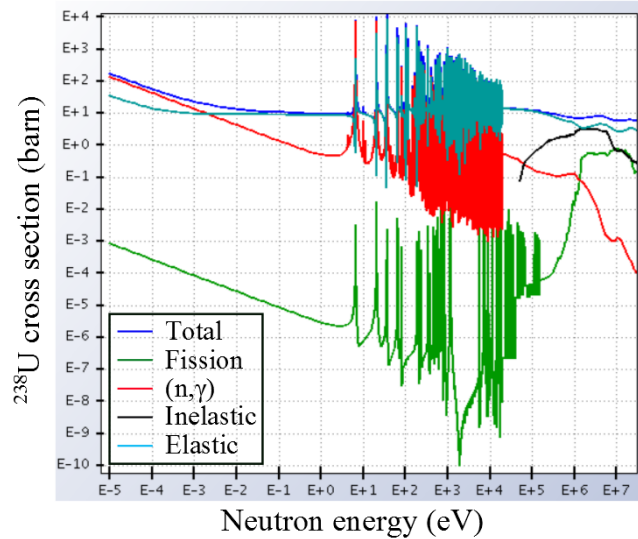


Figure 1.2: Evaluated nuclear data satisfies the condition that they are continuous in energy.

Figure 1.2 shows several evaluated cross section data of nuclide ^{238}U from the ENDF/B-VII.1 library and it gives a sense of the amount of data points required in order to faithfully reconstruct the complex resonances in a continuous-energy manner in the ACE-formatted pointwise nuclear data files. For computer codes which do not work with such detailed pointwise nuclear data, further data processing can be done and NJOY is also used to produce the other library formats for multigroup nuclear data. The idea is to average the pointwise data within specified energy groups (g) by an appropriate weighting function (w):

$$\langle \sigma \rangle_g = \frac{\int_{E_{g+1}}^{E_g} \sigma(E) w(E) dE}{\int_{E_{g+1}}^{E_g} w(E) dE} \quad (1.3)$$

By convention, the highest energy corresponds to the energy group number one. The choice of the weighting function $w(E)$ naturally comes from the definition of reaction rate [12]:

$$R = \int_{g+1}^g N \sigma(E) \phi(E) dE = N \cdot \frac{\int_{g+1}^g \sigma(E) \phi(E) dE}{\int_{g+1}^g \phi(E) dE} \cdot \int_{g+1}^g \phi(E) dE = N \langle \sigma \rangle_g \langle \phi \rangle_g \quad (1.4)$$

where $\langle \phi \rangle_g$ is called the integrated flux and $\langle \sigma \rangle_g$ the integrated cross section over energies between group $g+1$ and g .

Paradoxically, the precise flux is the unknown, sought-after solution of the Boltzmann transport equation which requires information of the nuclear data. It is said to be an *art* to make

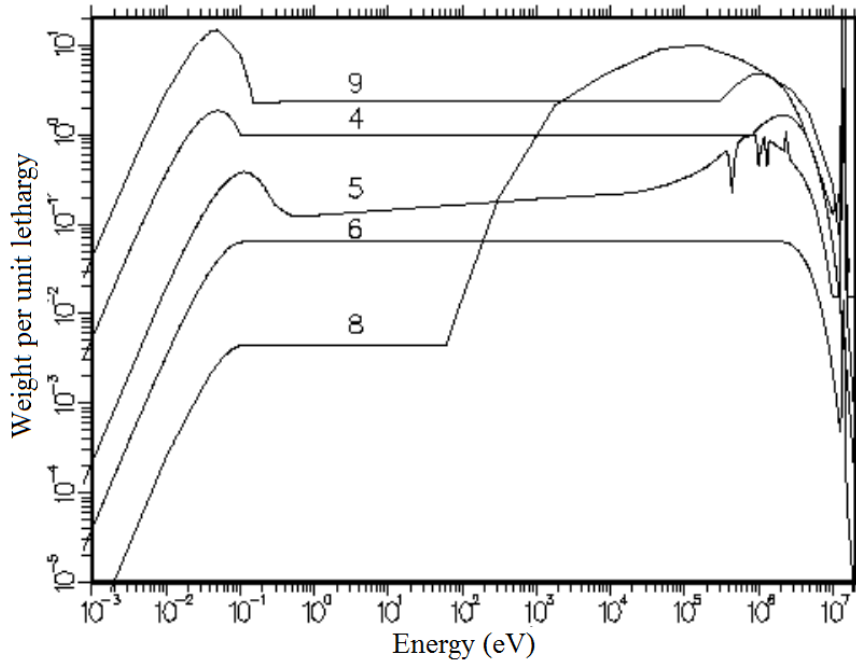


Figure 1.3: Different flux shapes as weighting function in NJOY.

a good guess for the within-group flux shape in NJOY [10]. Several options are provided by NJOY's GROUPT module as shown in Fig. 1.3. The flux shapes are usually divided into three regions: a fission spectrum, the $1/E$ -shape slowing down and the Maxwellian thermalization of neutrons. However, in the case of a strong absorber, at the energies of the resonances, the smooth flux shape has “dips” which are suppressions in the flux due to the increased probability of neutrons being absorbed in the medium. Fewer neutrons are available and reaction rates decrease. This phenomenon of reduced effectiveness of the resonance is known as the “self-shielding” of the resonance itself. In preparation of problem-dependent multigroup nuclear data, such effects must be taken into account by methods such as the Bondarenko shielding factor (more details in Chapter 2.2).

The choice of pointwise or multigroup nuclear data goes hand-in-hand with the choice of the computer codes for the applications of interest. The continuous-energy MCNP(X) code uses the ACE-formatted nuclear data and together they are highly suitable for criticality safety problems. However, it is important to remember that, even the ACE-formatted nuclear data are post-processed from evaluated data by processing codes such as NJOY. As the accuracy of neutronics codes improves, the uncertainty in the outputs of neutronics calculations can be traced back to the preparation of these nuclear data. At the different stages of data processing up until the particular nuclear data format used directly by the chosen neutronics code, there are assumptions and approximations which become the sources of uncertainty in nuclear data as explained next.

1.3 Nuclear data uncertainty

As seen in previous discussions, nuclear data undergo a series of processing steps to arrive at the suitable format for nuclear applications. A similar route is undertaken by the uncertainties in experimentally measured nuclear data which propagate through several stages of processing and become particular types of nuclear data uncertainties, often known as the “multigroup covariance matrices” that are used in this PhD work and related studies. In the previously mentioned time-of-flight experiment for nuclear data measurement, the count rate, i.e. the number of counts (of outgoing particles) per (energy, angle) channel·time are the raw data and they obey the Poisson statistics [7]. Performing consistent normalization ($a \pm \Delta a$) and background removal ($b \pm \Delta b$) on the experimental raw data (r_i, r_j) introduces correlations among experimentally measured cross sections (d_i, d_j). The experimental covariance is [7]:

$$V_{ij} = \langle \delta d_i, \delta d_j \rangle \quad (1.5)$$

where

$$\delta d_i = \delta \left(\frac{r_i - b}{a} \right) = \frac{\delta r_i - \delta b}{a} - (r_i - b) \frac{\delta a}{a^2} = \frac{\delta r_i - \delta b}{a} - d_i \frac{\delta a}{a} \quad (1.6)$$

Hence the experimental covariance can be calculated as

$$V_{ij} = \frac{\langle \delta r_i, \delta r_j \rangle + \langle \delta^2 b \rangle + d_i d_j \langle \delta^2 a \rangle}{a^2} = \frac{\Delta^2 r_{(i=j)} + \Delta^2 b + d_i d_j \Delta^2 a}{a^2} \quad (1.7)$$

The experimental covariances (V) are taken into account while the experimental cross sections are fitted with theoretical models, for example, described by R-matrix theory in the nuclear data processing code SAMMY [13]. Using generalized least-squares equations, the evaluated parameters P and their associated covariances M are best-fitted in the following [7]:

$$P = P_0 + MGV^{-1}(d - T) \quad \text{and} \quad M = (G^T V^{-1} G + M_0^{-1})^{-1} \quad (1.8)$$

where P_0 and M_0 are the initial guesses of P and M . T contains theoretical values for experimental data based on nuclear models and G is the sensitivity matrix (partial derivatives) of parameter T with respect to P . Results of the evaluated data P and associated covariance M are stored inside the ENDF-6 formatted files.

Codes such as NJOY have the formulation of the partial derivative $\partial\alpha/\partial P$ where α is the cross section. Hence the uncertainty $\delta\alpha$ is related to the evaluated data parameters P in the following way:

$$\delta\alpha = \delta\alpha(P_m, \dots, P_n) = \sum_m^n \frac{\partial\alpha}{\partial P_m} \delta P_m \quad (1.9)$$

Chapter 1. Quantifying nuclear data uncertainty

and the covariance of α is:

$$U(\alpha_i, \alpha_j) = \langle \delta \alpha_i, \delta \alpha_j \rangle = \sum_m \sum_n \frac{\partial \alpha}{\partial P_m} \langle \delta P_m, \delta P_n \rangle \frac{\partial \alpha}{\partial P_n} = \sum_m \sum_n \frac{\partial \alpha}{\partial P_m} M \frac{\partial \alpha}{\partial P_n} \quad (1.10)$$

To obtain multigroup covariance matrix, the flux weighting function is applied as before

$$\bar{U} = \int \phi(E) dE \int \phi(E') dE' \sum_{mn} \frac{\partial \alpha(E)}{\partial P_m} M_{mn} \frac{\partial \alpha(E')}{\partial P_n} \quad (1.11)$$

For certain nuclear data there are further mathematical constraints on the covariance matrix. For example, the prompt fission spectrum (χ) covariance matrix is normalized due to the “sum to zero” property [14]. It is cautioned that both too large (more than 50% of absolute cross section) or too small uncertainties should be considered unreliable and needed to be reviewed or rejected [14]. Mathematically, nuclear data covariance matrices have to be symmetric and positive semidefinite. The correlation matrix is defined in Eqn (1.12). Its diagonal elements are equal to 1 and off-diagonal elements between -1 and 1. The relative covariance matrix is defined in Eqn.(1.13). From its diagonal elements, the relative standard deviation of nuclear data can be obtained.

$$\text{CORR}(\alpha_i, \alpha_j) = \frac{\text{COV}(\alpha_i, \alpha_j)}{\sqrt{\text{VAR}(\alpha_i)} \sqrt{\text{VAR}(\alpha_j)}} \quad (1.12)$$

$$\text{RelCov}(\alpha_i, \alpha_j) = \frac{\text{COV}(\alpha_i, \alpha_j)}{\alpha_i \alpha_j} \quad (1.13)$$

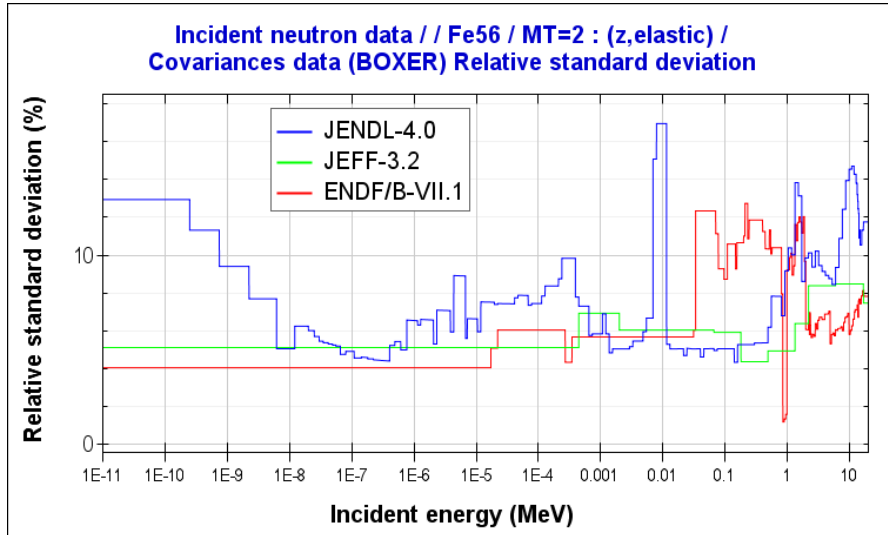


Figure 1.4: Relative uncertainties of $^{56}\text{Fe}(\text{elastic})$ from JENDL 4.0, JEFF-3.2 and ENDF/B-VII.1 nuclear data libraries.

An increasing number of nuclear data covariances is nowadays provided in the modern libraries listed in Table 1.1, yet there are discrepancies among them. As shown in Fig.1.4, the

1.4. Propagating nuclear data uncertainty by deterministic method

relative standard deviations of $^{56}\text{Fe}(n, \text{elastic})$ cross sections clearly have discrepancies, not related to numerical precision. Such difference is the main reason against the mixed use of covariances and nuclear data from different library evaluations for uncertainty propagation methods. Finally uncertainties should always be compiled along with the nuclear data, reflecting the methods used to determine them, whether by experiments, statistical evaluation or theoretical models [15].

1.4 Propagating nuclear data uncertainty by deterministic method

Deterministic method applied for nuclear data uncertainty propagation and quantification is based on the “propagation of moments” applied to the truncated first-order Taylor series. The variance (σ_R^2) of the system response R , i.e. the second central moment of the linearized R is computed as:

$$\sigma_R^2 = \vec{S}_\alpha \mathbf{V}_\alpha \vec{S}_\alpha^T \quad (1.14)$$

where $\vec{S}_\alpha = [S_{\alpha_1}, S_{\alpha_2}, \dots] = [\frac{\partial R}{\partial \alpha_1}, \frac{\partial R}{\partial \alpha_2}, \dots]$ is called the sensitivity coefficient of R with respect to inputs $\vec{\alpha}$, and \mathbf{V} is the covariance matrix of the inputs. Derivation of Eqn.(1.14) is given in Appendix A1. This deterministic approach (as opposed to the stochastic approach in the following Chapter 1.5) by Eqn.(1.14) is called colloquially the “Sandwich Rule” or “Sensitivity/Uncertainty” (S/U) method, both names are used interchangeably in this work.

It is important to distinguish that the covariance matrix (\mathbf{V}_α) is only a property of the inputs, while the sensitivity coefficient \vec{S}_α is dictated by the system properties (e.g. α could represent materials, densities, dimensions). Sensitivity coefficients represent the local change of the system due to the change of inputs. As the mathematical operation of Eqn.(1.14) shows, only inputs with large uncertainties when combined with large sensitivity will have a significant contribution to the variance of system output. Hence the examination of both the sensitivity coefficient and the uncertainty of the inputs is needed for the identification of important inputs.

Among deterministic neutronics codes, since the 1970s, one and two dimensional discrete ordinate S_N codes were already able to compute sensitivity coefficient of different system responses (e.g. dose rate, reaction rate) due to variations of inputs (e.g. cross section, material density), based on first-order adjoint weighted perturbation (AWP) theory [16]. More recent code systems such as SUS3D [16] and ERANOS [17] include the sensitivity capabilities for S_N transport or diffusion based calculations.

The development of sensitivity capabilities in Monte Carlo codes, in comparison has more difficulties due to its inherent statistical implementation. A simple illustration is given through the attempt to compute sensitivity coefficients by “direct perturbation” (DP): each input is varied by a small amount, one-at-a-time. The response R is measured at both its nominal and

perturbed states. The sensitivity coefficient is thus:

$$S^{DP} = \frac{R'(\alpha') - R_o(\alpha_o)}{\alpha' - \alpha_o} = \frac{\Delta R}{\Delta \alpha} \quad (1.15)$$

Such an operation simply involves one reference calculation ($R_o(\alpha_o)$) and the second calculation with a very slightly perturbed input ($R'(\alpha')$) so as to justify the linearity approximation around α_o . For Monte Carlo-based codes, the result of ($R' - R_o$) could be on the same order of magnitude as the statistical error inherent to Monte Carlo codes, producing erroneous S^{DP} . Correlated sampling [18] can be applied (as a variance reduction method in MCNP) which forces correlation between two similar calculations through the use of the same random number sequence. Hence each history track is identical except for those affected by the perturbed parameters. From the rule of error propagation, it can be seen that, a large, positive correlation (ρ) between the two calculations can reduce the variance of ΔR :

$$\sigma(\Delta R)^2 = \sigma(R')^2 + \sigma(R)^2 - 2\rho\sigma(R')\sigma(R) \quad (1.16)$$

Works by [19] and [20] demonstrated such capabilities. Nevertheless, applying direct perturbation to compute response perturbation due to each input variation still requires $K + 1$ calculations (for K number of input parameters, plus the nominal calculation) to sequentially obtain every sensitivity coefficient. Unless there are more system responses for which uncertainty quantifications are sought, than the number of input parameters, this brute-force approach is not recommended.

To compute sensitivity coefficients without repeatedly solving for the system solutions and to avoid the influence of statistical uncertainty, in MCNPX/MCNP the method of Differential Operator Sampling (DOS) is available which tallies the differential changes in the results of the response estimator due to the imposed perturbation in parameters such as cross section. The scores of what the neutrons would have done based on the perturbed cross sections are kept by DOS while performing the nominal simulation of neutron trajectories (see Appendix A2 for more details). In MCNPX/MCNP, DOS is implemented inside the ‘‘PERT CARD’’ module, with the assumption that the fission source distribution is unchanged which is known to degrade the accuracy of the perturbed flux, even though k_{eff} perturbation result is reliable [21]. PERT CARD also does not consider perturbations in $\bar{\nu}$ or χ .

The adjoint weighted perturbation (AWP) method is another option, which is more often implemented in deterministic codes. Based on the linear adjoint-based perturbation theory, sensitivity coefficient of k_{eff} to cross sections is determined by using both the forward (ϕ) and adjoint (ϕ^\dagger) fluxes [22]:

$$S_{k,\alpha} = \frac{dk/k}{d\alpha/\alpha} = \frac{\alpha}{k} \frac{k^2 d\rho}{d\alpha} = -\frac{\alpha}{k} \frac{\langle \phi^\dagger, (\frac{dL}{d\alpha} - \frac{1}{k} \frac{dM}{d\alpha}) \phi \rangle}{\langle \phi^\dagger, \frac{M}{k^2} \phi \rangle} \quad (1.17)$$

The derivation of $S_{k,\alpha}$ and the interpretation of adjoint flux can be found in Appendix A3.

1.5. Propagating nuclear data uncertainty by stochastic methods

Memory issues associated with Monte Carlo adjoint calculations have been solved (improved also by modern computing power) that AWP can now be found in multigroup TSUNAMI code and continuous-energy McCARD [23], MCNP6 [24]. The motivation to study the sensitivity and uncertainty of system responses other than k_{eff} has also led to the implementation of the “generalized perturbation theory” (GPT) which is in contrast to the “classic” AWP theory. Among Monte Carlo-based codes, SCALE6.1 TSUNAMI has developed such capability[25]. Table 1.2 summarizes major codes which employ DOS or AWP methods. DOS/FSP denotes the differential operator sampling method with fission source perturbation correction.

Monte Carlo codes		
Code	Energy	Method
MCNPX	Continuous	DOS
MCNP6	Continuous	DOS Classic AWP
McCARD	Continuous	Classic AWP, DOS/FSP
MVP[26]	Continuous	DOS/FSP
SCALE6.0	Multigroup	Classic AWP
MMKKENO[27]	Multigroup	DOS/FSP
Deterministic codes		
Code	Method	Sensitivity method
SCALE6.0	1D S_N 2D	Classic/Generalized AWP Generalized AWP
ERANOS	S_N , diffusion etc.	Classic/Generalized AWP
SUSD3D	S_N	Classic AWP
CASMO-4 (VTT inhouse)[28]	Method of Characteristic	Classic/Generalized AWP
DRAGON[29]	Method of Characteristic	Classic/Generalized AWP
SAGEP[30]	Diffusion	Generalized AWP

Table 1.2: Computer codes and corresponding deterministic-based methods to compute sensitivity coefficients.

1.5 Propagating nuclear data uncertainty by stochastic methods

The utilization of stochastic sampling within the field of nuclear engineering began with its applications in thermalhydraulics and reliability analysis. The motivation is to develop best-estimate modelling practices where realistic inputs and models are used and the evaluation of results must include their uncertainties. Instead of using conservative values for the model inputs, probability density functions (PDF) are assigned using the best available information. A sampling scheme is chosen to prepare the set of input data in accordance with the PDF assignment. The most straight-forward method is the simple random sampling (SRS) where each sample is created independently. However, the risk associated with SRS is that for a small number of samples, the sampling of inputs might explore the input domain in clusters by chance. This can be mitigated by stratified sampling schemes such as the Latin Hypercube

sampling (LHS) [31] where the user divides the PDF into strata of equal marginal probability and samples are made in each stratum. Though stratified sampling offers faster convergence than SRS, its implementation requires more administrative effort. Hence before being applied to actual model calculations, random samples from simple random sampling can be checked, discarded and regenerated easily if clustering is observed. Finally, the model of interest is calculated repeatedly with these sampled inputs and an equal number of output values is generated. Consequently, the output can now be represented and interpreted in terms of its probability distribution and statistical properties such as a sample mean and standard deviation.

The aforementioned stochastic sampling algorithms can also be applied to nuclear data uncertainty quantification. The sampling of the nuclear data and modifications can be made independently of the neutronics codes. But to reiterate Chapter 1.2, nuclear data and covariances are formatted differently depending on the needs of the computational codes and applications. Nuclear data in their most basic format can be found in compilations such as the EXFOR/CSISRS databases [5], the Atlas of Neutron Resonances [32]. These basic data are fitted with nuclear reaction models to generate evaluated nuclear data in the ENDF-6 format by nuclear reaction system codes, such as TALYS [33]. When TALYS is run many times, each with perturbed inputs of nuclear modelling parameters, perturbed ENDF6-formatted files are generated. Based on this sampling scheme with TALYS, the Total Monte Carlo (TMC) methodology offers the flexibility of reformatting ENDF-6 to continuous/pointwise-energy or multigroup format. As a stochastic sampling based method, it has the advantage of quantifying nuclear data uncertainty contribution for diverse applications such as PWR pincell burnup with SERPENT code [34], criticality safety with MCNP [35], ADS burnup calculation [36] with inventory code ACAB [37] etc. A by-product of the TMC sampling method is the automatic generation of ENDF-6 covariances [38], many of which can still be missing in other major nuclear data libraries. It is argued that, when the traditional method of preparing covariances by experiments is expensive and unable to provide comprehensive covariance information, TMC offers a solution based on uncertainty propagation from the point of view of theoretical nuclear physics. When nuclear model parameters are perturbed in accordance with their presumed uncertainties, the outputs of nuclear models, such as energy-dependent cross sections, resonance parameters, are obtained with statistical information as well. The mean and covariances for some nuclear data whose uncertainties were difficult to quantify experimentally become available. However, it will be shown in Chapter 3.3, the covariance differences between the TMC-generated TENDL nuclear data library and the other major libraries can be significant, due to the very different approaches.

Uncertainties from covariance data inside ENDF-6 formatted files can also be propagated into ENDF-6 formatted nuclear data by NUDUNA (NUclear Data UNcertainty Analysis), the “unified treatment for nuclear data uncertainties and systematic uncertainties” by AREVA NP GmbH. Nuclear data of neutron multiplicities, (resolved and unresolved) resonances, cross sections and angular distribution can be perturbed [39]. Since NUDUNA works directly with ENDF-6 formatted nuclear data files, they can be further reformatted by NJOY or PUFF

1.5. Propagating nuclear data uncertainty by stochastic methods

[40] into formats suitable for continuous-energy or multigroup-based computational codes. However, ENDF-6 format is for general-purpose and performing random sampling with cross section covariance matrices is numerically challenging for large data sets [39]. Moreover, uncertainty treatment for ENDF-6 formatted energy distribution data such as the fission spectrum has not been implemented[39].

Implemented by GRS (Gesellschaft für Anlagen- und Reaktorsicherheit, Germany), the XSUSA code uses stochastic sampling to propagate the multigroup nuclear data uncertainties through SCALE-based codes such as the 1D deterministic XSDRN code, 2D S_n transport solver NEWT, TRITON depletion sequence and the 3D Monte Carlo KENO-Va [41][42]. The relative covariances of nuclear data are used by XSUSA to generate a set of multiplicative perturbation factors (P_g), which can then be applied to the original multigroup cross sections on a group (g) to group basis:

$$\sigma_g \cdot P_g = \sigma'_g \quad (1.18)$$

where σ'_g is the perturbed multigroup cross section. Eqn(1.18) is an approximation because it perturbs the already self-shielded cross section σ_g by P_g values obtained from infinitely-diluted covariance data. Though substantial impact due to this inconsistency had not been observed in terms of the total nuclear data uncertainty contribution over the full energy range, it was corrected in the SAMPLER code of SCALE [43].

SAMPLER involves modifying the preparation steps of self-shielding factors in SCALE. CENTRM/PMC and BONAMI are two modules responsible for shielding cross sections in resolved and unresolved/fast resonance regions respectively. The former uses 1D discrete ordinate code for problem-dependent flux calculation to generate flux weighted, shielded multigroup cross sections (between 0 and 20keV). The latter is based on the Bondarenko method where the original infinitely-diluted multigroup cross section ($\sigma_g(\infty)$) is modified by pre-tabulated shielding factors ($f_g(\sigma_o)$). They are functions of the background cross section (σ_o):

$$\sigma_g(\sigma_o) = f_g(\sigma_o)\sigma_g(\infty) \quad (1.19)$$

In normal SCALE calculations, interpolated and pre-tabulated shielding factors can generate problem-dependent, self-shielded multigroup cross sections efficiently. In order to perturb self-shielded multigroup cross sections properly, the shielding factor is updated according to the affected cross section as well [43]:

$$f'_g(\sigma_o) = \frac{\sigma'_g(\sigma_o)}{\sigma'_g(\infty)} = \frac{\langle \frac{\sigma'_c(u)}{\sigma'_{c,t}(u)+\sigma_o} \rangle / \langle \frac{1}{\sigma'_{c,t}(u)+\sigma_o} \rangle}{\sigma'_g(\infty)} \quad (1.20)$$

where $\sigma'_g(\sigma_o)$ is the shielded MG cross section at a background σ_o , $\sigma'_g(\infty)$ is the perturbed infinitely-diluted MG cross section, $\sigma'_{c,t}(u)$ is the total of the perturbed pointwise cross sections in the material of interest.

Chapter 1. Quantifying nuclear data uncertainty

Uncertainty results from SAMPLER for an LWR criticality benchmark experiment show close agreement with the TSUNAMI-3D “Sandwich Rule” method, for example 0.44% vs. 0.46% with 300 random samples[43]. Similarly, uncertainties in pin power and isotopic content as a function of burnup due to nuclear data are also examined in [43]. It is clear that the capability of the stochastic sampling-based method to compute uncertainties of arbitrary output parameter is a big advantage over the deterministic-based methods.

As seen in the case of SAMPLER, the modification of the nuclear data must be consistent, which sometimes relies on the accessibility of computer source code. Another such example is the CASMO-5MX code, which is an in-house modified version of CASMO-5M at PSI to perform uncertainty quantification for nuclear data by stochastic sampling. The direct perturbation method is available for computing the first-order sensitivity coefficients to be used in the Sandwich Rule. The stochastic-sampling option performs simple random sampling, using multigroup nuclear data covariances whose structures can be changed by auxiliary code called ANGELO-LAMBDA[16]. Due to the proprietary format of nuclear data, the self-shielding effect has not been taken into account in CASMO-5MX. The perturbation factors obtained by sampling the infinitely-diluted nuclear data covariances are applied to CASMO-5M resonance-range nuclear data without updating the original shielding factors. It is reasoned that self-shielding is a negative feedback effect; as a result, the CASMO-5MX uncertainty methodology would overestimate the nuclear data uncertainty contributions [44]. It is also not feasible to separate the elastic scattering, inelastic scattering, (2,2n) and (n,3n) reactions from a “combined scattering matrix” format for these data. As explained in [4], calculations have to be performed in NJOY to derive “scattering fractions” for the nuclides of interest (impact of temperature and background cross section variations are found to be insignificant[44]).

Data format	Code name
EXFOR/CSISRS	TALYS/TMC
ENDF-6	NUDUNA
Multigroup	CASMO-5MX, XSUSA, SAMPLER

Table 1.3: Existing codes based on stochastic sampling approach work with specific nuclear data and covariance formats.

Table 1.3 summarizes the methods mentioned above and the types of nuclear data formats for which their implementations are tailored, which are relatively simple as long as the formats and the generation process of respective nuclear data are understood. For another example, the ENDL format by the Lawrence Livermore National Lab (LLNL) is sampled with the in-house tool KIWI code [45], part of the “extensive framework for quantitative measurement of uncertainty (QMU) studies” at LLNL.

As an attractive alternative to the deterministic sensitivity/uncertainty-based methods in the previous section, stochastic-sampling methods are expected to gain more wide usage due to increasing modern computing power. Already, an integration between deterministic “Sandwich Rule” and sampling methods has been proposed by Cabellos as a hybrid method

for burnup applications [46]. It formulates that the evolution of k_{eff} uncertainty is attributable to two components at each burnup step t :

$$\text{var}(k)_t = [S_k V_\alpha S_k^T]_t + [S_N V_N S_N^T]_t \quad (1.21)$$

where S_k is the sensitivity coefficient of k due to cross sections α and S_N is the sensitivity coefficient of k due to isotopic number density (N). For each burnup step, SCALE/TRITON is used to compute the isotopic number densities and they are used as nominal inputs in TSUNAMI code to calculate S_k and S_N . V_N is the covariance of number density due to cross section, fission yield and/or decay data, which are sampled by an inventory code (ACAB [37]) at each burnup step. ACAB performs many depletion calculations to determine the number densities for each sample at the end-of-burnup-step. Hence, statistical information is acquired to produce the burnup-step-dependent V_N , which is not possible to be generated otherwise by the TSUNAMI method.

1.6 Contribution of PhD on NDUQ by SS for MCNPX

As presented in this Chapter, each of the major neutronics codes has at least one approach to quantify nuclear data uncertainty (see Tables 1.2 and 1.3) and they are continuously improving. On one hand, the adjoint weighted perturbation has been expanded from the classic to generalized theory of perturbation. Perturbation of the fission source is taken into account for differential operator sampling method as well. On the other hand, stochastic sampling-based methods, even though a late-comer compared to deterministic “Sandwich Rule” methods, are gaining wider usage because of increasing modern computing power. The choice of uncertainty quantification method depends largely on the problem under investigation and consequently on the type of neutronics code and nuclear data format.

To reiterate from Chapter 1.1, at PSI there is strong demand for nuclear data uncertainty quantification in criticality safety assessment and burnup credit validation basis for the storage and transport of Swiss spent LWR nuclear fuel. Hence the uncertainty quantification method suitable for our problems has to be compatible with MCNPX and able to provide uncertainty for variables in addition to k_{eff} . Among the existing codes discussed in this chapter, only NUDUNA and TMC provide the closest solution to our problem. What is proposed in this PhD work has to have additional contributions to the existing solutions, which are investigated in the following three aspects.

1.6.1 Mixing of continuous-energy and multigroup

In the existing methods, nuclear data are either in multigroups or in ENDF6 format. The manipulation of the former format is certainly much easier. However as shown by SAMPLER's improvement over XSUSA, self-shielding effect must be treated properly upon the perturbation of multigroup data. An additional step is also required (though not mentioned previously) for

aligning the different group structures which might exist between the nuclear data and the covariance data.

Given the different types of nuclear data and consequently their usage by corresponding codes (i.e. multigroup or continuous energy), it is important to assess the effect of code difference on the propagated nuclear data uncertainty. In [39], NUDUNA was applied to generate perturbed ENDF6-formatted nuclear data which were subsequently converted to the continuous-energy ACE format used by MCNP and to the 238-group format for SCALE6.0/KENO V.a. The nuclear uncertainty contributions in k_{eff} for the fast-spectrum Godiva benchmark [47] has been found to be essentially unaffected by multigroup discretization (e.g. 955 pcm in MCNP vs. 953 pcm in KENO). This study indicates that multigroup nuclear data, when perturbed by the same underlying uncertainties (on the same ENDF6-level) as the continuous-energy were, do not introduce additional uncertainty to k_{eff} uncertainty due to the coarser energy resolution.

The use of ENDF6 format by NUDUNA (as well as TMC) is versatile but incompatible with the multigroup covariance libraries used by TSUNAMI, SAMPLER etc. The verification and validation of NUDUNDA and TMC against other methods which do not use ENDF6 format are difficult in terms of separating uncertainty contributions from methodological effects, or from nuclear data directly because of the different source/format of nuclear data uncertainties.

To be able to propagate nuclear data uncertainties through MCNP/MCNPX, there in fact exists another “native” nuclear data format of MCNP(X) called ACE. The mixing of continuous/pointwise-energy nuclear data and multigroup uncertainties was already implemented in the SAMPLER code as discussed previously. Such mixing can also be directly applied to ACE-formatted nuclear data to propagate nuclear data uncertainties in the multigroup format, with the advantage that the self-shielding effect is taken into account during neutronics calculations.

1.6.2 Stochastic sampling with MCNPX

The implementation of stochastic sampling is relatively easier than that of the deterministic methods requiring sensitivity coefficients because neutronics codes do not have to be retrofitted. However, an affordably large enough number of perturbed samples is expected in order to satisfy the statistical convergence in sampling methods. This criterion becomes a challenge for Monte Carlo-based codes in certain applications, such as full-core nuclear reactor problems, because of their longer computational time. Even though the intended applications in this PhD work are relatively simpler (e.g. spent fuel assembly, transport casks etc.) a practical sample size is a genuine concern for a stochastic sampling method for MCNPX.

To that aim, GRS and NRG [48],[34] have both proposed methods to lift the burden of computational time for complex models. Their algorithms involve 1) relaxing the statistical convergence criterion for each Monte Carlo calculation by decreasing the number of neutron histories and 2) changing the random seed in each sample of neutronics calculation to separate statistical error due to Monte Carlo codes and the k_{eff} uncertainty contributed by nuclear data. They

have shown that a reduction in computational time can be achieved without compromising uncertainty results.

1.6.3 Sensitivity from stochastic sampling

Stochastic sampling (SS) methods are expeditious for quantifying *total* uncertainties. However, when *individual* uncertainty contribution is desired, SS methods with especially Monte Carlo-based codes become inefficient since each parameter has to be perturbed separately, amounting to many samples to be calculated. In this aspect, the AWP-based methods are advantageous because of the ability to compute sensitivity coefficients of all inputs using only a forward and an adjoint calculations. The total uncertainty is calculated as the sum of individual uncertainties.

Basic sensitivity analyses have been performed [3] through the determination of linear correlation coefficients, such as Pearson or Spearman coefficients. They quantify the strength of association between individual inputs and the output as a way to rank important inputs. This approach is applied in Chapter 3.5 and is shown to be not equivalent to the determination of sensitivity coefficient.

It is hence very desirable to establish a consistent method for the determination of important inputs, based on a set of quantities which can be computed using both sensitivity coefficient-based approach and the stochastic sampling-based implementation. In Chapter 4, the global sensitivity analysis is presented as a mean to rank important inputs in terms of their variance contributions.

Chapter's key message

Nuclear data uncertainty quantification (NDUQ) is an active research field given its practical importance. Analogous to the two types of neutron transport methods - deterministic or stochastic, existing computer tools for NDUQ also fall into either the deterministic propagation of moments (also known as S/U and "Sandwich Rule") or stochastic sampling/Monte Carlo methods. They can be further differentiated by the types of nuclear data with which the tools are compatible. Several of these NDUQ methods will be used to provide verification and validation of the central contribution of this PhD work, that is a global sampling-based tool for continuous-energy MCNPX to propagate and quantify nuclear data uncertainty contributions.

2 Building NUSS-SRS for ACE-formatted nuclear data

The ACE format is one of the native nuclear data formats readable by the continuous-energy transport code MCNPX. In this chapter, the ACE format is first described along with MCNPX. In order to develop a tool to perturb ACE-formatted nuclear data using multigroup nuclear data uncertainties, the procedures to prepare multigroup (MG) nuclear data covariances by NJOY are examined. The two different formats (ACE and MG) are consolidated under certain assumptions for the development of the “NUSS-SRS” (Nuclear data **U**ncertainty **S**tochastic **S**ampling - **S**imple **R**andom **S**ampling) tool in this PhD work. With MATLAB and shell scripts for mathematical operations and data parsing respectively, the steps to generate perturbed ACE files for MCNPX calculations are presented.

2.1 MCNP(X) and ACE-formatted nuclear data

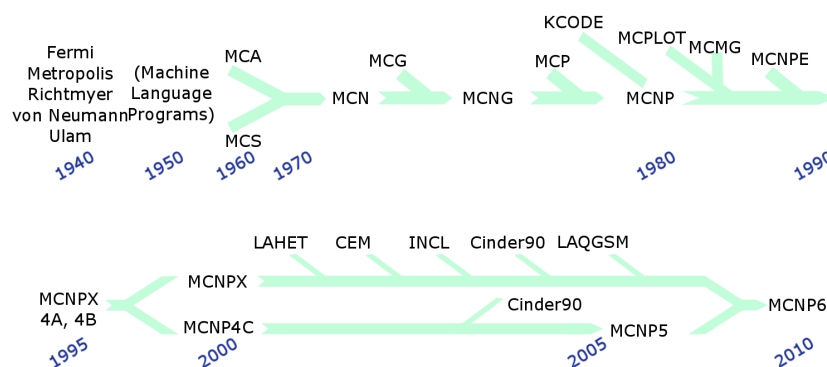


Figure 2.1: Historic development of MCNP and MCNPX (see https://mcnpx.lanl.gov/opendocs/misc/LAUR08_3475.ppt).

The Monte Carlo N-Particle (MCNP) is a general purpose particle transport code for applications of neutron, photon, electron or coupled neutron/photon/electron. It has evolved over six decades as shown in Fig.2.1 and in 1995, the MCNP-eXtended (MCNPX) became available as a result of the ‘MCNP 4B and LAHET’ code-merger project. MCNPX includes all the capabilities

Chapter 2. Building NUSS-SRS for ACE-formatted nuclear data

of MCNP 4C, as well as the capabilities to model many different particles over a broad range of energies. In 2011, the MCNP6 was released as the merger between MCNP5 and MCNPX into a single package after five years of effort by the developers of MCNP and MCNPX. It is said that the last separated versions MCNP5 v 1.6.0 and MCNPX v 2.7.0 are maintained for upcoming years, but no more future releases except to continue the version MCNP6.

For this PhD work, MCNPX v2.7.0 is used to perform calculations for the historical reason that at PSI, MCNPX has been used for both nuclear engineering and high energy physics applications. Nevertheless, the input structure is the same for MCNP or MCNPX. Both can use the ACE-formatted nuclear data for particle transport calculations.

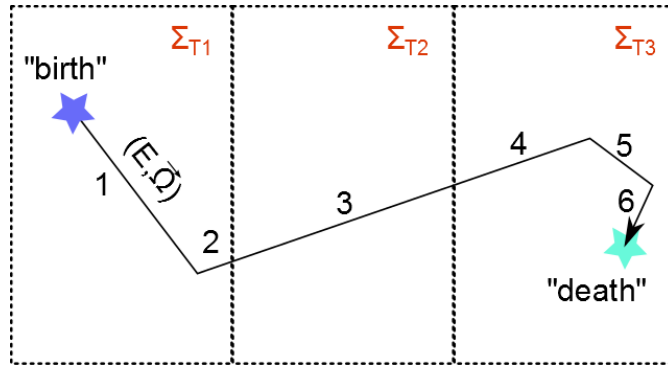


Figure 2.2: Example of a particle traversing through 3 regions with different macroscopic cross sections Σ_T , leaving 6 tracks until its “death” by absorption.

As a Monte Carlo-based code, MCPNX simulates particle transport and interaction in the medium. Illustrated by Fig. 2.2, a particle is generated from a source with energy E and a direction $\vec{\Omega}$. There is a probability ξ of undergoing a collision at the end of the first track which is described by Eqn.(2.1). In Monte Carlo simulation, a random probability is assigned and the distance travelled (L) is calculated.

$$\xi = \int_0^L \Sigma_{T1} e^{-\Sigma_{T1} \cdot x} dx \quad \therefore \quad L = \frac{-\ln(1 - \xi)}{\Sigma_{T1}} \quad (2.1)$$

At the site of collision, the nuclide with which the simulated particle (e.g. neutron) has an interaction is identified. The probability of an absorption of neutron by the target nucleus is $\frac{\sigma_a}{\sigma_T}$ where σ_a is the sum of all (neutron, x) cross sections given the outgoing particle x is anything but a neutron. The probability of a scattering event is $\frac{\sigma_s}{\sigma_T}$, and the outgoing neutron can be generated by an elastic (el) or inelastic (in) collision with probabilities:

$$P_{el} = \frac{\sigma_{el}}{\sigma_{in} + \sigma_{el}} = \frac{\sigma_{el}}{\sigma_T - \sigma_a} \quad \text{and} \quad P_{in} = \frac{\sigma_{in}}{\sigma_{in} + \sigma_{el}} = \frac{\sigma_{in}}{\sigma_T - \sigma_a} \quad (2.2)$$

The thermal motion of the target nucleus is taken into account by either the “free gas thermal” model or $S(\alpha, \beta)$ treatment, both of which make adjustments to the scattering cross section of the target nucleus for low-energy reactions. The use of $S(\alpha, \beta)$ is important for molecular

binding effects such as in water. The energy, direction and energy-direction correlation of the outgoing neutrons (or other types of particles such as photons, protons) are given by the so-called “ENDF laws”. For example, “Law 7” means the “Simple Maxwell Fission Spectrum”:

$$f(E_{\text{in}} \rightarrow E_{\text{out}}) = C \times \sqrt{E_{\text{out}}} e^{-E_{\text{out}}/T(E_{\text{in}})} \quad (2.3)$$

where $T(E_{\text{in}})$ is the nuclear temperature tabulated as a function of incoming neutron energy. In MCNP(X), the outgoing fission neutron energy is sampled by a rejection scheme where random numbers ξ_1 to ξ_4 are drawn from [0,1] and ξ_1, ξ_2 are rejected when $\xi_1^2 + \xi_2^2 > 1$:

$$E_{\text{out}} = -T(E_{\text{in}}) \left(\frac{\xi_1^2 \ln \xi_3}{\xi_1^2 + \xi_2^2} + \ln \xi_4 \right) \quad (2.4)$$

The number of fission neutron as a function of incident neutron energy is an average value $\bar{\nu}(E_{\text{in}})$ and hence for individual fission reaction, the actual number of fission neutron N_p is determined by the following condition:

$$N_p = \begin{cases} I & \text{if } \xi > \bar{\nu}(E_{\text{in}}) - I \\ I + 1 & \text{if } \xi \leq \bar{\nu}(E_{\text{in}}) - I \end{cases}$$

where I is the largest integer less than $\bar{\nu}(E_{\text{in}})$ and ξ is the random number.

The aforementioned steps essentially drive the simulation of the transport of neutrons. A fixed source problem is where a neutron source is given to MCNPX and random walks of neutrons are tallied (i.e. recorded) for information of interest such as fluence, flux, reaction rate, energy deposition etc. On the other hand, a criticality problem is where a population of source neutrons is seeded in the medium of interest and their random walks are tracked until a converged fission source distribution is obtained. At the beginning, all of the seed neutrons will be destroyed by absorption or escape, but some of those that are absorbed can cause fission. Fission neutrons are generated and become the source neutrons for the next cycle until all are destroyed. Many cycles later, the sites of the source neutrons will aggregate at locations where the probability of fission is high and the fission source distribution becomes stable. MCPNX uses three k_{eff} estimators to tally information over the cycles of neutron population:

Collision Estimator

$$k^c = \frac{1}{N} \sum_s W_s \left[\frac{\sum_i \theta_i \cdot \bar{\nu}_i \cdot \sigma_{f_i}}{\sum_i \theta_i \cdot \sigma_{t_i}} \right] \quad (2.5)$$

where N = number of source neutrons for the current cycle

s = summed over all collisions in a cycle where fission is possible

i = summed over all nuclides involved in the i^{th} collision

W_s =weight of particle entering collision s
 (also the number of neutrons entering collisions)
 θ_i =atomic fraction for isotope i
 $\bar{\nu}_i$ =average prompt or total fission neutrons
 σ_{t_i} =total microscopic cross section of isotope i in the material
 σ_{f_i} =microscopic fission cross section of isotope i in the material

Absorption Estimator

$$k^a = \frac{1}{N} \sum_s \left(W_s \frac{\bar{\nu}_i \sigma_{f_i}}{(\sigma_{a_i} + \sigma_{f_i})} \right) \quad (2.6)$$

where N =number of source neutrons for the current cycle
 s =summed over all capture events in the i^{th} isotope
 W_s =weight of particle entering each capture event s
 $\bar{\nu}_i$ =average prompt or total fission neutrons
 σ_{f_i} =microscopic fission cross section of isotope i in the material
 $\sigma_{a_i} + \sigma_{f_i}$ =microscopic capture cross section of isotope i in the material

Track Length Estimator

$$k^{tl} = \frac{1}{N} \sum_l \left(W_l \left(L \rho \sum_i \theta_i \bar{\nu}_i \sigma_{f_i} \right) \right) \quad (2.7)$$

where N =number of source neutrons for the current cycle
 l =summed over all neutron trajectories
 W_l =weight of particle on trajectory l
 ρ =the atomic density in the cell
 L =the trajectory track length from the last event
 i =summed over all collision in a cycle where fission is possible
 θ_i =atomic fraction for isotope i
 $\bar{\nu}_i$ =average prompt or total fission neutrons
 σ_{f_i} =microscopic fission cross section of isotope i in the material

Looking at Fig. 2.2, a “collision estimator”, Eqn.(2.5) would register a score for each fission at collision; an “absorption estimator” (Eqn.2.6) would only register when the neutron is absorbed and fission reaction occurs. However, neither estimator would register a score in region 2 because no interactions occur there along track 3. A “track length estimator” (Eqn.2.7) is more suitable for keeping record of the length of each track. Since each estimator works best only in certain configurations, a combined estimator for k_{eff} is used as the best final estimate of k_{eff} in MCNPX.

The Central Limit Theorem (CLT) is relied upon to estimate the confidence interval of the final estimated mean value of k_{eff} . Let $E[k]$ denote the true population mean of k_{eff} . For each cycle of neutron transport, the mean value of the sample k_{eff} is k_{eff}^n . According to CLT, \bar{k}_{eff} , the mean value of k_{eff}^n which have been sampled independently from the identical distribution (i.e. the distribution of the said population) of finite mean and variance value, would approach a normal distribution for a large sample size N as N approaches infinity. The standard deviation of k_{eff}^n (denoted as $S_{\bar{k}}$) would also approach σ which is the standard deviation of a normal distribution as N approaches infinity. Hence the confidence interval set up by $S_{\bar{k}}$ and \bar{k}_{eff} would approximate the PDF of a normal distribution as and the true population mean of k_{eff} lies within specific confidence intervals:

$$\begin{aligned} \bar{k}_{\text{eff}} - S_{\bar{k}} < E[k] < \bar{k}_{\text{eff}} + S_{\bar{k}} & \sim 68\% \text{ of time} \\ \bar{k}_{\text{eff}} - 2S_{\bar{k}} < E[k] < \bar{k}_{\text{eff}} + 2S_{\bar{k}} & \sim 95\% \text{ of time} \\ \bar{k}_{\text{eff}} - 3S_{\bar{k}} < E[k] < \bar{k}_{\text{eff}} + 3S_{\bar{k}} & \sim 99\% \text{ of time} \end{aligned}$$

In preparing MCNPX calculations, the minimum inputs must describe the geometry, materials, neutron source and of course include nuclear data. The ACE format is one of the eight classes of nuclear data tables readable by MCNPX. The ACE-formatted nuclear data can be type 1 (sequential, ASCII, 80 characters per record) or type 2 (direct-access, binary) interchangeable by an auxiliary processing program MAKXSF. In the MCNPX input file, a DATAPATH can be specified to direct MCNPX to the folder of the intended nuclear data files. MCNPX looks inside DATAPATH for a file named `xmdir` (see Appendix B1 for example) for the isotope identifiers (ZAID) in MCNPX input’s material specification.

Looking inside an ACE-formatted nuclear data, for example hydrogen ^1H in Fig.2.3, one must appreciate the well-structured comprehensiveness of the ACE format. This example file contains a total of 4506 lines of data which can be divided into different parts:

- Header: Material identification (e.g. 1001 .00c) is associated with the particular library (e.g. ENDF7_1) and general information such as atomic weight ratio (e.g. 0.999167) and incident neutron energy (e.g. 2.5301E-08MeV).
- NXS Array and JXS Array: Counters, flags and pointers are given so as to describe the expected length of data points, the number of reactions, and locations of these reactions etc. The explanations for the NXS, JXS values are given in Appendix B2 for Fig. 2.3.

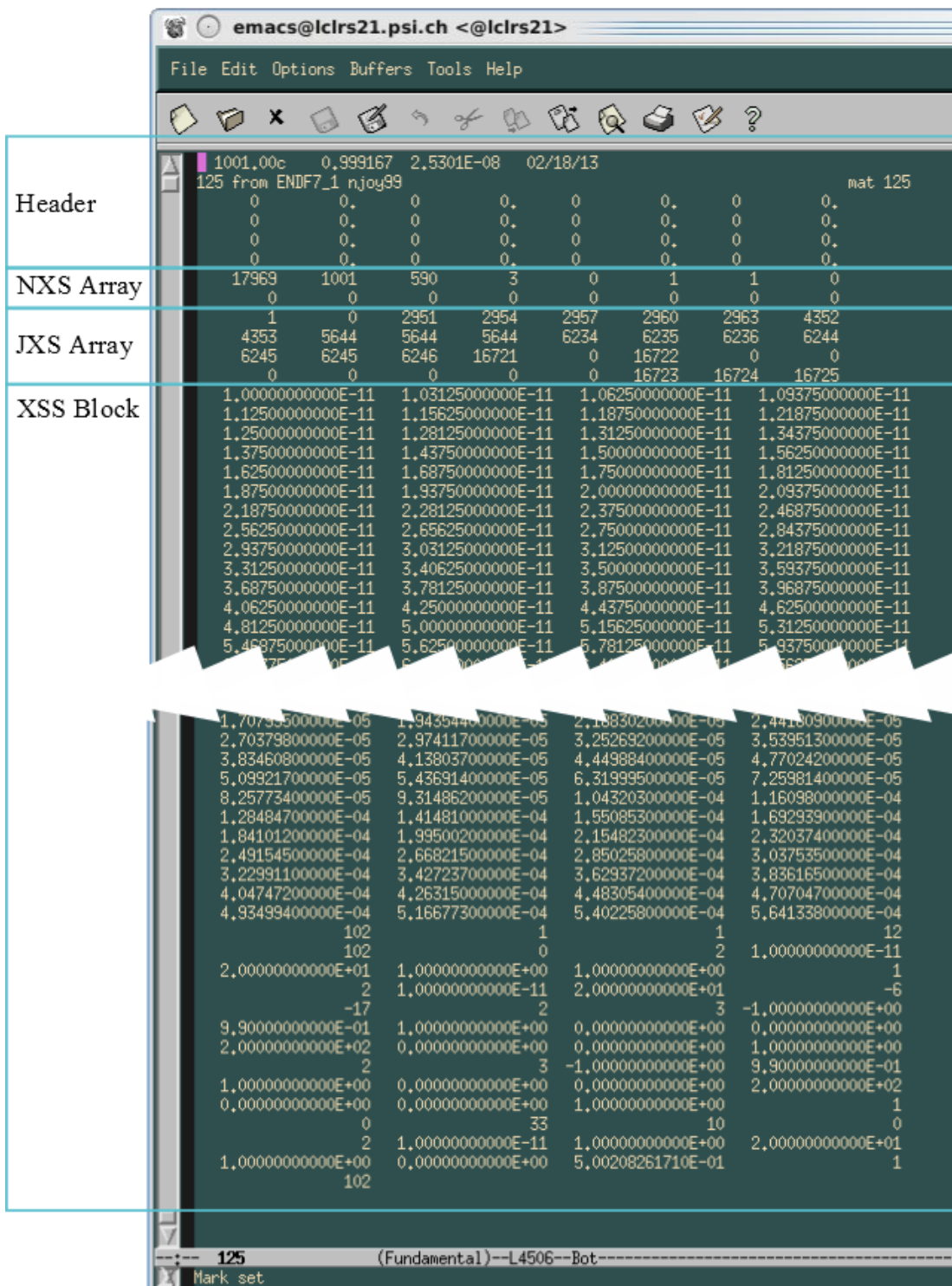


Figure 2.3: Example of ACE-formatted nuclear data file for isotope MAT=125, i.e. ^1H .

- XSS Block: Nuclear data are organized into 21 blocks. It begins with a unionized energy grid (e.g. the first entry is $1.0000000000\text{E}-11$, i.e. 1×10^{-11} MeV), followed by the total

cross section, total absorption cross section, elastic cross sections, all three of which use the same, unionized uniform energy grid. For other reactions, reaction-specific energy grids are specified in terms of pointers to the starting energy location in the uniform energy grid. For example, (n,2n) of ^{235}U data are only available at high energy ($E > 2\text{keV}$) therefore, its energy grid is pointed to the corresponding partial segment of the unionized grid.

2.2 NJOY and the generation of groupwise covariances

The NJOY nuclear data processing system converts ENDF-6 format into other formats for practical nuclear applications. It is also used to generate multigroup nuclear data covariances. As mentioned in Chapter 1.2, multigroup data are essentially weighted pointwise data by the neutron flux. Hence a look at how NJOY produces pointwise (i.e. ACE-formatted) nuclear data is first presented.

In the ENDF-6 formatted file, different interpolations laws (not necessarily linear) and resonance parameters are given to describe the continuous-energy evaluated nuclear data. The RECONR module of NJOY is responsible for creating a unified energy grid, where a linear relation is possible between each energy point with a user-defined error tolerance. The search of the energy grid points is illustrated in Fig. 2.4 where midpoints are added to create the first linearized energy grid for elastic cross section; this grid is then used for the next cross section (e.g. (n,2n)) where more midpoints are added to create a denser energy grid. After going through all partial cross sections, the total cross section in the same pointwise unionized energy grid is obtained as the sum of the partial cross sections.

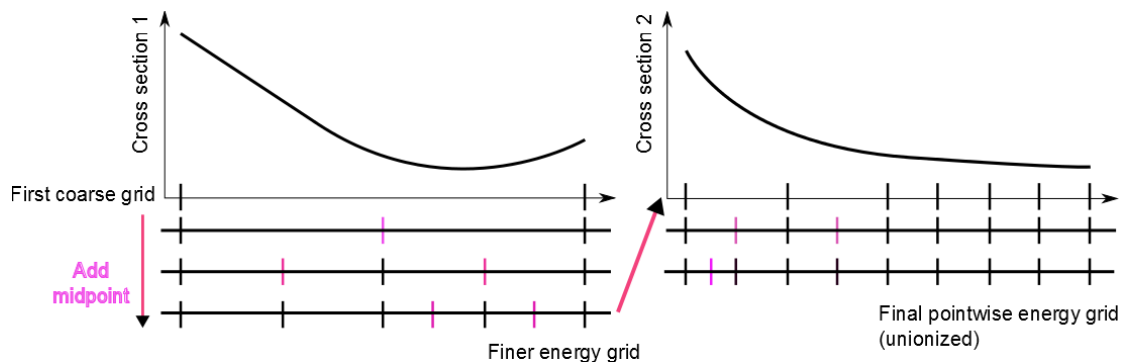


Figure 2.4: Schematic of increasing the number of energy grid points to construct linearly interpolated pointwise data for a unionized energy grid.

The pointwise cross sections from RECONR module are for zero-temperature and then they are Doppler broadened by the BROADR module. The temperature effect is especially important for cross section at the resonance energy range since high-energy fission neutrons have to slow down to thermal energies and the probability of absorption is affected by the many resonances. The BROADR module not only performs cross section adjustment based on the temperature

provided, but it also has to modify the previously unionized energy grid to a new grid which can describe the broadened cross sections. At the energy range of unresolved resonances, resonances are too close to be specified individually; so the ENDF-6 format gives average values on their widths, probability distributions, spacing instead. NJOY's UNRESR module generates the "effective" self-shielded cross sections as a smooth function of energy (without explicit resonance peaks). For MCNPX specifically, the PURR module prepares probability tables in the ACE file. Finally the ACER module generates an output file in the ACE format for the processed nuclear data, as well as updating the corresponding information in the `xsd.ir` file and consistency checks for the ACE format.

Multigroup nuclear data can be prepared by the GROUPT module which uses built-in weighting functions (i.e. typical flux shapes shown in Fig.1.3) to obtain the infinitely-diluted multigroup cross sections. Bondarenko method and "flux calculator" are two options [49] in GROUPT to generate self-shielded multigroup data. Narrow Resonance approximation is assumed for the former method, which simulates suppression to the weight flux shape due to resonances. The latter is used for broad and intermediate-width resonances; it solves the slowing-down integral equation point by point using total and elastic cross sections from RECONR.

Similar to GROUPT, the ERRORR module relies on the same method of weighting function to compute multigroup covariances for infinitely-diluted cross sections. Let $\text{cov}(x(E), y(E'))$ be the covariance of energy-dependent cross sections $x(E)$ and $y(E')$ in ENDF-6 format. Since flux-weighted cross section X_g and $Y_{g'}$ for $x(E)$ and $y(E')$ are:

$$X_g = \frac{\int_g x(E) w(E) dE}{\int_g w(E) dE} \approx \frac{\sum_E w(E) x(E)}{\bar{w}_g} = \sum_E a(E) x(E) \quad (2.8)$$

$$Y_{g'} = \frac{\int_{g'} y(E') w(E') dE'}{\int_{g'} w(E') dE'} \approx \frac{\sum_{E'} w(E') y(E')}{\bar{w}_{g'}} = \sum_{E'} b(E') y(E') \quad (2.9)$$

The covariance of multigroup cross sections becomes

$$\begin{aligned} \text{cov}(X_g, Y_{g'}) &= E \left[\left(\sum_E a(E) x(E) - \sum_E a(E) x_o(E) \right) \left(\sum_{E'} b(E') y(E') - \sum_{E'} b(E') y_o(E') \right) \right] \\ &= \sum_{E, E'} a(E) b(E') E [(x(E) - x_o(E)) (y(E') - y_o(E'))] \\ &= \sum_{E, E'} a(E) b(E') \text{cov}(x(E), y(E')) \end{aligned} \quad (2.10)$$

Table 2.1 shows the content of various types of File "MF" in the ENDF-6 formatted data file. For the resonance parameters stored in "MF2" and "MF32", a new module ERRORJ [50] has been integrated into ERRORR for NJOY 2012. It is invoked to compute resonance covariances when certain advanced options are specified in the provided ENDF-6 data file. Otherwise, the contributions of the resonance uncertainties are automatically added in addition to the

2.2. NJOY and the generation of groupwise covariances

processing of “MF33” multigroup cross section covariances. The angular distribution of secondary particle is given as tabulated distribution or as Legendre polynomial coefficients in “MF4”, while in “MF34” only the covariances for Legendre coefficients are given.¹ The energy distribution of secondary particles is stored in “MF5”. The corresponding covariance matrix in “MF35” has to comply the “zero-sum” constraint, a mathematical property of the covariance matrix of the normalized energy distribution for which the matrix elements have sums (in any row or column) equal to 0.

File	Content	File	Content
MF 1	$\bar{v}_{\text{prompt}}, \bar{v}_{\text{delayed}}$	MF 31	covariance for \bar{v}
MF 2	resonance parameters	MF 32	covariance for resonance parameters
MF 3	reaction cross sections	MF 33	covariance for cross sections
MF 4	angular distributions for emitted particles expressed as normalized probability distributions	MF 34	covariance for angular distributions of emitted particles
MF 5	energy distribution for emitted particles expressed as normalized probability distributions	MF 35	covariance for energy spectra of emitted particles

Table 2.1: Examples of “MF file” in the ENDF-6 format and their intended nuclear data.

During this PhD work, NJOY is primarily used to generate multigroup covariances (see Appendix B3 for an NJOY input example). In the beginning and before the release of ENDF/B-VII.1 evaluated nuclear data library, the SCALE6-44group covariance library [51] was applied extensively due to the lack of alternatives. The energy group structure consists of 22 fast and 22 thermal energy groups. Fig.2.5 shows that SCALE6-44g is designed to accommodate certain isotopes’ resonances. The flux weighting function used is based on a 17×17 Westinghouse PWR assembly (M4.2.2 from [52]). When another user-defined group structure is desired, the ANGELO2.3 auxiliary code could be used by applying a flat flux weighting function onto the SCALE6-44g covariance data. Speed is traded with lower accuracy in such a simple interpolation scheme especially when the new group structure is very different from the original. Using NJOY to generate covariance matrix in user-defined group structure becomes practical when the ENDF/B-VII.1 evaluated nuclear data library was released. It includes covariance data for 190 materials (versus 26 materials in ENDF/B-VII.0, 37 materials in JEFF-3.1 and 401 materials in SCALE6-44g). In Chapter 3.2, ENDF/B-VII.1 evaluated nuclear data covariances are processed flexibly into various group structures such as the SCALE6-44g, or 30-, 80-group, using appropriate weighting functions.

¹ACE format uses 32 equiprobable cosine bins for scattering.

Chapter 2. Building NUSS-SRS for ACE-formatted nuclear data

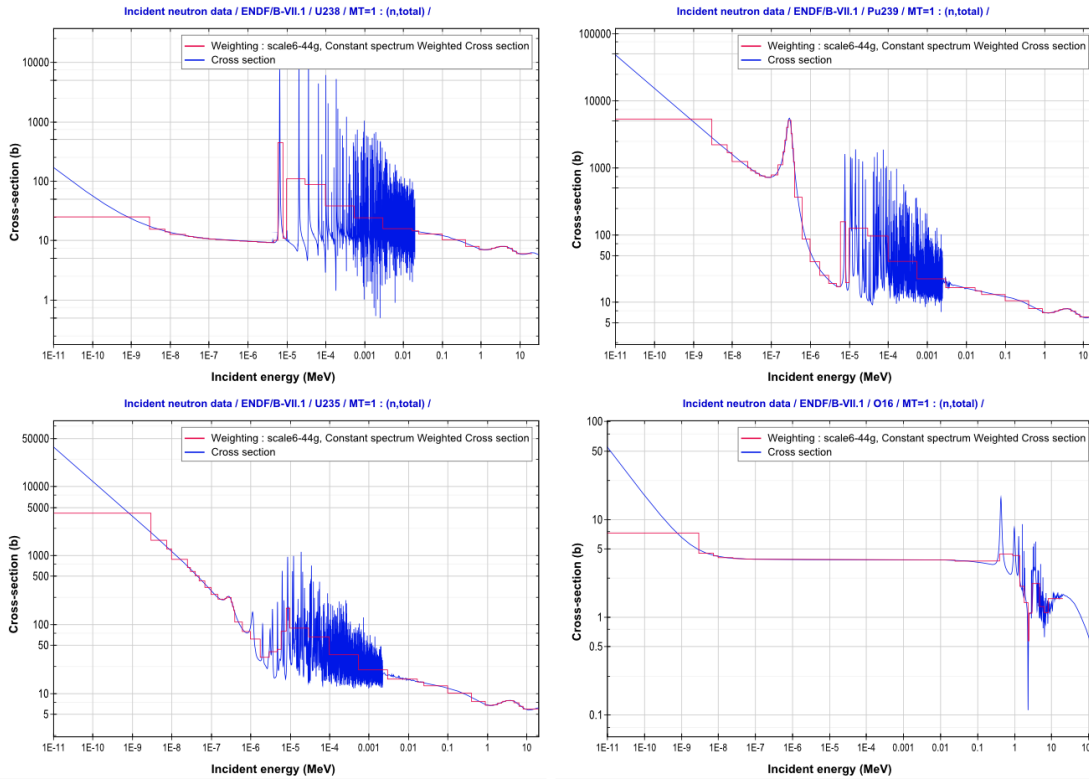


Figure 2.5: Energy bounds of the SCALE6-44g covariance group structure are selected to accommodate features of various nuclide cross sections. Flat weighting function is used when the plots are produced in the JANIS plotting program.

2.3 NUSS-SRS implementation

NUSS-SRS consists of MATLAB programs and unix shell scripts. The former provides mathematical calculations and the latter is for file manipulation. Shown in Fig. 2.6 NUSS-SRS has five stages of operation. The processing of multigroup covariance matrices by NJOY is stage 1. Stages 2 to 5 of NUSS-SRS are presented with the focus on the organization and workflow of computer programs written to complete the sampling and modification of ACE files. But first and foremost, the core assumptions in relation to the nuclear data properties for the development of the NUSS-SRS tool are laid down here.

2.3.1 Assumption and limitation

Within-group correlation

It is assumed that, pointwise nuclear data within each energy group is fully correlated. Eqn.(2.11) illustrates this assumption that a scalar factor (p) can be applied to the point-

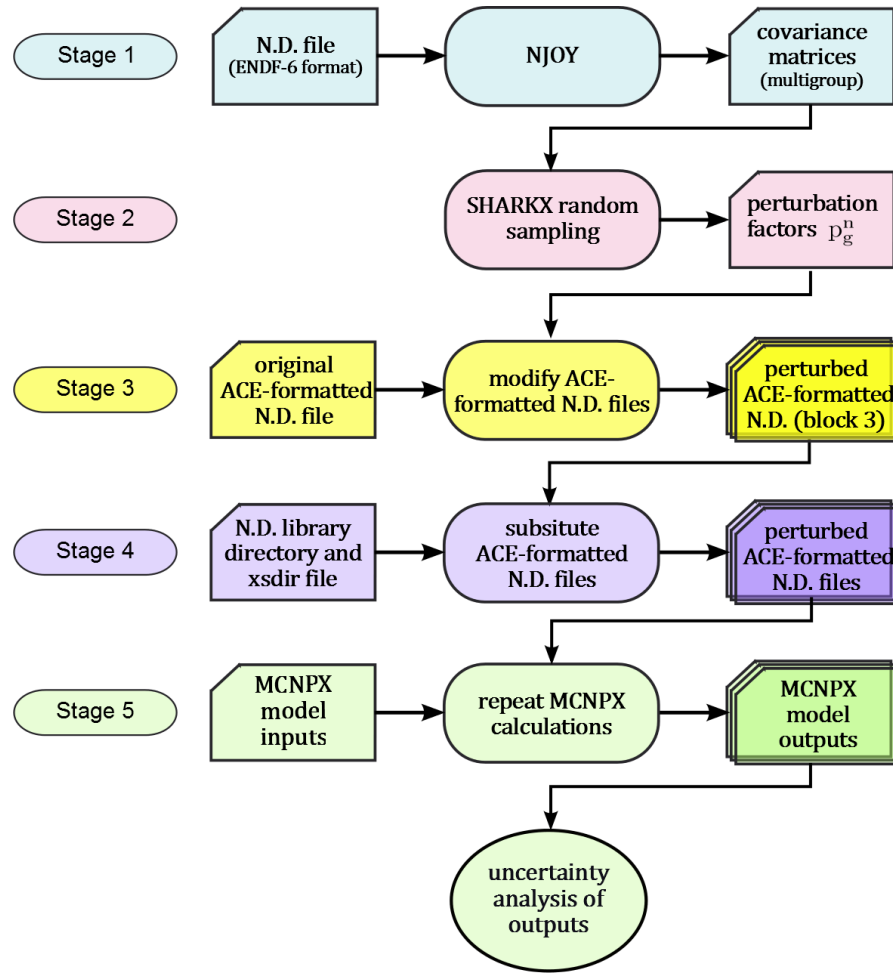


Figure 2.6: Workflow of NUSS is divided into five stages.

wise nuclear data:

$$\tilde{\alpha}'_g = p\tilde{\alpha}_g = p \cdot (\alpha_{g_1}, \alpha_{g_2}, \alpha_{g_3}, \dots, \alpha_{g_m}) = (p\alpha_{g_1}, p\alpha_{g_2}, p\alpha_{g_3}, \dots, p\alpha_{g_m}) \quad (2.11)$$

The advantage of ACE-formatted pointwise nuclear data comes from working with the unionized energy grid by which cross sections between energy points can be linearly interpolated. Depicted in Fig.2.7, the cross sections through random sampling will on average lie within the respective $\pm 1\sigma$ (68%) of the time. The cross sections between E_a and E_b will be interpolated by MCNPX during execution and will also lie within the marked range of values which are determined by the adjacent perturbed cross section values because of the linearly-interpolated relation required by the ACE format.

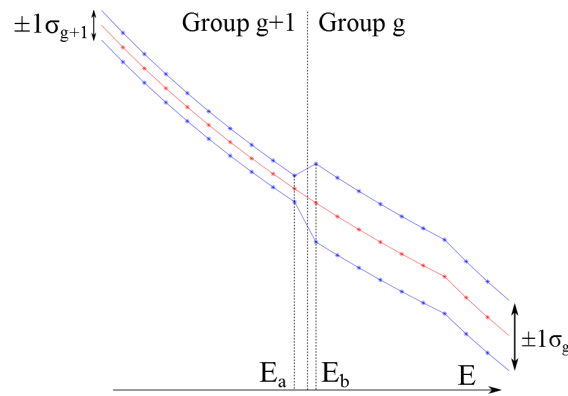


Figure 2.7: Pointwise ACE nuclear data across the boundary of the multigroup energy structure have a smooth transition and their uncertainties are still bounded.

Probability distribution function of nuclear data

Nuclear data are assumed to have multivariate normal distribution. The normality assumption can be traced back to the time-of-flight experiments in Chapter 1.2 for basic nuclear data measurements. The raw data counts have Poisson distribution; but at high count rates, Poisson distribution is approximately normal [7]. The normality assumption of the inputs which are fitted by least-squares, leads to the property that, the linear least-squares estimator is also the maximum likelihood estimator. Hence the evaluated nuclear data from least-squares fitting can be considered the “best” estimates for nuclear data [7].

A consequence of the normal distribution assumption is the possibility of negative-valued nuclear data samples in case of a large uncertainty for a small-valued cross section. The fix for such physical violation is to impose a zero-cutoff for negative cross sections. This practice inevitably biases the mean value of the sampled cross sections (see Chapter 3.3). In this work, the multivariate-normal assumption is applied while acknowledging the implications mentioned above. For future works, log-normal distribution could be applied instead of normal distribution which has been done by Žerovnik[53] for the resonance parameter.

2.3.2 MATLAB programs for modifying nuclear data

The organization of the NUSS system is shown in Fig.2.8. The “Scripts” folder contains the MATLAB-scripted programs to perform the tasks of Stage 2 and 3 of Fig.2.6. The “Nuclear data” and “Group structure” are static folders. The former provides the original ACE-formatted nuclear data files and multigroup covariances, which have been prepared by NJOY preparation in Stage 1 of Fig.2.6. The energy group structures with their energy boundary values are stored in “Group Structure” folder as text files; they correspond to the group structure of the covariance libraries and are used to partition the pointwise ACE formatted nuclear data. The dynamic folders are “Workdir” and “Make_Pert_Factors” which are created by the shell script “setfolder.sh”. The “Template” folder contains holders of information which are to be copied

into the “Workdir” and “Make_Pert_Factors” and modified according to individual problems. They establish the initial parameters for the MATLAB-scripted “NUSS_p.m” program for the new set of perturbed ACE libraries to be generated.

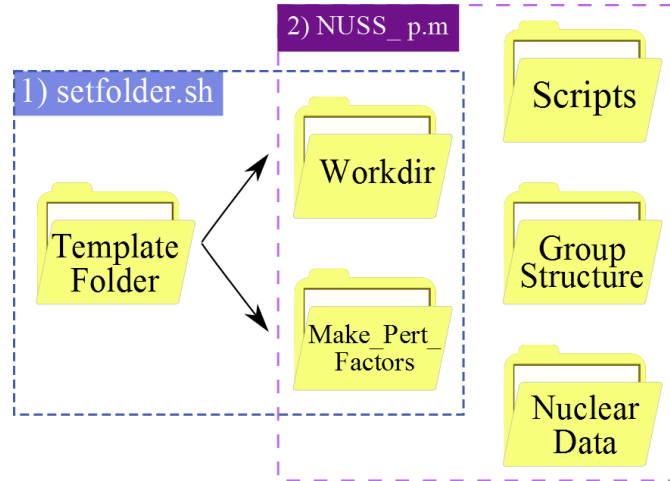


Figure 2.8: The “setfolder.sh” script sets up the problem-specific “Workdir” and “Make_Pert_Factors” folders. The “Nuclear data” and “Group structure” and “Scripts” folders are static and used by “NUSS_p.m” program.

The program flow of “NUSS_p.m” is shown in Fig.2.9. Its first part (i.e. “If sharkx_flag is equal to 1”) is responsible for sampling the multigroup covariances² and generating the perturbation factors \mathbf{P} to be used in the second part (i.e. “if pert_flag is equal to 1”).

The mathematical procedure to obtain the perturbation factors from multigroup covariance data is based on the assumption of multivariate normal distributions for nuclear data. Keeping all quantities relative, the built-in MATLAB function to obtain the *relative* random samples is simply:

$$\mathbf{P} = \text{mvnrnd}(\text{ones}(N, K), \mathbf{M}, N)$$

in which the function $\text{ones}(N, K)$ generates an $N \times K$ matrix filled with ones for N number of random samples and K number of inputs. Inside mvnrnd , the *relative* covariance matrix \mathbf{M} of size $K \times K$ is decomposed into two matrices:

$$\mathbf{M} = \mathbf{L} \cdot \mathbf{U} \quad \text{where } \mathbf{U} = \mathbf{L}^T \text{ and both are of size } K \times K \quad (2.12)$$

Depending on the property of the covariance matrix, being positive definite or positive semidefinite or neither, the decomposition is achieved by either Cholesky or eigen-decomposition algorithms, or an ad hoc fix of the covariance matrix is required. Details are presented in Appendix A4.

²SHARKX.m is part of the PSI’s CASMO-5MX Nuclear Data Uncertainty Quantification (NDUQ) toolset [54] and has been adopted to perform the sampling of multigroup nuclear data covariances.

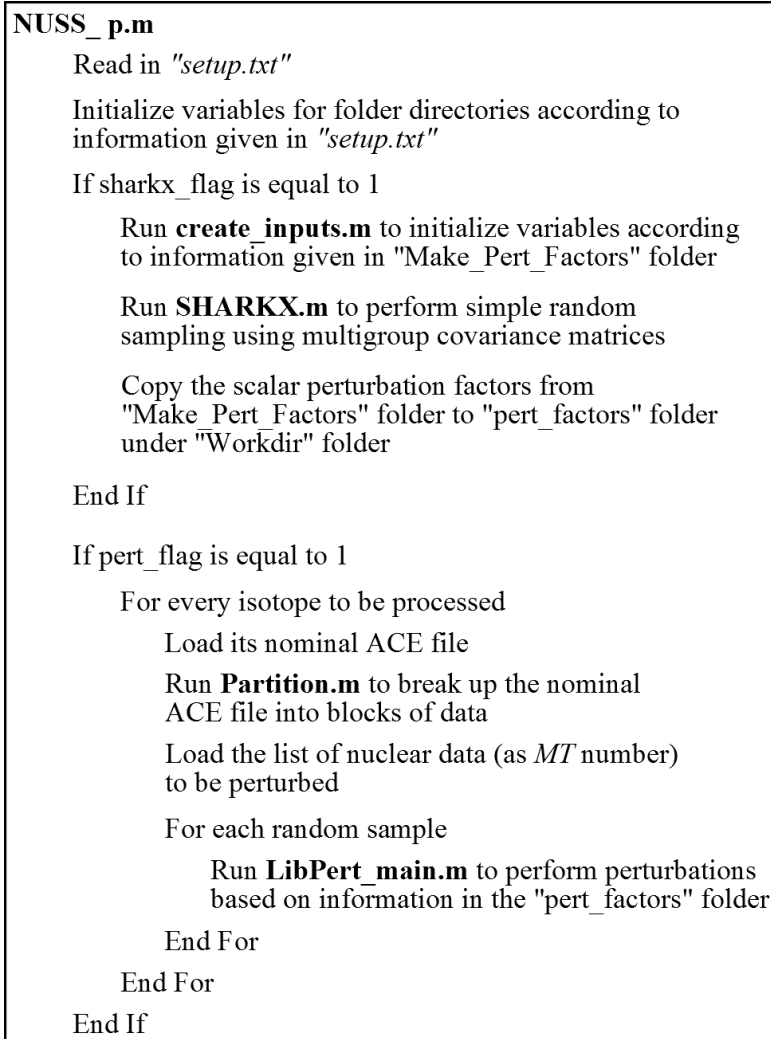


Figure 2.9: Program flow of “NUSS_p.m”.

Matrix \mathbf{V} of size $[N \times K]$ is generated, whose columns are independent sample sets of random numbers drawn from the standard normal distribution. Mathematically the `mvrnd` output \mathbf{P} is obtained as:

$$\mathbf{P} = \mathbf{V} \cdot \mathbf{U} + \mathbf{1} \quad (2.13)$$

where matrix $\mathbf{1}$ is generated by function `ones(N,K)` and the relative random samples in matrix \mathbf{P} are by definition the perturbation factors:

$$p = \frac{\alpha'}{\alpha_o} \quad (2.14)$$

The perturbed nuclear data $\alpha' = \alpha_o \times p$ are multivariate-normally distributed according to the given variance covariance matrix. The proof for the above algorithm is given in Appendix A5.

Next, the perturbation of the ACE-formatted nuclear data is initiated by **Partition.m** which literally partitions the XSS Block of the ACE file (see previously in Fig.2.3) into individual blocks. Fig.2.10 is an example log file (for ^{235}U) generated by **Partition.m**. The four-column XSS Block is first reshaped into a one-column vector called “data” and then divided into respective sections. Block indices are labelled in the first column (block_ind). The unionized energy grid is given in the first section of the XSS data and shall be referred to as the “energy” vector. The second and third columns (data[i] and data[f]) refer to the initial and final locations of the individual nuclear data (explained in the explanation column). For each nuclear data (labelled by “MT” numbers), the starting location of its energy grid is also recorded (see energy [...] column).

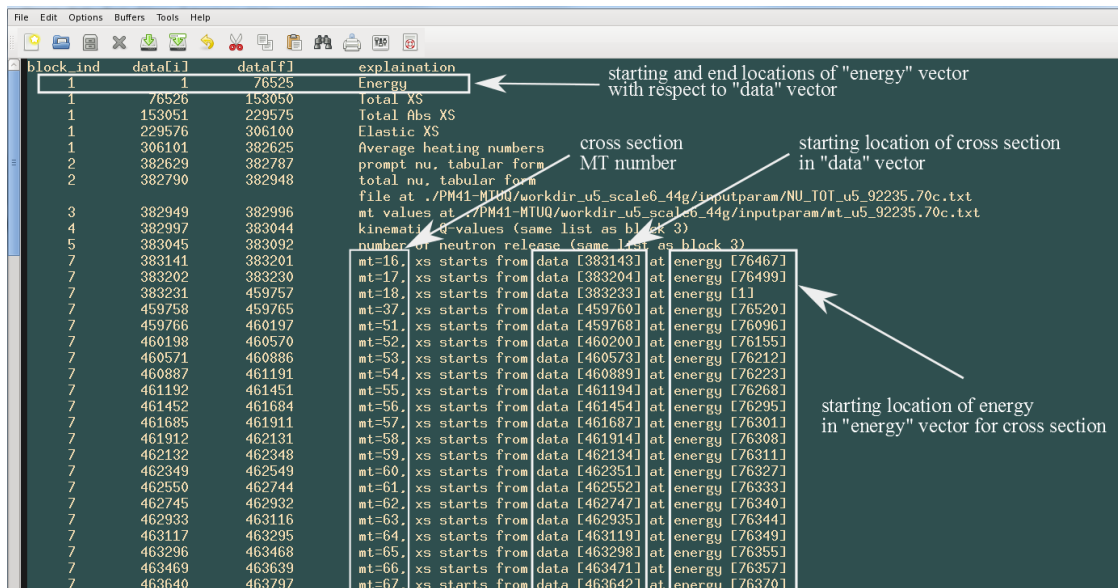


Figure 2.10: MATLAB program “Partition.m” reads the ACE file and generates a log file to provide clear explanation of the partition.

After partitioning the ACE file, the **LibPert_main.m** program is run to perform perturbations on the pointwise data (see Fig.2.11). Because we have partitioned the nuclear data vector, it is easy to locate each cross section and its pointwise energy grid structure. The pointwise energy grid and cross sections are one-to-one; therefore the pointwise data can be divided into the same number of groups as the multigroup energy structure. For each segment, a scalar perturbation factor p is applied:

$$\vec{\alpha}'_g = p \vec{\alpha}_g = p \cdot (\alpha_{g_1}, \alpha_{g_2}, \alpha_{g_3}, \dots, \alpha_{g_m}) = (p\alpha_{g_1}, p\alpha_{g_2}, p\alpha_{g_3}, \dots, p\alpha_{g_m}) \quad (2.15)$$

where $\vec{\alpha}_g$ represents the segment of the pointwise data points α_{g_i} bounded by energy group g between E_{g_1} and E_{g_m} . The single perturbation factor p is applied uniformly to the pointwise data points.

After the perturbation of specific pointwise data, the consistency within the ACE file must

```

LibPert_main.m
  perturb.m
    For each requested MT number
      If MT  $\neq$  2, 1018, 452, 455 or 456
        Get the list of available cross section in ACE file
        If requested MT is 4 (for (n,n'))
          Expand the requested MT list to include MT =50 ~91
          if they exist in the cross section list in ACE file
          For each MT in the updated requested MT list
            new_data is generated by pert_xs.m
          End For
        Else
          new_data is generated by pert_xs.m
        End If
      Else If requested MT = 2 (for elastic scattering)
        new_data is generated by pert_escatt.m
      Else If requested MT = 452 (for average fission yield)
        new_data is generated by pert_nu.m
      Else If requested MT=1018 (for fission spectrum)
        new_data is generated by pert_chi.m
      End If
    End perturb.m
    save "new_data" in the 4-column XSS Block format in text files
  End LibPert_main.m

```

Figure 2.11: MATLAB program “LibPert_main.m” performs perturbation on the ACE-formatted cross sections. Depending on the type of reaction, different perturbation programs are applied to match the implicit sum rule in ACE files.

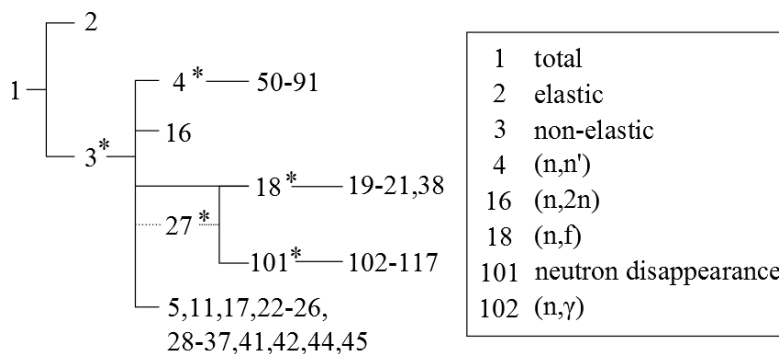


Figure 2.12: ENDF-6 format sum rule for cross sections. MT 3,4,18,27,101 are redundant if one or more of the constituting MTs are present.

be retained because the “sum-rule” defined by the ENDF-6 format is also inherited by the

ACE format. Fig.2.12 shows the relationship among the cross sections labelled by their MT numbers. For example, when MT=102 is perturbed, cross sections of MT=101, 27, 3 and 1 are all required to be updated if they exist in the ACE file.

For regular cross section perturbation, the total cross section The difference between the pointwise perturbed cross section and original cross section is calculated and added to other relevant cross sections (denoted as α_{sum}) as guided by the sum rule:

$$\Delta \vec{\alpha}'_g = \vec{\alpha}'_g - \vec{\alpha}_g = (\Delta \alpha_{g_1}, \dots, \Delta \alpha_{g_m})$$

$$\vec{\alpha}'_{\text{sum},g} = \vec{\alpha}_{\text{sum},g} + \Delta \vec{\alpha}'_g = (\alpha_{\text{sum},g_1} + \Delta \alpha_{g_1}, \dots, \alpha_{\text{sum},g_m} + \Delta \alpha_{g_m})$$

The sum rule of Fig.2.12 does not apply to the average total fission neutron yield ($\bar{\nu}$, MT=452) or fission spectrum (χ , MT=1018). The $\bar{\nu}$ data in a tabular form³ are modified by multiplying with the perturbation factors. Current version of NUSS-SRS perturbs only $\bar{\nu}$, without updating the prompt and delayed fission neutron yield sections in the ACE file. This does not affect criticality calculation in MCNPX because only the average total fission neutron yield ($\bar{\nu}$) data are used.

For fission spectrum χ in ACE format, the so-called “continuous tabular distribution” (Law 4) is used which includes 1) outgoing particle energy grid, 2) the probability density (PDF) and 3) cumulative density functions (CDF). Because the exact numerical precision used to compute the original CDF from PDF is unclear for a given ACE file, the following steps are taken which do not involve numerical integration. Instead the new CDF is computed by adding the amount of perturbation on top of the original CDF:

- Original data in ACE file:

$$\text{PDF}_g = \vec{f}_g = [f_{g_1}, \dots, f_{g_m}]$$

$$\text{CDF}_g = \vec{c}_g = [c_{g_1}, \dots, c_{g_m}]$$

- After perturbation:

$$\text{PDF}'_g = \vec{f}'_g = [f'_{g_1}, \dots, f'_{g_m}]$$

$$\Delta \vec{f} = \vec{f}'_g - \vec{f}_g = [\Delta f_{g_1}, \Delta f_{g_2}, \dots, \Delta f_{g_m}]$$

- Obtain incremental increase in each energy group (ΔE):

$$\Delta \text{CDF}_g = [\Delta f_{g_1} \Delta E_{g_1}, \Delta f_{g_2} \Delta E_{g_2}, \dots, \Delta f_{g_m} \Delta E_{g_m}] = [\Delta c_{g_1}, \dots, \Delta c_{g_m}]$$

³Polynomial function form is also probable but has not been encountered.

- Compute the cumulative increase of CDF in each energy group:

$$\begin{aligned}\Delta\text{CCDF}_g &= \left[\Delta c_{g_1}, (\Delta c_{g_1} + \Delta c_{g_2}), (\Delta c_{g_1} + \Delta c_{g_2} + \Delta c_{g_3}), \dots, \sum_{i=1}^m \Delta c_{g_i} \right] \\ &= [cc_{g_1}, cc_{g_2}, \dots, cc_{g_m}]\end{aligned}$$

- Finally the new CDF and PDF are calculated and normalized:

$$\begin{aligned}\text{CDF}'_g &= (\text{CDF}_g + \Delta\text{CCDF}_g) / \text{normalization} \\ &= [c_{g_1} + cc_{g_1}, c_{g_2} + cc_{g_2}, \dots, c_{g_m} + cc_{g_m}] / (c_{g_m} + cc_{g_m}) \\ \text{PDF}'_g &= [f'_{g_1}, \dots, f'_{g_m}] / (c_{g_m} + cc_{g_m})\end{aligned}$$

As shown in this section, the modifications of the ACE-formatted data are relatively straightforward. However due to the more limited availability of covariance data than ACE data, the following procedures are implemented:

- In the case of total inelastic reaction MT=4, its covariance is given instead of individual covariances for the discrete level excitation cross sections from MT=50 to MT=91. Hence, when modifying MT=4 cross section, the **perturb.m** program checks if MT=50~91 exist in ACE file. It is implemented such that the perturbation factors obtained from MT=4 covariance data are applied to all available MT=50~91 cross sections. It is feasible because the incident energy grid points used for MT=4 covers all sets of MT=50 to 91.
- χ tabulated data in ACE-format are given in terms of incoming neutron energies. However there is very limited covariance data for χ which are supposed to cover an energy range from 0.1eV to 500keV. Hence the current implementation of NUSS-SRS is such that, only one χ covariance data is processed by NJOY (usually there is indeed only one given χ data). It is used to modify all the ACE-formatted χ data regardless of the incoming neutron energies.

2.3.3 Link to MCNPX on MERLIN

MCNPX is installed on PSI's high performance computing cluster (MERLIN) where the nominal ACE-formatted nuclear data libraries are also located. The perturbed ACE nuclear data files are not stored on merlin but remain on PSI's AFS (the "Andrew File System" distributed file system) due to the large amount of nuclear data in terms of memory usage and the lack of backup capability on MERLIN. Access and retrieval of perturbed ACE files from AFS folders such as "Nuclear Data" and "Workdir" are accomplished by shell scripts on MERLIN as part of the NUSS-SRS tool. A problem-dependent ACE nuclear data library is set up on MERLIN which feeds each sample set of the perturbed ACE files to MCNPX calculations. Fig.2.13 summarizes

the substitution of the ACE files in the dynamic library on merlin by the prepared samples of perturbed ACE files on AFS.

```

runNUSS.sh
initialize variables for AFS "Workdir", NUSS output directories etc.
check if the requested ACE files (to be replaced) exist
reset each ACE file by copying from the original source

For each set (ie. sample) of the ACE files to be perturbed
    run create_pert_lib.sh to substitute the nominal ACE files with
    the perturbed ACE files from AFS
    submit MCNPX job on merlin in parallel-computing setting
    check If MCNPX calculation is finished successfully
End For
End runNUSS.sh

```

```

create_pert_lib.sh
look inside the current sample in the "Workdir" on AFS to get
the list of ACE file names to be substituted and their ZAID written
in the xsdir file
For each file name (ie. isotope)
    make the substitution on merlin by subs_pert_data.sh
End For
End create_pert_lib.sh

```

Figure 2.13: On merlin, a dynamic library consists of ACE files which are to be substituted by the perturbed ACE files from AFS "Workdir" folder. After each substitution, an MCNPX calculation is launched on merlin and has to finish successfully before the next substitution.

2.3.4 Output analysis methods

The final stage of NUSS involves the extraction of MCNPX output of interest (such as k_{eff} , reaction rate) from MCNPX output files by shell scripts, followed by the statistical analysis in MATLAB. Each MCNPX calculation is performed with one (for single isotope-reaction) or a set of uniquely perturbed ACE files (for multiple isotope-reactions). After N samples, a distribution of k_{eff} values is obtained and the mean and variance of the sample are:

$$\bar{k} = \frac{1}{N} \sum_{n=1}^N k_n \quad \text{and} \quad V_k = \frac{1}{N-1} \sum_{n=1}^N (k_n - \bar{k})^2 \quad (2.16)$$

The spread of k_n values, in terms of V_k is caused by both the statistical uncertainty of MCNPX-calculated k_n , as well as the nuclear data uncertainties:

$$V_k = V_{\text{ND}} + V_{\text{MC}} \quad (2.17)$$

Chapter 2. Building NUSS-SRS for ACE-formatted nuclear data

The contribution of Monte Carlo statistical uncertainty V_{MC} is estimated to be [34]:

$$V_{MC} \approx \frac{1}{N} \sum_{n=1}^N s_n \quad (2.18)$$

where s_n is the MCNPX-calculated k_n 's (statistical) variance for sample n . The nuclear data uncertainty contribution is therefore:

$$V_{ND} = V_k - V_{MC} = \frac{1}{N-1} \sum_{n=1}^N (k_n - \bar{k})^2 - \frac{1}{N} \sum_{n=1}^N s_n \quad (2.19)$$

Now suppose all s_n values are similar, the ratio between $\sqrt{V_{MC}}$ and $\sqrt{V_k}$ says:

$$\sqrt{\frac{1}{N} \sum_{n=1}^N s_n / \sqrt{V_k}} \approx \sqrt{s_n} / \sqrt{V_k} \quad (2.20)$$

For example, to restrict the contribution from statistical uncertainty so that most of the V_k captures nuclear data uncertainty and only 1% of the $\sqrt{V_k}$ comes from the overall statistical error V_{MC} , the individual sample k_n statistical error should be restricted to 1 pcm for a $\sqrt{V_k}$ of 100 pcm, which is computationally challenging.

In theory, as N increases, V_{ND} converges to nuclear data uncertainty contribution in k_{eff} . Restricted by the feasibility of running many MCNPX calculations, a confidence interval is useful for knowing the reliability of the estimated nuclear data uncertainty contributions. It is assumed that the underlying k_{eff} population is normally distributed with a true variance (σ^2) contributed by nuclear data uncertainty and statistical uncertainty. This is based on the observation that, linearity holds for k_{eff} as a function of nuclear data when perturbations are small⁴. As nuclear data samples are prepared from simple random sampling (specifically, independent and identically distributed) of multivariate normal distributions, it can be shown that the random variable W has χ^2 distribution:

$$W = \frac{\sum_{n=1}^N (k_n - \bar{k})^2}{\sigma^2} = \frac{(N-1)V_k}{\sigma^2} \sim \chi_{N-1}^2 \quad (2.21)$$

where χ_{N-1}^2 is the χ^2 distribution with $N-1$ degree of freedom, and $k_n = \{k_1, \dots, k_N\}$ of the smaller set of samples and \bar{k} the sample mean. For a desired probability level of $(1-\alpha)$ for W , critical values $\chi_{\alpha/2, N-1}^2$ and $\chi_{1-\alpha/2, N-1}^2$ of the χ^2 distribution can be looked up for a given degree of freedom $N-1$ from the tabulated probability table of χ^2 :

$$\text{Prob} \left(\chi_{\alpha/2, N-1}^2 \leq W \leq \chi_{1-\alpha/2, N-1}^2 \right) = (1-\alpha) \cdot 100\% \quad (2.22)$$

⁴If k_{eff} is not sensitive to a cross section, the k_{eff} sample variance is still dominated by statistical uncertainty. If nuclear data uncertainty is so large that negative nuclear data samples are generated, they are replaced by zero values as shown in Fig.3.12 in Chapter 3.3. This can alter the k_{eff} sample mean and variance estimation. Linearity might not be observed in this case. In case of non-normal population distributions, formulas for the variance of sample variance are shown in [55].

After rearranging W and σ^2 , the confidence interval shown below would contain the true σ^2 of k_{eff} for $(1-\alpha)\cdot 100\%$ of the time, if the sampling procedures would be repeated to obtain a set of V_k values (i.e. by sampling of nuclear data and calculation of k_{eff}):

$$\left[\sigma_{\text{lower}}^2, \sigma_{\text{upper}}^2 \right] = \left[\frac{(N-1)V_k}{\chi_{1-\alpha/2, N-1}^2}, \frac{(N-1)V_k}{\chi_{\alpha/2, N-1}^2} \right] \quad (2.23)$$

As a result, the $(1-\alpha)\cdot 100\%$ confidence interval for σ is $[\sigma_{\text{lower}}, \sigma_{\text{upper}}]$.

Chapter's key message

The implementation of NUSS-SRS is essentially simple thanks to the transparent ACE format, but not easy because of the large amount of data (often on the order of megabyte per nuclide) to be parsed and modified. The NUSS-SRS tool eliminates the manual process of ACE file modification which can be extremely error-prone given the amount of ASCII texts and the number of perturbed ACE files to be manipulated. The performance of NUSS-SRS is going to be verified in the next chapter when it is compared to existing methods for nuclear data uncertainty quantification.

3 Evaluating NUSS-SRS against existing methods and its applications

The Nuclear data Uncertainty Stochastic Sampling (NUSS) tool with the simple random sampling (SRS) method is verified in three ways. First, the implementation of NUSS-SRS is tested in a direct perturbation manner by using pre-defined perturbation factors. The results are compared with those generated by MCNPX's PERT CARD module in terms of the sensitivity coefficients of k_{eff} to nuclear data. Next, simple random sampling is applied and k_{eff} uncertainty due to nuclear data uncertainties is compared with that calculated by the "Sandwich Rule". Sensitivity coefficients are provided by TSUNAMI and whenever available, PERT CARD. The third comparison is done between NUSS-SRS and the Total Monte Carlo (TMC) methodology to assess the propagation of nuclear data uncertainties at the levels of ACE-format or basic nuclear data.

Upon verifying NUSS-SRS, the effect of multigroup structures of the covariances on the propagated nuclear data uncertainties is examined. It is to assess whether the commonly used SCALE6 44-group structure is adequate or excessive. Similarly, the existing practice of computing Pearson and Spearman correlation coefficient as sensitivity indicator is questioned. Instead, the squared value of the corresponding correlation coefficient is used to estimate the associated input variances in the total output variance.

Finally, two applications of NUSS-SRS are presented and discussed. They are the UAM pincell and criticality safety assessment benchmarks in consideration of nuclear data uncertainties.

3.1 NUSS Direct perturbation versus MCNPX PERT CARD

Direct perturbation means varying inputs one-at-a-time and the difference between the perturbed output and the reference can easily be associated to the output's sensitivity to this single input's variation. In Chapter 1.4, Eqn.(1.15) gives the absolute sensitivity coefficient. Here the relative sensitivity coefficient from direct perturbation (DP) is also given:

$$S^{DP} = \frac{(R(\alpha') - R(\alpha_o)) / R(\alpha_o)}{(\alpha' - \alpha_o) / \alpha_o} \quad (3.1)$$

Chapter 3. Evaluating NUSS-SRS against existing methods and its applications

where the relative input variation can be written in terms of the perturbation factor p of Eqn(2.11):

$$\frac{\alpha' - \alpha_o}{\alpha_o} = \frac{p\alpha_o - \alpha_o}{\alpha_o} = p - 1 = \Delta p \quad (3.2)$$

The relative input variation Δp represents how far away the perturbed value is from the reference. Here we let it be calculated as the multiple (γ) of the relative standard deviation of the input (multigroup nuclear data):

$$\Delta p_g = \gamma \cdot \sigma_{rel,g} \quad \text{for } g = 1, \dots, G \text{ groups} \quad (3.3)$$

To verify the sensitivity coefficients calculated by NUSS direct perturbation, PERT CARD module of MCNPX is applied. Its differential operator sampling (DOS) method [18] computes the small change in particle track lengths due to a perturbed input parameter θ . In criticality problems, fission source distribution for each cycle is given by the location of fissions at the end of previous cycle. When the source fission source distribution is converged, k_{eff} can be calculated as the neutron production from fission per source particle (N) [56]:

$$k = \frac{1}{N} \int_V dV \int_E dE \chi(E) \int_{E'} dE' v(E') (N\sigma_f(E')) \Phi(r, E') \quad (3.4)$$

where the value of $\Phi(r, E)$ can be obtained from the track-length tally in MCNPX. When perturbations in inputs such as cross sections are introduced to the system, there is no guarantee that the source distribution remains the same. However, in PERT CARD, the unperturbed source distribution is still used to for the calculation of perturbed k_{eff} , in effect approximating the perturbed flux as the actual flux resulted from a perturbed source distribution. By Taylor expansion up to the second order without cross terms:

$$\Delta k \approx \frac{\partial k}{\partial \theta} \Delta \theta + \frac{1}{2!} \frac{\partial^2 k}{\partial \theta^2} (\Delta \theta)^2 \quad (3.5)$$

the derivatives $\frac{\partial k}{\partial \theta}$ and $\frac{\partial^2 k}{\partial \theta^2}$ are calculated concurrent to the normal transport calculation during the active cycles where the change in track lengths Φ are tallied (further details in Appendix A2). Δk from Eqn.(3.5) is used directly even though it in fact includes second order perturbation contribution:

$$S^{PC} = \frac{\Delta k / k}{\Delta \theta / \theta} \quad (3.6)$$

To perform PERT CARD perturbation, a fictitious material is first created, with compositions containing the modified isotopic density as a means to perturb cross section. Suppose parameter Σ is the macroscopic cross section and $\Sigma = N\sigma$. The perturbed value Σ' is $((1 + \Delta p)N)\sigma$ which is equivalent to $N((1 + \Delta p)\sigma)$. An example of PERT CARD entry is shown below:

3.1. NUSS Direct perturbation versus MCNPX PERT CARD

```
pert1:n cell=1 mat=101 rho=4.16e-2 RXN=18 ERG=8.19E+00,2.00E+01 METHOD=1
```

which sets up a perturbation calculation `pert1` for neutron particles (n) in geometry `cell=1`, where the original material is replaced by a fictitious (i.e. perturbed) material (`mat=101`) defined in the material card section of the input file, with an adjusted density `rho`. By PERT CARD, a particular cross section $\Sigma(r, E)$ (`RXN=18`) at specific incident neutron energy range (`ERG` between 8.19MeV and 20MeV) can be perturbed. `METHOD=1` is the default for asking PERT CARD to calculate both $\frac{\partial k}{\partial \Sigma} \Delta \Sigma$ and $\frac{\partial^2 k}{\partial \Sigma^2} \Delta \Sigma^2$.

For verifying S^{DP} of NUSS and S^{PC} of MCNPX PERT CARD, the ^{239}Pu Jezebel benchmark is used. It is a well-characterized benchmark with an experimental k_{eff} of 1.000 ± 0.002 . Its simple physical structure as a bare spherical assembly allows the easy modelling and short computation time in MCNPX. The reference calculation produces $k_{\text{eff}} = 0.99980 \pm 0.00006$ with ENDF/B-VII.1 nuclear data library and by 1×10^5 neutrons for 900 active cycles. Listed in Fig. 3.1, the nominal atom densities are given in the Benchmark specification document and are used in the MCNPX input file. The atom density values in PERT CARD are obtained by multiplying corresponding “factor” values, which are equal to $1 + \Delta p$ with arbitrary Δp .

Benchmark values		Nominal values					Perturbed values			
Isotope	atom density (per barn-cm)	abundance	molar mass (g/mol)	atom density (per barn-cm)	mass(g)	weight %	factor	atom density (per barn-cm)	mass(g)	weight %
239Pu	3.7047E-02	1.0E+00	239.05216	3.7047E-02	1.4706E+01	94.21%	1.03	3.8158E-02	1.5147E+01	94.37%
240Pu	1.7512E-03	1.0E+00	240.05381	1.7512E-03	6.9806E-01	4.47%	1	1.7512E-03	6.9806E-01	4.35%
241Pu	1.1674E-04	1.0E+00	241.05685	1.1674E-04	4.6729E-02	0.30%	1	1.1674E-04	4.6729E-02	0.29%
Ga	1.3752E-03	0.60108	68.925574	8.2661E-04	9.4608E-02	0.61%	1	8.2661E-04	9.4608E-02	0.59%
		0.39892	70.924701	5.4859E-04	6.4610E-02	0.41%	1	5.4859E-04	6.4610E-02	0.40%
				initial density	total mass			perturbed density	total mass	
				4.0290E-02	1.5610E+01			4.1402E-02	1.6051E+01	

Figure 3.1: Material compositions for the Jezebel benchmark.

As a fast critical system, the sustained fission reaction is driven by fission reaction in the fast energy range. Fig.3.2 shows the pointwise ACE-formatted cross sections of $^{239}\text{Pu}(n,f)$ and its relative standard deviations in SCALE6-44g structure. First, NUSS perturbs the pointwise data in each of the 44 groups sequentially by an amount of γ times the corresponding relative standard deviation $\sigma_{\text{rel,g}}$. Three γ values are applied to obtain the sensitivity coefficients from NUSS direct perturbation. MCNPX PERT CARD is also applied to compute the sensitivity coefficients by introducing the same amount of changes ($1 + \Delta p$) in the atomic density of ^{239}Pu in the model.

Plotted in Fig.3.3, groups 1 to 12 correspond to an energy range from 25keV to 20MeV (see Appendix B4 for individual group boundaries). Sensitivity coefficients are found to be negligible below 25keV due to the negligible reaction rates, confirming the “insensitivity” of k_{eff}

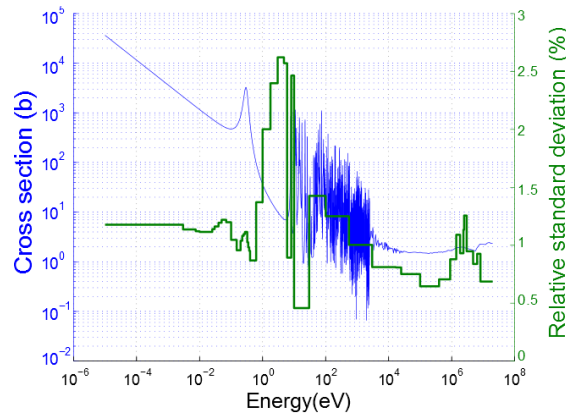


Figure 3.2: ACE pointwise cross section data of $^{239}\text{Pu}(n,f)$ from ENDF/B-VII.1 library and the relative standard deviation from SCALE6-44g library.

to changes in the (n,fission) cross section below this energy. More importantly, it can be observed that the precision and accuracy of sensitivity coefficients by NUSS direct perturbation procedure improve as γ increases (in both negative and positive direction) because perturbed k_{eff} is more distinguishable from the MCNPX statistical uncertainty (about 6pcm^1).

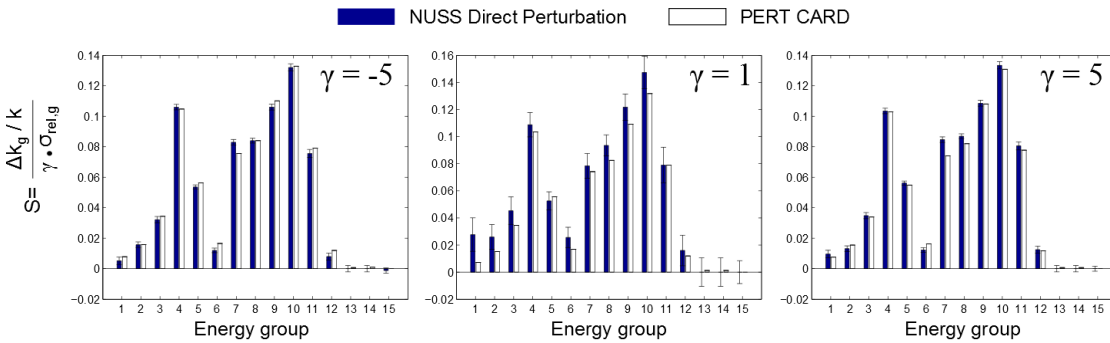


Figure 3.3: Direct perturbation in NUSS is performed to verify accuracy by comparing sensitivity coefficients calculated by MCNPX PERT CARD.

k_{eff} uncertainty due to nuclear data has been computed by the “Sandwich Rule” for the three γ cases and presented in Table 3.1. The average relative difference of NUSS-DP and PERT CARD results is 4.3%. In the next section where NUSS-SRS (i.e. stochastic sampling approach) is applied, it is equivalent to using a mix of γ values to obtain variance of sampled k_{eff} due to nuclear data perturbations.

3.2 NUSS-SRS versus TSUNAMI

In this section, TSUNAMI of SCALE6 is applied to compare with NUSS-SRS. The former computes k_{eff} sensitivity coefficients by first-order perturbation theory (see Appendix A3) for the

¹At a statistical uncertainty of 6pcm for k_{eff} , PERT CARD gives zero statistical uncertainty for Δk results.

γ	-5	1	5	Average
NUSS-DP	0.348	0.391	0.357	0.365
PERT CARD	0.353	0.349	0.346	0.350
$\frac{(DP-PC)}{PC}$	1.4%	12%	3.2%	4.3%

Table 3.1: k_{eff} uncertainty due to nuclear data $^{239}\text{Pu}(n,f)$ uncertainties by direct perturbation and deterministic “Sandwich Rule” method.

deterministic “Sandwich Rule” calculation of k_{eff} uncertainty due to nuclear data uncertainties. TSUNAMI-1D and TSUNAMI-3D are available in SCALE6 and they employ $S_{N=32}$ discrete ordinate and KENO multigroup Monte Carlo code respectively for the calculation of forward and adjoint fluxes. The nuclear data structure is 238-group so that the sensitivity coefficients from TSUNAMI are originally in 238-group. They are collapsed (i.e. summed over energy groups) into 44-group and folded with the default 44-group “SCALE6-44g” nuclear data covariances (see Appendix B4 for more details of the 238- and 44-group structures).

Uncertainties associated to the following nuclear data are considered: elastic (n,n), inelastic (n,n'), (n,2n), (n,f), (n, γ) cross sections and ($\bar{\nu}$), (χ) nuclear data. With NUSS-SRS, 300 perturbed ACE-formatted nuclear data files (original data from ENDF/B-VII.1 library and covariances also from SCALE6-44g library) are generated, one reaction at a time. From the subsequent 300 MCNPX calculations, the standard deviation of 300 k_{eff} values due to the perturbed reaction is calculated. The “total” uncertainty is obtained by perturbing all reactions simultaneously. In that case, inter-reaction correlations are taken into account by including inter-reaction covariances in the matrix decomposition (see Eqn.(2.12)) during sampling. However, correlations between partial and total cross section are not taken into account, meaning the total cross section uncertainties themselves are not considered.

NUSS-SRS, TSUNAMI-1D, TSUNAMI-3D, as well as MCNPX’s PERT CARD are applied to the Jezebel benchmark which was already seen in previous Section 3.1. A second fast-spectrum criticality benchmark, called “Godiva” is considered too. It is a 93-wt% enriched bare uranium metal sphere denoted as “hmf-001” from the ICSBEP Handbook. The isotopes of interest are ^{239}Pu in Jezebel and ^{235}U in Godiva.

Fig.3.4 plots the standard deviation of k_{eff} samples over the sample size as a “moving standard deviation (σ_k)”. The larger uncertainty contributors (e.g. $^{239}\text{Pu}(\bar{\nu})$, $^{235}\text{U}(n,\gamma)$) have more fluctuations in their moving σ_k , which might be difficult to judge for their convergence at a sample size of 300. In the case of $^{235}\text{U}(n,\gamma)$, large fluctuations are observed and σ_k convergence is verified with a larger sample size as shown in Fig.3.5. The 95% confidence intervals of σ_k of two sample sizes are included (see Eqn.(2.23)). By comparison, it could be concluded that at 300 samples, the σ_k value is underestimated.

Fig.3.6 and Fig.3.7 compare the NUSS-SRS results of σ_k in Fig.3.4 and alternative methods of TSUNAMI and PERT CARD based on the deterministic “Sandwich Rule”. Both systems

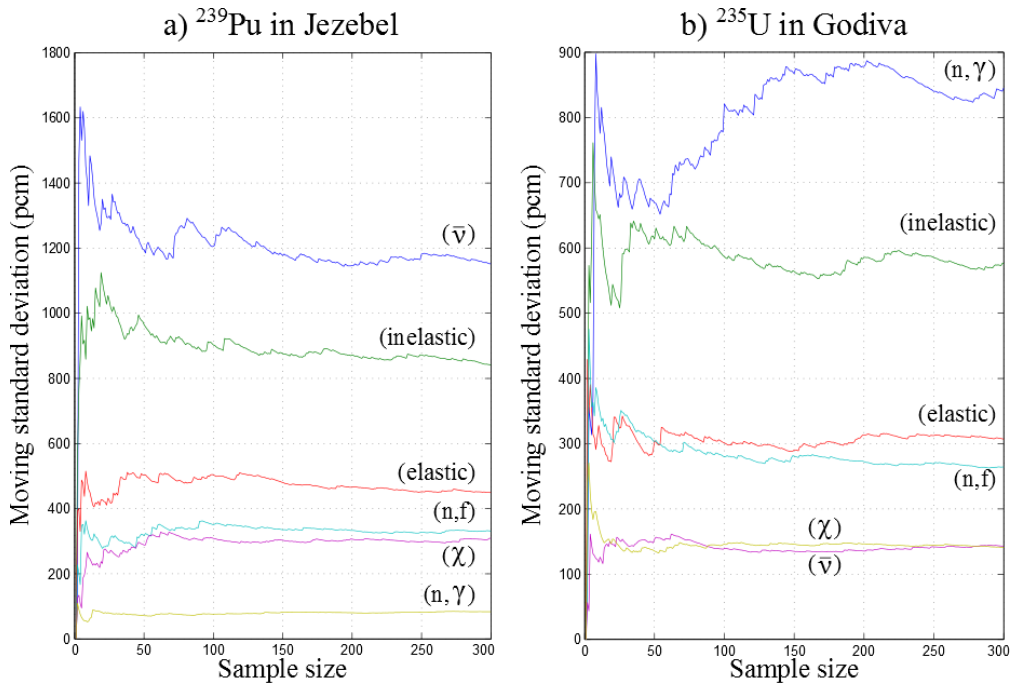


Figure 3.4: k_{eff} standard deviation values in terms of sample sizes up to 300.

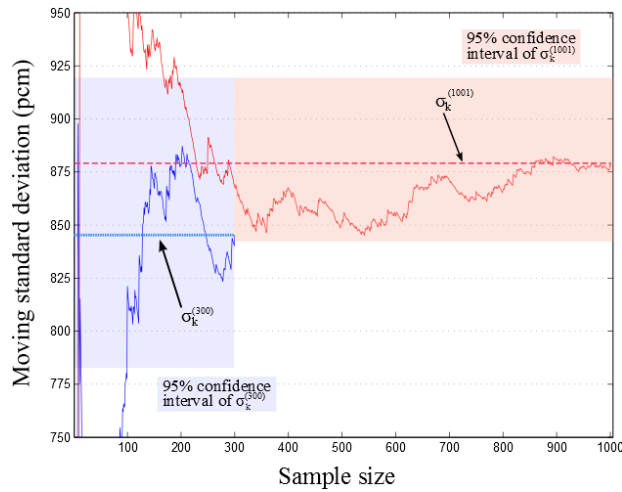


Figure 3.5: k_{eff} standard deviation values in terms of sample sizes for 300 and 1001 for $^{235}\text{U}(n,\gamma)$ in Godiva. The 95% confidence interval is included for the standard deviation of 300 samples. The interval includes the standard deviation of 1001 samples which is approximately 50pcm greater.

are insensitive to threshold (from 6MeV) reaction (n,2n) which is thus omitted in the figures. PERT CARD lacks the capability for $\bar{\nu}$ and χ perturbation. Guided by the confidence bound, the NUSS results agree in general with TSUNAMI and PERT CARD. Given individual MCNPX statistical uncertainty around 30 pcm, statistical uncertainties (V_{MC}) in proportion to nuclear data uncertainty contribution (V_{ND}) become 10% or more when $\sqrt{V_k}$ is less than 300 pcm.

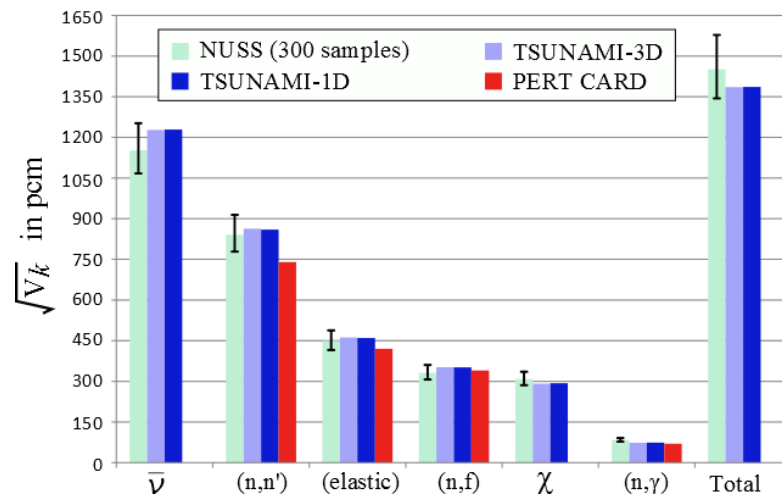


Figure 3.6: SCALE6-44g ^{239}Pu nuclear data uncertainties are propagated through MCNPX for the Jezebel benchmark and quantified in terms of standard deviations of 300-sampled k_{eff} by NUSS including statistical uncertainty and 95% confidence intervals. Alternatively k_{eff} uncertainty is calculated from “Sandwich Rule” with sensitivities from TSUNAMI and PERT CARD.

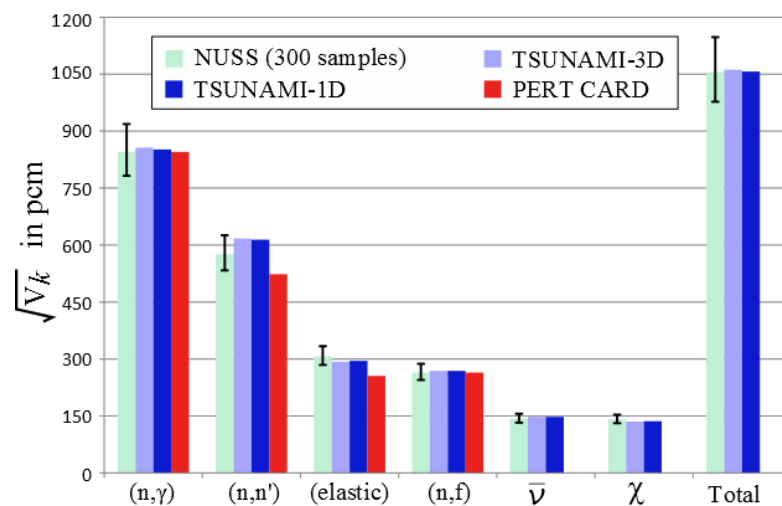


Figure 3.7: SCALE6-44g ^{235}U nuclear data uncertainties are propagated through MCNPX for the Godiva benchmark and quantified in terms of standard deviations of 300-sampled k_{eff} by NUSS including statistical uncertainty and 95% confidence intervals. Alternatively k_{eff} uncertainty is calculated from “Sandwich Rule” with sensitivities from TSUNAMI and PERT CARD.

3.3 NUSS-SRS versus TMC

As introduced in Chapter 1.5, the Total Monte Carlo (TMC) methodology from NRG is also a stochastic sampling approach but it samples from basic nuclear data and nuclear data model parameters. Fig.3.8 shows the process of TMC which runs the TALYS nuclear reaction

Chapter 3. Evaluating NUSS-SRS against existing methods and its applications

code repeatedly with perturbed nuclear model parameters and generates samples of ENDF-6 formatted nuclear data files. These perturbed ENDF-6 formatted files can then be processed by NJOY into, for example ACE-formatted nuclear data files for MCNPX calculations.

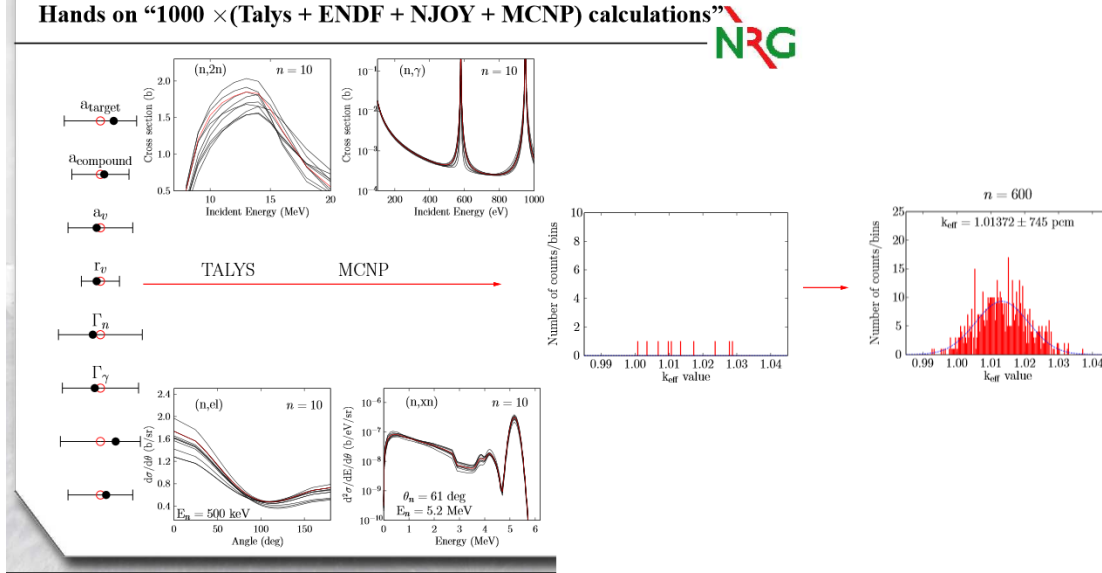


Figure 3.8: Nuclear model parameters are perturbed to generate random ENDF-6 formatted nuclear data files. Perturbed ENDF-6 formatted nuclear data are processed into ACE files for MCNP(X) calculations and a spread of k_{eff} outputs is obtained.

Unlike NUSS and deterministic “Sandwich Rule” methods, TMC does not need multigroup covariance matrices. But they can be produced as the by-product of the TMC process. The TENDL covariance library [57] is prepared from the covariance and correlations of random ENDF-6 formatted nuclear data:

$$V_{ij} = \frac{1}{N} \sum_{n=1}^N (\alpha_i^n - \alpha_i^o) (\alpha_j^n - \alpha_j^o) \quad \text{and} \quad C_{ij} = \frac{V_{ij}}{\sqrt{V_{ii}} \sqrt{V_{jj}}} \quad (3.7)$$

where α^o is the nominal nuclear data and α^n the perturbed data as a result of the n^{th} random sample by TALYS code. Correlation matrix (C_{ij}) is obtained as usual.

By NJOY, the TENDL covariances in ENDF-6 format can then be processed into application-ready multigroup covariances. Available at the time of the study in [58], TENDL-2011 covariance evaluations were used by NUSS as uncertainty sources for ^{239}Pu in Jezebel and ^{235}U for Godiva benchmarks to assess their k_{eff} uncertainty contributions. To make consistent comparison, MCNPX calculations use both TENDL-2011 ACE-formatted nuclear data and the TENDL-2011 covariances in 44-group structures. Meanwhile, PERT CARD is applied to provide additional verification check on the NUSS result.

Results of Jezebel and Godiva by TMC (fast TMC to be specific [34]) are provided from NRG [59] and plotted in Fig.3.9 and 3.10 alongside the NUSS and PERT CARD results. Noticeable

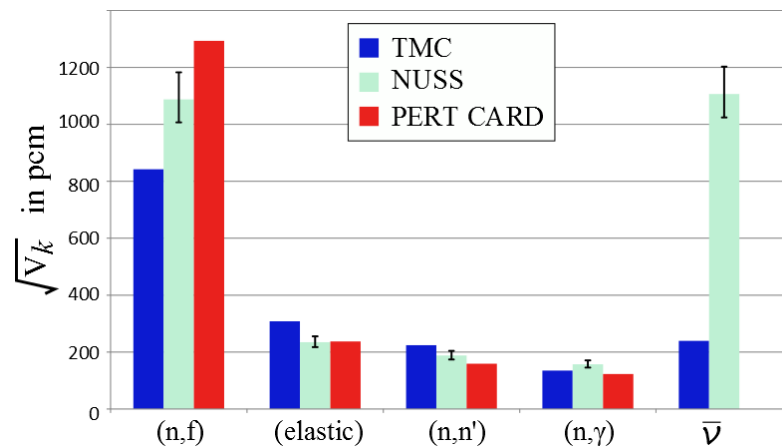


Figure 3.9: k_{eff} uncertainties due to ^{239}Pu nuclear data uncertainty from TENDL-2011 library in Jezebel benchmark by NUSS (300 samples) are compared with Total Monte Carlo (TMC) and MCNPX PERT CARD methods.

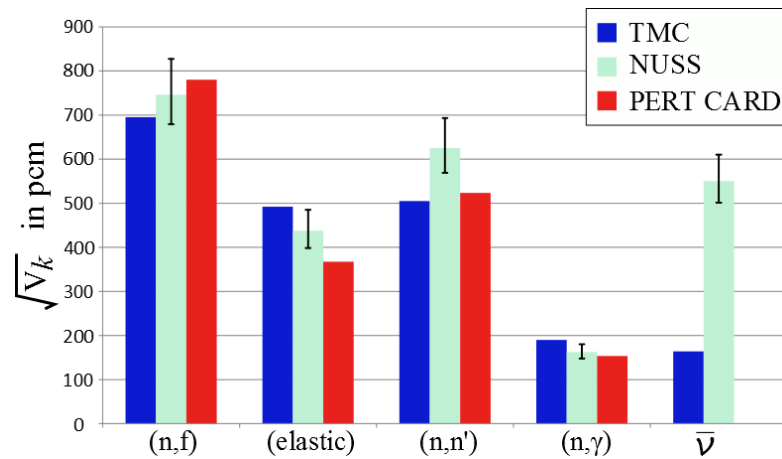


Figure 3.10: k_{eff} uncertainty due to ^{235}U nuclear data uncertainty from TENDL-2011 library in Godiva benchmark by NUSS (200 samples) are compared with Total Monte Carlo (TMC) and MCNPX PERT CARD methods.

differences are found in $^{239}\text{Pu}(n,f)$, $^{239}\text{Pu}(\bar{\nu})$ of Jezebel and $^{235}\text{U}(\bar{\nu})$ of Godiva. The discrepancy in k_{eff} uncertainty results is suspected to be due to the quality of the corresponding TENDL 2011 covariance data as explained in the following.

In Fig.3.11, the correlation matrix and relative standard deviation of the $^{239}\text{Pu}(n,f)$ cross section evaluation from TENDL are shown. Unreliable uncertainty values (400% relative standard deviation) are present around 10^4eV , corresponding to energy group numbers 13 and 14. Sampling from this covariance data in NUSS led to non-Gaussian distribution of perturbation factors as shown in Fig.3.12 where in groups 13 and 14, perturbation factors have been restricted to be non-negative and deviated from the mean value of 1. This biasing of sampled nuclear data could affect the k_{eff} sample mean and variance by NUSS. Similarly, the large

Chapter 3. Evaluating NUSS-SRS against existing methods and its applications

uncertainties in groups 13 and 14 contribute significantly to the k_{eff} uncertainty calculated by the deterministic Sandwich Rule. PERT CARD of MCNPX was used to obtain sensitivity coefficients (\vec{S}) and they are combined with the TENDL covariance matrix in Sandwich Rule:

$$\sigma^2 = \vec{S}V\vec{S}^T = \sum_i^G \sum_j^G S_i V_{ij} S_j$$

Normally, the above summation is over all energy groups (i.e. $G=44$ in case of 44-group), resulting in $\sigma=1293$ pcm for $^{239}\text{Pu}(n,f)$ by PERT CARD, shown in Fig.3.9. Now, if the summation is only up to group 12² so as to remove the excessive uncertainty contributions from groups 13 and 14, σ is reduced to 1029 pcm and is within the 95% confidence bound of NUSS-calculated result in Fig.3.9.

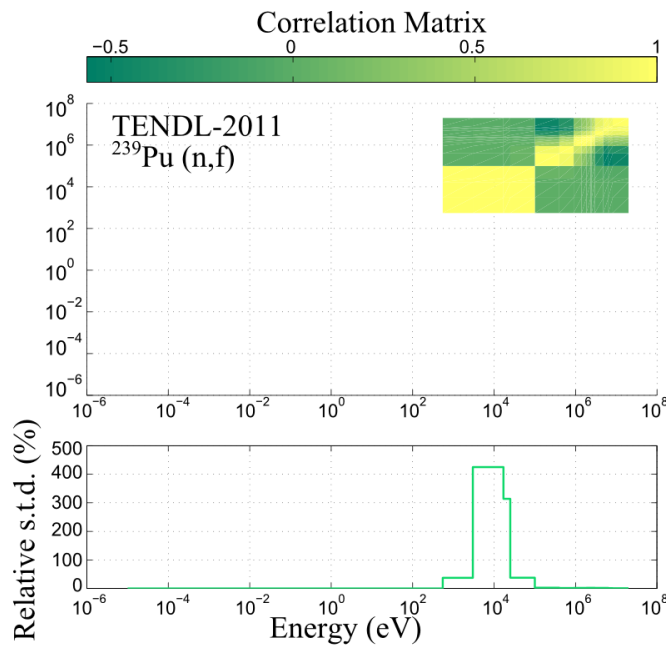


Figure 3.11: TENDL-2011 correlation and relative standard deviation (s.t.d.) for $^{239}\text{Pu}(n,f)$.

In the cases of $^{239}\text{Pu}(\bar{\nu})$ and $^{235}\text{U}(\bar{\nu})$, NUSS results are much larger than TMC results. There is no PERT CARD results because it does not compute Δk due to $\bar{\nu}$ perturbations. Alternatively, sensitivity coefficients from TSUNAMI-3D can be applied with the TENDL covariances to estimate k_{eff} uncertainty from $^{239}\text{Pu}(\bar{\nu})$ and $^{235}\text{U}(\bar{\nu})$. They are equal to 1306 pcm and 544 pcm respectively and comparable to k_{eff} uncertainties by NUSS, even though TSUNAMI sensitivity coefficients were obtained using KENO-3D and ENDF/B-VII.0 nuclear data. This implies that the implementation of NUSS for $\bar{\nu}$ is not incorrect. Then the discrepancy between NUSS and TMC for $\bar{\nu}$ uncertainty contribution is likely due to the quality of the TENDL-2011 covariance data. The correlation matrices, as well as the relative standard deviations of $^{239}\text{Pu}(\bar{\nu})$ and

²For fast spectrum Jezebel, summation up to group 16 gives the same k_{eff} uncertainty of 1293 pcm because above group 16, k_{eff} sensitivities are zero.

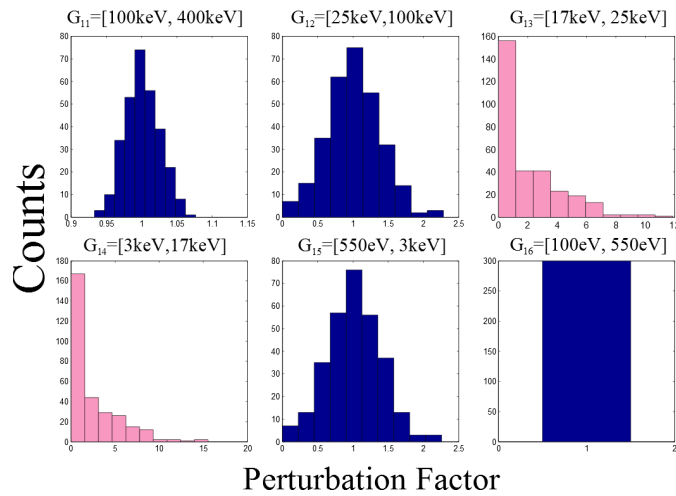


Figure 3.12: For $^{239}\text{Pu}(n,f)$, some perturbation factors are skewed due to the large uncertainties in certain energy groups (see Fig.3.11). Perturbation factors must be greater than zero by physical requirement.

$^{235}\text{U}(\bar{\nu})$ are compared to the ones in SCALE6-44g covariance library in Fig.3.13 and Fig.3.14. Clearly, TENDL-2011 evaluations are much different from SCALE6-44g, showing high level of correlations below 10^4 eV and a sharp drop of uncertainty above 1 MeV. This observation partially explains that k_{eff} uncertainty due to $^{235}\text{U}(\bar{\nu})$ from TENDL-2011 is larger than that from SCALE6-44g (550 pcm vs. 148 pcm). Since NUSS results clearly depend on the magnitude of the nuclear data covariances, the most plausible explanation is that the TENDL-2011 covariances for $^{239}\text{Pu}(\bar{\nu})$ and $^{235}\text{U}(\bar{\nu})$ are much larger than those inside the TMC-generated random ENDF-6 formatted nuclear data files, which we did not have access at the time of the above calculations.

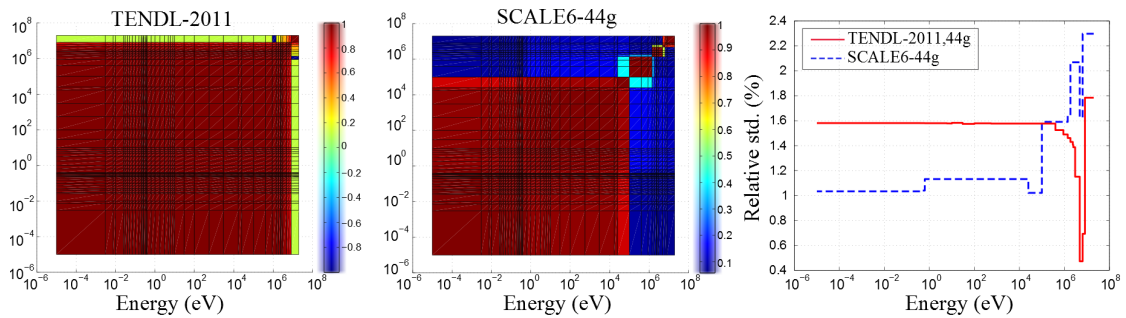


Figure 3.13: TENDL-2011 and SCALE6-44g (sourced from ENDF/B-VII.0) correlation matrices and relative standard deviation (std.) for $^{239}\text{Pu}(\bar{\nu})$.

At the time of this writing, the 2014 version of TENDL covariances is available [60]. With the help of D. Rochman (one of the authors of TENDL), ENDF-6 formatted data of $^{239}\text{Pu}(\bar{\nu})$ and $^{235}\text{U}(\bar{\nu})$ (i.e. file MF31) in TENDL-2014 are obtained separately. Fig.3.15 and Fig.3.16 show the relative standard deviations in 44-group and MF31 energy grids. The 44-group nuclear data

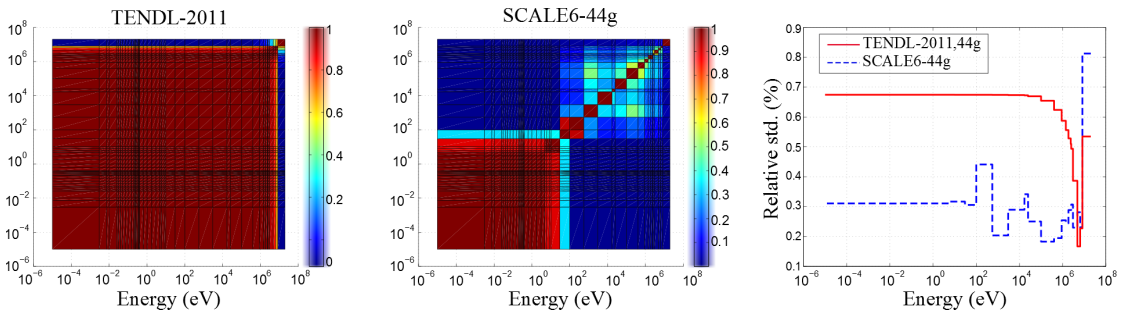


Figure 3.14: TENDL-2011 and SCALE6-44g (sourced from JENDL-3.3) correlation matrices and relative standard deviation (std.) for $^{235}\text{U}(\bar{\nu})$.

uncertainties are much smaller in the 2014 version, and comparable to the $\bar{\nu}$ uncertainties in file MF31 which are produced by TMC. Using the TENDL-2014 44-group covariance data, NUSS generates 400 perturbed ACE files (original from TENDL-2014 too) for k_{eff} uncertainty quantification. Shown in Table 3.2, results of NUSS and TMC are much closer for TENDL-2014 comparison than for TENDL-2011 as seen before. There are still small differences in k_{eff} uncertainty between NUSS and TMC, which can be explained by the smaller uncertainty values given by 44-group than by original MF31 data in fast energy range as seen in Fig. 3.15 and Fig.3.16. It is outside the scope of this PhD work to investigate the cause of the difference in 44-group and MF31 uncertainty data³. But it is expected that, when multigroup covariances are prepared such that they agree well with MF31 uncertainties, the k_{eff} uncertainty due to nuclear data uncertainties as quantified by NUSS (using multigroup covariances) can be equivalent to that by TMC method.

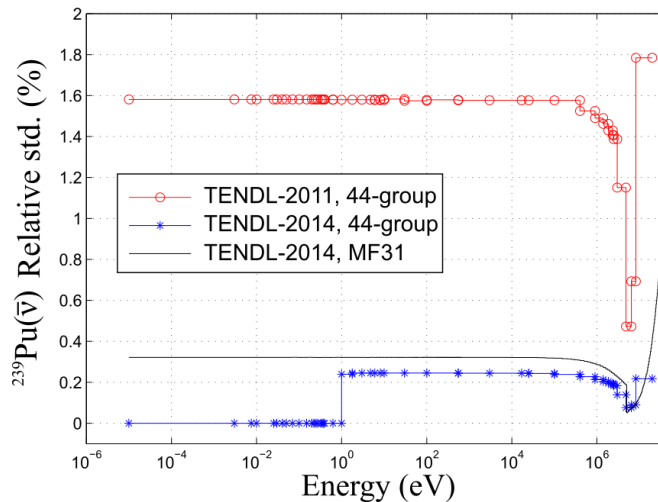


Figure 3.15: $^{239}\text{Pu}(\bar{\nu})$ uncertainty given by TENDL-2011 and TENDL-2014 evaluations. From TENDL-2014, MF31 data correspond to $\bar{\nu}$ and are processed by NJOY into 44-group structure.

³Some issue with the processing of 44-group covariance from File MF31 is still present for $^{239}\text{Pu}(\bar{\nu})$, as shown by the zero relative standard deviation values given by TENDL-2014, 44-group in Fig.3.15. But for the current fast spectrum Jezebel benchmark, nuclear data uncertainties below 10^2 eV is inconsequential.

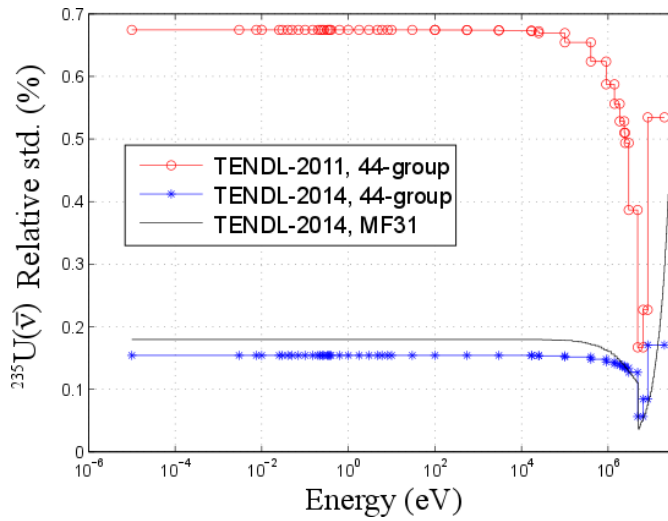


Figure 3.16: $^{235}\text{U}(\bar{\nu})$ uncertainty given by TENDL-2011 and TENDL-2014 evaluations. From TENDL-2014, MF31 data correspond to $\bar{\nu}$ and are processed by NJOY into 44-group structure.

TENDL	$^{239}\text{Pu}(\bar{\nu})$		$^{235}\text{U}(\bar{\nu})$	
	TMC	NUSS	TMC	NUSS
2011	239	1106	164	550
2014	237	182	158	142

Table 3.2: The most updated 2014 version of TENDL covariances give more comparable k_{eff} uncertainty results (in pcm) between NUSS and TMC.

3.4 Energy-group-structure effect in NUSS-SRS

The performance of NUSS was verified against both PERT CARD and TSUNAMI methods. However, as shown by the comparison study between NUSS and TMC, it should be emphasized that uncertainty results ultimately depend on the accuracy of the employed nuclear data uncertainties. Furthermore, the accuracy of nuclear data uncertainty refers to both the magnitude and the employed energy group structure of the variance/covariance data.

The SCALE6-44g covariance library uses a 44-group structure consisting of 22 thermal and 22 fast groups (see Fig.2.5) in order to accommodate various cross section features in the wide range of energies. However as the Jezebel and Godiva benchmarks are fast systems, a finer group structure in the fast energy range and fewer details in the thermal range is sufficient. The 30- and 80-group structures are part of NJOY's list of built-in group structures for fast fission systems [10]. The three group structures are compared in terms of the tallied flux spectra for Jezebel and Godiva in Fig.3.17.

So far, the SCALE6-44g and TENDL covariances are applied. To generate 30- and 80-group covariances, the ENDF/B-VII.1 covariance library, released in 2011 is used in the following. The focus here is on nuclear data which have noticeable differences between SCALE6-44g and

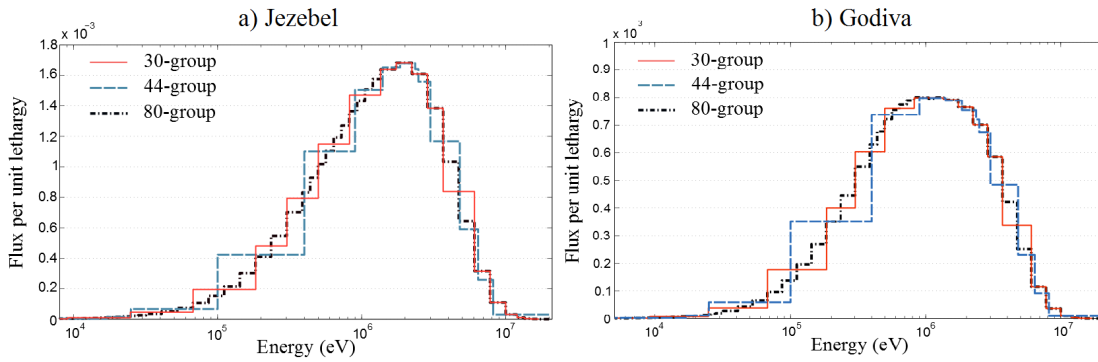


Figure 3.17: Neutron flux spectra for Jezebel and Godiva benchmarks in different multigroup structures, tallied by MCNPX.

ENDF/B-VII.1 covariance libraries. A strong example which illustrates the importance of the accuracy of nuclear data uncertainty in NUSS is by the quantification of $^{239}\text{Pu}(\bar{\nu})$ uncertainty in Jezebel. As shown in Figure 3.18, the discrepancy between the two libraries leads to very different k_{eff} standard deviation (1152 pcm vs. 86 pcm). In comparison, the effect of different energy group structures is minor as shown in Figure 3.19. The corresponding correlation matrices are provided in Figure 3.20.

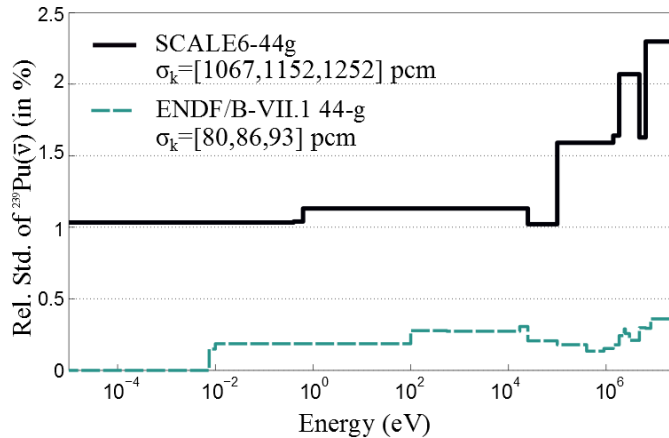


Figure 3.18: Larger uncertainty of $^{239}\text{Pu}(\bar{\nu})$ from SCALE6-44g results in much higher k_{eff} uncertainty in Jezebel. 95% confidence intervals are given in brackets.

Figure 3.21 shows the uncertainties of $^{235}\text{U}(n,f)$ in both libraries and in three group structures (30 vs. 44 vs. 80 groups). Corresponding correlation matrices are shown in Figure 3.22. Even though large variations are observed below 30 keV, k_{eff} uncertainty in Godiva benchmark from $^{235}\text{U}(n,f)$ does not vary substantially. This is again due to the low neutron flux level below 30 keV (see Fig.3.17b) which implies a low reaction rate of $^{235}\text{U}(n,f)$ below the fast energy range in Godiva and perturbations in $^{235}\text{U}(n,f)$ there have a limited effect on the overall flux and hence on k_{eff} .

The above results show that using the 30-, 44- and 80-group structures leads to similar k_{eff}

3.4. Energy-group-structure effect in NUSS-SRS

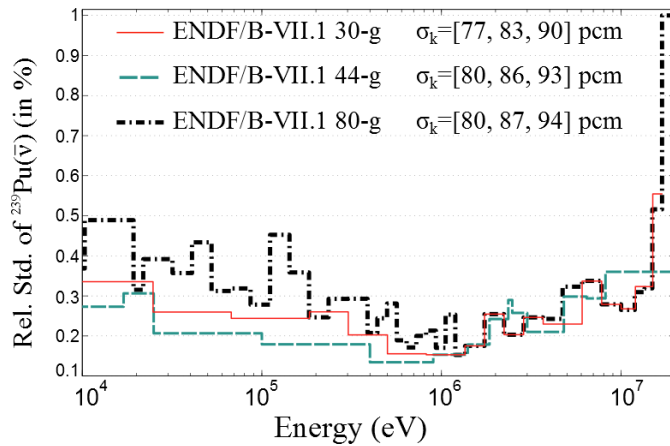


Figure 3.19: Uncertainty of $^{239}\text{Pu}(\bar{\nu})$ from ENDF/B-VII.1 libraries in three different energy group structures. The impact on k_{eff} uncertainty contribution (bounded by 95% confidence interval) due to different group structure is minor. See Appendix A6 for explanations on the large uncertainty difference below 10^6 eV.

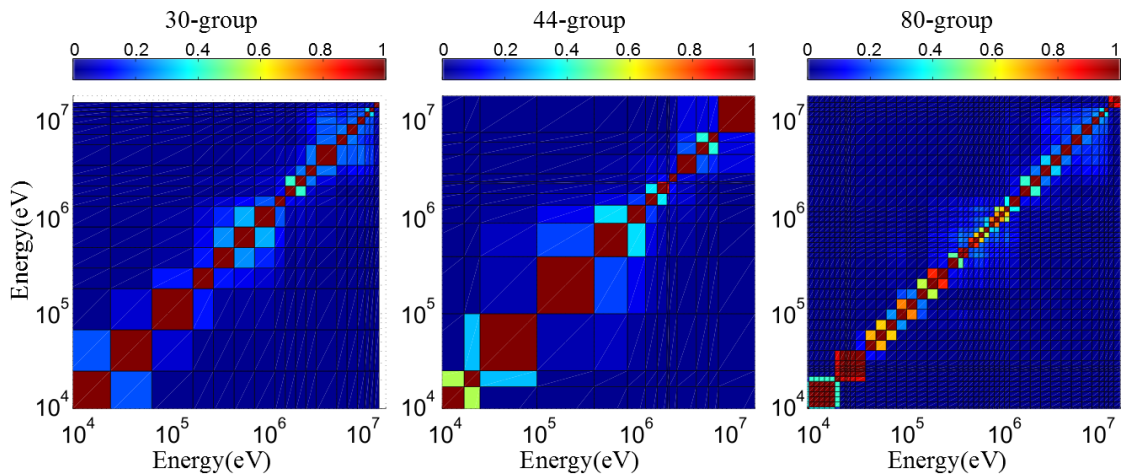


Figure 3.20: Correlation matrices of $^{239}\text{Pu}(\bar{\nu})$ from ENDF/B-VII.1 library in three different energy group structures.

uncertainty precision. It is emphasized again that the number of groups is less meaningful than their locations, whether they reflect the system (related to the flux spectrum) under investigation. As the number of groups decreases, it is expected that the k_{eff} uncertainty precision is going to deteriorate. Without applying NUSS-SRS but only with the Sandwich Rule, k_{eff} uncertainty variation due to different energy group structures is illustrated below.

The default 238-group sensitivity coefficient calculated by TSUNAMI is collapsed into another groupwise structure by summing the sensitivity ($S(E)$) values within energy group g spanning

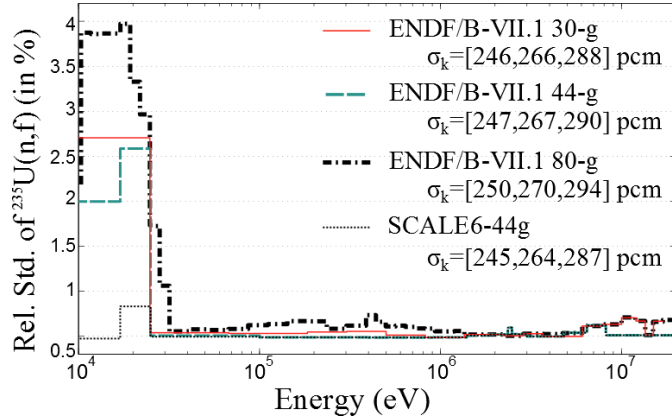


Figure 3.21: Relative standard deviation of $^{235}\text{U}(n,f)$ nuclear data from SCALE6-44g and ENDF/B-VII.1 libraries. The impact on k_{eff} uncertainty contribution due to different group structure is minor.

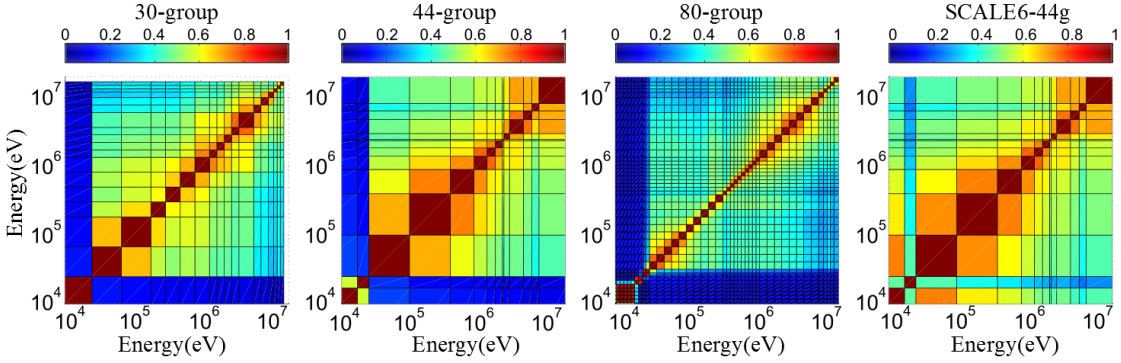


Figure 3.22: Correlation matrices of $^{235}\text{U}(n,f)$ from ENDF/B-VII.1 library in three different energy group structures and from SCALE6-44g covariance library.

energies E_{g+1} and E_g :

$$S'(g) = \sum_{E=E_{g+1}}^{E_g} S(E) \quad (3.8)$$

Multigroup covariances are prepared using ENDF/B-VII.1 covariance library and NJOY, after which the k_{eff} uncertainties are calculated by the Sandwich Rule and shown in Fig.3.23. Keeping in mind that, the 44-group structure has 22 groups in the fast energy range, its k_{eff} uncertainty result is only slightly higher than the result of 10-group and 5-group structures. The difference between 238-group and 44-group uncertainties is also small. In the opposite direction, reducing number of groups to 2-group or 1-group structures has doubled more than twice the k_{eff} uncertainty value and clearly resulted in a stronger adverse effect on the precision of k_{eff} uncertainty.

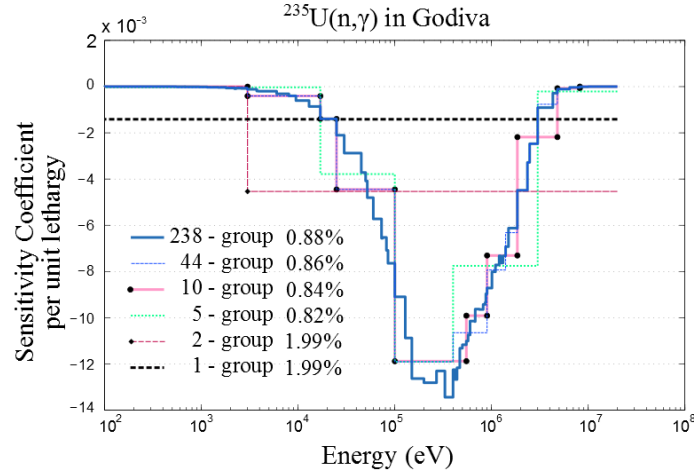


Figure 3.23: Sensitivity coefficients in 238-group from TSUNAMI are collapsed into various group structures and the corresponding relative k_{eff} uncertainties are calculated.

3.5 Sensitivity analysis with NUSS-SRS

With NUSS-Simple Random Sampling (SRS), the total uncertainty contributed by multiple inputs can be calculated. However, due to the black-box approach of NUSS-SRS, the relationship between individual input and the output has to be quantified indirectly. Recall Eqn.(3.1) for the sensitivity coefficient and now for every random sample:

$$S_{k,\alpha} = \frac{\Delta k/k}{\Delta \alpha/\alpha} \xrightarrow{\text{for each sample}} S_{k,\alpha,\text{samp}} = \frac{(k^{\text{samp}} - k^{\text{ref}})/k^{\text{ref}}}{(\alpha^{\text{samp}} - \alpha^{\text{ref}})/\alpha^{\text{ref}}} = \frac{k^{\text{samp}}/k^{\text{ref}} - 1}{p - 1} \quad (3.9)$$

By expressing $S_{k,\alpha,\text{samp}}$ with the perturbation factor p , the behaviour of $S_{k,\alpha,\text{samp}}$ can be observed for each sample variation. In Fig.3.24 the first 20 groups of the 44-group $^{239}\text{Pu}(\bar{\nu})$ cross section in the Jezebel benchmark are examined. The scatter plot in each window is between the values of $(p - 1)$ and $(k^{\text{samp}}/k^{\text{ref}} - 1)$. Visual inspection suggests linear relation between nuclear data input and k_{eff} for energy groups 4 to 12, especially for group 8 between 1.4 MeV and 1.85 MeV. In contrast, the association between input and output variations for group 13 and above is weak as shown by the higher degree of dispersion of scattered data points. Group 13 corresponds to incident neutron energy of 25 keV and from previous discussions (see flux spectra in Fig.3.17) that below this energy the k_{eff} value is not affected by cross section perturbations.

To make use of the k_{eff} random samples obtained by simultaneous sampling of nuclear data, scatter plots provide qualitative information of the relation between nuclear data and k_{eff} . Quantitative information is provided through the calculation of correlation coefficients:

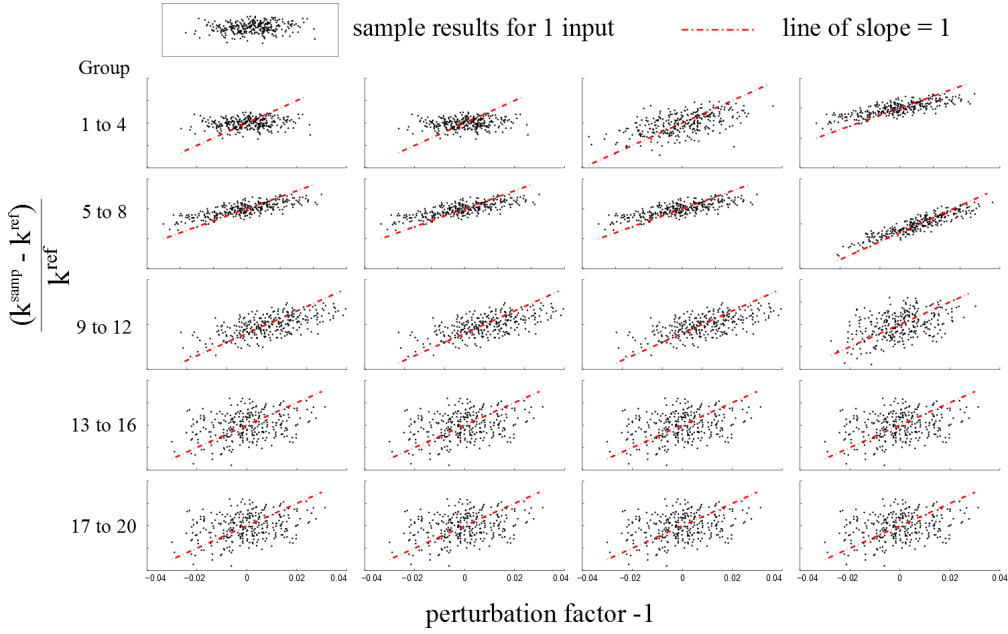


Figure 3.24: Scatter plots for $^{239}\text{Pu}(\bar{\nu})$ show the strength of association between relative change in k_{eff} and relative change in cross section. The closer the sample results are to the red dotted line, the higher the linear association. The first 20 groups cover energies from 20MeV down to 6eV.

$$r_p = \frac{\sum_i^N (X_i - \bar{X})(Y_i - \bar{Y})}{\sqrt{\sum_i^N (X_i - \bar{X})^2} \sqrt{\sum_i^N (Y_i - \bar{Y})^2}} \quad (3.10)$$

$$r_s = \frac{\sum_i^N (R(X_i) - \bar{R}_X)(R(Y_i) - \bar{R}_Y)}{\sqrt{\sum_i^N (R(X_i) - \bar{R}_X)^2} \sqrt{\sum_i^N (R(Y_i) - \bar{R}_Y)^2}} \quad (3.11)$$

where r_p is called the Pearson correlation coefficient and r_s the Spearman rank correlation coefficient. $R(\dots)$ denotes the use of the ranking instead of the actual value and $\bar{R}_X = (\sum_i^N R(X_i))/N$. As their names suggest, they measure how much the inputs and output are correlated, in other words, how much inputs and output vary together in comparison to the degree they vary independently. Plotted in Fig.3.25, the large coefficient values from energy groups 4 to 8 imply high correlations, which have been observed in the scatter plots of Fig.3.24. The correlation coefficient is different from sensitivity coefficient however, in that the former is a global analysis of all inputs simultaneously and statistically, and the latter is based on the local observation, made one-at-a-time. The good agreement between the results of Pearson and Spearman correlation coefficients implies linear relation between k_{eff} and nuclear data. In this case, sensitivity coefficient of linear system is a constant ratio of $\Delta k / \Delta \alpha$. In fact, when the Pearson correlation coefficient is squared, Eqn.(3.12) can estimate the shared variance

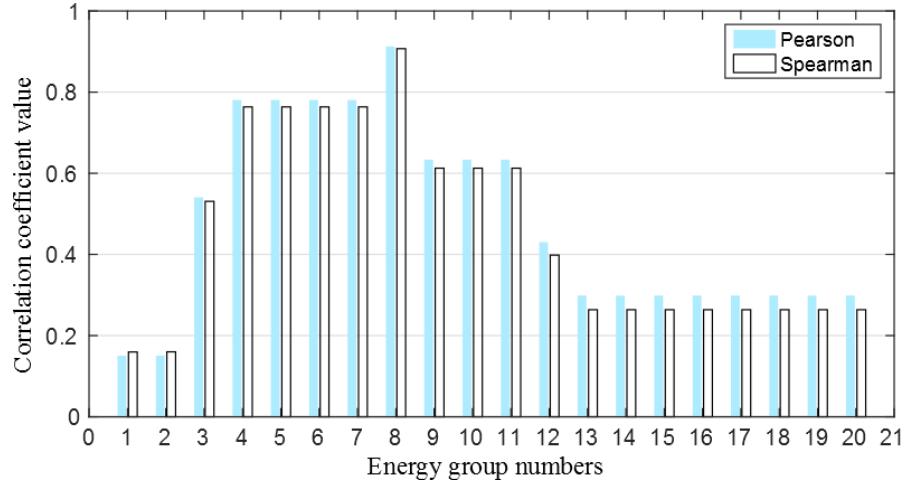


Figure 3.25: Pearson and Spearman correlation coefficient results for $^{239}\text{Pu}(\bar{\nu})$ in Jezebel benchmark.

between k_{eff} and nuclear data:

$$r_p^2 = \left(\frac{\sum_i^N (X_i - \bar{X})(Y_i - \bar{Y})}{\sqrt{\sum_i^N (X_i - \bar{X})^2} \sqrt{\sum_i^N (Y_i - \bar{Y})^2}} \right)^2 = \left(\frac{\text{COV}(X, Y)}{\sqrt{\text{VAR}(X)} \sqrt{\text{VAR}(Y)}} \right)^2 \approx \frac{a^2 \cdot \text{VAR}(X)}{\text{VAR}(Y)} \quad (3.12)$$

The numerator of Eqn.(3.12) is analogous to the quantity calculated by the Sandwich Rule: $S_\alpha^2 \cdot \text{VAR}(\alpha)$, except a is a statistical parameter derived from the set of samples. The detailed derivation is given in Appendix A7.

By substituting $(k^{\text{samp}}/k^{\text{ref}} - 1)$ as Y_i and $(p - 1)$ as X_i , the k_{eff} variance fraction due to $^{239}\text{Pu}(\bar{\nu})$ in Jezebel is estimated and shown in Fig.3.26. It can be seen that energy group 8 is responsible for more than 80% of the total k_{eff} variance contribution, even though the corresponding sensitivity coefficient as shown in Fig.3.3 is only at the 4th place. In addition, the approach of correlation coefficient has no problem of handling inputs correlations. The similar values of r_p^2 (and r_s^2) for groups 3 to 7, groups 9 to 11 and groups 13 to 20 indicate exactly that these inputs are similar to each other in terms of their variance contributions to k_{eff} variance.

In nuclear data uncertainty quantification, sensitivity coefficient has long been used to identify important inputs, in terms of the perturbation in k_{eff} due to perturbation in the inputs. To extract the equivalent sensitivity information however is not straight-forward as shown here for the sampling-based NUSS-SRS tool, due to the fact that inputs have been sampled simultaneously in accordance with their correlations. An attempt to identify important input is taken by calculating the variance contribution instead of the sensitivity coefficient which is a local parameter. The linear relationship between nuclear data and k_{eff} allows the estimation of variance fraction by the squared value of Spearman or Pearson correlation coefficients, which can be calculated using the existing results from simple random sampling. Even though the use of squared value of correlation coefficient is shown to be efficient, without additional

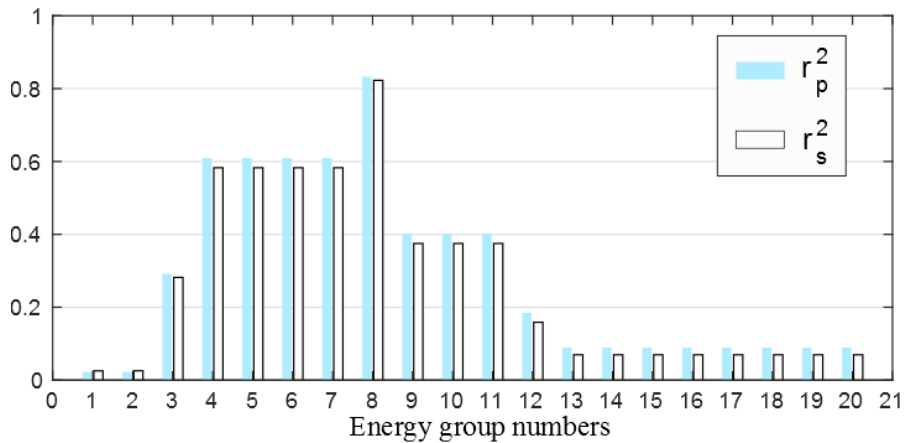


Figure 3.26: The squared of Pearson r_p and Spearman r_s correlation coefficients give estimate of how much the total variance is contributed by each input if the output is linearly dependent on the inputs.

computational effort after simple random sampling calculations, it should be emphasized that sensitivity coefficient and variance fraction should not be compared directly. Otherwise, inconsistent conclusions are drawn for the identification of influential inputs. Further theoretical development of a sampling-based sensitivity analysis will be shown in Chapter 4.

3.6 UAM Pincell application by NUSS-SRS

Standard reactor core calculations are performed based on few-group homogenized cross sections which typically have been prepared a priori with a lattice transport code. At the nuclear fuel pin cell level, calculations for the homogenization and condensation of cross sections represent a basic component of the multiscale process leading to reactor core-level computations. Quantifying uncertainties from indispensable nuclear data inputs at the pin cell level provides a quantitative measure of the nuclear data uncertainty contributions in later stages of neutronics calculations.

With the accurate continuous-energy MCNPX and pointwise/continuous energy nuclear data, NUSS has been applied to quantify nuclear data uncertainty for four pin cell benchmarks which belong to the “OECD/NEA Uncertainty Analysis in Modelling (UAM) Light Water Reactor Benchmark” [61]. Some of the important benchmark parameters are listed in Table 3.3 with the computed k_{inf} by MCNPX.

For these four cases, nuclear data uncertainties of the major fuel components ^{235}U and ^{238}U are from the SCALE6-44g covariance library and ENDF/B-VII.1[62]. The latter has been prepared in the same 44-group energy structure as SCALE6-44g. NUSS-SRS is applied to calculate the top k_{inf} uncertainty contributors and their combined contributions and the results are shown in Figures 3.27 and 3.28. The cases in which ^{235}U and ^{238}U nuclear data are perturbed simultaneously are labeled as “ $^{235}\text{U}^{238}\text{U}$ ”. An additional set of calculations was

3.6. UAM Pincell application by NUSS-SRS

Cases	Fuel Temp.	Mod. Temp.	$k_{\text{inf}}(\sigma_{MC}$ in pcm)	Fuel Enrichment	Pitch
1.PB-2 HZP	552.8K	552.8K	1.33916(33)	2.93%	18.75mm
2.PB-2 HFP	900K	557K, 40% void	1.22231(36)		
3.TMI-1 HZP	551K	551K	1.42358(36)	4.85%	14.427mm
4.TMI-1 HFP	900K	562K	1.40586(36)		

Table 3.3: Pin cell specifications and MCNPX-computed k_{inf} with statistical uncertainty in brackets, using ENDF/B-VII.1 nuclear data evaluation. PB-2 and TMI-1 are Peach Bottom-2 BWR and Three Mile Island-1 PWR. HZP and HFP are the hot zero power and hot full power conditions.

performed by perturbing also the structural materials consisting of hydrogen, oxygen and zirconium (labeled as “U & S.M.”). Their nuclear data uncertainties are found to contribute insignificantly to the k_{inf} uncertainty.

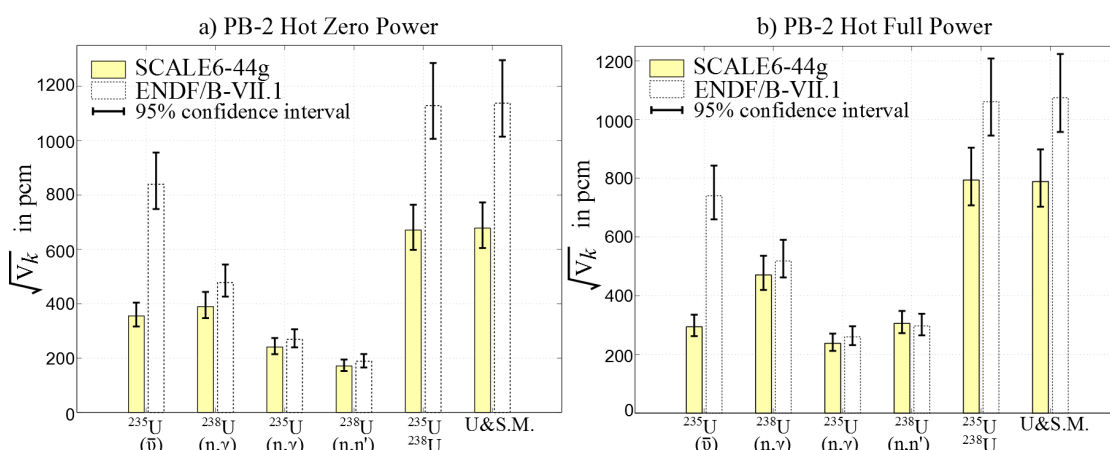


Figure 3.27: NUSS calculation of k_{inf} sample standard deviation (with 130 samples) for PB-2 a) hot zero power and b) hot full power pincell benchmarks.

It has also been found that the largest discrepancy between SCALE6-44g and ENDF/B-VII.1 belongs to the $^{235}\text{U}(\bar{\nu})$ contribution. It clearly influences the combined uncertainty contributions, which are very different depending on the covariance library used. The different evaluations of $^{235}\text{U}(\bar{\nu})$ in various covariance libraries are shown in Figure 3.29. In SCALE6-44g, $^{235}\text{U}(\bar{\nu})$ uncertainty is taken from JENDL-3.3 library. Along with JENDL 4.0, the JENDL-based $^{235}\text{U}(\bar{\nu})$ uncertainty is underestimated in comparison to ENDF/B-VII.1 (same as JEFF3.1.1 and JEFF3.1.2.) The ENDF/B-VII.1 evaluation gives the highest uncertainty evaluation at 0.7%, approximately double of those given by JENDL-3.3 and JENDL-4.0. Consequently, the uncertainty contributions from $^{235}\text{U}(\bar{\nu})$ uncertainty are dominating in the case of ENDF/B-VII.1 covariances and are also about twice as the ones calculated by the use of JENDL-3.3 (in SCALE6) covariances.

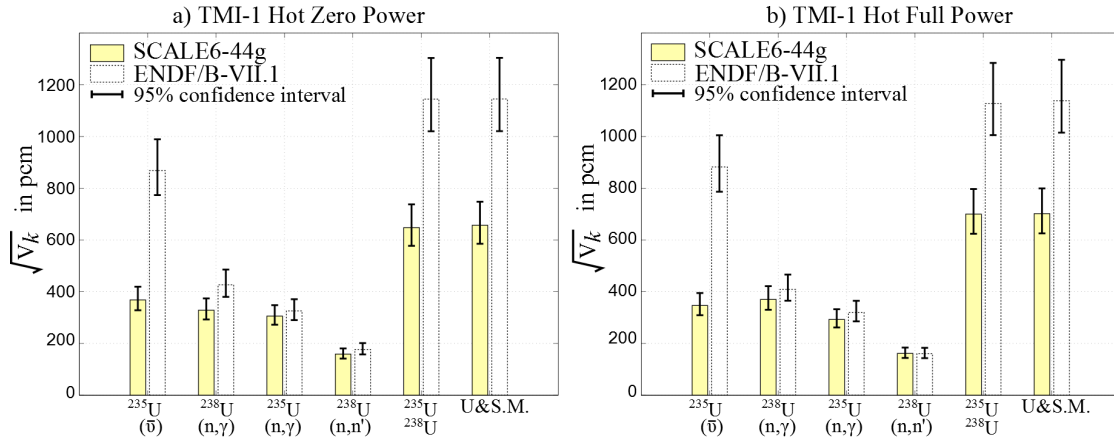


Figure 3.28: NUSS calculation of k_{inf} sample standard deviation (with 130 samples) for TMI-1 a) hot zero power and b) hot full power pin cell benchmarks.

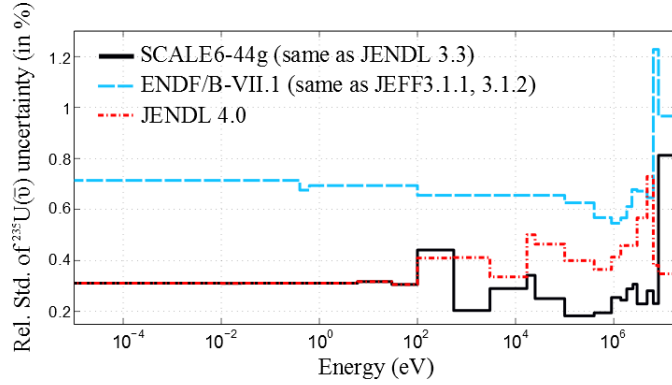


Figure 3.29: Relative standard deviation of $^{235}\text{U}(\bar{\nu})$ nuclear data from SCALE6-44g (taken from JENDL-3.3) and ENDF/B-VII.1 libraries. The ENDF/B-VII.1 uncertainty is twice as much as the SCALE6-44g, resulting in higher k_{inf} uncertainty due to $^{235}\text{U}(\bar{\nu})$ for the UAM pin cell benchmarks.

With stochastic sampling, the propagation of nuclear data uncertainties to system response parameter other than the multiplication factor (k_{eff} , k_{inf}) can be easily investigated. One-group reaction rate (R) and flux (ϕ) have been tallied in MCNPX and used to determine the one-group fission and absorption cross sections (Σ), as well as the associated one-group uncertainties due to nuclear data uncertainties:

$$\Sigma_g = \frac{R_g}{\phi_g}, \quad \bar{\Sigma}_g = \frac{1}{N} \sum_{i=1}^N \Sigma_{g,i} \quad \text{and} \quad \text{VAR}(\Sigma_g) = \frac{1}{N-1} \sum_{i=1}^N (\Sigma_{g,i} - \bar{\Sigma}_g)^2. \quad (3.13)$$

^{235}U and ^{238}U cross sections are perturbed simultaneously and their uncertainties are propagated through MCNPX. Table 3.4 shows the one-group cross sections and relative standard deviations (with a sample size of 130). Their values are compared to the corresponding results obtained from CASMO-5MX stochastic sampling calculations published in [44].

3.7. UACSA application by NUSS-SRS

	NUSS		CASMO-5MX/SS	
	Value	relstd (%)	Value	relstd (%)
PB-2 HZP				
$^{235}\text{U } \Sigma_f$	49.70	0.924	49.69	1.020
$^{235}\text{U } \Sigma_a$	60.50	0.810	60.47	1.010
$^{238}\text{U } \Sigma_f$	0.0934	3.740	0.0939	3.760
$^{238}\text{U } \Sigma_a$	0.923	1.190	0.915	1.090
PB-2 HFP				
$^{235}\text{U } \Sigma_f$	33.10	1.12	32.8	1.23
$^{235}\text{U } \Sigma_a$	41.09	0.96	40.72	1.23
$^{238}\text{U } \Sigma_f$	0.086	4.80	0.088	4.55
$^{238}\text{U } \Sigma_a$	0.86	1.37	0.85	1.10
TMI-1 HZP				
$^{235}\text{U } \Sigma_f$	35.20	0.93	35.28	1.05
$^{235}\text{U } \Sigma_a$	43.49	0.82	43.57	1.05
$^{238}\text{U } \Sigma_f$	0.101	3.49	0.101	3.59
$^{238}\text{U } \Sigma_a$	0.919	1.19	0.911	1.10
TMI-2 HFP				
$^{235}\text{U } \Sigma_f$	34.40	0.98	34.31	1.07
$^{235}\text{U } \Sigma_a$	42.56	0.85	42.44	1.06
$^{238}\text{U } \Sigma_f$	0.100	3.95	0.101	3.62
$^{238}\text{U } \Sigma_a$	0.941	1.27	0.934	1.11

Table 3.4: One-group cross sections with relative standard deviations (relstd) are calculated from multigroup reaction rates and fluxes which are perturbed due to nuclear data uncertainty in NUSS. Note that absorption cross section (Σ_a) here includes fission cross section (Σ_f).

3.7 UACSA application by NUSS-SRS

In modern criticality safety assessment (CSA) studies, the use of a specific computer modelling code and nuclear data library is validated against suitable experimental evidence. Uncertainties from sources such as nuclear data however can permeate throughout criticality calculations, and contribute to the discrepancy between calculated and experimental values. The OECD/NEA/WPNCs Expert Group on Uncertainty Analyses for Criticality Safety Assessment (UACSA) has been organized for the exact purpose to compare different CSA validation methods (see Fig.3.30). Specifically, UACSA-Phase I focuses on the propagation of nuclear data uncertainty [63]. Technological parameter uncertainties are considered in UACSA-Phase II and implicit sensitivity coefficient effects in UACSA-Phase III.

PSI's participation in UACSA-Phase I is an application of the existing PSI CSA methodology, based on a "validation suite" of 149 benchmarks which were selected from the ICSBEP handbook with certain criteria [64]. They are representative of Swiss Light Water Reactor (LWR) spent fuel configurations in terms of fuel enrichment, moderation ratio, fuel rod pitch size and spectrum-related observables such as the average neutron energy causing fission, average neutron lethargy causing fission, etc. The coverage of the selected parameters is associated

Chapter 3. Evaluating NUSS-SRS against existing methods and its applications

Organisation Country	Criticality Calculation		Validation of Criticality Calculation		
	Code	Nuclear Data	Similarity Assessment	Method for Bias and Bias Uncertainty Establishment	Software Tool
AREVA Germany	SCALE 5.1 [2] Monte Carlo	ENDF/B-V 44-gr. or 238-gr. ENDF/B-VI 238-gr.	<i>S/U-based parameter c_k</i> [3]. <i>Expert judgment</i>	Bayesian MC regression analysis [4]	TSUNAMI-IP MOCADATA
CEA France	CRISTAL [5] (TRIPOLI-4.3) Monte Carlo	JEF-2.2 CE (Continuous Energy)	Benchmark quality. <i>S/U-based parameter r</i> . <i>Sensitivity profiles calculated using APOLLO2 code and multigroup cross sections</i>	Representativity method (GLLSM based)	R.I.B. [6]
EMS Sweden	SCALE 5.1 Monte Carlo	ENDF/B-VI 238-gr.	<i>Expert judgment</i> based on benchmark quality. <i>S/U-based parameter c_b</i> . Other parameters may be used.	<i>Expert judgment,</i> <i>including</i> <i>consideration of</i> <i>benchmark quality</i> <i>and correlations</i> [7]	TSUNAMI-IP
JAEA Japan	MVP II [8] Monte Carlo	JENDL-3.2 CE	<i>Expert judgment</i>	Statistical method	None
IPPE Russia	MMKKENO [9] Monte Carlo	ABBN 299-gr. Subgroups	Benchmark quality. <i>Sensitivity comparison,</i> χ^2 filter, <i>Expert judgment</i>	GLLSM based	INDECS [10]
IRSN France	CRISTAL (APOLLO2- MORET 4) Monte Carlo	CEA93.V6 (JEF-2.2 172-gr.)	Physical parameters, <i>Expert judgment</i>	Trending analysis (trend vs combined parameters)	MACSENS [11]
KINS Korea	SCALE 6.0 [12] Monte Carlo	ENDF/B-VII.0 238-gr.	EALF, <i>S/U-based parameter c_k</i> . <i>Expert judgment</i>	Statistical method	TSUNAMI-IP
ORNL USA	SCALE 6.0 Monte Carlo	ENDF/B-VII.0 238-gr.	H/X, EALF and others or <i>S/U-based parameter c_k</i>	Trending analysis	USLSTATS TSUNAMI-IP
			<i>S/U-based parameter c_k</i> χ^2 filter	GLLSM based	TSURFER
PSI Switzerland	MCNPX [13] Monte Carlo	ENDF/B-VII.0 CE JEFF-3.1 CE	<i>Expert judgment,</i> <i>benchmark quality and</i> <i>analysis of physical</i> <i>parameters</i>	Statistical method	None

Figure 3.30: Summary of participants, criticality codes, nuclear data, criticality validation methods, and software tools in UACSA-Phase I.

to the so-called Area of Applicability (AoA). According to the ANSI/ANS-9.1-1998 Standard for *Nuclear Criticality Safety in Operation with Fissionable Materials Outside Reactors*, AoA is defined as [65]:

The limiting ranges of material compositions, geometric arrangements, neutron energy spectra, and other relevant parameters (such as heterogeneity, leakage, interaction, absorption, etc.) within which the bias of a calculational method is established.

For each of the 149 benchmarks, MCNPX is used to compute the k_{eff} (denoted as k_n^{cal} for

$n = 1, \dots, 149$). The k_{eff} value difference to the respective experimental k_{eff} (denoted as k_n^{bench}) is the computational bias β_n . Over the 149 cases, a weighted average of computational bias $\langle \beta_c \rangle$ is determined as:

$$\langle \beta_c \rangle = \frac{\sum_{n=1}^N w_n \beta_n}{\sum_{n=1}^N w_n} \quad \text{where} \quad \beta_n = k_n^{\text{cal}} - k_n^{\text{bench}} \quad \text{and} \quad w_n = \frac{1}{\sigma_n^2} \quad (3.14)$$

The individual uncertainty of parameter β_n is determined by

$$\sigma_n = \sqrt{(\sigma^{\text{bench}})_n^2 + (\sigma^{\text{cal}})_n^2} \quad (3.15)$$

where σ^{bench} is the benchmark uncertainty reported in the ICSBEP Handbook and σ^{cal} is the MCNPX statistical uncertainty which can be reduced by the user-defined neutron history size (about 20 pcm in all calculations presented here). As $\sigma^{\text{cal}} \ll \sigma^{\text{bench}}$, experiments with a smaller σ^{bench} are considered more important, hence are given more “weight” to the calculation of $\langle \beta_c \rangle$. Calculated by MCNPX with nuclear data libraries JEFF-3.1 and ENDF/B-VII.0, the distribution and values of β_n are shown in Fig.3.31.

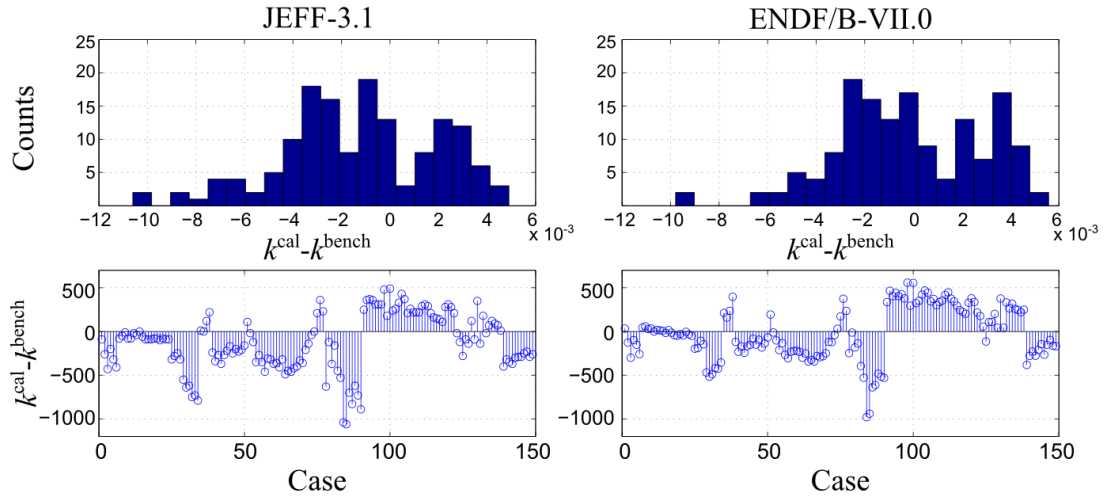


Figure 3.31: The values of $k^{\text{cal}} - k^{\text{bench}}$ are shown in histograms and by benchmark cases.

The spread of the individual β_n is quantified by Eqn.(3.16). Together with $\langle \beta_c \rangle$, their values are shown in Table 3.5. The computational bias is positive in the case of ENDF/B-VII.0 and much less than that of JEFF-3.1, suggesting the improvement of nuclear data quality leading to smaller individual computational biases. On the other hand, the change of library affects only slightly the value of s , which indicates the dispersion of β_n is contributed more by benchmark experimental and modelling uncertainties than nuclear data uncertainty.

$$s = \left[\frac{\frac{1}{N-3} \sum_{n=1}^N w_n \cdot (\beta_n - \langle \beta_c \rangle)^2}{\frac{1}{N} \sum_{n=1}^N w_n} \right]^{1/2} \quad (3.16)$$

Chapter 3. Evaluating NUSS-SRS against existing methods and its applications

Library	$\langle \beta_c \rangle$	s
JEFF-3.1	-97 pcm	348 pcm
ENDF/B-VII.0	+9 pcm	325 pcm

Table 3.5: Change of nuclear data libraries affect computational bias β_c but the spread of individual bias (s) is less affected.

Next, the UACSA-Phase 1 exercise requested participants to apply their methodologies to predict the value of k_{eff} for an application case. The predicted k_{eff} is estimated by adjusting the calculated k_{eff} with the computational bias:

$$k_{\text{app}}^{\text{pred}} = k_{\text{app}}^{\text{cal}} - \beta_c \quad (3.17)$$

One of the suggested application cases is the LCT-040-010 benchmark from the ICSBEP Handbook. Fig.3.32 shows that four 18×18 rod assemblies of uranium dioxide are contained in borated square canister; they are water-moderated and reflected by A33-type steel. The UO_2 fuel rods have an enrichment of 4.738% by weight and the cladding of aluminum alloy AGS. The configuration approximates the physical condition of shipping casks and high-density fuel-assembly storage [47]. The experiment was conducted at CEA in the late 1970s, via a subcriticality approach extrapolated to criticality. Hence it serves as an application, even though its experimental k_{eff} and uncertainty are known already. With JEFF-3.1 and ENDF/B-VII.0 nuclear data, the MCNPX-calculated k_{eff} values and statistical uncertainties of the LCT-040-010 benchmark are presented in Table 3.6. The difference between the calculated and the actual (experimental) k_{eff} is defined as the observed bias; it is on the same order of magnitude as the experimental k_{eff} uncertainty (Δk^{bench}).

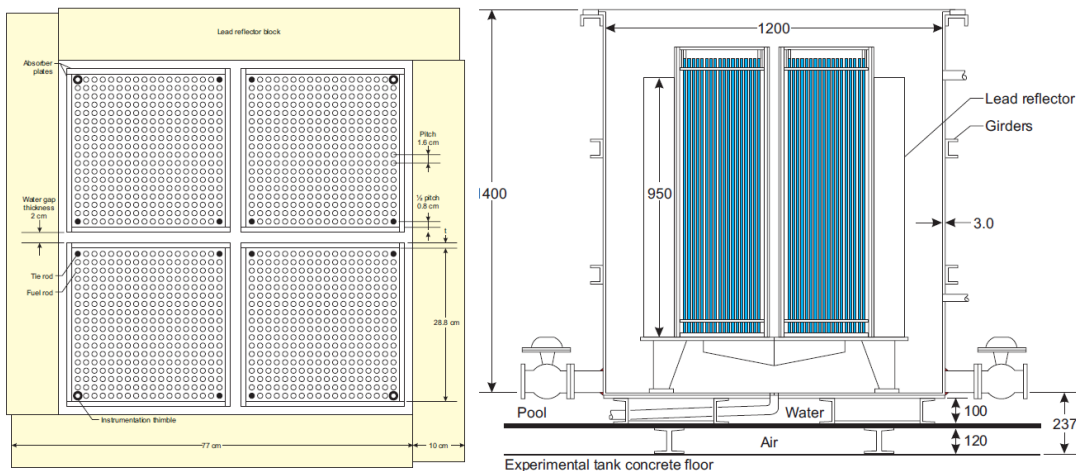


Figure 3.32: The bird view and vertical cross section view of the “LCT-040-010” experiment apparatus.

Focusing on the case of ENDF/B-VII.0 library, the predicted k_{eff} (see Eqn.(3.17)) and calculated k_{eff} are compared in Fig.3.33. PSI results are plotted as “Participant 1” and the difference

3.7. UACSA application by NUSS-SRS

k^{bench}	Δk^{bench}	library	k^{mcnpX}	β^{obs}
1.00000	460 pcm	JEFF-3.1	$0.99500 \pm 20\text{pcm}$	-500 pcm
		ENDF/B-VII.0	$0.99428 \pm 17\text{pcm}$	-572 pcm

Table 3.6: Δk^{bench} is the benchmark experimental k_{eff} uncertainty. The observed bias is $\beta^{\text{obs}} = k^{\text{mcnpX}} - k^{\text{bench}}$.

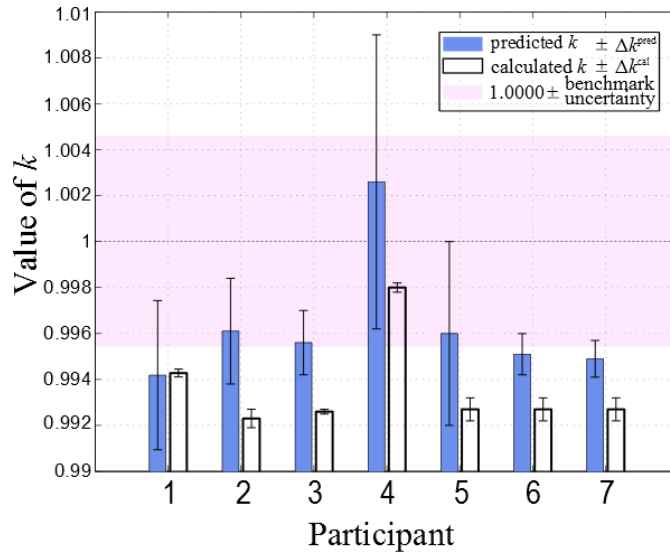


Figure 3.33: PSI results are plotted under “Participant 1”. The predicted k is calculated from Eqn.(3.17). The Δk^{pred} value is given by s from Eqn(3.16).

between k^{pred} and k^{cal} is the value of $\langle \beta_c \rangle$, equal to 9 pcm as shown in Table 3.5. Results of other participants of UACSA-1 using LCT-040-010 benchmark are also plotted. All k^{cal} values are outside the experimental uncertainty of the critical k^{exp} value, except for Participant 4 (from JAEA). Note that in the original PSI contribution to UACSA-1 and in [66], application case experimental uncertainty and MCNPX statistical uncertainty are included in the Δk^{pred} as $\sqrt{s^2 + \sigma_{\text{spec}}^2 + \sigma_{\text{MC}}^2}$. Here Δk^{pred} only contains s and benchmark uncertainty (σ_{spec}) is given separately.

As a further assessment for the application case bias uncertainty quantification, NUSS-SRS has been applied to compute the uncertainty of the observed bias due to nuclear data uncertainties (denoted as ΔND). The uncertainties of ^{235}U and ^{238}U are taken from the SCALE-6 covariance library⁴ and propagated by NUSS (with ENDF/B-VII.0 ACE files) for the calculated k_{eff} . The total uncertainty contribution from both ^{235}U and ^{238}U is found to be 562 pcm (95% confidence interval at [491pcm, 657pcm]). This is greater than the experimental uncertainty of 460pcm (Δk^{bench} in Table 3.6), which suggests the uncertainty values of ^{235}U and ^{238}U could be over-estimated. Top uncertainty contributors are obtained by running NUSS-SRS independently for each isotope-reaction. The results are plotted in Fig.3.34 and compared with the TSUNAMI

⁴The covariances of ^{235}U and ^{238}U in SCALE6-44g library are taken from ENDF/B-VII.0 covariances

Chapter 3. Evaluating NUSS-SRS against existing methods and its applications

results which were reported in [67]. They have used TSUNAMI-3D with ENDF/B-VI nuclear data and SCALE5-44g covariance library.

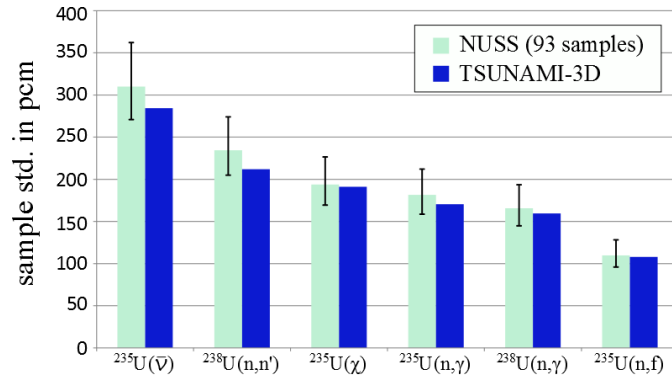


Figure 3.34: Top uncertainty contributors for LCT-040-010 benchmark are calculated by NUSS. From 93 samples and at 95% confidence interval, they are in good agreement with the TSUNAMI results reported at OECD/NEA WPNCs EG UACSA 2nd meeting, 2008.

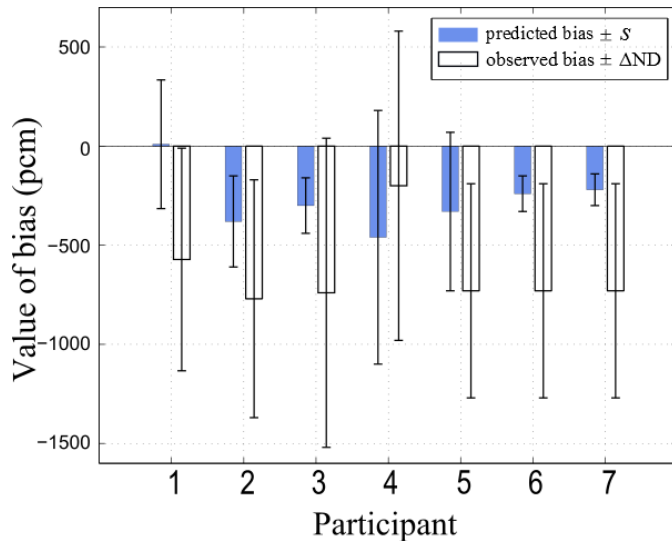


Figure 3.35: Predicted bias $\langle \beta_c \rangle$ and uncertainty s by Eqn.(3.14) and Eqn.(3.16) are plotted under “Participant 1”. Nuclear data uncertainty (^{235}U and ^{238}U from SCALE6-44g library) contribution component of the observed bias uncertainty is shown.

Finally, both the predicted and observed biases with respective uncertainties are plotted in Fig.3.35, where participant 1 corresponds to PSI results. Recall the predicted bias and uncertainty are results of the chosen computational method (i.e. the use of MCNPX and ENDF/B-VII.0 nuclear data library for PSI), but they have not considered nuclear data uncertainties in Eqn.(3.14) and (3.16). Currently, the lower limit of the predicted bias uncertainty (i.e. predicted bias - s) does not cover the observed bias of -572pcm for the application case, which is also observed in other participants’ results (except for participant 4). It is again reminded

that for this application case, the experimental uncertainty is in fact known (460pcm) which could explain the relatively large observed bias. However, for future CSE applications which are without experimental value and uncertainties, the quantification of nuclear data uncertainty becomes imperative and will be accomplished by NUSS-SRS in future works: the values of computational bias and s of the current PSI CSE methodology are updated by including nuclear data uncertainties into Eqn.(3.15) for each of the validation suite benchmarks:

$$\sigma_n = \sqrt{(\sigma^{\text{bench}})_n^2 + (\sigma^{\text{cal}})_n^2 + (\sigma^{\text{ND}})_n^2} \quad (3.18)$$

Chapter's key message

The focus of this chapter was to demonstrate the proof-of-concept of the NUSS-SRS tool for the propagation of nuclear data uncertainties through MCNPX. It has been shown that for problems of various complexity (from simple spherical assembly, pin cell model to fuel-rod assembly), NUSS-SRS was successful at obtaining the same k_{eff} uncertainty due to nuclear data uncertainties as the other existing methods such as TSUNAMI, PERT CARD. The verification of the implementation of NUSS-SRS lays the foundation for the development of global sensitivity analysis in the sampling manner in the next chapter.

4 Introducing variance-based global sensitivity analysis

In Chapter 3, the stochastic-sampling based NUSS tool has been compared and verified with both the “Sandwich Rule” and existing stochastic-sampling methods. This chapter begins with the motivation for developing in NUSS the capability to conduct sensitivity analysis, followed by the theory and methods of the FAST and RBD methods. The derivation of variance decomposition by the local-based “Sandwich Rule” method is also given so that it shall provide verification and comparison for NUSS in Chapter 5.

4.1 Motivation for global sensitivity analysis

Sensitivity analysis is needed when in addition to the total propagated uncertainty, the knowledge of the proportions of top input uncertainty contributors is desired. For the nuclear data measurement community, identifying important inputs assists in the prioritization of more accurate and precise experiments, such that on the reduction in their uncertainty level can lead to significant reduction of uncertainty in nuclear system calculations. NUSS is a “global” approach, where the nuclear data input variations depend on assumed probability density functions. This global approach works for a wide range of applications regardless of the linearity of the system. However, it becomes inefficient when in addition to the total uncertainty contribution, individual nuclear data uncertainty contribution is desired. For every case of comparison between NUSS and another method in Chapter 3, each isotope-reaction uncertainty quantification is done independently, by running hundreds of MCNPX calculations. Given the abundance of nuclear data inputs in terms of energy groups, reaction channels and many isotopes, the number of inputs renders the task of obtaining the uncertainty contribution of individual nuclear data by the simple random sampling-based NUSS to be inefficient. Using NUSS-SRS to determine the list of top uncertainty contributors without a priori knowledge of the ranking of their contribution, becomes especially computation-prohibitive for complex systems.

The problems of large input set and complex system simulation are certainly not unique to nuclear data uncertainty quantifications. These problems have been tackled by global

sensitivity analysis for diverse applications such as chemical reaction rate [68], nuclear waste depository [69] and hydrology studies [70]. Existing methods previously developed for other applications are adopted in the second stage of NUSS tool development to expand NUSS's capability to derive individual nuclear data uncertainty contributions. The flexibility as a global-based method and the advantage of working with ACE-formatted nuclear data in continuous-energy code MCNPX can also be maintained.

Presented in Chapter 3.5, a method based on the squared value of Pearson/Spearman correlation coefficient was shown to be able to apportion individual input variance contributions, using the existing randomly sampled results. The limitation however is the requirement of linear relation between input and output. A more general theory of variance analysis is in demand, both to validate the aforementioned simplistic approach and to anticipate problems of non-linear nature.

4.2 Variance decomposition by global sensitivity analysis

The sensitivity of the system to inputs is measured by the variance contribution due to individual inputs. The rational is, an important input to which the output is very sensitive, is responsible for a large portion of the output variance. It is not to be confused with the sensitivity coefficient of the Sandwich Rule, which describes only the linear relation between the system response and input, and is not affected by the input uncertainties.

For a single variable function $f(x)$ with $p(x)$ as the probability density function (PDF) of x , the expectation and variance of $f(x)$ are respectively:

$$E[f(x)] = \int f(x)p(x)dx$$

$$V[f(x)] = \int f^2(x)p(x)dx - \left(\int f(x)p(x)dx\right)^2$$

When a model has multiple inputs, $f(\vec{x}) = f(x_1, \dots, x_n)$, the joint PDF of inputs can be expressed as

$$p(\vec{x}) = \begin{cases} p(x_1, \dots, x_n) & \text{for correlated inputs} \\ \hat{p}(x_1)\hat{p}(x_2)\cdots\hat{p}(x_n) & \text{for uncorrelated inputs} \end{cases} \quad (4.1)$$

where $\hat{p}(x_i)$ is called the marginal probability density distribution.

Hence, the expectation and variance of a multidimensional function $f(\vec{x})$ are

$$E_f = E[f(\vec{x})] = \int f(\vec{x})p(\vec{x})d\vec{x} \quad (4.2)$$

$$V_f = V[f(\vec{x})] = \left(\int f^2(\vec{x})p(\vec{x})d\vec{x}\right) - (E[f(\vec{x})])^2 \quad (4.3)$$

4.2. Variance decomposition by global sensitivity analysis

The derivation of the input variance contribution is demonstrated through a two-input function $f(s, t)$ in Fig.4.1, where the sampled values of $f(s, t)$ are plotted against the variation of input s along the x-axis. The dependence on input t manifests as the dispersed sampled values along the y-axis. The red curve corresponds to the conditional expectation of f when s is fixed (i.e. “conditioned”) at various values (s') according to $\hat{p}(s)$. The conditional probability density at each fixed s' is:

$$\tilde{p}_t = p(s, t|s') = \begin{cases} \frac{p(s, t)}{\hat{p}(s)} & \text{if } s \text{ and } t \text{ are correlated} \\ \frac{\hat{p}(s)\hat{p}(t)}{\hat{p}(s)} = \hat{p}(t) & \text{if } s \text{ and } t \text{ are uncorrelated} \end{cases} \quad (4.4)$$

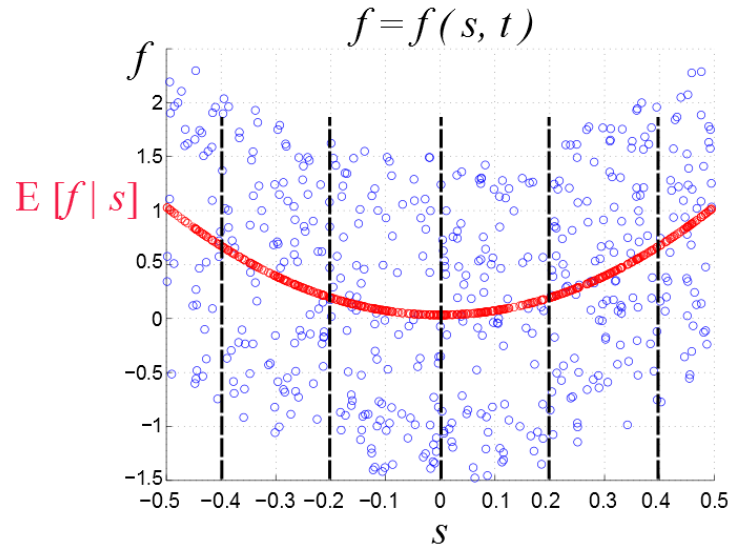


Figure 4.1: Illustration of the formulation of the variance of f due to input s uncertainty.

The variance of the conditional expectation $E[f(s, t|s')]$, i.e. the variance of the values along the red curve in Fig.4.1 is calculated as:

$$\begin{aligned} & V[E[f(s, t|s')]] \\ &= \int (E[f(s, t|s')])^2 \hat{p}(s') ds' - \left(\int E[f(s, t|s')] \hat{p}(s') ds' \right)^2 \end{aligned} \quad (4.5)$$

$$\begin{aligned} &= \int \left(\int f(s, t|s') \tilde{p}_t dt \right)^2 \hat{p}(s') ds' - \left(\int \left(\int f(s, t|s') \tilde{p}_t dt \right) \hat{p}(s') ds' \right)^2 \\ &= \int \left(\int f(s, t|s') \tilde{p}_t dt \right)^2 \hat{p}(s') ds' - \left(\int f(s, t|s') p(s', t) ds' dt \right)^2 \quad \text{using Eqn.(4.1)} \\ &= \int \left(\int f(s, t|s') \tilde{p}_t dt \right)^2 \hat{p}(s') ds' - (E[f])^2 \end{aligned} \quad (4.6)$$

Eqn.(4.6) is the analytical formula for the variance of conditioned input variable s which could

be computed numerically by evaluating the double-integrals in the brute-force manner: the total number of f evaluation is equal to $N_s \times N_t + N_{st}$ where N_s is the sampling points from $\hat{p}(s)$, N_t from \tilde{p}_t , and N_{st} from the joint PDF $p(s, t)$ for $E[f]$. Even if using only 100 samples for each of N_s , N_t and N_{st} , the number of total sample runs to determine the variance contribution of each input can become prohibitive. Clearly, brute-force method is better reserved for problems with small input dimensions, which often are the opposite for nuclear data uncertainty quantification problems. The alternative approach is explained in the following sections.

4.3 Theory of FAST for uncorrelated inputs

The Fourier Amplitude Sensitivity Test (FAST) method was proposed by Cukier et.al. [68], aiming to apportion the total output variance by individual input parameters. The fundamental idea is to simultaneously vary all input variables \vec{x} by a single control parameter s . Instead of sampling randomly to compute the double integrals of Eqn.(4.6) as in the case of "blackbox" simple random sampling, a transformation of the K inputs x_i of the model $f(\vec{x})$ is shown in Eqn.(4.7) where the individual x_i is dependent on frequency ω_i and a control parameter s :

$$x_i = \frac{1}{2} + \frac{1}{\pi} \arcsin(\sin(\omega_i s)) \quad \text{where } -\pi \leq s \leq \pi, \text{ and } i = 1, 2, \dots, K \quad (4.7)$$

According to the Weyl Theorem [71], it is true that,

$$\int_{\Omega^K} (f(\vec{x}))^m d\vec{x} = \lim_{T \rightarrow \infty} \frac{1}{2T} \int_{-T}^T (f(\vec{x}(s)))^m ds \quad \text{where } m = 1, 2, 3, \dots \quad (4.8)$$

given $(x_1(s), x_2(s), \dots, x_K(s))$ is a well-designed exploring curve which can get arbitrarily close to any point \vec{x} in the K -dimensional input space Ω^K (so-called "space-filling") as the path of integration from $s = -\infty$ to $+\infty$. Since numerical integration between $-\infty$ to $+\infty$ is impossible, integer frequencies ω_i are used such that the integration can be done on a closed loop of period $T = 2\pi$, instead of the asymptotically space-filling curve. With an exemplary 3-input case, $\vec{x} = \{x_1, x_2, x_3\}$, Fig.4.2 shows the transformed values of x_1 , x_2 and x_3 , controlled by a single s through Eqn.(4.7) with different ω values associated with each x . The trajectory of $(x_1(s), x_2(s), x_3(s))$ is plotted in Fig.4.3 which is periodic between $(0,0,0)$ and $(1,1,1)$ because of the use of integer ω values.

Next, the value of m in Eq.(4.8) is set to 1 and 2 :

$$\int_{\Omega^K} f(\vec{x}) d\vec{x} \approx \frac{1}{2\pi} \int_{-\pi}^{\pi} f(s) ds \quad (4.9)$$

$$\int_{\Omega^K} f^2(\vec{x}) d\vec{x} \approx \frac{1}{2\pi} \int_{-\pi}^{\pi} f^2(s) ds \quad (4.10)$$

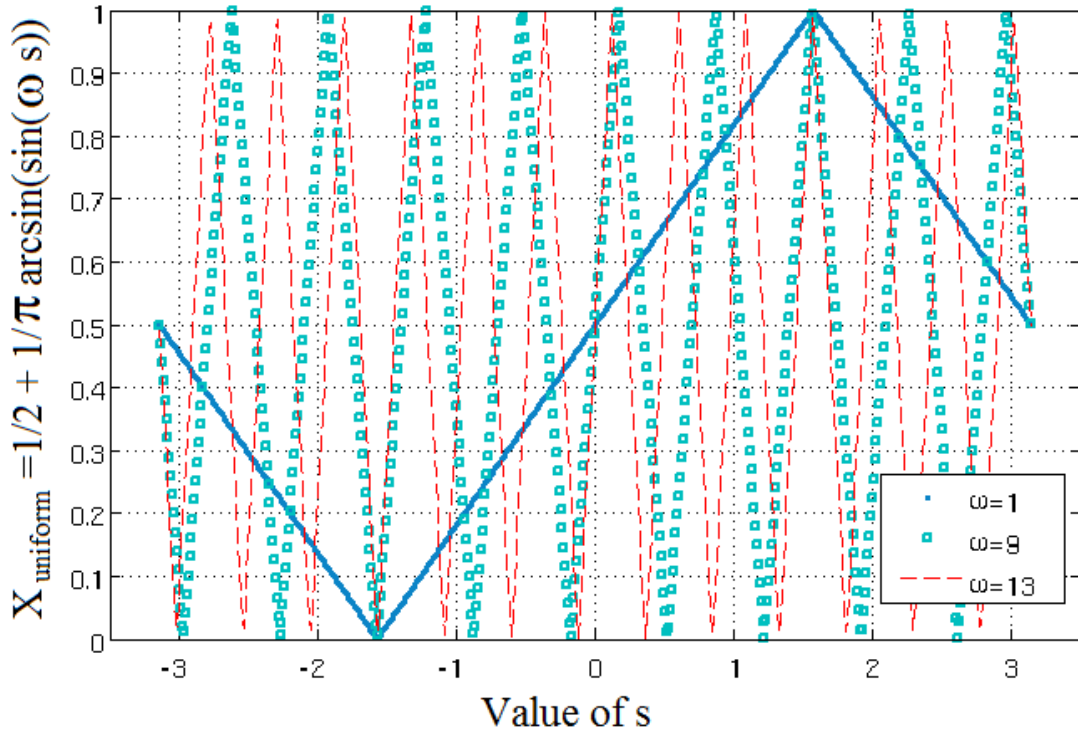


Figure 4.2: Periodic X values are generated simultaneously with ω and the control variable s .

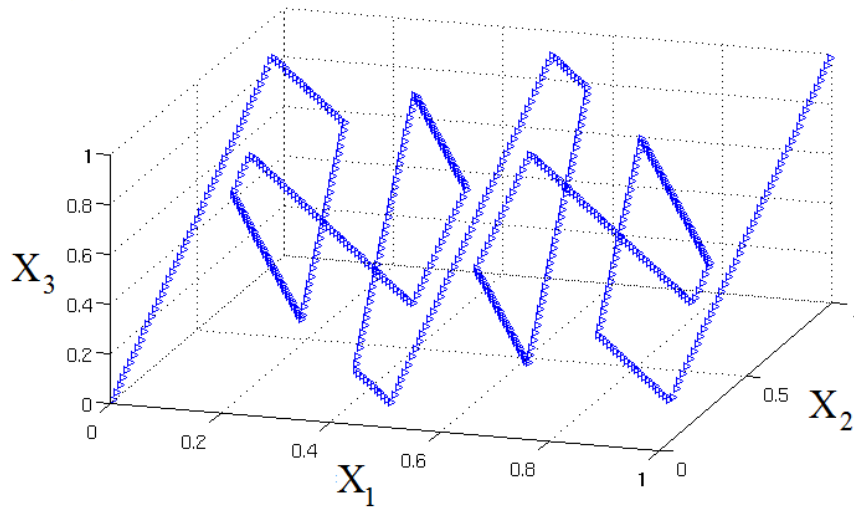


Figure 4.3: As s varies, the same path shown here is traced periodically by input points in the input space (x_1, x_2, x_3) as a result of the individual periodic inputs in Fig.4.2.

which allows the evaluation of variance of $f(\vec{x})$ by the variance of $f(s)$:

$$V[f] = \int f^2(\vec{x}) d\vec{x} - \left(\int f(\vec{x}) d\vec{x} \right)^2 \approx \frac{1}{2\pi} \int_{-\pi}^{\pi} f^2(s) ds - \left(\frac{1}{2\pi} \int_{-\pi}^{\pi} f(s) ds \right)^2 \quad (4.11)$$

Chapter 4. Introducing variance-based global sensitivity analysis

The purpose of parametrizing x_i in Eqn.(4.7) is the effective retrieval of the frequency-dependence associated to individual input x_i when the model output $f(s)$ is analyzed in terms of Fourier series:

$$f(s) = \sum_{\omega=-\infty}^{\infty} (A_{\omega} \cos(\omega s) + B_{\omega} \sin(\omega s)) = A_0 + 2 \sum_{\omega=1}^{\infty} (A_{\omega} \cos(\omega s) + B_{\omega} \sin(\omega s)) \quad (4.12)$$

A_0 is the value of $f(s)$ at $s = 0$ and $f(s)$ is symmetric for real-valued $f(\vec{x})$ values. Substituting Eqn(4.12) into Eqn(4.11) gives the simple formulation of $V[f]$ in terms of the Fourier coefficients A_{ω} and B_{ω} :

$$\begin{aligned} V[f] &= \int f^2(\vec{x}) d\vec{x} - \left(\int f(\vec{x}) d\vec{x} \right)^2 \\ &\approx \frac{1}{2\pi} \int_{-\pi}^{\pi} |f(s)|^2 ds - \left(\frac{1}{2\pi} \int_{-\pi}^{\pi} f(s) ds \right)^2 \\ &= 2 \sum_{\omega=1}^{\infty} (A_{\omega}^2 + B_{\omega}^2) \quad (\text{see derivation in Appendix A8}) \\ &= 2 \sum_{\omega=1}^{\infty} \Lambda_{\omega} \end{aligned}$$

where $\Lambda_{\omega} = A_{\omega}^2 + B_{\omega}^2$ is called the power spectrum of $f(s)$. The interpretation of the power spectrum is that $f(s)$ is a signal and each frequency contains a portion of the signal's power. Hence the larger the amplitude (i.e. portion) in certain frequency, the more important (i.e. the output is sensitive to) the corresponding input is.

Since each ω_i is associated to the original x_i , the variance contribution from input $x_i(\omega_i, s)$ can be determined by adding its harmonics (as selected by integer h) of the corresponding frequency ω_i as depicted in Fig.4.4:

$$V_i = 2 \sum_{h=1}^{\infty} (A_{h \times \omega_i}^2 + B_{h \times \omega_i}^2) \quad (4.13)$$

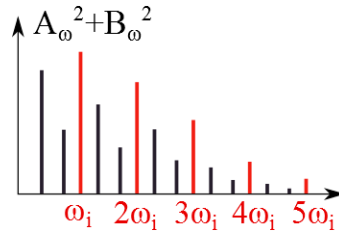


Figure 4.4: Schematic of the power spectrum. The variance contribution of each input is equal to the summation of the harmonics of the corresponding ω_i components.

Limitation of FAST in terms of input size

In Eqn.(4.13), when $h \times \omega_i$ of V_i and $h' \times \omega_j$ of V_j are multiples of each other, an “interference in harmonics” occurs due to the use of integer frequency values. Continuing with the example in Fig.4.2, the individual variance contributions are:

$$\begin{aligned} \text{For } x_1 : \omega_1 = 1, \quad V_1 &= 2 (\Lambda_1 + \Lambda_2 + \Lambda_3 + \dots + \Lambda_9 + \dots + \Lambda_{13} + \dots) \\ x_2 : \omega_2 = 9, \quad V_2 &= 2 (\Lambda_9 + \Lambda_{18} + \Lambda_{27} + \dots) \\ x_3 : \omega_3 = 13, \quad V_3 &= 2 (\Lambda_{13} + \Lambda_{26} + \Lambda_{39} + \dots) \\ V_{\text{total}} &= 2 \sum_i \Lambda_i \end{aligned}$$

In V_1 , there are contribution from Λ_9 and Λ_{13} which are the first harmonics of V_2 and V_3 power spectra. Input x_1 is said to be in interference with x_2 at the 9th harmonic because V_1 and V_2 are no longer calculated from independent sets of Λ values. Similarly, x_1 and x_3 interfere at the 13th harmonic, x_2 and x_3 at the 9×13 th harmonic.

The effect of interference can be seen in Fig.4.5 where the variance fractions of inputs (i.e. $\frac{V_i}{V_{\text{total}}}$) in an example model $Y = X_1 + X_2 + X_3$ are calculated. The analytical solution of V_i/V_{total} is equal to $\frac{1}{3}$ for all three inputs. Calculated by FAST, the values of variance fraction, V_i/V_{total} as a function of harmonics order are converged after harmonics order of 5 as shown in Fig.4.5. However, for input x_1 , its V_1/V_{total} value are observed to be augmented at the 9th and 13th harmonics because of the contributions from X_2 and X_3 variances: $9 \times \omega_1$ and $13 \times \omega_1$ coincide with $1 \times \omega_2$ and $1 \times \omega_3$. Hence, a maximum harmonics order of 8 should be set for this example to limit interferences. In general, the modified version of Eqn.(4.13) below is used to consider only up to the harmonics order M which is free of interference for a given set of N samples:

$$V_i = 2 \sum_{h=1}^{h=M} \Lambda_{h \times \omega_i} \tag{4.14}$$

For models with a small number of inputs, harmonics interference can be minimized by choosing frequencies which are far away from each other such that the summation of Eqn.(4.14) can keep a high harmonics order M , before reaching the first interference. The trade-off is however the minimum number of samples required to avoid “aliasing” effect as shown in Fig.4.6. For the reconstruction of the “true” (also unknown) signal with limited sample size, the minimum sampling rate, known as the Nyquist rate, has to be twice the maximum frequency component (i.e. $M \times \max(\omega_i)$). According to [68][72] the minimum sample size is calculated as:

$$N_{\text{min}} = 2 \times M \times \max(\omega_i) + 1 \tag{4.15}$$

Previously, the ω_i values are desired to be sparsely spaced from each other. Consequently N_{min} increases quickly as a function of the number of inputs, as shown in Fig.4.7. The choice of frequency values to avoid harmonics interference and the dependence of N_{min} on the

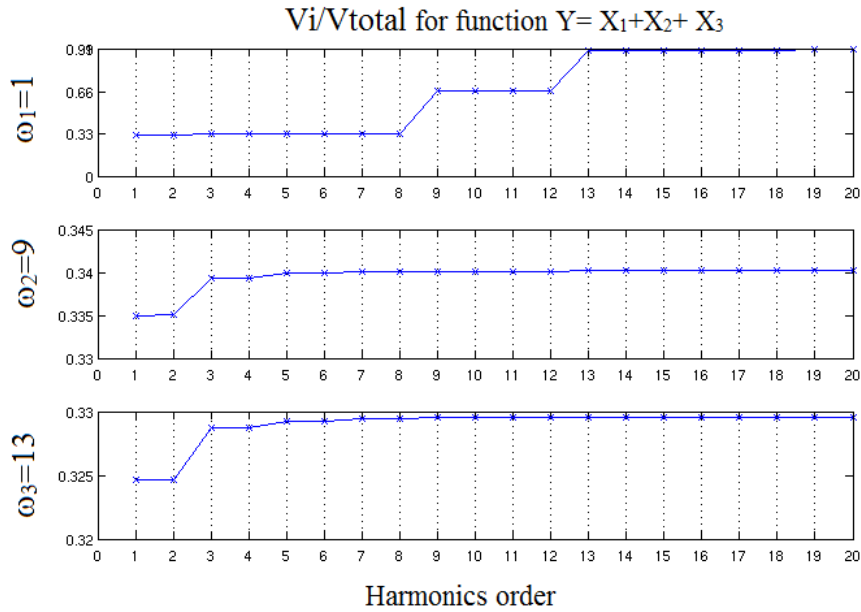


Figure 4.5: Interference of V_2 and V_3 in V_1 due to the overlapping Λ_9 and Λ_{13} .

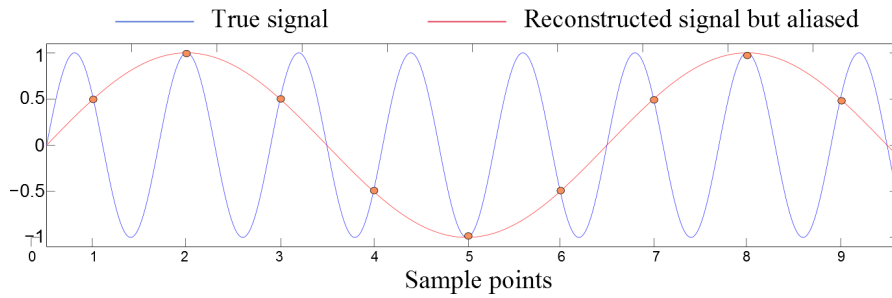


Figure 4.6: Aliasing occurs when the number of sample points is insufficient to reconstruct the true signal. Instead, a lower-frequency signal is made.

$\max(\omega_i)$ essentially limit the otherwise elegant FAST method from tackling problems of high dimensionality. Unfortunate for FAST, there are often more than 30 nuclear data inputs to be included to the uncertainty analysis.

4.4 RBD for correlated inputs

Random Balance Design (RBD) is based on the original (or sometimes called “classic”) FAST method described above. First proposed by Tarantola [73] for uncorrelated inputs, the RBD method has since been updated by Xu [74] to include correlations between inputs. Compared to the classic FAST, the first two steps of the RBD algorithm in the following are able to eliminate the dimensionality limitation:

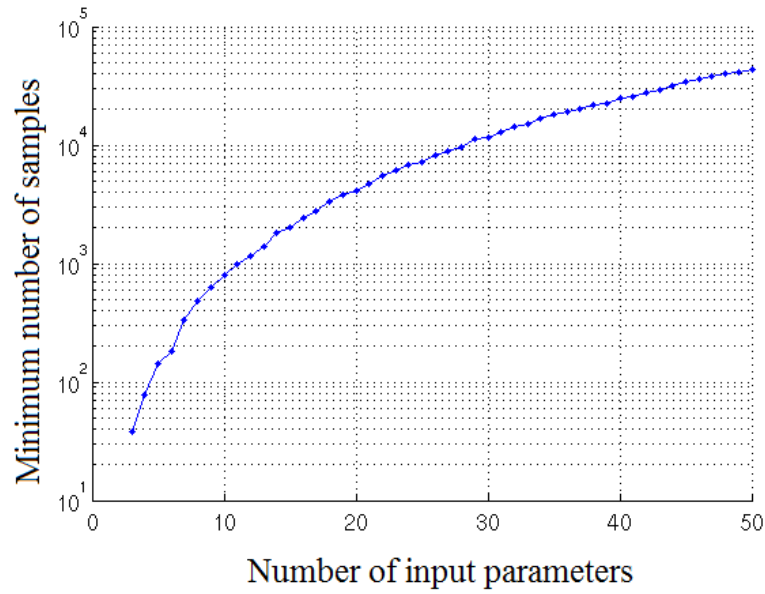


Figure 4.7: The minimum number of samples as a function of the number of input parameters according to Eqn.(4.15).

1. Instead of a unique frequency for each input, a common-frequency ω_c is used to generate $\vec{x}_c = \vec{x}(\omega_c, s)$ where effectively, $\vec{x}_1 = \vec{x}_2 = \vec{x}_3 \cdots \vec{x}_K$ and elements inside \vec{x}_c follow the standard normal distribution.
2. Create a matrix \tilde{X} in which the row vectors \tilde{x}_i have elements from independent permutations of the original vector \vec{x}_c elements.

$$\tilde{X} = \begin{pmatrix} \vec{x}_1 \\ \vec{x}_2 \\ \vdots \\ \vec{x}_K \end{pmatrix} \tag{4.16}$$

Fig.4.8 depicts the randomly permuted vector elements (right column) from the original \vec{x}_c (left column). Note that the permutation does not alter the respective probability density function of each vector \vec{x}_i . The order of permutation of each \vec{x}_i is recorded and will be used in Step (6). A second matrix \tilde{X}_s has to be created by “stretching” the permuted and standard-normal distributed elements in \tilde{x}_i according to the actual given values of mean and standard deviation of the corresponding nuclear data.

3. Correlations among the otherwise independent \vec{x}_i are imposed through the Iman-Conover’s method [75]: the desired correlation is approximated by a rank correlation such that the desired correlation is attained not exactly, but asymptotically for large sample sizes:

- Similar to the NUSS-SRS method, a Cholesky decomposition of the nuclear data

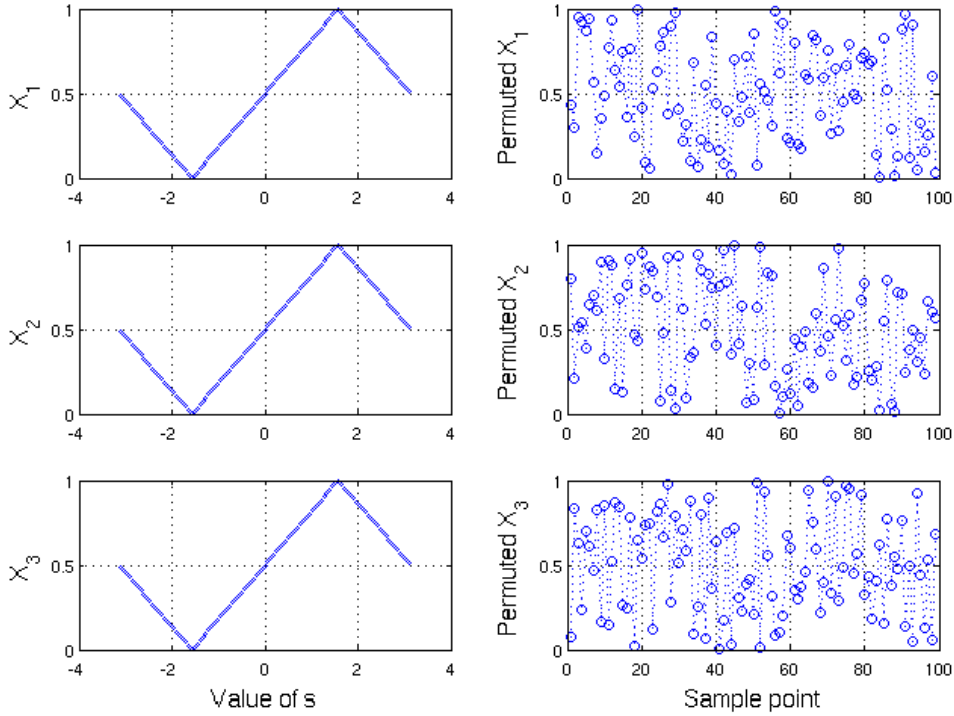


Figure 4.8: Permutation of the $x(s)$ values which are generated by the common frequency.

covariance matrix (V) is performed and the lower triangular matrix (A) is applied onto matrix \tilde{X} :

$$T = A \cdot \tilde{X} + M_o \quad (4.17)$$

with $M_o = [\bar{\mu} \bar{\mu} \bar{\mu} \cdots \bar{\mu}]$ is of size $[K \times N]$ and $\bar{\mu}$ is the column vector containing the mean values of the K inputs. Hence the row vectors of matrix T are correlated according to V and elements in each row vector still preserve the normal distribution.

- The ranking of elements in each row of T is obtained and the elements in the corresponding row of \tilde{X}_s are re-ordered using the ranking information, such that the rank correlation of \tilde{X}_s is the same as T .
4. Same as in NUSS-SRS, perturbation factors are obtained as the ratio between the newly sampled inputs (\tilde{X}_s) and their nominal values (M_o). They are applied to modify the ACE-formatted nuclear data.
 5. MCNPX is run using these perturbed nuclear data to obtain output values $\tilde{Y} = \{y_1, y_2, \dots, y_N\}$.
 6. For each of the i^{th} input, re-order $\{y_1, y_2, \dots, y_N\}$ according to the recorded orders in Step (2), i.e. in the initial order of samples for the i^{th} input before permutation.

The aforementioned steps are illustrated in Fig.4.9 at the end of this chapter using a generic two-input example model in [74]. At step 6a) and 6b), in order to recover the Fourier spectrum information carried by the $x(\omega_c, s)$ values prior to the random permutation, the output values are re-arranged. Each re-ordering leads to a distinct power spectrum Λ^i . The total variance is as the sum of amplitudes:

$$V_{\text{total}} = 2 \times \sum_{\omega=1} \Lambda_{\omega}^i \quad (4.18)$$

The total sum of Λ_{ω}^i is always the same for any i . The partial variance due to i^{th} input is estimated by summing the amplitudes of the power spectrum at the multiples of the characteristic frequency up to a user-defined harmonics order M :

$$V_i = 2 \times \sum_{h=1}^M \Lambda_{h \times \omega_c}^i \quad (4.19)$$

4.5 Variance decomposition by Sandwich Rule

In Chapter 3.5, it has been shown that the computation of individual input variance contribution can result in a different ranking of “important inputs” from that based on sensitivity coefficients. Since sensitivity coefficient is the local rate of change of the output parameter due to input variation, it is a property of the system. Its derivation is either based on the assumption of a linear system or is limited to the consideration of input uncertainties around the nominal local input (α) values and system response (R):

$$V(R) = SVS^T = \sum_{i=1} \left(\frac{\partial R}{\partial \alpha_i} \right)^2 \cdot \text{VAR}(\alpha_i) + \sum_{i=1} \sum_{j \neq i} \left(\frac{\partial R}{\partial \alpha_i} \right) \left(\frac{\partial R}{\partial \alpha_j} \right) \cdot \text{COV}(\alpha_i, \alpha_j) \quad (4.20)$$

Without loss of generality, for a system of 3-input, the total system variance $V(R)$ is:

$$V_{3\text{-inp}} = S_1 \sigma_1^2 S_1 + 2S_1 \sigma_{12} S_2 + S_2 \sigma_2^2 S_2 + 2S_2 \sigma_{23} S_3 + S_3 \sigma_3^2 S_3 + 2S_1 \sigma_{13} S_3 \quad (4.21)$$

Next, the formulation for individual input variance contribution is derived intuitively. Suppose the value of input α_1 is known which changes the number of components in the total variance calculation changes 9 terms to 4 terms as the dimension of the problem decreases from 3-input to 2-input:

$$\begin{pmatrix} \mathbf{S}_1 \sigma_1^2 \mathbf{S}_1 & \mathbf{S}_1 \sigma_{12} \mathbf{S}_2 & \mathbf{S}_1 \sigma_{13} \mathbf{S}_3 \\ \mathbf{S}_2 \sigma_{21} \mathbf{S}_1 & S_2 \sigma_2^2 S_2 & S_2 \sigma_{23} S_3 \\ \mathbf{S}_3 \sigma_{31} \mathbf{S}_1 & S_3 \sigma_{32} S_2 & S_3 \sigma_3^2 S_3 \end{pmatrix} \xrightarrow{2\text{-input}} \begin{pmatrix} S_2 \sigma_2^2 S_2 & S_2 \sigma_{23} S_3 \\ S_3 \sigma_{32} S_2 & S_3 \sigma_3^2 S_3 \end{pmatrix} \quad (4.22)$$

Chapter 4. Introducing variance-based global sensitivity analysis

The sum of the bolded terms represents the reduction of total output variance if the value of α_1 becomes known. Intuitively, it shall correspond to the variance contribution of α_1 :

$$V_1 = V_{3\text{-input}} - V_{2\text{-input}} = S_1\sigma_1^2 S_1 + 2S_1\sigma_{12}S_2 + 2S_1\sigma_{13}S_3 \quad (4.23)$$

Similarly,

$$V_2 = S_2\sigma_2^2 S_2 + 2S_1\sigma_{12}S_2 + 2S_2\sigma_{23}S_3 \quad (4.24)$$

$$V_3 = S_3\sigma_3^2 S_3 + 2S_1\sigma_{13}S_3 + 2S_2\sigma_{23}S_3 \quad (4.25)$$

The formula for individual variance contribution is therefore generalized as:

$$V_i = S_i\sigma_i^2 S_i + 2 \cdot \sum_{j \neq i} S_i\sigma_{ij}S_j \quad (4.26)$$

The larger the amount of reduction, the more important input α_1 is, as measured by its variance contribution to the total variance. If inputs are uncorrelated, the individual input variance is simply:

$$V_i = S_i\sigma_i^2 S_i \quad (4.27)$$

The comparison between local and global sensitivity analysis is essentially between Eqn.(4.26) or Eqn.(4.27) with Eqn.(4.6).

Chapter's key message

This chapter presented the FAST and RBD methods to answer the call for a sensitivity analysis methodology in Chapter 4.1. While the simple random sampling or deterministic “Sandwich Rule” methods can be found in many existing works as shown in Chapters 1.4 and 1.5, the variance-decomposition theory of FAST and RBD is first-of-its-kind for the application of nuclear data uncertainty quantification. In order to make consistent comparison between the Sandwich Rule and the sampling-based approaches, Chapter 4.5 presented a heuristic method to break up the deterministic Sandwich Rule formula into components associated to individual inputs. The implementation and demonstration of the variance decomposition capability in the upgraded NUSS-RF are given in the next chapter.

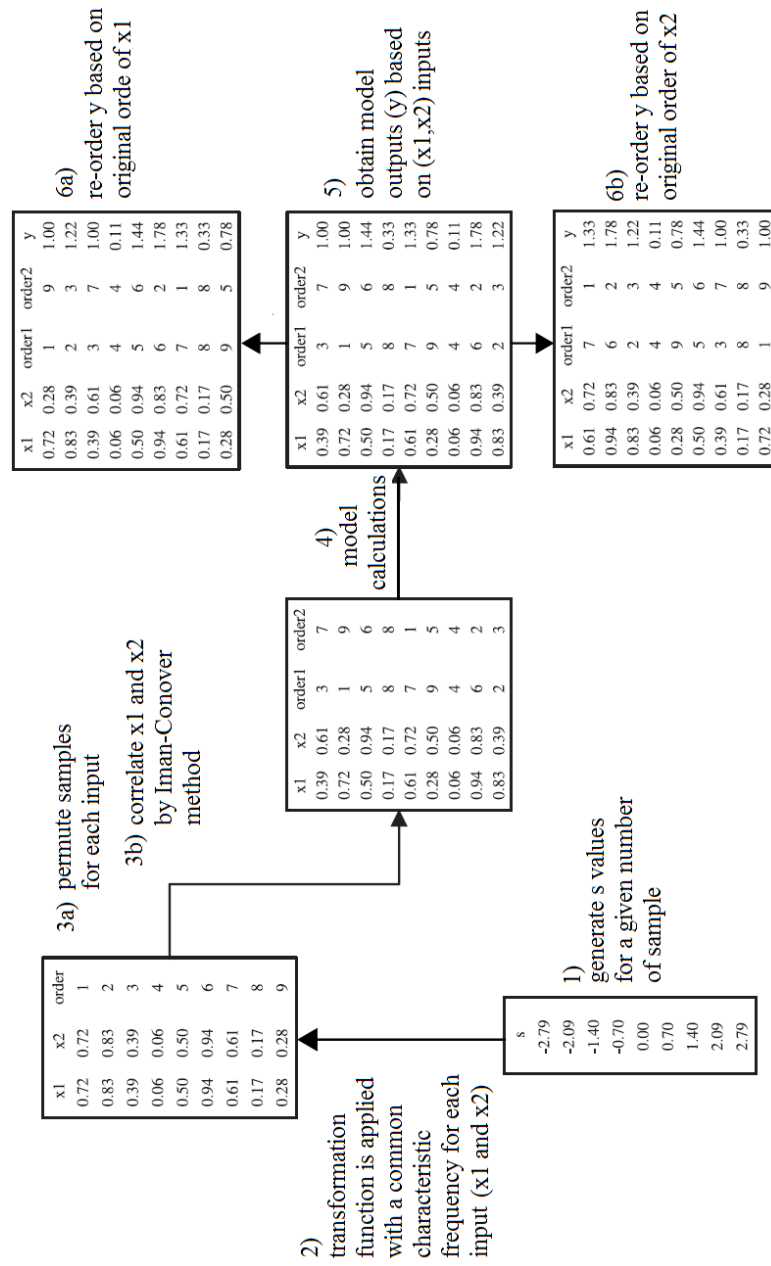


Figure 4.9: Steps of the RBD method are illustrated through a 2-input model.

5 Implementing NUSS-RF and its applications

This chapter first presents the implementation of FAST and Random Balance Design (RBD) into the NUSS tool, as the complementary capability of sensitivity analysis for nuclear data. Three mathematical test cases are analyzed for the verification and comparison between RBD and the “Sandwich Rule”-based variance decomposition results. Applied to the Jezebel, Godiva and UAM Pincell benchmarks, NUSS-RF examines nuclear data uncertainty contributions depending on the various levels of correlations. Discrepancies between the global-based NUSS-RF and local-based “Sandwich Rule” method are analyzed and discussed.

5.1 Introducing NUSS-RF

The expansion of NUSS-SRS to NUSS-RF is shown in Fig.5.1. The highlighted modules constitute the sensitivity analysis capability of NUSS-RF. In Stage 2 of NUSS’s calculation scheme where perturbation factors are prepared for the modification of ACE-formatted nuclear data, random balance design (RBD) is available as the alternative sampling module to the simple random sampling (SRS). Inside the MATLAB-scripted RBD module “random balance design sampling”, the algorithm follows the steps given previously in Chapter 4.4 and outlined in Fig.5.2. The following outputs are generated:

- Perturbation factors: as defined by Eqn.(2.14), they are groupwise factors to be applied uniformly to the pointwise ACE-formatted nuclear data, in the same manner as in NUSS-SRS by Eqn.(2.15).
- Re-ordering information: as illustrated by steps 6a) and 6b) in Fig.4.9, the MCNPX sample output are re-ordered to recover the initial periodicity.

From Stage 3 to 5 of Fig.5.1, the same procedures are conducted to perturb ACE files for repeated MCNPX calculations. The sensitivity analysis of MCNPX outputs is accomplished by first re-ordering the MCNPX sample outputs and applying Fourier transform to them, followed by the calculation of the components of the output power spectrum. To compute the result of

Eqn.(4.19), the program “RBD_getSI.m” shown in Fig.5.3 is used.

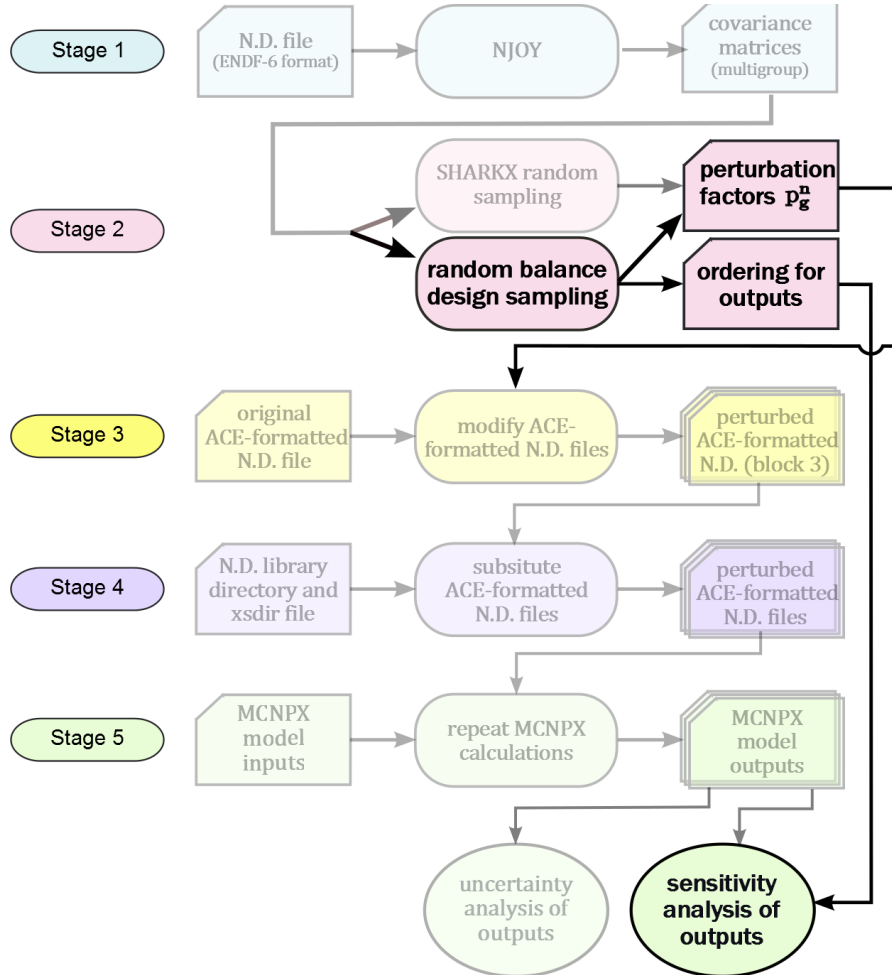


Figure 5.1: Module “random balance design sampling” is selected instead of the “SHARKX random sampling” to generate perturbation factors for the modification of ACE files. The “ordering for output” information will be used to perform “sensitivity analysis outputs” for the variance decomposition calculations.

5.2 Verification by analytical functions

MATLAB programs RBD_makeInp.m and RBD_getSI.m to accomplish RBD can be tested outside of the NUSS framework. Perturbation factors from RBD sampling can be generated and applied to test functions to simulate the sampled values of the input parameters. In the following, the verification of the MATLAB programs is presented through the comparison of numerical results to analytical solutions of three test functions.


```

RBD_makeInp.m
 $\omega$  = user-defined common frequency
N = number of samples
h = user-defined harmonics order
k = number of inputs
create vector  $s_0$  of length N
create matrix  $p = k$  sequences of permuted intergers
create  $s$  by using  $p$  to duplicate and permute elements inside  $s_0$ 
create uncorrelated, uniformly-distributed samples:
 $X = 1/2 + \text{asin}(\sin(\omega s))/\pi$ 
transform  $X$  into standard-normal samples  $X'$ 
apply function cholcov to decompose covariance matrix and
apply the decomposed triangular matrix to  $X'$  to generate
correlated and standard-normal samples  $X''$ 
get the ranking of the correlated samples  $X''$ 
"stretch" the standard-normal samples  $X'$  by the given
mean and standard deviations to become  $X'''$ 
re-order elements inside  $X'''$  according to the ranking
of elements in  $X''$  (Iman-Conover method)
calculate the perturbation factor by each sample
for each input
keep record of the "re-order" of  $X'''$ 

```

Figure 5.2: MATLAB program “RBD_makeInp.m” generates groupwise perturbation factors by random balance sampling on the covariance matrix. It also keeps track of the re-ordering of inputs by the Iman-Conover method.

```

RBD_getSI.m
For each input, given  $\omega$  and harmonics h values
re-order output  $y$  (of size N) accordingly
Fourier transform of output:  $Y = \text{fft}(y)/N$ 
calculate power spectrum:  $P_i = \text{abs}(Y).^2$ 
calculate total sample variance:  $V_t = (\text{sum}(P_i(2:N))) * N / (N-1)$ 
calculate sample variance for this particular input:
components = (1:h) *  $\omega$ 
 $V_i = \text{sum}(P_i(\text{components}+1)) * N / (N-1)$ 
calculate variance fraction:  $V_i/V_t$ 
End For

```

Figure 5.3: MATLAB program “RBD_getSI.m” computes the total and individual input variances, as well as the variance fraction denoted by “SI”. Appendix A9 has more details on the use of Fourier transform in MATLAB.

Test 1

A simple additive and linear model y is used:

$$y = x_1 + x_2 + x_3 \quad (5.1)$$

with the following correlation (C) and covariance (M) matrix. The variances of individual inputs are the values in the diagonal of matrix M .

$$C = \begin{bmatrix} 1 & 0 & 0 \\ 0 & 1 & \rho \\ 0 & \rho & 1 \end{bmatrix} \quad \text{and} \quad M = \begin{bmatrix} \sigma_1^2 & 0 & 0 \\ 0 & \sigma_2^2 & \rho\sigma_2\sigma_3 \\ 0 & \rho\sigma_2\sigma_3 & \sigma_3^2 \end{bmatrix} = \begin{bmatrix} 1^2 & 0 & 0 \\ 0 & 1^2 & 2\rho \\ 0 & 2\rho & 2^2 \end{bmatrix}$$

This model was studied in [76] which used a copula-based sampling approach to obtain the variance fractions (also known as sensitivity indices in global sensitivity analysis [77]). Here the same case is examined with the random balance design algorithm. Analytical solutions of the total variance and variance decomposition are shown below (derivations in Appendix A10):

$$\hat{V}_{\text{tot}} = \sigma_1^2 + \sigma_2^2 + \sigma_3^2 + 2\rho\sigma_2\sigma_3 = 6 + 4\rho \quad (5.2)$$

$$\hat{V}_1 = \sigma_1^2 = 1 \quad (5.3)$$

$$\hat{V}_2 = (\sigma_2 + \rho\sigma_3)^2 = (1 + 2\rho)^2 \quad (5.4)$$

$$\hat{V}_3 = (\sigma_3 + \rho\sigma_2)^2 = (2 + \rho)^2 \quad (5.5)$$

On the other hand, according to the deterministic Sandwich Rule approach, the output variance is calculated as:

$$\sigma_y^2 = SMS^T = \begin{bmatrix} \frac{dy}{dx_1} & \frac{dy}{dx_2} & \frac{dy}{dx_3} \end{bmatrix} \begin{bmatrix} 1 & 0 & 0 \\ 0 & 1 & 2\rho \\ 0 & 2\rho & 4 \end{bmatrix} \begin{bmatrix} \frac{dy}{dx_1} \\ \frac{dy}{dx_2} \\ \frac{dy}{dx_3} \end{bmatrix} \quad (5.6)$$

With $\frac{dy}{dx_1} = \frac{dy}{dx_2} = \frac{dy}{dx_3} = 1$ and Eqn.(4.26), the individual input variance contributions are:

$$V_1 = 1 \quad V_2 = 1 + 2(2\rho) \quad V_3 = 4 + 2(2\rho) \quad (5.7)$$

The total variance is:

$$V_{\text{tot}} = 1 + 1 + 2(2\rho) + 4 = 6 + 4\rho \quad (5.8)$$

Comparing analytical solutions \hat{V} 's with the V 's from Sandwich Rule, differences are observed for the two correlated inputs x_2 and x_3 :

$$\hat{V}_2 = V_2 + (2\rho)^2 \quad \text{and} \quad \hat{V}_3 = V_3 + (1 \cdot \rho)^2 \quad (5.9)$$

5.2. Verification by analytical functions

As a linear model, the Sandwich Rule method does not need to assume the truncation of higher order terms of the model. Hence \hat{V}_{tot} and V_{tot} are the same. The extra term $(2\rho)^2$ in \hat{V}_2 shall be interpreted as the contribution of x_3 variance weighted by the correlation coefficient ρ between x_2 and x_3 . Similar explanation can be given for $(1\rho)^2$ in \hat{V}_3 . Only when $\rho = 0$, the two formulations have the same result.

For various values of ρ between x_2 and x_3 , and with sample sizes from 301 to 901, Fig. 5.4 shows the averaged variance fraction values for the three inputs. Except for the smallest sample size of 301, the effectiveness of determining the correct ranking as well as the values of individual input variance contributions is relatively stable for sample size above 901.

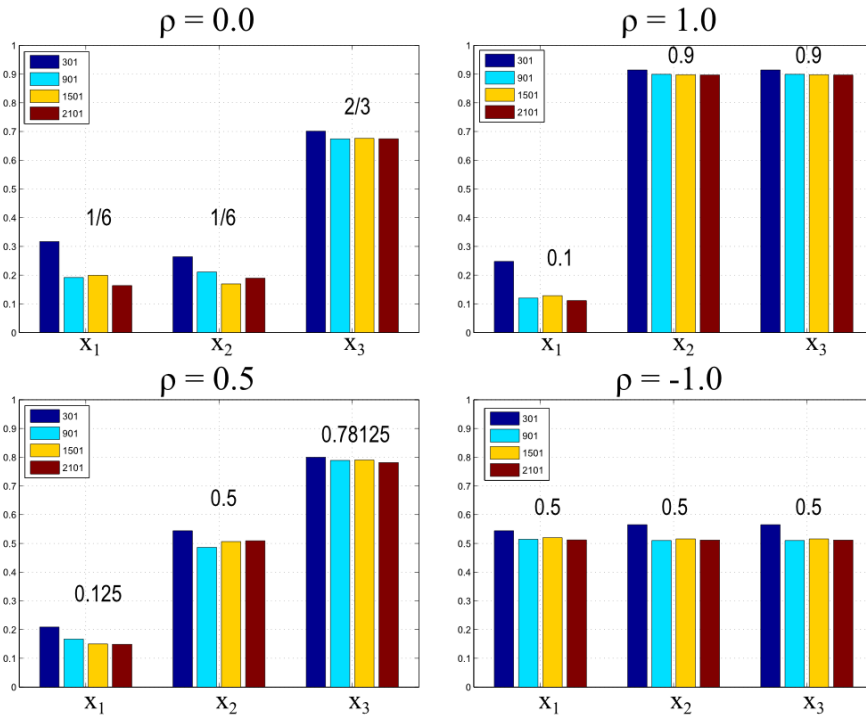


Figure 5.4: Variance fractions of x_1, x_2, x_3 are calculated by RBD using a sample size of 301, 901, 1501 or 2101, each is repeated three times to obtain an average variance fraction value. Harmonics order is set to be 20. Analytical solutions are labelled accordingly.

To confirm the accuracy of RBD, a large sample size of 9999 is used. As listed Table 5.1, the averaged variance fraction values and their standard deviations are resulted from ten RBD calculations, each of which used 9999 samples. The analytical and numerical results are in good agreement. In coincidence, when $\rho = -0.5$, the value of \hat{V}_2 becomes zero from the Eqn.(5.4) when $2\rho = -1$.

For completeness of method comparison, the variance fractions are also estimated through the squared value of the Pearson correlation coefficient (r_p^2) which as shown in Chapter 3.5 works in the case of linear systems. Fig.5.5 shows that RBD and r_p^2 , both are sampling-based approaches have good agreement with the analytical values. On the other hand, it is known

Chapter 5. Implementing NUSS-RF and its applications

Correlation		V_1/V_{tot}	V_2/V_{tot}	V_3/V_{tot}
$\rho=0$	Analytical	0.167	0.167	0.669
	RBD	0.168(6)	0.169(8)	0.665(3)
$\rho=1$	Analytical	0.1	0.9	0.9
	RBD	0.103(3)	0.8958(4)	0.8958(4)
$\rho=0.5$	Analytical	0.126	0.502	0.784
	RBD	0.123(6)	0.500(4)	0.779(2)
$\rho=-1$	Analytical	0.5	0.5	0.5
	RBD	0.499(3)	0.499(4)	0.499(4)
$\rho=-0.5$	Analytical	0.251	0.000	0.564
	RBD	0.254(8)	0.0038(9)	0.562(2)

Table 5.1: Analytical and numerical results of variance fraction for $y = x_1 + x_2 + x_3$ are compared, for different correlations between x_2 and x_3 . The notation of 0.123(6) means 0.123 ± 0.006 . In RBD, $\omega_c=1$ and $M=20$ are used in Eqn.(4.19).

from Eqn.(5.9) that the Sandwich Rule-based approach gives different variance fraction results when the correlations among inputs are non-zero.

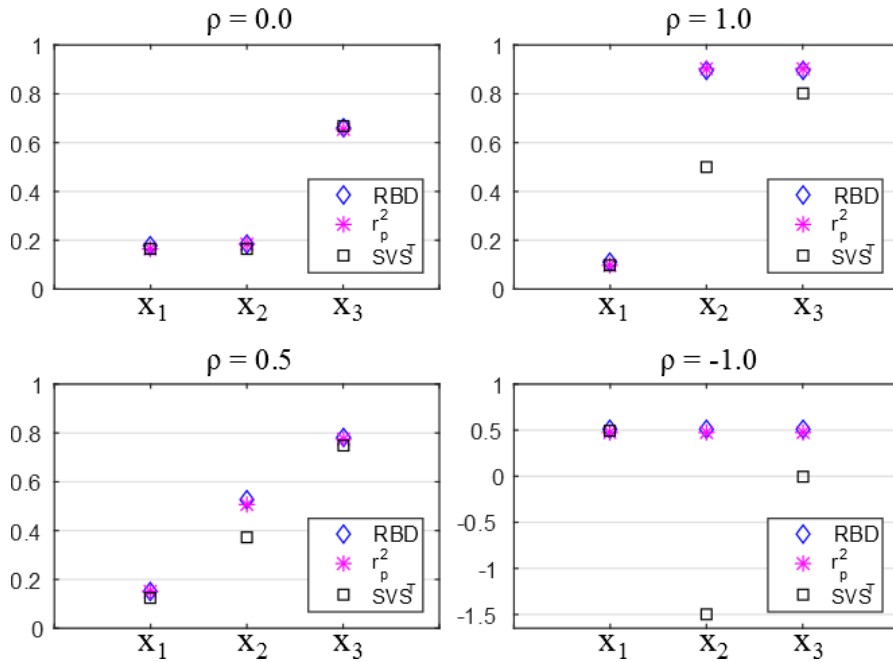


Figure 5.5: RBD and the squared value of the Pearson correlation coefficient (r_p^2) reproduce the analytical variance fractions for the linear model $y = x_1 + x_2 + x_3$ with various correlation (ρ_{23}) values. Negative variance fraction from local-based Sandwich Rule is due to large negative ρ_{23} values.

Test 2

The second test model [76] has four inputs with interactions among themselves:

$$y = x_1 \cdot x_3 + x_2 \cdot x_4 \quad (5.10)$$

where each input as a random variable has a normal distribution with the following mean and standard deviation values (denoted as $\sim N(\mu, \sigma)$):

$$X_1 \sim N(0, 4) \quad X_2 \sim N(0, 2) \quad X_3 \sim N(250, 20) \quad X_4 \sim N(400, 30) \quad (5.11)$$

The covariance matrix of the inputs is given below, considering x_1, x_2 are correlated by 0.3, x_3 and x_4 by -0.3:

$$M = \begin{bmatrix} \sigma_1^2 & \sigma_{12} & 0 & 0 \\ \sigma_{21} & \sigma_2^2 & 0 & 0 \\ 0 & 0 & \sigma_3^2 & \sigma_{34} \\ 0 & 0 & \sigma_{43} & \sigma_4^2 \end{bmatrix} = \begin{bmatrix} 4^2 & 4 \times 2 \times 0.3 & 0 & 0 \\ 2 \times 4 \times 0.3 & 2^2 & 0 & 0 \\ 0 & 0 & 20^2 & 20 \times 30 \times (-0.3) \\ 0 & 0 & 30 \times 20 \times (-0.3) & 30^2 \end{bmatrix}$$

From the point of view of the Sandwich Rule, the first-order sensitivity coefficients are:

$$S = \left[\frac{\partial y}{\partial x_1} \quad \frac{\partial y}{\partial x_2} \quad \frac{\partial y}{\partial x_3} \quad \frac{\partial y}{\partial x_4} \right] = \left[x_3 \quad x_4 \quad x_1 \quad x_2 \right] \quad (5.12)$$

which is not a constant vector anymore. By using the mean value of each input, the sensitivity coefficient vector at the “mean” point is:

$$S = \left[\mu_3 \quad \mu_4 \quad \mu_1 \quad \mu_2 \right] = \left[250 \quad 400 \quad 0 \quad 0 \right] \quad (5.13)$$

Consequently, the total variance of y is:

$$V_{\text{tot}} = SMS^T = \mu_3^2 \sigma_1^2 + \mu_4^2 \sigma_2^2 + \mu_1^2 \sigma_3^2 + \mu_2^2 \sigma_4^2 + 2\mu_3 \sigma_{12} \mu_4 + 2\mu_1 \sigma_{34} \mu_2 \quad (5.14)$$

$$= \mu_3^2 \sigma_1^2 + \mu_4^2 \sigma_2^2 + 2\mu_3 \sigma_{12} \mu_4 \quad (5.15)$$

which is different from the analytical solution of total variance of y (given in [76]) due to the truncation of the second-order terms in the Taylor expansion of y (see Appendix A11):

$$\hat{V}_{\text{tot}} = \mu_3^2 \sigma_1^2 + \mu_4^2 \sigma_2^2 + 2\mu_3 \sigma_{12} \mu_4 + \sigma_1^2 \sigma_3^2 + \sigma_2^2 \sigma_4^2 + 2\sigma_{12} \sigma_{34} \quad (5.16)$$

$$= V_{\text{tot}} + \sigma_1^2 \sigma_3^2 + \sigma_2^2 \sigma_4^2 + 2\sigma_{12} \sigma_{34} \quad (5.17)$$

Chapter 5. Implementing NUSS-RF and its applications

The individual input variance contributions are [76],:

$$\hat{V}_1 = \sigma_1^2 \left(\mu_3 + \mu_4 \rho_{12} \frac{\sigma_2}{\sigma_1} \right)^2 \quad \text{and} \quad \hat{V}_2 = \sigma_2^2 \left(\mu_4 + \mu_3 \rho_{12} \frac{\sigma_1}{\sigma_2} \right)^2 \quad (5.18)$$

$$\hat{V}_3 = \sigma_3^2 \left(\mu_1 + \mu_2 \rho_{34} \frac{\sigma_4}{\sigma_3} \right)^2 = 0 \quad \text{and} \quad \hat{V}_4 = \sigma_4^2 \left(\mu_2 + \mu_1 \rho_{34} \frac{\sigma_3}{\sigma_4} \right)^2 = 0 \quad (5.19)$$

The zero values of \hat{V}_3 and \hat{V}_4 indicate that these two inputs have no variance contributions. This can be visually confirmed by samples of the four inputs vs. the value of y are shown in scatter plots in Fig.5.6. The bottom-left scatter plot shows that as the value of x_3 varies, there is equal probability for y to be above or below zero (due to $\mu_1 = \mu_2 = 0$). By Eqn.(4.6), the variance of the conditional expectation of y for fixed x_3 , i.e. V_3 is found to be zero. Similarly, $V_4=0$.

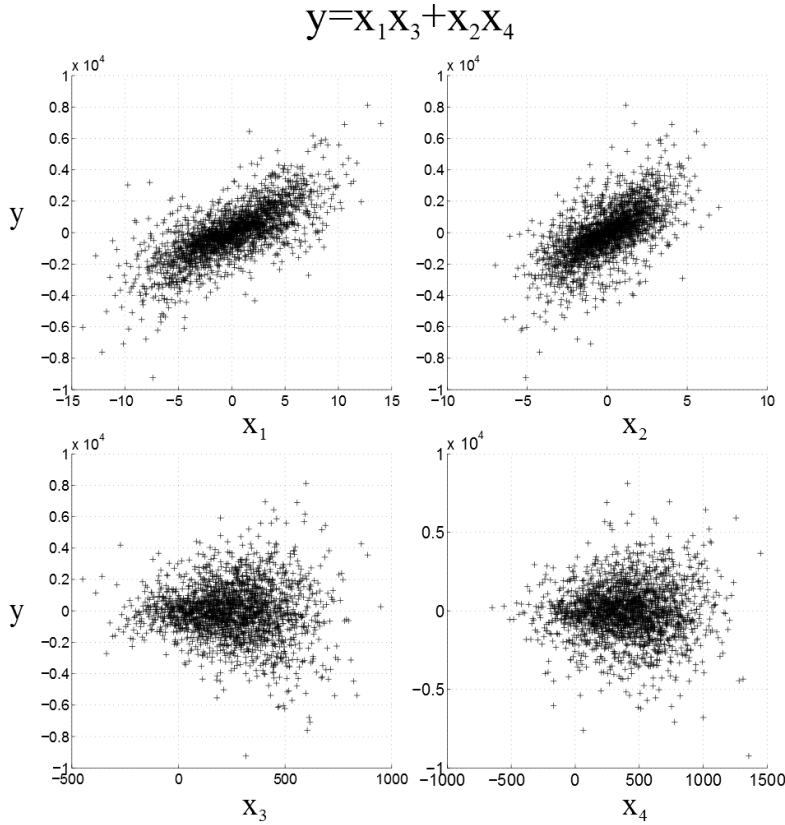


Figure 5.6: Scatter plots for the results from simple random sampling on inputs x_1 to x_4 for model $y = x_1 x_3 + x_2 x_4$.

Shown in Table 5.2, RBD algorithm is able to obtain numerical results which are in good agreement with the analytical solutions. Numerical calculations are performed by running RBD ten times, each having $N=9999$ samples to obtain the mean and standard deviation values. For V_3/V_{tot} and V_4/V_{tot} which should have zero values, the precision of RBD's results is affected by the statistical uncertainty of a finite sample size, as statistical uncertainty is considered the

signal noise, occupying any frequencies in the power spectrum representation [78].

Correlation		V_1/V_{tot}	V_2/V_{tot}	V_3/V_{tot}	V_4/V_{tot}
$\rho=0$	Analytical	0.379	0.242	0	0
	RBD	0.370(10)	0.240(6)	0.0025(9)	0.0024(5)
$\rho_{12} = \rho_{34} = 0.3$	Analytical	0.507	0.399	0	0
	RBD	0.505(6)	0.403(8)	0.0043(9)	0.0037(9)

Table 5.2: Analytical and numerical results of input variance fractions for test function $y = x_1 x_3 + x_2 x_4$. The use of notation, e.g. 0.370(10) implies 0.370 ± 0.010 . In RBD, $\omega_c=1$ and $M=20$ are used in Eqn.(4.19).

Test 3

A popular test case commonly known as the G-function of Sobol's is a non-linear and non-monotonic model:

$$f = \prod_{i=1}^n g_i(x_i) \quad \text{where} \quad g_i(x_i) = \frac{|4x_i - 2| + a_i}{1 + a_i} \quad (5.20)$$

where $0 \leq x_i \leq 1$ uniformly and $a_i \geq 0$. The analytical solutions of variances for uncorrelated x_i inputs are [74]:

$$V_i = \frac{1}{3(1 + a_i)^2} \quad \text{and} \quad V = \prod_{i=1}^n (V_i + 1) - 1 \quad (5.21)$$

In Fig.5.7, the non-linear and non-monotonic distribution of f values is shown for various values of a . As a result, the variance fraction estimation by the squared value of Pearson/Spearman correlation coefficient (r^2) is unreliable in this case. Fig.5.8 shows the respective results from RBD and r^2 as compared to the analytical solutions. With a sample size of 9999, RBD is able to reproduce the analytical solutions.

Results in Tables 5.1, 5.2 and Fig.5.8 have served to validate the implemented RBD algorithm for both linear and nonlinear, uncorrelated and correlated cases. In these test cases, the number of samples is chosen to be large enough for the desired convergence (as indicated by the standard deviations). In practise, it is impractical to use as a large sample size as here. Quantification of statistical error due to finite sample size has not been considered in this PhD thesis and remains as future work. In the following sections, NUSS-RF with the RBD capability is applied for nuclear data uncertainty quantification applications, with the focus of identifying the top uncertainty contributors.

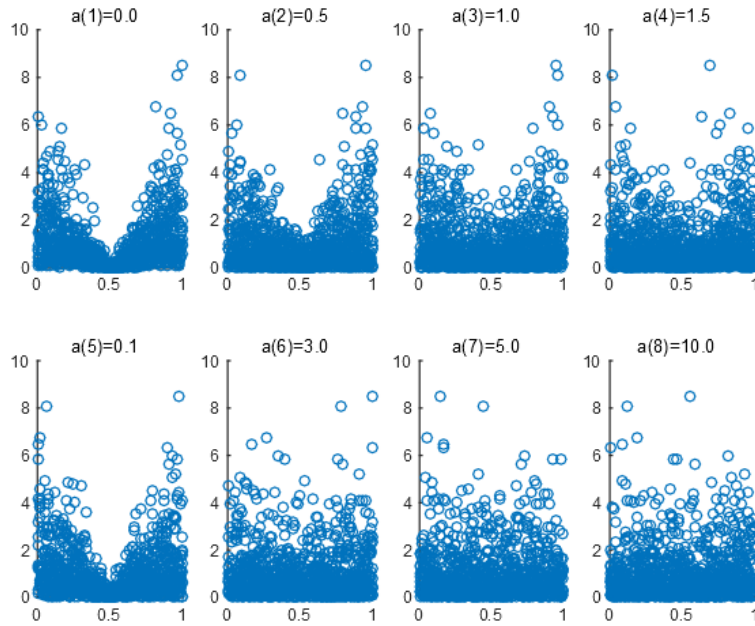


Figure 5.7: Scatter plots of the g-function model output y with respect to each input which is associated with a distinct a constant.

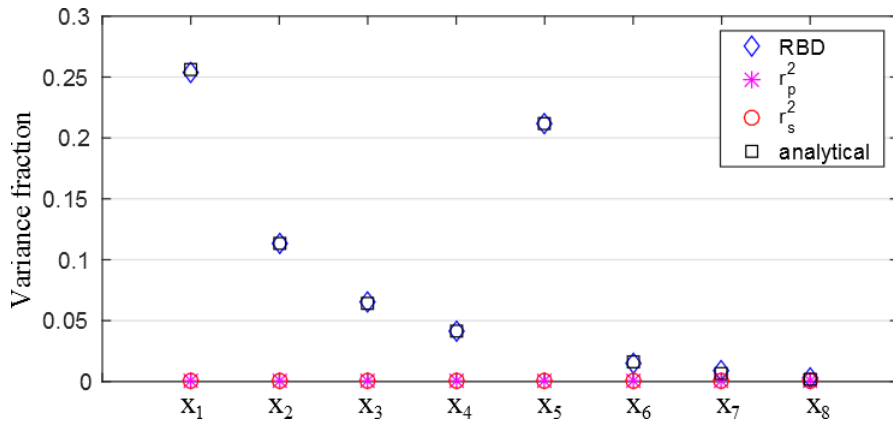


Figure 5.8: The approach by the squared of Pearson/Spearman correlation coefficients (r_p^2, r_s^2) fails because of the non-linearity of the g-function, but RBD is able to reproduce the analytical solutions. Sample size here is 99999.

5.3 Application for small correlation: Jezebel and Godiva

For the application of NUSS-RF for nuclear data uncertainty and sensitivity analysis, the two bare metal spherical criticality assembly benchmarks, namely the ^{239}Pu -fuelled Jezebel and ^{235}U -fuelled Godiva are used. Their fast neutron spectra can be recalled in Fig.3.17 in Chapter 3.4. The isotope-reactions chosen for the demonstration of NUSS-RF capability are $^{239}\text{Pu}(n,f), ^{239}\text{Pu}(\bar{\nu})$ in Jezebel and $^{235}\text{U}(n,f), ^{235}\text{U}(n,\gamma)$ in Godiva. Their uncertainties

5.3. Application for small correlation: Jezebel and Godiva

are taken from the SCALE6-44g covariance library and shown in Fig.5.9 to Fig.5.12, along with the sensitivity coefficient (S_k) profiles obtained by TSUNAMI. By default, S_k values in TSUNAMI are in a 238-group structure. They are then collapsed into the 44-group structure and combined with the SCALE6-44g covariance data for k_{eff} uncertainty calculation. In the Sandwich Rule-based approach (i.e. local sensitivity analysis), individual input variance contributions are determined by Eqn.(4.26) and Eqn.(4.27) for correlated and uncorrelated cases respectively. In the global sensitivity analysis approach, NUSS-RF calculations are performed using ENDF/B-VII.1 nuclear data in MCNPX for the calculation of k_{eff} values and the same SCALE6-44g covariances for the nuclear data uncertainty propagation. A sample size of 1001 is used.

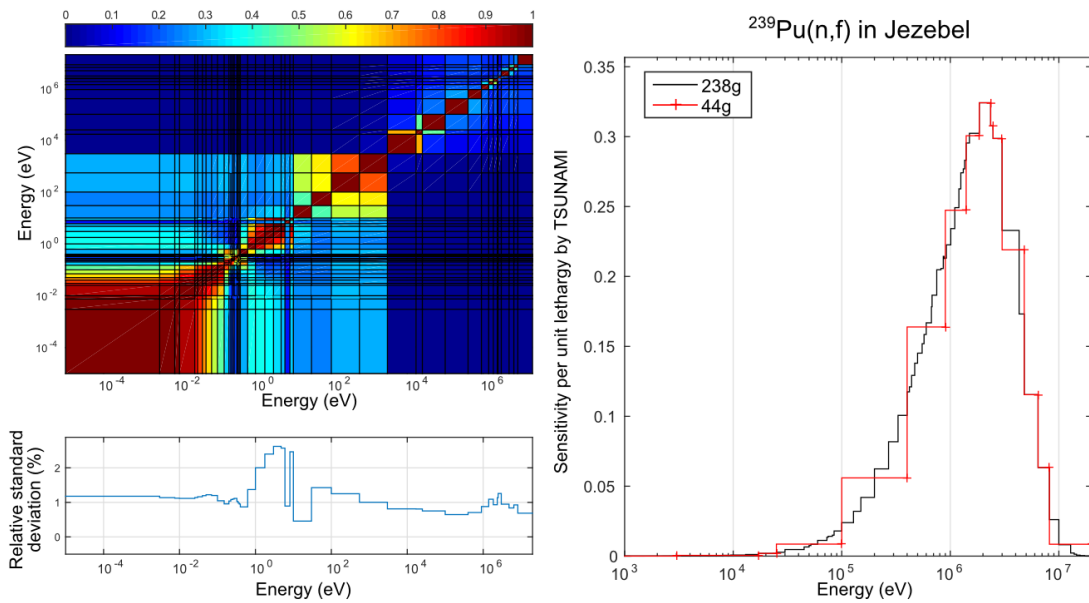


Figure 5.9: Correlation matrix and relative standard deviations for $^{239}\text{Pu}(n,f)$, given by the SCALE6-44g covariance library in a 44 energy-group structure. Sensitivity coefficients are obtained by TSUNAMI.

Here, not only the energy-integrated uncertainty contribution (i.e. total k_{eff} uncertainty) is of interest, the energy-dependent individual uncertainty contribution is examined. As the energy group structure consists of 44 groups, the total number of inputs is equal to 44. Two scenarios are investigated in the following: the groupwise cross sections are assumed to be uncorrelated first, followed by the consideration of correlations.

Scenario 1: Correlations are set to zero

Table 5.3 lists the k_{eff} uncertainty due to ^{239}Pu in Jezebel and ^{235}U in Godiva uncertainties, assuming the energy-dependent correlations are zero. The good agreement in k_{eff} uncertainty between NUSS-RF and the Sandwich Rule approach means the higher order effect (i.e. $\mathcal{O}(\Delta^2, \dots) = k - k_o - S_k \Delta\alpha$) which is omitted by the Sandwich Rule is negligible. It is on the same order of magnitude as the statistical uncertainty.

Chapter 5. Implementing NUSS-RF and its applications

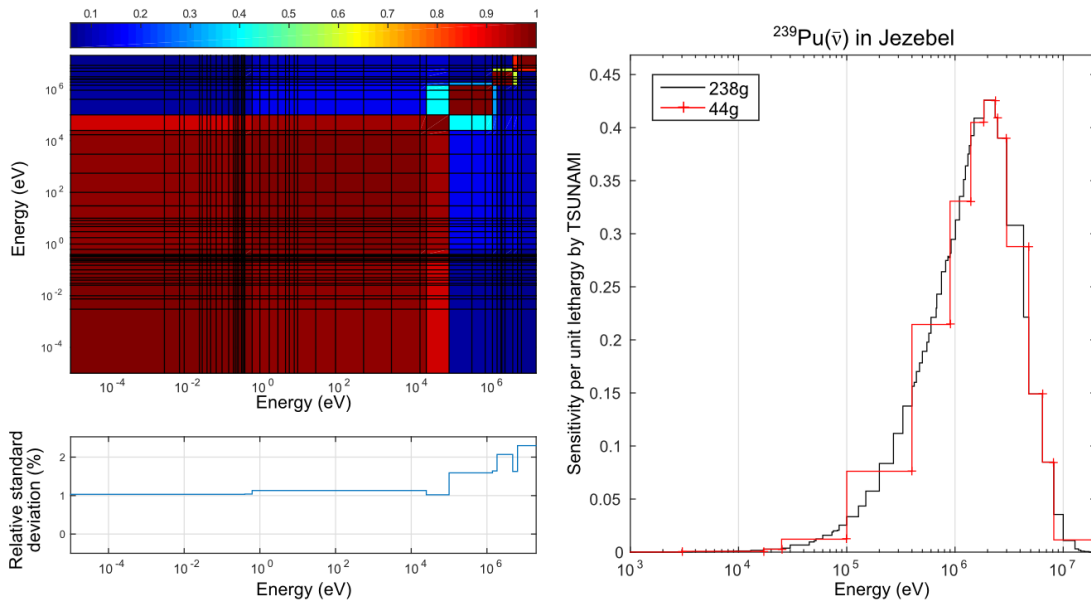


Figure 5.10: Correlation matrix and relative standard deviations for $^{239}\text{Pu}(\bar{\nu})$, given by the SCALE6-44g covariance library in a 44 energy-group structure. Sensitivity coefficients are obtained by TSUNAMI.

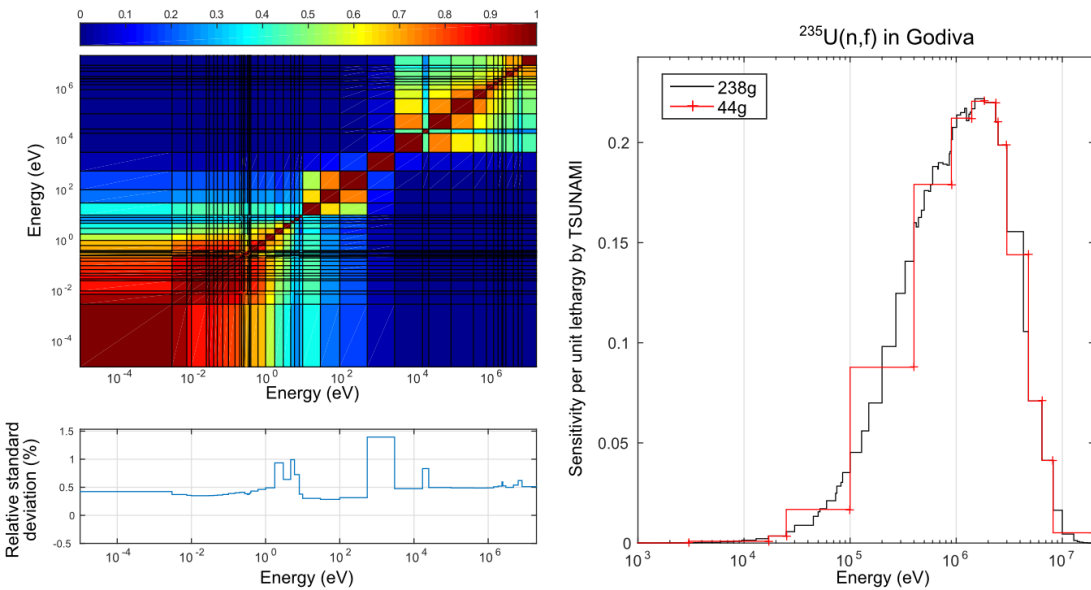


Figure 5.11: Correlation matrix and relative standard deviations for $^{235}\text{U}(n,f)$, given by the SCALE6-44g covariance library in a 44 energy-group structure. Sensitivity coefficients are obtained by TSUNAMI.

Next, the total k_{eff} uncertainty is decomposed in terms of energy-dependent variance contributions. In Fig.5.13 to Fig.5.16, the variance fraction results show distinctly the separated groups of high and low-variance inputs. k_{eff} uncertainty mainly comes from uncertainties

5.3. Application for small correlation: Jezebel and Godiva

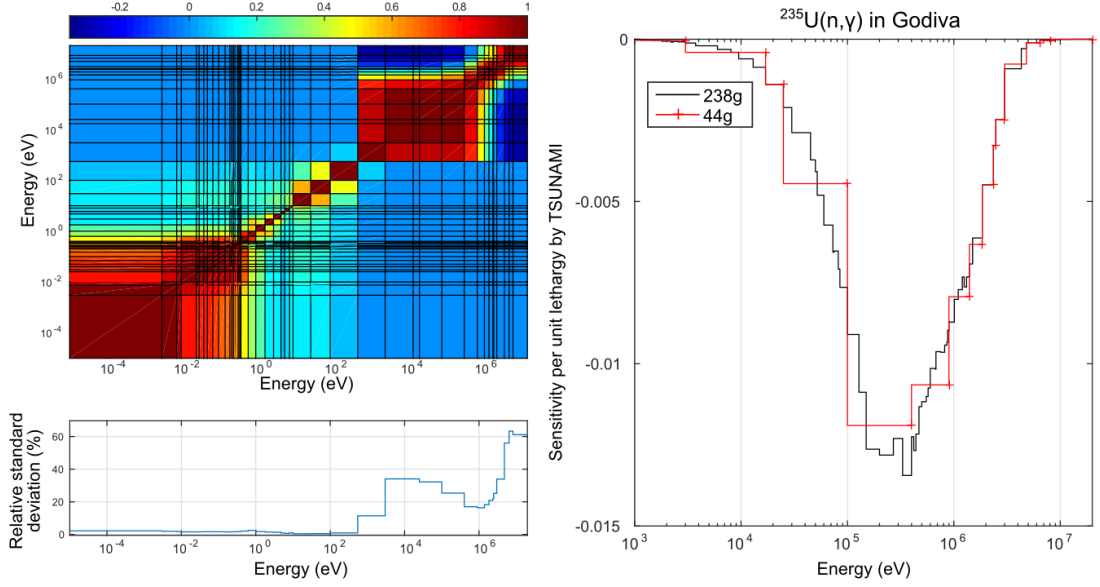


Figure 5.12: Correlation matrix and relative standard deviations for $^{235}\text{U}(n,\gamma)$, given by the SCALE6-44g covariance library in a 44 energy-group structure. Sensitivity coefficients are obtained by TSUNAMI.

Case	NUSS-RF	SVS^T
$^{239}\text{Pu}(n,f)$	225 pcm	219 pcm
$^{239}\text{Pu}(\bar{\nu})$	601 pcm	591 pcm
$^{235}\text{U}(n,f)$	124 pcm	119 pcm
$^{235}\text{U}(n,\gamma)$	478 pcm	492 pcm

Table 5.3: Good agreement in k_{eff} uncertainty values calculated by sampling-based NUSS-RF and first-order Sandwich Rule (SVS^T) methods, assuming uncorrelated nuclear data.

of cross sections in the fast energy range since both Jezebel and Godiva are fast-spectrum systems. Below 10^4eV , sensitivity coefficients are zero, hence the corresponding variance fractions obtained from Sandwich Rule are zero. In comparison, the fluctuations in variance fractions by NUSS-RF are due to statistical uncertainty of the sampling-based approach. Also the propagation of MCNPX statistical uncertainty into variance decomposition is not separated from nuclear data uncertainty contribution currently.

Estimation of Sensitivity Coefficients

Given the good agreement between NUSS-RF and Sandwich Rule methods, sensitivity coefficients can be derived from the variance fraction calculated by NUSS-RF. Since correlations are assumed to be zero, Eqn.(4.27) can be rearranged:

$$V_i = S_i \text{var}(\alpha_i) S_i \rightarrow |S_i| = \sqrt{\frac{V_i}{\text{var}(\alpha_i)}} \quad (5.22)$$

Chapter 5. Implementing NUSS-RF and its applications

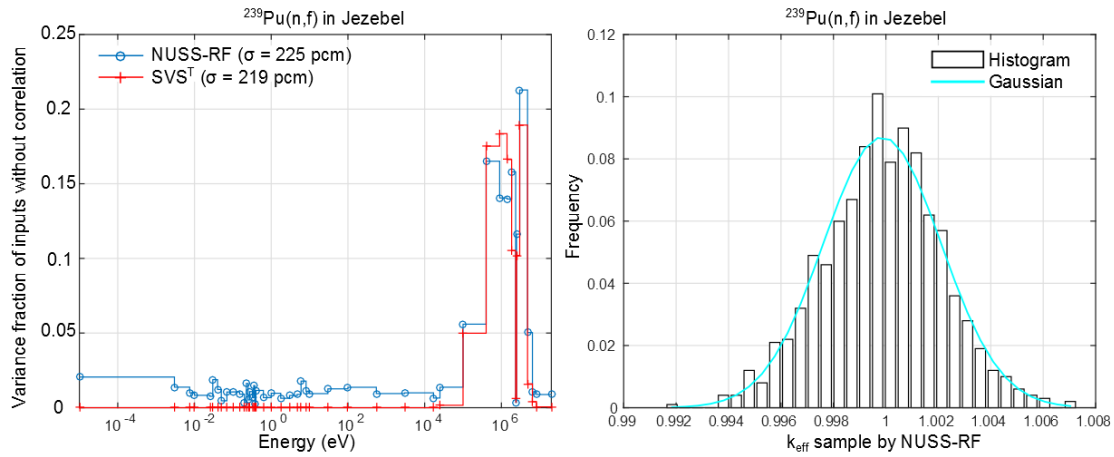


Figure 5.13: Variance fractions for uncorrelated inputs of 44-group $^{239}\text{Pu}(n,f)$ and the total uncertainties (σ) are similar by NUSS-RF and “Sandwich Rule” methods.

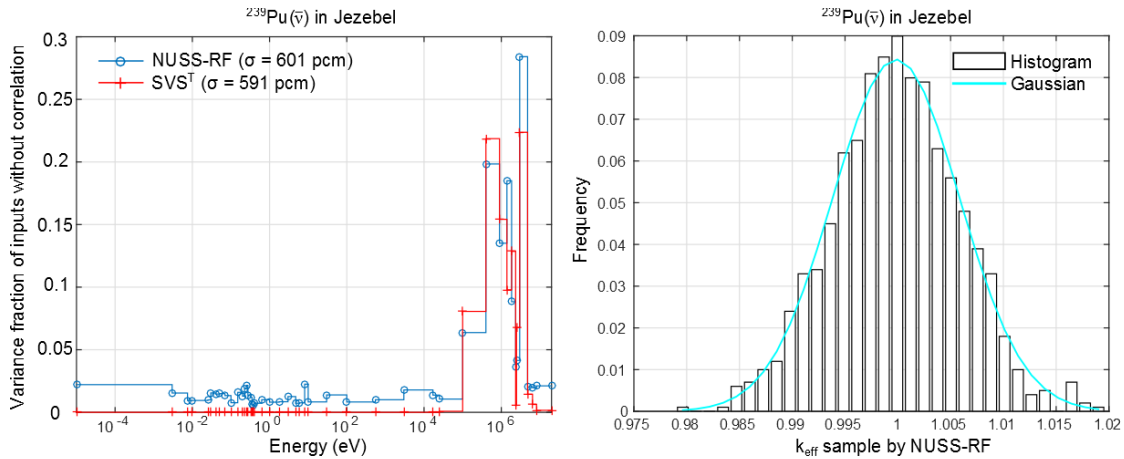


Figure 5.14: Variance fractions for uncorrelated inputs of 44-group $^{239}\text{Pu}(\bar{\nu})$ and the total uncertainties (σ) are similar by NUSS-RF and “Sandwich Rule” methods.

where $\text{var}(\alpha_i)$ is the variance of individual input (i.e. variance of cross section α at energy group i).

In Fig.5.17 and Fig.5.18, sensitivity coefficient profiles has been estimated from NUSS-RF sampling method and are compared to TSUNAMI-calculated S_k . The spikes in the NUSS-RF-calculated sensitivity coefficients are due to the normalization by “unit per lethargy” (i.e. divided by a small lethargy value). Eqn.(5.22) is also applicable for computing sensitivity coefficients for any system output parameters if the corresponding input covariances and input-output linearity exist. It should be kept in mind that linearity is the premise of first-order sensitivity coefficient in the Sandwich Rule. Strictly speaking, $|S_i|$ is an averaged value of $\partial k / \partial \alpha_i$. Also, the sign of the sensitivity coefficient from Eqn(5.22) cannot be determined as illustrated by the $^{235}\text{U}(n,\gamma)$ sensitivity estimation in Fig.5.18.

5.3. Application for small correlation: Jezebel and Godiva

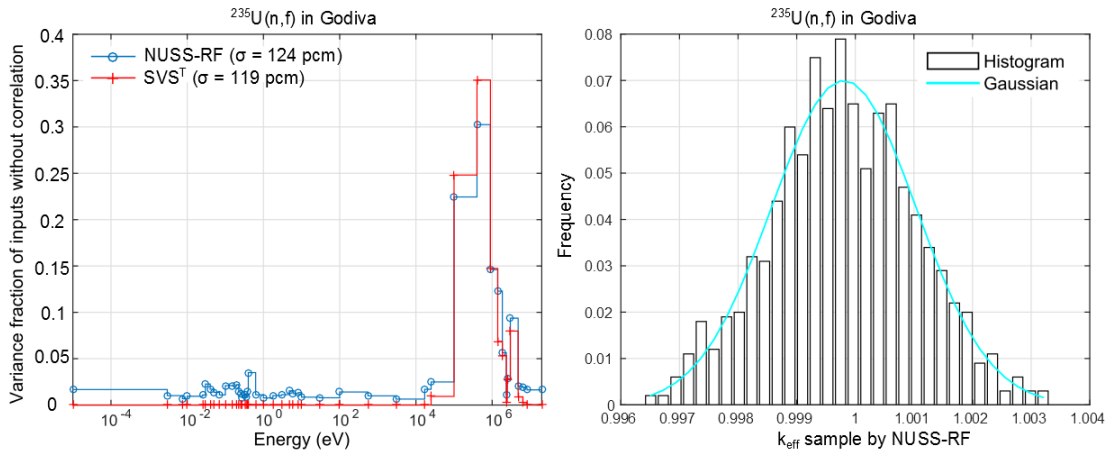


Figure 5.15: Variance fractions for uncorrelated inputs of 44-group $^{235}\text{U}(n,f)$ and the total uncertainties (σ) are similar by NUSS-RF and “Sandwich Rule” methods.

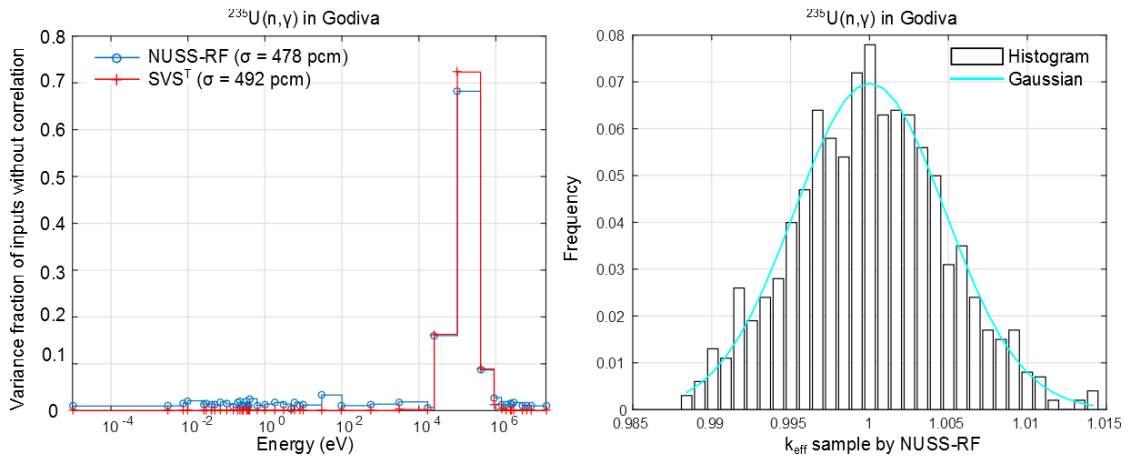


Figure 5.16: Variance fractions for uncorrelated inputs of 44-group $^{235}\text{U}(n,\gamma)$ and the total uncertainties (σ) are similar by NUSS-RF and “Sandwich Rule” methods.

Scenario 2: Correlations are included

NUSS-RF sampling is performed with the original $^{239}\text{Pu}(n,f)$, $^{239}\text{Pu}(\bar{\nu})$, $^{235}\text{U}(n,f)$ and $^{235}\text{U}(n,\gamma)$ covariances. The total k_{eff} uncertainties are larger now as shown in Table 5.4 as compared to Table 5.3. The variance fraction are also obtained with NUSS-RF and the Sandwich Rule (by Eqn.(4.26)). They are still in good agreement due to the linearity of the systems. However, the maximum variance fraction values (in %) listed in Table 5.4 reveal the two methods decompose the total k_{eff} variance differently.

In Fig.5.19 to Fig.5.22, the variance fractions are normalized by the maximum variance fraction values by the two methods respectively. The differences between NUSS-RF and Sandwich Rule has to be due to the presence of correlations. In particular, the correlations in the fast energy region of cross sections $^{235}\text{U}(n,f)$ and $^{235}\text{U}(n,\gamma)$ lead to a more pronounced “change of shape”

Chapter 5. Implementing NUSS-RF and its applications

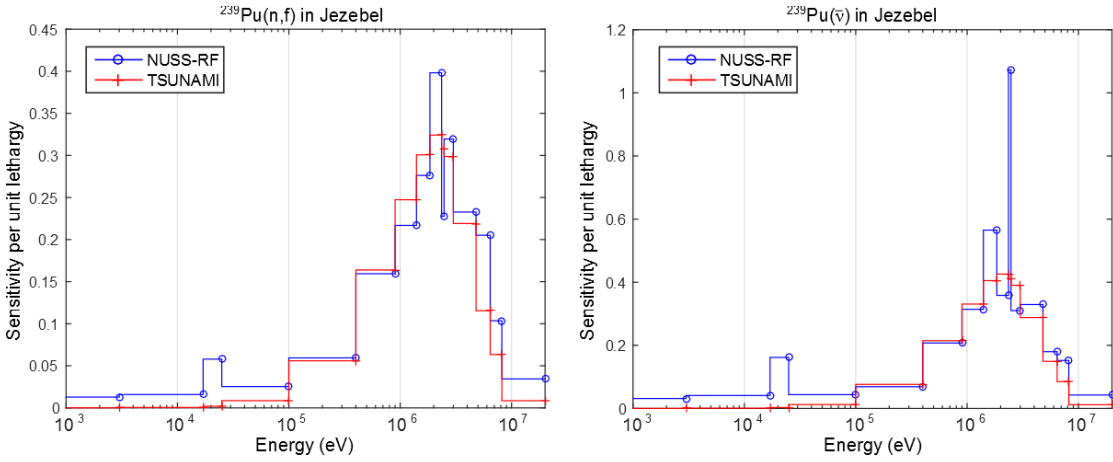


Figure 5.17: Sensitivity coefficients are derived from NUSS-RF (Eqn.(5.22)) and compared to TSUNAMI results.

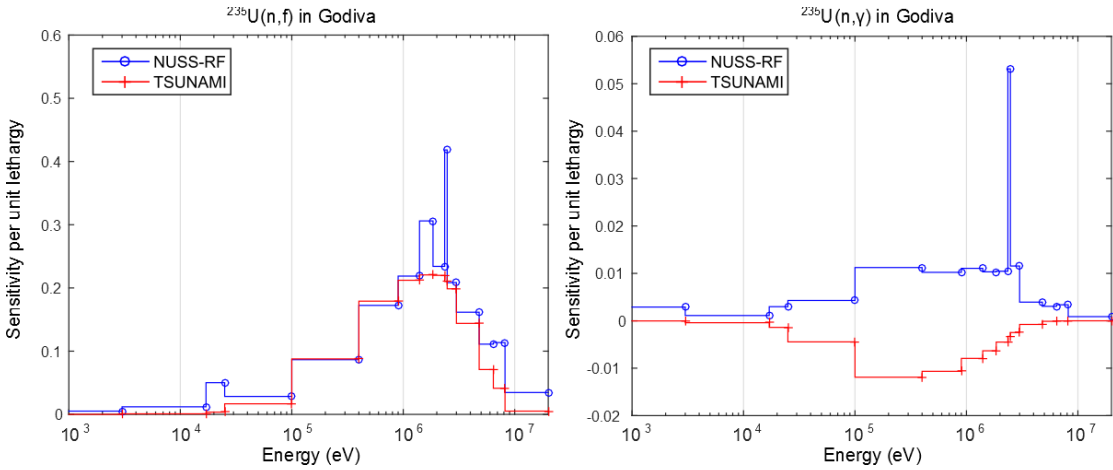


Figure 5.18: Sensitivity coefficients are derived from NUSS-RF (Eqn.(5.22)) and compared to TSUNAMI results.

Case	NUSS-RF	max VF	SVS^T	max VF
$^{239}\text{Pu}(n,f)$	352 pcm	0.423	352 pcm	0.254
$^{239}\text{Pu}(\bar{\nu})$	1243 pcm	0.839	1228 pcm	0.310
$^{235}\text{U}(n,f)$	272 pcm	0.750	268 pcm	0.393
$^{235}\text{U}(n,\gamma)$	851 pcm	0.941	862 pcm	0.719

Table 5.4: Good agreement in k_{eff} uncertainty values calculated by sampling-based NUSS-RF and first-order Sandwich Rule (SVS^T) methods when cross sections are correlated. However, the variance fraction distributions are different as seen by the maximum variance fraction (VF) values.

of the variance fraction profile in Fig.5.21 and Fig.5.22. In comparison, the correlations for $^{239}\text{Pu}(n,f)$ in the fast energy region are less than 0.3, hence the shape of the variance fraction

5.4. Application for large correlation: PB2-HZP

plot has changed only slightly comparing Fig.5.19 and Fig.5.13, albeit the overall increase of individual variance fractions as a result of the addition of covariance contributions.

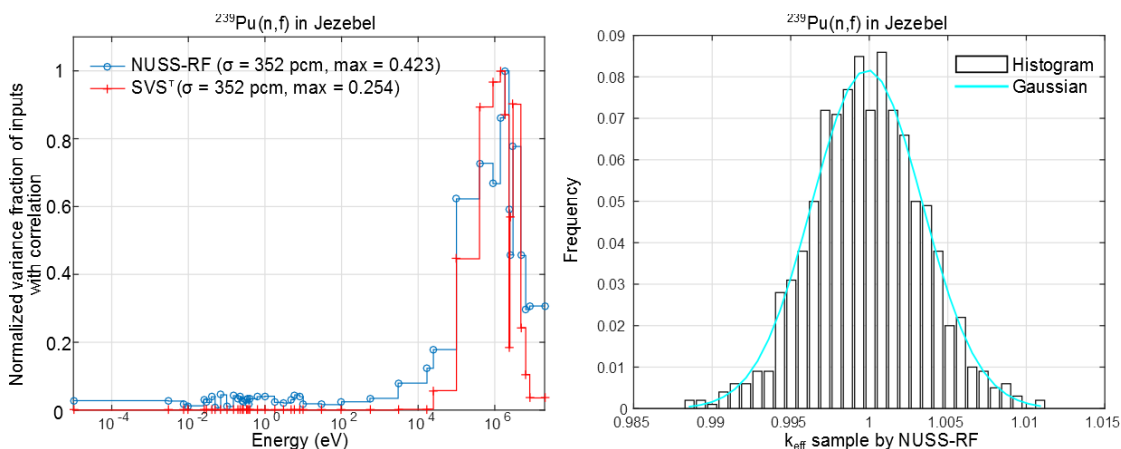


Figure 5.19: Normalized variance fractions ($V_i/\sigma^2/\text{max}$) for correlated inputs of 44-group $^{239}\text{Pu}(n,f)$. Difference between NUSS-RF and Sandwich Rule methods increases with the level of input correlations, but the total uncertainties (σ) by both methods are in good agreement.

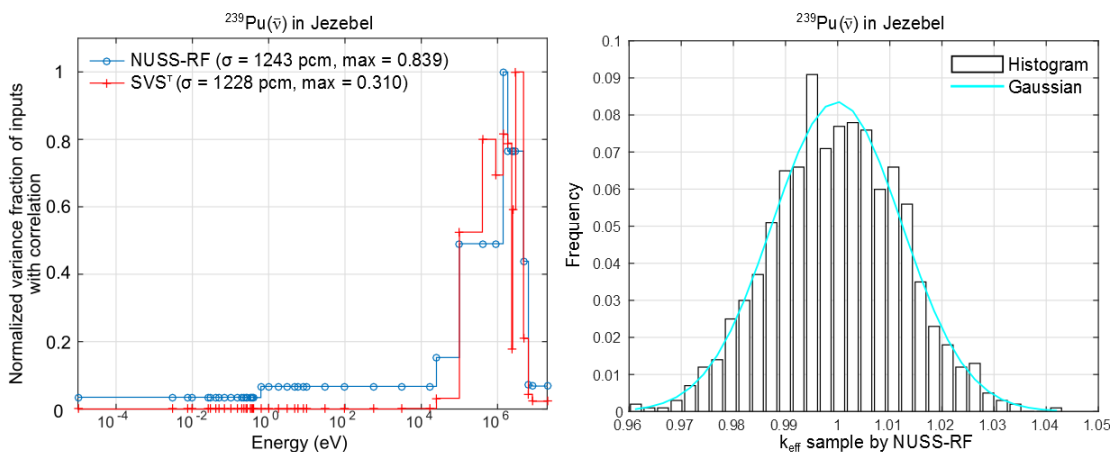


Figure 5.20: Normalized variance fractions ($V_i/\sigma^2/\text{max}$) for correlated inputs of 44-group $^{239}\text{Pu}(\bar{\nu})$. Difference between NUSS-RF and Sandwich Rule methods increases with the level of input correlations, but the total uncertainties (σ) by both methods are in good agreement.

5.4 Application for large correlation: PB2-HZP

Moving from fast to thermal spectrum benchmarks, NUSS-RF is applied to the PB-2 hot zero power pin-cell model from the UAM benchmarks. The specification of the pincell can be found again in Table 3.3 in Chapter 3.6. When the SCALE6-44g covariance data are used, the top uncertainty contributor has been found to be $^{238}\text{U}(n,\gamma)$ by NUSS-SRS (see Fig.3.27 a). Fig.5.23 shows the correlation matrix of $^{238}\text{U}(n,\gamma)$ from SCALE6-44g covariance library, and the sensitivity coefficient profiles from TSUNAMI.

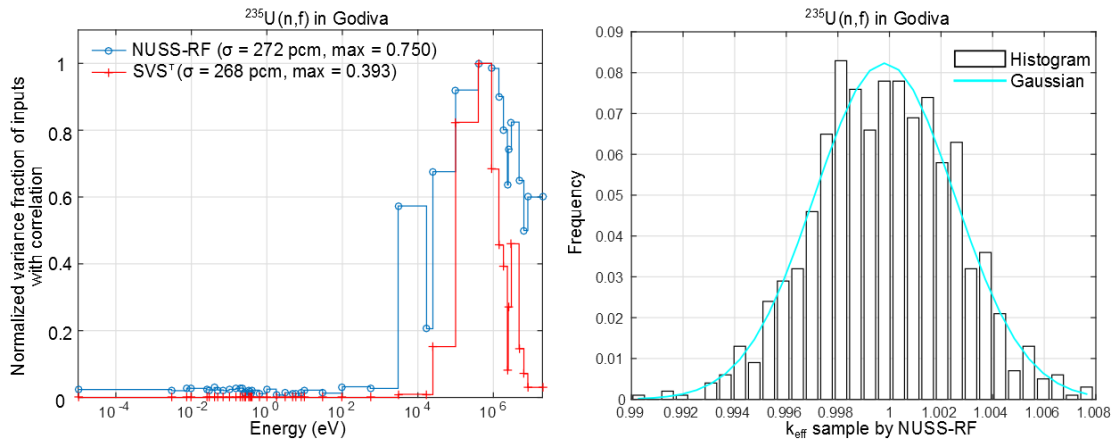


Figure 5.21: Normalized variance fractions ($V_i/\sigma^2/\max$) for correlated inputs of 44-group $^{235}\text{U}(n,f)$. Difference between NUSS-RF and Sandwich Rule methods increases with the level of input correlations, but the total uncertainties (σ) by both methods are in good agreement.

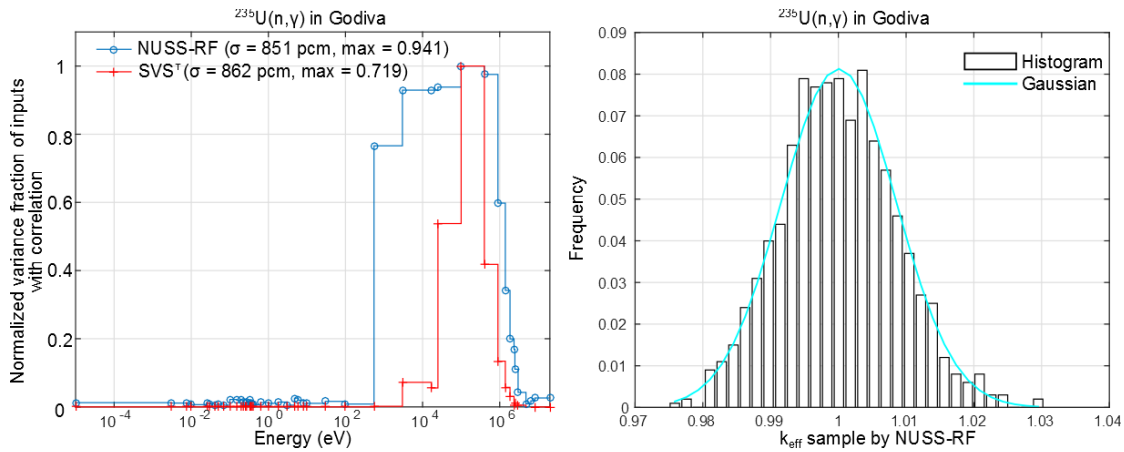


Figure 5.22: Normalized variance fractions ($V_i/\sigma^2/\max$) for correlated inputs of 44-group $^{235}\text{U}(n,\gamma)$. Difference between NUSS-RF and Sandwich Rule methods increases with the level of input correlations, but the total uncertainties (σ) by both methods are in good agreement.

In Fig.5.24, the variance fractions of uncorrelated inputs as calculated by NUSS-RF (1001 samples¹) and Sandwich Rule methods are plotted. In the latter method, the 44-group sensitivity coefficients have been calculated by MCNPX’s PERT CARD module instead of the TSUNAMI-calculated sensitivity coefficients in order. A standard deviation σ of 168 pcm is obtained from NUSS-RF sampling and it is in excellent agreement with the k_{eff} uncertainty of 167 pcm by the Sandwich Rule. It can also be seen that most of the variance contributions are located at the resonance energy range between 10 eV and 10^4 eV, corresponding to the large sensitivities in 238-group in Fig.5.23. In addition, around 0.1 eV there is noticeable uncertainty contribution due to neutron flux thermalization.

¹RBD algorithm requires an odd number of samples.

5.4. Application for large correlation: PB2-HZP

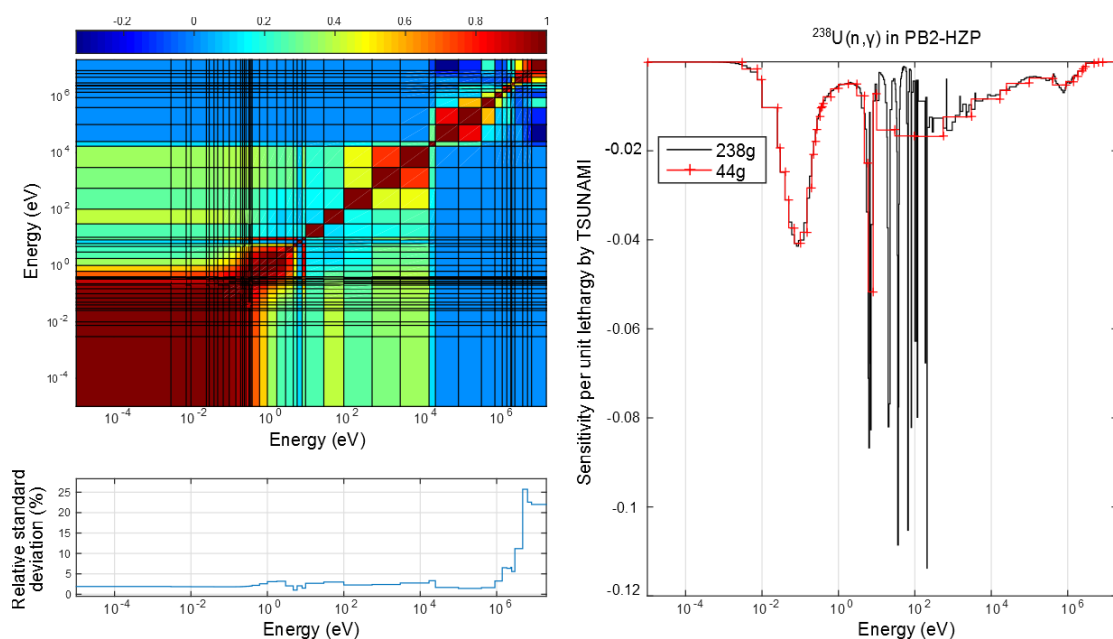


Figure 5.23: SCALE6-44g correlation matrix for cross section $^{238}\text{U}(n,\gamma)$ and sensitivity profiles calculated by TSUNAMI.

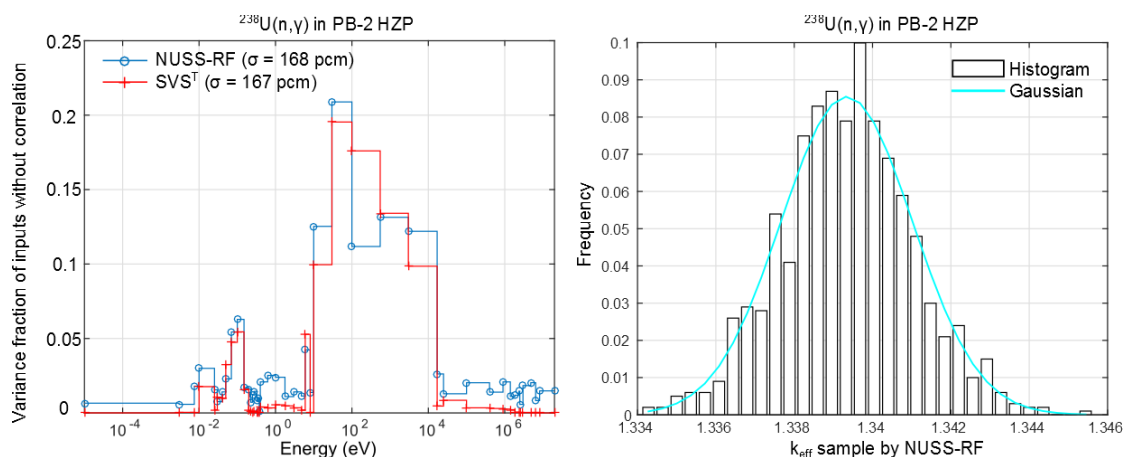


Figure 5.24: Variance fractions for uncorrelated inputs of 44-group $^{238}\text{U}(n,\gamma)$ show good agreement between NUSS-RF and “Sandwich Rule”. k_{eff} samples by NUSS-RF exhibit Gaussian (normal) shape and the total uncertainties (σ) by both methods are in good agreement.

In the case of correlated inputs, Fig.5.25 shows discrepancies in both the magnitude of variance fractions and the energy groups which are responsible for the most uncertainties. Between 10^{-5} eV and 0.35 eV in the thermal energy range, inputs have similar variance fraction values which is seen as the smooth blue curve. This is caused by the strong and long-ranged correlations of $^{238}\text{U}(n,\gamma)$ in the corresponding energy groups as shown in Fig.5.23. Intuitively, random samples of highly correlated inputs (see the correlation matrix of $^{238}\text{U}(n,\gamma)$) also have high correlations, as visualized in the scatter plots in Fig.5.26. From sampling of the inputs

Chapter 5. Implementing NUSS-RF and its applications

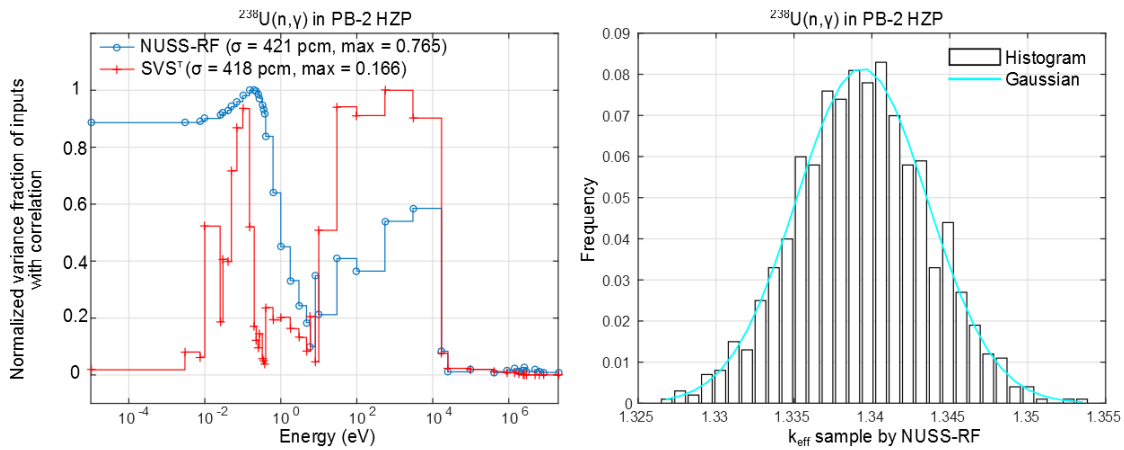


Figure 5.25: Normalized variance fractions ($V_i/\sigma^2/\max$) for correlated inputs of 44-group $^{238}\text{U}(n,\gamma)$. Difference between NUSS-RF and Sandwich Rule methods increases with the level of input correlations. k_{eff} samples by NUSS-RF exhibit Gaussian (normal) shape and the total uncertainties (σ) by both methods are in good agreement.

covariance matrix, the perturbation factors of the neighbouring energy groups can be seen to vary linearly with the reference group which is set to correspond to the input with the maximum variance fraction. As a result, even though k_{eff} is in fact not sensitive to cross sections below 10^{-2}eV , scatter plots in Fig.5.27 show linear variations between k_{eff} and perturbation factor in these groups.

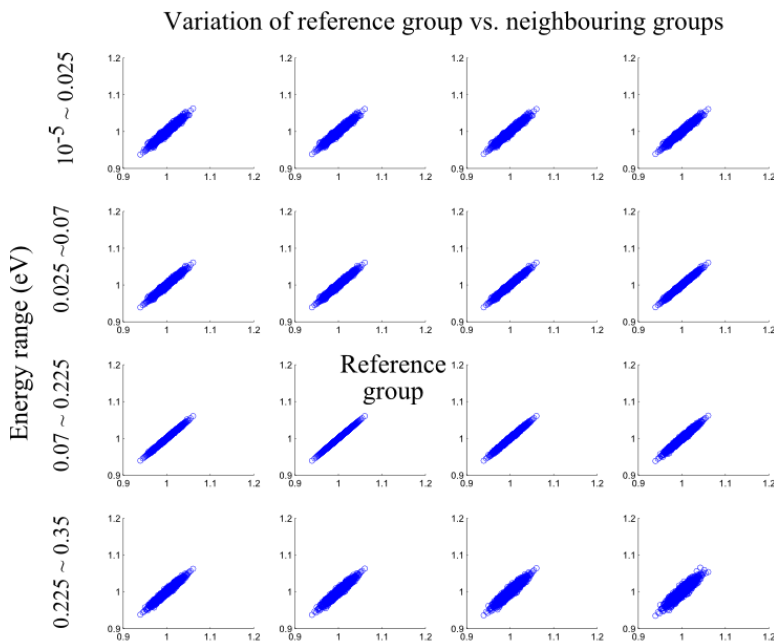


Figure 5.26: High correlations in the thermal groups of $^{238}\text{U}(n,\gamma)$ lead to their similar perturbation factors prepared by random sampling.

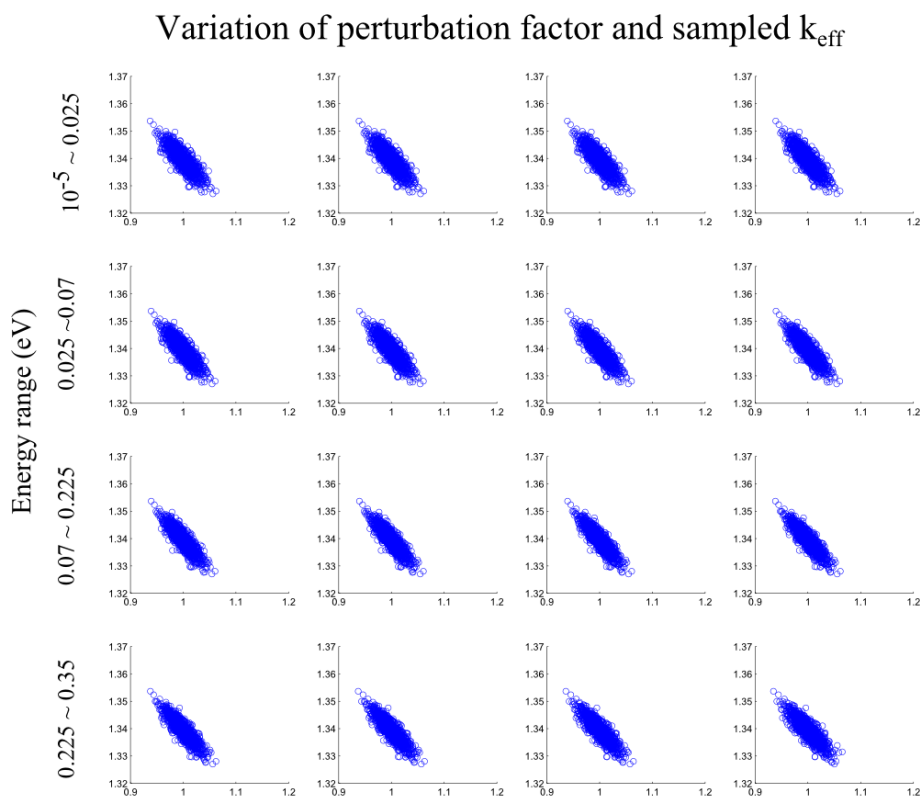


Figure 5.27: k_{eff} samples vary with perturbation factors in a similar manner in thermal groups due to the similar variation of perturbation factors shown in Fig.5.26.

Chapter's key message

The motivation for the development of NUSS-RF is to efficiently associate important nuclear data with their high variance contribution in k_{eff} uncertainty. The capability to decompose total k_{eff} variance into individual input variance contribution is based on Random Balance Design, a global sensitivity method, as opposed to the conventional first-order “Sandwich Rule” approach. It has been shown that, only in the case of uncorrelated inputs and linear systems, Sandwich Rule results of input variance contributions are in agreement with the those computed by the global-based NUSS-RF. In nuclear data uncertainty quantification problems, the correlations among nuclear data (in energy groups, in reaction pairs etc.) should not be neglected in order to quantify the total k_{eff} uncertainty correctly. The same total k_{eff} uncertainty is decomposed differently into individual variance contributions by the two methods. NUSS-RF has been verified through analytical equations. Therefore, the fact that nuclear data are correlated compels the use of NUSS-RF instead of the Sandwich Rule for the decomposition of total k_{eff} uncertainty due to nuclear data uncertainties into individual contributions.

6 Conclusion and future work

In this PhD work, a computational tool called NUSS (Nuclear data **U**ncertainty **S**tochastic **S**ampling) has been developed to perform nuclear data uncertainty propagation and quantification. As its name suggests, the concept of stochastic sampling (SS) has been implemented in NUSS, as opposed to the conventional deterministic first-order moment propagation approach. Between the time of the PhD proposal in 2010 and the commencement of the PhD project in 2011, several SS-based codes for nuclear data uncertainty quantification (NDUQ) were conceived. While their works had certainly validated the idea of SS for NDUQ, they had only investigated the same simple random sampling (SRS) scheme and could not be easily applied to the need at PSI which is to include nuclear data uncertainty quantification through Monte Carlo code MCNP/MCNPX for criticality safety assessment and burnup credit validation applications. The goal of this PhD work therefore is to develop the computational tool NUSS specifically for MCNPX and to extend the NDUQ capabilities beyond those of the existing SS-based tools.

This final chapter of the thesis consists of a summary of previous chapters and reiterates the scientific contributions of this PhD work. Unresolved issues are brought forward which shall be considered as future works.

6.1 Chapterwise summary

Chapter 1 began with an overview of the on-going activities in the field of nuclear data uncertainty quantification in which PSI had participated, namely the OECD/NEA/NSC/WPRS Expert Group on Uncertainty Analysis in Modelling (UAM-LWR) and OECD/NEA/NSC/WPNCS Expert Group on Uncertainty Analysis Criticality Safety Assessment (UACSA). The benchmarks set up by these working parties have been used during the development of NUSS tool for verification and validation purposes. Before the different methods to perform NDUQ were surveyed, the formats of nuclear data and nuclear data uncertainties were presented. The key point was to understand that nuclear data uncertainties originate from experimental measurements and theoretical models. They can acquire correlations after propagating through a

chain of formatting processes to become the multigroup nuclear data covariance matrices to be used by NUSS. Reliable multigroup nuclear data covariances are required also in the conventional NDUQ method based on the first-order moment propagation (commonly known as “Sandwich Rule”) method. It combines nuclear data covariances with the sensitivity coefficients to determine the second moment of the linearized system response k_{eff} . Alternatively, sampling-based methods were introduced with the emphasis on the types of nuclear data formats they were compatible with. The variety of nuclear data formats considered by these methods spans from experimental measurements and theoretical model parameters (i.e. TMC method) to multigroup (i.e. XSUSA). With the understanding of nuclear data formats and existing NDUQ methods, the motivation of implementing a sampling-based tool for MCNPX was presented, along with specific areas to be researched in this PhD work.

Chapter 2 presented the implementation of the NUSS-SRS (i.e. with **Simple Random Sampling** capability) tool, starting with an explanation of the continuous-energy Monte Carlo code MCNPX and the pointwise-energy ACE format for nuclear data. Understanding the data structure of ACE format was crucial for introducing random perturbations to the nuclear data of interest. Equally important was the sum rules that specify which cross sections need to be updated consistently upon the modification of certain partial cross sections. ACE formatted data were generated by NJOY, the nuclear data processing code which has also been applied mainly for the generation of multigroup nuclear data covariances in this PhD work. The first of the five steps of NUSS-SRS workflow involved the preparation of multigroup covariances. The assumption that nuclear data are multivariate normal must be laid out for the implementation of random sampling method in NUSS and this assumption is shared by existing SS-based codes which also use multigroup covariances. The sampling of multigroup covariance data and the modification of the ACE-formatted data were accomplished by MATLAB and shell scripts. The advantage of perturbing ACE files is the seamless interface between these ACE files and MCNPX as long as the aforementioned sum rules are respected. Thanks to the well-documented ACE format, NUSS implementation was relatively straight-forward. Nuclear data (n, n) , (n, n') , $(n, 2n)$, $(n, \text{fission})$, (n, γ) , $\bar{\nu}$ and χ in ACE format can be perturbed and their uncertainties propagated through MCNPX calculations. Finally NUSS analyzes the outputs of MCNPX calculations in terms of the sample mean, sample variance and confidence interval for the variance.

In Chapter 3, NUSS-SRS was evaluated against both the “Sandwich Rule” and other SS-based approaches. First-order sensitivity coefficient (S_k) has been generated by NUSS through one-at-a-time perturbation on well-defined inputs instead of the usual random sampling mode. Groupwise S_k of NUSS and MCNPX’s PERT CARD module were compared for the same amount of perturbations in the cross section data. Due to Monte Carlo statistical errors, NUSS direct perturbation of small magnitudes gives less precision on k_{eff} uncertainty as expected. On the other hand, PERT CARD is implemented to handle small perturbations but assumes unperturbed fission source distribution. NUSS-SRS was then compared to TSUNAMI which is based on the first-order adjoint perturbation theory and the “Sandwich Rule” for the determination of k_{eff} uncertainty due to nuclear data uncertainties ($\sigma_k^2 = S_k V S_k^T$). The

results of NUSS-SRS and TSUNAMI were in good agreement when the same covariance data libraries were used. NUSS and TSUNAMI require multigroup covariance data, in contrast to the SS-based TMC method. The comparison between TMC and NUSS-SRS showed the propagation of nuclear data uncertainties at the levels of nuclear data model (in TMC) and of ACE files (NUSS-SRS) were comparable with some exceptions due to possibly the questionable quality of certain TENDL-2011 covariance data. Improvement of NUSS and TMC comparison is obtained with TENDL-2014 covariances. Indeed the outcome of NUSS calculations depend greatly on the quality of nuclear data covariances. For the considered benchmark cases (Jezebel and Godiva), the group structure variation was also found to have relatively minor impact on NUSS results. Finally, NUSS-SRS was applied to the UAM pincell and UACSA benchmarks.

Chapter 4 was dedicated to the variance-based global sensitivity analysis. It was motivated by the ineffectiveness of simple random sampling for sensitivity analysis, in terms of the decomposition of total variance into individual input contributions. The FAST (Fourier Amplitude Sensitivity Testing) is an elegant method to decompose variances. But its use was limited to a small number of uncorrelated inputs. The RBD (Random Balance Design) method which is built upon FAST has overcome the challenges of large number of inputs and the correlations among them. As a promising method for NDUQ, RBD was chosen to be implemented in the second part of NUSS, called NUSS-RF to calculate the variance contributions of correlated inputs. Unlike simple random sampling which has been implemented in other sampling-based codes, RBD for NDUQ is first-of-its-kind. Variance decomposition according to the “Sandwich Rule” formulation was also presented.

In Chapter 5, RBD was shown to be integrated into the NUSS tool, as an alternative option from the simple random sampling (SRS) technique. The addition of RBD module did not require retrofitting the NUSS tool in that perturbation factors from RBD could be generated using only the covariance matrices and be applied to perform the modification of ACE files in the same manner as the SRS option. Three mathematical benchmarks were used for both the verification of RBD implementation and the comparison of RBD and local sensitivity “Sandwich Rule” method. As the analytical solutions are known, they reveal that the global and local-based approaches arrived at the same variance decomposition formulae when the inputs were uncorrelated. In case of correlated inputs, the local “Sandwich Rule” approach gave lower estimates of decomposed variance than the global approach. From the three mathematical benchmarks, the implementation of RBD as part of NUSS was verified. It was then applied to Jezebel, Godiva fast benchmarks and the UAM pincell benchmarks. Same observations were made that NUSS-RF results were in good agreement with the conventional “Sandwich Rule” method when the nuclear data inputs were uncorrelated. Before the application of RBD for NDUQ, the local approach had been the only effective means to determine the sensitivity coefficient of output to input variation. Now NUSS-RF is capable of not only pinpointing which inputs are influential in terms of their individual variance contributions, but also estimating energy-dependent sensitivity coefficient through mathematical manipulation (Eqn.(5.22)). As the level of correlation increased, discrepancies between global NUSS-RF and

local “Sandwich Rule” widened. It is observed that, even though the system may be sensitive to only certain nuclear data, the high correlations between these particular nuclear data and other insensitive nuclear data can cause similar (i.e. correlated) variance contributions. As a result, nuclear data with low k_{eff} sensitivity would be considered unimportant in the “Sandwich Rule” approach, but might be considered important in NUSS-RF if they are highly correlated to nuclear data with high k_{eff} sensitivity. The global-based NUSS-RF predicts a larger k_{eff} uncertainty contribution by all these correlated nuclear data collectively than the “Sandwich Rule” approach.

In the current Chapter 6, the work performed in this PhD project has been summarized. In the following, the scientific contributions are highlighted which pave for several research directions to be pursued further in the future.

6.2 Contribution summary and future work

In the beginning of the thesis in Chapter 1.6, the research focus and scientific contribution of this PhD project were listed to be:

1. Mixing of continuous-energy and multigroup nuclear data formats
2. Stochastic sampling of nuclear data with MCNPX
3. Sensitivity from stochastic sampling

Through the presented PhD work, these areas have been addressed and the main achievements of research activities are highlighted below. Given the limited duration of the project, areas of research which deserve further examination upon completion of the current PhD project are discussed as future works.

Mixing of continuous-energy and multigroup formats

NUSS has been implemented such that the perturbation of the pointwise ACE-formatted nuclear data is in a groupwise manner, matching the multigroup structure of the nuclear data covariances. Such implementation can also be found in the SAMPLER code of SCALE6 to obtain the correctly perturbed self-shielded multigroup cross sections. In this PhD work, SCALE6-44g, ENDF/B-VII.1 and TENDL-2011 covariances in multigroup structures have been applied. The ability to propagate these multigroup uncertainties through pointwise ACE nuclear data files and continuous-energy MCNPX was verified with alternative NDUQ methods (i.e. TSUNAMI, PERT CARD). The k_{eff} uncertainty due to nuclear data as calculated by NUSS was as refined as the number of energy groups carried by the covariances. In the preliminary assessment of covariance matrix group structure effect on k_{eff} uncertainty, using fast-spectrum Jezebel and Godiva benchmarks, it was shown that from 30 to 44 to 80 groups, the k_{eff} uncertainty varies insignificantly as compared to the change of covariance matrices. If

pointwise covariances (from ENDF-6 format) are directly fed into NUSS, the algorithm would not discriminate in theory, even though numerically the decomposition of an enormous matrix (dimension of hundreds of thousands squared) is extremely difficult. Furthermore, as the current evaluation of nuclear data covariance is suspected to be overestimated, the refinement of energy groups is likely ineffective for acquiring more accurate quantification of nuclear data uncertainty contribution. In the other direction, by reducing the number of groups to one or two groups, the deterioration of nuclear data uncertainty contribution result was apparent as shown in Chapter 3.4. Since in SS-based method, the “cost” of computation time depends on the sample size, not on the number of energy groups (which is opposite in “Sandwich Rule”-based method), the reliability (i.e. appropriate flux weighting functions and locations of group boundaries) of the multigroup covariances was the most important.

Future work

The current implementation of NUSS is limited to energy-dependent cross section and nuclear data (n,n) , (n,n') , $(n,2n)$, $(n,\text{fission})$, (n,γ) , $\bar{\nu}$ and χ . For other nuclear data such as $S(\alpha,\beta)$, angular distribution and resonances, the scheme to perturb them in ACE format using multigroup or ENDF-6 formatted covariances remains as future work. It is expected that the main task would involve ensuring the mixing of different nuclear data formats for these data is consistent.

For $S(\alpha,\beta)$ information stored in separate files from the usual ACE-formatted nuclear data files, they must be specifically included in the MCNPX input file in order to treat thermal neutron scattering by molecules and crystalline solids (as moderator materials) correctly. In ENDF-6 format, File MF7 MT4, the incoherent inelastic scattering law is given in tables of S dependent on α (momentum transfer parameter) for various values of β (energy transfer parameter). Then through NJOY’s THERMR and ACER modules, the $S(\alpha,\beta)$ data are formatted into tables which are organized in blocks, containing energy dependent inelastic and elastic scattering cross sections, coupled energy-angle distributions for inelastic scattering and angular distributions for elastic scattering. Though a very important nuclear data, $S(\alpha,\beta)$ has limited uncertainty information which prompted studies to generate best-estimated data of $S(\alpha,\beta)$ [79] or its covariance matrix[80], both by sampling-based techniques.

For secondary particle angular distribution, their covariances are located in the ENDF-6 format File MF34, with the actual angular distribution data in File 4. Using NJOY, the uncertainty and correlation data can be prepared, for example shown in Fig.6.1 where the average cosine angle μ and relative uncertainty $\Delta\mu/\mu$ are plotted against incident neutron energy E . Fig.6.1 has simplified the many details of angular distribution as shown in Fig.6.2. To describe such details, the ACE format uses 32 equiprobable cosine bins to represent the angular probability distribution at given incident energies.

Resonance parameter uncertainties can be found in ENDF-6 format File MF32. Resonance widths are strictly positive quantities, yet a random sampling based on the normal distribution assumption could result in negative values when sampled from large uncertainties. Hence,

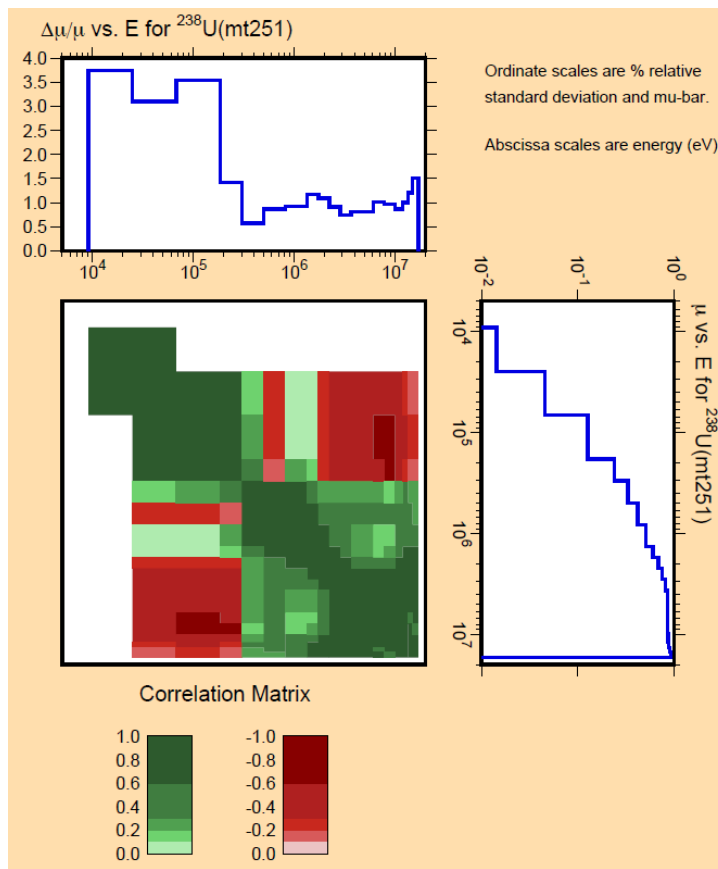


Figure 6.1: Example of angular distribution covariance data formatted by NJOY (P.296).

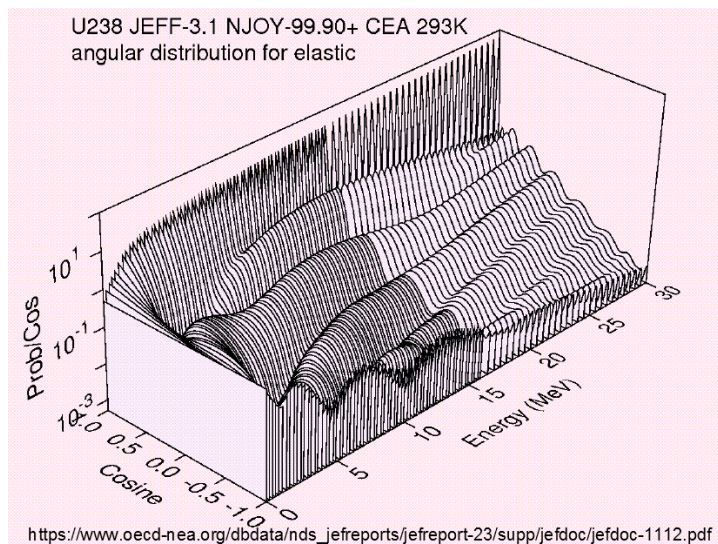


Figure 6.2: Example of angular probability distribution.

the use of lognormal distribution has been proposed [81]. Certainly such issue is not limited to resonance parameters, but also cross sectional and probability data. The basic assumption

of normal distribution deserves further examination. On the other hand, motivated by a different challenge, which is to reduce the size of ENDF-6 formatted files (due to large amount of information in File MF32), the conversion of File MF32 data into File MF33 is done by the SCALE PUFF-IV code for processing ENDF uncertainty data into multigroup covariance matrices [82] for selected isotopes in ENDF/B-VII.1 library such as ^{239}Pu , ^{235}U and ^{238}U . Hence, when multigroup covariances are prepared using ENDF/B-VII.1 files, resonance uncertainties are implicitly included in the cross section uncertainties (for MT=1,2,18,102). However, an independent quantification of resonance parameter uncertainties is still of great interest and should be examined in future works.

Stochastic sampling with MCNPX

NUSS-SRS has been implemented specifically for MCNPX and the sampling approach is reliable as shown by the comparison studies between NUSS and deterministic “Sandwich Rule” methods. As a “blackbox” approach, NUSS-SRS is un-intrusive to MCNPX routine calculations, which allowed the correct fission source distribution to be established in each sample case. Furthermore, the choice of MCNPX output for which uncertainty can be quantified is flexible thanks to the “blackbox” approach. More precisely, the parameter of interest is in fact not the sample mean itself, but the sample variance. Depending on the run-time of MCNPX calculations, various sample sizes have been used from about 100 to over 1000. Certainly, the larger the sample size, the more converged the sample mean is, and similarly the sample variance. However, in this PhD work, it has been argued that, the current nuclear covariance data are likely to be overestimated. Using a smaller number of samples though cannot guarantee the sample variance values are converged, the lower precision of the propagated uncertainty from over-estimated covariance data is compensated by the use of confidence intervals. It has been assumed that, the underlying population of k_{eff} is normal by the multivariate normal distribution assumption of nuclear data. Consequently, the distribution of sample k_{eff} variance is the χ^2 distribution from which the confidence interval can be calculated.

Future work

With sampling, the choice of output parameter for which uncertainty can be quantified is more flexible than that from the deterministic classic perturbation methods. In this PhD, NUSS has been applied to compute the 1-group cross section with uncertainties for the UAM-Phase 1 exercise. What naturally follows is to complete the UAM-Phase 1b exercise which is the propagation of nuclear data uncertainty through burnup calculation. The output parameters of interest include k_{eff} , reaction rates, collapsed cross sections and nuclide concentrations. Existing results [4][46][83] for UAM-Phase 1b exercise can provide verification for NUSS. To perform these benchmarked burnup calculations, two options can be considered: MCNPX/CINDER or SERPENT, both of which are Monte Carlo-based codes and use ACE-formatted nuclear data. While Monte Carlo codes provide accurate calculation of flux in both energy space and detailed physical locations, nuclear data uncertainties are naturally propagated through depletion calculations at each burnup step into the perturbed fluxes, reaction rates

and isotope densities. At PSI, MCNPX/CINDER has been compared to CASMO-4E code for nuclide density calculations, verified with experiments at the PSI's PROTEUS reactor [84]. Studies of combining SERPENT and sampling-based nuclear data perturbation for assembly-type problems have been done by TMC [34][85] and can provide verifications for NUSS application with SERPENT.

Nuclear data uncertainty quantification is part of the comprehensive uncertainty quantification. Other sources of uncertainty in MCNPX calculation include manufacturing and technological parameter uncertainties. Hence, at PSI, a systematic tool called MTUQ for quantifying non-nuclear data parameter uncertainties has been developed for MCNPX based on stochastic sampling method [86]. MTUQ is capable of introducing perturbation to geometry and material properties (i.e. so-called manufacturing and technological parameters) according to the given parameter uncertainties and probability distributions, taking into account certain physical constraints. Studies of spent fuel transport casks can be conducted in MCNPX with the quantification of output uncertainty due to manufacturing and technological parameters by MTUQ, as well as nuclear data uncertainty contribution by NUSS.

Sensitivity from stochastic sampling

In this PhD, sensitivity analysis refers specifically to the determination of individual input variance contributions in proportion to the total variance of a system output. Conventionally, in order to determine the ranking of inputs in terms of their uncertainty contributions, individual input can be sampled one-by-one in which case correlations between inputs cannot be taken into account. Also, the total number of MCNPX calculations is equal to the number of inputs multiplied by the number of random samples, making such operation time consuming. The squared value of Pearson correlation coefficient can be calculated to estimate the variance contributions apportioned to individual inputs, but is limited to linear systems. Now with NUSS-RF, a more efficient and flexible way of estimating the ranking of inputs is available. Unlike existing "blackbox"-type simple random sampling methods where the relation between inputs and outputs is inferred through statistical regression analysis, the first-of-its-kind NUSS-RF, based on Random Balance Design prepares the sampling of inputs by design (i.e. not "blackbox"). As shown in Chapter 5.3 with the 44-input problems (i.e. 44 energy group-wise cross sections of the same isotope-reaction), NUSS-RF is capable of decomposing the k_{eff} variance into 44 cross section variance contributions. The consideration of correlations among inputs has a significant impact on the variance decomposition results from NUSS-RF compared to those from the deterministic "Sandwich Rule" approach. It has been found that inputs with higher correlations have more similar variance contribution, consequently can be considered similarly important.

The deterministic "Sandwich Rule" approach had always been used as the reference of verification for sampling-based uncertainty quantification. However, in terms of decomposition of total variance into individual input variance contributions, "Sandwich Rule" results are different from those of RBD as shown by three mathematical benchmarks, as well as in nuclear

data uncertainty applications. When it is desired to rank nuclear data by their uncertainty contributions in the system response such as k_{eff} , different ranking is expected from “Sandwich Rule” versus NUSS-RF.

Global sensitivity analysis is to be distinguished from the first-order sensitivity coefficient which can be determined by direct perturbation, differential operator sampling (DOS) or adjoint weighted perturbation (AWP) methods. With Random Balance Design in NUSS-RF, it has been shown possible to disentangle the sensitivity coefficients from the variance decomposition results through Eqn.(5.22) as if they are uncorrelated. Since NUSS-RF can efficiently compute the individual variances, sensitivity coefficients (although only in absolute values) of system responses different from k_{eff} can be estimated, which are not possible with the current deterministic methods such as the classic AWP or DOS for NDUQ problems.

Future work

The current implementation of NUSS-RF does not provide a confidence interval to the result of variance decompositions as in the NUSS-SRS approach for σ_k^2 . The precision of NUSS-RF results depends not only on the size of samples, but also on the use of harmonics order in the summation of the power spectrum amplitudes. The current version of NUSS-RF uses the same harmonics order for all inputs. However, ideally, inputs with lower importance, manifested by a smaller variance should be computed with a smaller harmonics order so as to avoid adding up the noise components.

The efficiency of NUSS-RF for automatic decomposing individual input variances has been shown in cases of single energy-dependent reaction in this PhD work. However, in NDUQ, the more relevant uncertainty information is sometimes the energy-integrated isotope-reaction uncertainty contribution. For example the UAM-Phase 1 exercise in Chapter 3.6 focuses only on the top five uncertainty contributors which make up more than 90% of the total output uncertainty. To quantify uncertainty in a similar manner, the few-group covariance data can be used in NUSS-RF to reduce to fewer number of inputs. However, as seen in Chapter 3.4, a coarse energy group structure leads to the overestimation of uncertainty contributions. Visual inspection of the groupwise cross section uncertainties can be used to rank the inputs in terms of uncertainty contributions. However, the amount of uncertainty due to a single reaction cannot be easily isolated from other reactions which are correlated to it.

6.3 Concluding remarks

This PhD work aimed to quantify nuclear data uncertainties for the continuous-energy MC-NPX code through the approach of stochastic sampling. It has been accomplished with the implementation of the NUSS systematic tool, which enabled research activities such as the comparison of various nuclear data covariance libraries, the quantification of k_{eff} uncertainty in benchmarks chosen by OECD/NEA working party expert groups (UAM and UACSA), as well as the development of global sensitivity analysis focusing on the efficient calculation

Chapter 6. Conclusion and future work

of individual input variance contributions. Even though the current PhD work has yet to be applied more broadly to actual applications such as criticality safety and burnup credit, it has first and foremost demonstrated the proof of concept. NUSS has the feasibility and flexibility of working with continuous-energy Monte Carlo codes which are required for high fidelity nuclear system simulations. The quantification of simulation uncertainty due to nuclear data uncertainties is also expected to motivate the improvement of nuclear data and covariances.

Appendix

A Derivations

A1 Sandwich Rule

First order approximation is the key in the derivation of the Sandwich Rule. In the Taylor expansion of the response R :

$$\begin{aligned}
 R(\alpha_1, \dots, \alpha_k) &= R(\vec{\alpha}_o) + \sum_i^k \left(\frac{\partial R}{\partial \alpha_i} \right)_{\vec{\alpha}_o} \Delta \alpha_i + \frac{1}{2} \sum_{i_1, i_2}^k \left(\frac{\partial^2 R}{\partial \alpha_{i_1} \partial \alpha_{i_2}} \right)_{\vec{\alpha}_o} \Delta \alpha_{i_1} \Delta \alpha_{i_2} + \dots \\
 &\quad + \frac{1}{n!} \sum_{i_1, \dots, i_n}^k \left(\frac{\partial^n R}{\partial \alpha_{i_1} \dots \partial \alpha_{i_n}} \right)_{\vec{\alpha}_o} \Delta \alpha_{i_1} \dots \Delta \alpha_{i_n} \\
 &\approx R(\vec{\alpha}_o) + \sum_i^k \left(\frac{\partial R}{\partial \alpha_i} \right)_{\vec{\alpha}_o} \Delta \alpha_i = R_o + \sum S_i \Delta \alpha_i
 \end{aligned} \tag{1}$$

Let $p(\alpha_1, \dots, \alpha_k)$ denote the joint probability density function of $(\alpha_1, \dots, \alpha_k)$. The definition of the second central moment is:

$$\begin{aligned}
 \mu_2(R) &= E[(R - R_o)^2] \approx \int \left(\sum_i^k S_i \Delta \alpha_i \right)^2 p(\vec{\alpha}) d\vec{\alpha} \\
 &= \int \left(\sum_i^k (S_i \Delta \alpha_i)^2 + 2 \sum_{i \neq j}^k S_i \Delta \alpha_i \Delta \alpha_j S_j \right) p(\vec{\alpha}) d\vec{\alpha} \\
 &= \sum_i^k S_i^2 \left(\int \delta \alpha_i^2 p(\vec{\alpha}) d\vec{\alpha} \right) + 2 \sum_{i \neq j}^k S_i \left(\int \delta \alpha_i \delta \alpha_j p(\vec{\alpha}) d\vec{\alpha} \right) S_j
 \end{aligned} \tag{2}$$

Recognizing the variance and covariance terms:

$$\int \delta \alpha_i^2 p(\vec{\alpha}) d\vec{\alpha} = \int (\alpha_i - \alpha_{i,o})^2 p(\vec{\alpha}) d\vec{\alpha} = \text{var}(\alpha_i) \tag{3}$$

$$\int \delta \alpha_i \delta \alpha_j p(\vec{\alpha}) d\vec{\alpha} = \int (\alpha_i - \alpha_{i,o})(\alpha_j - \alpha_{j,o}) p(\vec{\alpha}) d\vec{\alpha} = \text{cov}(\alpha_i, \alpha_j) \tag{4}$$

Putting Eqn. (3) and (4) into Eqn. (2), the variance of the response is obtained as the product of sensitivity coefficient vectors and the covariance matrix of inputs:

$$\mu_2(R) = \text{var}(R) = \sum_i^k S_i^2 \cdot \text{var}(\alpha_i) + 2 \sum_{i \neq j}^k S_i \text{cov}(\alpha_i, \alpha_j) S_j = \vec{S} \mathbf{V}_\alpha \vec{S}^T \quad (5)$$

The above formulation is known as the “propagation of moments” method and can be found in Section III.F of [87]. There, more complex equations for propagation of high-order moments are also given.

A2 Differential Operator Sampling

Full derivations of the Differential Operator Sampling (DOS) method in MCNPX can be found in [88][89]. It is based on Taylor series expansion of the response change (Δc) at first and second orders:

$$\Delta c = \sum_{n=1} \frac{1}{n!} \frac{d^n c}{dv^n} (\Delta v)^n \approx \frac{dc}{dv} \Delta v + \frac{1}{2} \frac{d^2 c}{dv^2} \Delta v^2 = u_1 \Delta v + u_2 \Delta v^2 \quad (6)$$

where Δv is the fractional change of input (e.g. density, concentration, macroscopic cross section [88]). Specifically, the response c is the track-length estimate tally in MCNPX:

$$c_{j'} = \sum_{j'} t_{j'} q_{j'} \quad (7)$$

where $t_{j'}$ is the tally response estimator of path segment j' and $q_{j'}$ the probability of path segment j' . Substituting Eqn.(7) into the first-order coefficient of Eqn.(6):

$$u_1 = \frac{dc}{dv} = \frac{d}{dv} \left(\sum_{j'} t_{j'} q_{j'} \right) \quad (8)$$

$$= \sum_{j'} \left(t_{j'} \frac{dq_{j'}}{dv} + q_{j'} \frac{dt_{j'}}{dv} \right) \quad (9)$$

$$= \sum_{j'} t_{j'} q_{j'} (P_{1,j'} + R_{1,j'}) \quad (10)$$

The two terms are expanded in the following:

$$P_{1,j'} = \frac{1}{q_{j'}} \frac{dq_{j'}}{dv} \quad \text{substituting } q_{j'} = \prod_{k=0} r_k \quad (11)$$

$$= \sum_k \frac{dr_k}{dv_{j'}} \frac{1}{r_k} \quad (12)$$

$$= \sum_k \beta_{k,j'} \quad (13)$$

where r_k is the probability of track k within the segment j' .

$$R_{1,j'} = \frac{1}{t_{j'}} \frac{dt_{j'}}{dv_{j'}} \quad \text{where } t_{j'} = \lambda_k \sum_{c \in C} x_c(E) \quad \text{and } dv = \frac{dx_b(h)}{x_b(h)} \quad (14)$$

$$= \sum_{b \in B} \sum_{h \in H} \frac{x_b(h)}{\sum_{c \in C} x_c(h)} \frac{\partial}{\partial x_b(h)} \left(\sum_{c \in C} x_c(h) \right) \quad (15)$$

$$= \frac{\sum_{c \in B} \sum_{E \in H} x_c(E)}{\sum_{c \in C} x_c(E)} \quad (16)$$

where tally response $t_{j'}$ is a linear function of some combination of reaction cross sections, B and E are a set of cross sections and the energy interval for cross sections to be perturbed. $R_{1,j'}$ is the fraction of reaction rate tally involved in the perturbation. If all cross sections in the tally are perturbed by the same amount over all energies, $R_{1,j} = 1$ (e.g. in cases of density perturbation). The history-based estimator for first-order perturbation is:

$$\langle u_1 \rangle = \frac{1}{N} \sum_i \left(\sum_{j'} \left(\sum_{k=0} \beta_{j',k} + R_{1,j'} \right) t_{j'} \right) \quad (17)$$

Without derivation details, the second order perturbation $\langle u_2 \rangle$ is:

$$\langle u_2 \rangle = \frac{1}{2N} \sum_i \left(\sum_{j'} \left(\sum_{k=0} (\alpha_{j',k} - \beta_{j',k}^2) + \left(\sum_{k=0} \beta_{j',k} + R_{1,j'} \right)^2 - R_{1,j}^2 \right) t_{j'} \right) \quad (18)$$

Finally, the total perturbation is the sum of the two orders of perturbation:

$$\langle c \rangle = \langle u_1 \rangle \Delta v + \langle u_2 \rangle \Delta v^2 \quad (19)$$

A3 First-order Adjoint Perturbation Method

The steady state Boltzmann equation is written in the operator form as an eigenvalue problem:

$$L\phi = \frac{1}{k} M\phi \quad (20)$$

where L and M denote the unperturbed ‘‘loss’’ (i.e. streaming, collision and scattering) and ‘‘gain’’ (fission) operators. ϕ and k are the unperturbed flux and k_{eff} values respectively. Now, introducing perturbations to the operators, which result in perturbations in k and ϕ as well:

$$(L + \Delta L)(\phi + \Delta\phi) = \frac{1}{k + \Delta k} (M + \Delta M)(\phi + \Delta\phi) \quad (21)$$

The assumption that $\Delta k/k \ll 1$ for very small amount of perturbation to ensure linearity around nominal value and the use of binomial approximation lead to:

$$\frac{1}{k + \Delta k} = \frac{1}{k(1 + \Delta k/k)} \approx \frac{1}{k} (1 - \Delta k/k) = \frac{1}{k} - \frac{\Delta k}{k^2} \quad (22)$$

Appendix . Appendix

In terms of reactivity ρ which is $\rho = \frac{k-1}{k}$:

$$\frac{1}{k + \Delta k} \approx \frac{1}{k} - \Delta\rho \quad \text{given} \quad \Delta\rho \approx \frac{\Delta k}{k^2} \quad (23)$$

Eqn(21) is rearranged after the substitution of $\Delta\rho$ and the omission of second and third high order terms:

$$\mathcal{O}(\Delta^2, \Delta^3) = (\Delta L - \frac{1}{k} \Delta M)\phi + (L - \frac{1}{k} M)\Delta\phi + \Delta\rho M\phi \quad (24)$$

$$= \frac{1}{k} \Delta M \Delta\phi - \Delta\rho (\Delta M\phi + M\Delta\phi + \Delta M\Delta\phi) \approx 0 \quad (25)$$

On one hand, in the so-called ‘‘forward’’ manner, the perturbation in reactivity can be obtained by using the perturbed flux $\Delta\phi$:

$$\Delta\rho \approx - \frac{(\Delta L - \frac{1}{k_o} \Delta M)\phi_o + (L_o - \frac{1}{k_o} M_o)\Delta\phi}{M_o\phi_o} \quad (26)$$

However, repeatedly solving for $\Delta\phi$ as a result of each perturbed parameter is impractical for systems with many parameters. The alternative method to circumvent this is to use an adjoint flux ϕ^\dagger , which has the properties:

$$L^\dagger \phi^\dagger = \frac{1}{k^\dagger} M^\dagger \phi^\dagger, \quad \langle \phi^\dagger, L\phi \rangle = \langle L^\dagger \phi^\dagger, \phi \rangle, \quad \langle \phi^\dagger, \frac{1}{k} M\phi \rangle = \frac{1}{k^\dagger} \langle M^\dagger \phi^\dagger, \phi \rangle \quad (27)$$

Applying ϕ^\dagger as a weighting function to each term in Eqn.(26) and integrating (as $\langle \dots \rangle$) over the phase space (r, Ω, E):

$$\Delta\rho \approx - \frac{\langle \phi^\dagger, (\Delta L - \frac{1}{k} \Delta M)\phi \rangle + \langle \phi^\dagger, (L - \frac{1}{k} M)\Delta\phi \rangle}{\langle \phi^\dagger, M\phi \rangle} = - \frac{\langle \phi^\dagger, (\Delta L - \frac{1}{k} \Delta M)\phi \rangle}{\langle \phi^\dagger, M\phi \rangle} \quad (28)$$

The second term in the numerator which contains the $\Delta\phi$ has been eliminated because of the adjoint relations:

$$\langle \phi^\dagger, (L - \frac{1}{k} M)\Delta\phi \rangle = \langle (L^\dagger - \frac{1}{k^\dagger} M^\dagger)\phi^\dagger, \Delta\phi \rangle = \langle 0, \Delta\phi \rangle = 0 \quad (29)$$

In Eqn.(28), the calculation of perturbed reactivity (consequently the value of k_{eff}) requires the determination of the forward and adjoint fluxes which will be calculated only once, instead of the repeated calculation of $\Delta\phi$ in Eqn.(26).

The sensitivity coefficient of k with respect to nuclear data Σ_x is therefore[22]:

$$S_x = \frac{dk/k}{d\Sigma_x/\Sigma_x} = \frac{\Sigma_x k^2 d\rho}{k d\Sigma_x} = - \frac{\Sigma_x \langle \phi_o^\dagger, (\frac{dL}{d\Sigma_x} - \frac{1}{k} \frac{dM}{d\Sigma_x})\phi \rangle}{\langle \phi^\dagger, \frac{M}{k^2}\phi \rangle} \quad (30)$$

$$\text{where} \quad \frac{dk}{d\Sigma_x} = \frac{d\rho}{d\Sigma_x} k^2 \quad (31)$$

The adjoint flux ϕ^\dagger (synonyms are adjoint function, importance function) is generally interpreted as the response of a prescribed detector contributed by the neutrons at their current location, and by their progenies (i.e. “offspring”). Imagine in the analog Monte Carlo simulation, source neutrons undergo chains of reactions and eventually (after many neutron generations) the progenies of the source neutrons will attain an equilibrium distribution, corresponding to the so-called fundamental eigen-mode of the forward neutron transport equation (ie. forward neutron flux). At this asymptotic generation, the prescribed detector would only measure the “surviving” progenies of source neutrons which are considered to have high importance. Hence the name “importance function” is used to describe the detector response. Pseudo-particles can be simulated by modifying several physics parameters in the forward simulation and transporting them “backward”. This method, implemented in TSUNAMI of SCALE6 KENO-3D requires more particle histories because the pseudo-particles have to scatter up to fast energies to the initiating fission event through the absorbing medium [90]. Alternatively, the “iterated fission probability” method works by keeping rigorous score-recording of progenies [91]. The intense memory requirement issue was addressed and in MCNP6 such capability is available to compute k_{eff} sensitivity coefficients to nuclear data, including scattering energy-angle transfer distributions [24].

A4 Decomposition of Covariance Matrix

To decompose the covariance matrix (M) into the upper and lower triangular matrices using Cholesky decomposition, the MATLAB built-in function `chol` can be applied given that the M is positive definite:

$$xMx^T > 0 \quad \text{for any non-zero vector } x \quad (32)$$

For example, matrix M_1 is positive definite:

$$M_1 = \begin{bmatrix} 9 & 6 \\ 6 & 5 \end{bmatrix} \quad \text{because} \quad xM_1x^T = (3x_1 + 2x_2)^2 + x_2^2 > 0 \quad (33)$$

On the other hand, matrix M_2 is positive semidefinite:

$$M_2 = \begin{bmatrix} 9 & 6 \\ 6 & 4 \end{bmatrix} \quad \text{because} \quad xM_1x^T = (3x_1 + 2x_2)^2 \geq 0 \quad (34)$$

Matrix M_3 is not positive semidefinite:

$$M_3 = \begin{bmatrix} 9 & 6 \\ 9 & 3 \end{bmatrix} \quad \text{because} \quad xM_3x^T = (3x_1 + 2x_2)^2 - x_2^2 \quad (35)$$

When the matrix is positive semidefinite, it has non-negative eigenvalues, for example, equal to 0 and 13 for the second matrix M_2 . For this case, MATLAB’s `cholcov` function is used

Appendix . Appendix

instead. It is based on eigendecomposition algorithm.

The **Cholesky factorization algorithm** begins with taking the element in first row and first column to be m_{11} and designating the rest of the matrix by three block matrices:

$$M = \begin{bmatrix} m_{11} & M_{21}^T \\ M_{21} & M_{22} \end{bmatrix} = \begin{bmatrix} l_{11} & 0 \\ L_{21} & L_{22} \end{bmatrix} \begin{bmatrix} l_{11} & L_{21} \\ 0 & L_{22}^T \end{bmatrix} = \begin{bmatrix} l_{11}^2 & l_{11}L_{21}^T \\ l_{11}L_{21} & L_{21}L_{21}^T + L_{22}L_{22}^T \end{bmatrix} \quad (36)$$

Solving for l_{11} and L_{21} are simply:

$$l_{11} = \sqrt{m_{11}} \quad \text{and} \quad L_{21} = \frac{1}{l_{11}}M_{21} \quad (37)$$

To solve for L_{22} ,

$$M_{22} - L_{21}L_{21}^T = L_{22}L_{22}^T \quad (38)$$

which is to apply the Cholesky factorization algorithm of Eqn.(36) to $M_{22} - L_{21}L_{21}^T$. The above algorithm works on each row of M until it becomes triangular.

Cholesky decomposition of a positive definite matrix is straight-forward. In case of positive semidefinite matrix, the same algorithm results in an upper and lower matrices that are not exactly triangular any more:

$$M = \begin{bmatrix} 81 & 54 & 27 \\ 54 & 45 & 21 \\ 27 & 21 & 10 \end{bmatrix} \quad \text{with} \quad l_{11} = \sqrt{81} = 9 \quad L_{21} = \frac{1}{9} \begin{bmatrix} 54 \\ 27 \end{bmatrix} = \begin{bmatrix} 6 \\ 3 \end{bmatrix} \quad (39)$$

$$L_{22}L_{22}^T = \begin{bmatrix} 45 & 21 \\ 21 & 10 \end{bmatrix} - \begin{bmatrix} 6 \\ 3 \end{bmatrix} \begin{bmatrix} 6 & 3 \end{bmatrix} = \begin{bmatrix} 9 & 3 \\ 3 & 1 \end{bmatrix} = \begin{bmatrix} 3 & 0 \\ 1 & 0 \end{bmatrix} \begin{bmatrix} 3 & 1 \\ 0 & 0 \end{bmatrix} \quad (40)$$

The decomposed result is:

$$\begin{bmatrix} 81 & 54 & 27 \\ 54 & 45 & 21 \\ 27 & 21 & 10 \end{bmatrix} = \begin{bmatrix} 9 & 0 & 0 \\ 6 & 3 & 0 \\ 3 & 1 & 0 \end{bmatrix} \begin{bmatrix} 9 & 6 & 3 \\ 0 & 3 & 1 \\ 0 & 0 & 0 \end{bmatrix} = U_c^T U_c \quad (41)$$

Nevertheless, the matrix U_c can be used to generate multivariate normally distributed samples of size N in the following manner:

$$Z = \text{randn}(N, K) \quad \text{where } K \text{ is number of inputs} \quad (42)$$

$$R_c = Z \cdot U_c \quad \text{where dimension of } R \text{ is } [N \times K] \quad (43)$$

The decomposition of a positive semidefinite matrix is not unique, meaning there exists other

possible decomposition factors. If the matrix is not positive definite, chol will fail upon finding non-positive eigenvalues.

Alternative the **Eigendecomposition** approach decomposes the covariance matrix into its eigenvalues and eigenvectors:

$$M = PDP^{-1} = \left(PD^{\frac{1}{2}}\right)\left(D^{\frac{1}{2}}P^{-1}\right) \quad (44)$$

where matrix P contains the eigenvectors of M in each column, hence orthogonal and $P^{-1} = P^T$. The diagonal of the diagonal matrix D contains the eigenvalues. By applying “eigendecomposition” to the same M of Eqn.(39), it can be seen that a different decomposition is obtained (by MATLAB’s eig function):

$$P = \begin{bmatrix} 0.1048 & 0.6189 & 0.7784 \\ 0.3145 & -0.7632 & 0.5645 \\ -0.9435 & -0.1856 & 0.2746 \end{bmatrix} \quad \text{and} \quad D = \begin{bmatrix} 0 & 0 & 0 \\ 0 & 6.3153 & 0 \\ 0 & 0 & 129.6847 \end{bmatrix} \quad (45)$$

$$\left(D^{\frac{1}{2}}P^{-1}\right) = \begin{bmatrix} 0 & 0 & 0 \\ 1.5554 & -1.9179 & -0.4665 \\ 8.8646 & 6.4282 & 3.1277 \end{bmatrix} \quad (46)$$

When MATLAB function cholcov is applied, the output is $D^{\frac{1}{2}}P^{-1}$ with all zero-value row vector(s) omitted:

$$\text{cholcov}(M) = U_e = \begin{bmatrix} 1.5554 & -1.9179 & -0.4665 \\ 8.8646 & 6.4282 & 3.1277 \end{bmatrix} \quad (47)$$

If matrix M is positive definite, the decomposition is unique and hence cholcov and chol have the same output ($U_c=U_e$). The following matrix operation is used instead of Eqn.(42) to generate random samples:

$$Z = \text{randn}(N, k) \quad \text{where } k \text{ is the reduced rank of } M \quad (48)$$

$$R_e = Z \cdot U_e \quad \text{where dimension of } R \text{ is } [N \times K] = [N \times k] \times [k \times K] \quad (49)$$

Using the same random numbers generated by Eqn.(42) with 5000 samples, the covariance of the random samples generated by Eqn.(43) and Eqn.(49) can be compared with the original covariance matrix M :

$$\text{cov}(R_c) = \begin{bmatrix} 82.586 & 54.941 & 27.49 \\ 54.941 & 45.597 & 21.303 \\ 27.49 & 21.303 & 10.156 \end{bmatrix} \quad \text{vs.} \quad \text{cov}(R_e) = \begin{bmatrix} 81.516 & 54.181 & 27.118 \\ 54.181 & 45.154 & 21.072 \\ 27.118 & 21.072 & 10.037 \end{bmatrix} \quad (50)$$

In certain cases, the NJOY-processed relative covariance matrix for nuclear data does not satisfy the positive (semi)definite condition by including negative eigenvalues. The following **ad hoc fix for negative definite matrix** has been implemented in SHARKX and is adopted in NUSS. Recall the relation between correlation (Λ) and covariance (C) matrices:

$$\Lambda(x_i, x_j) = \frac{C(x_j, x_j)}{\sigma_{x_i} \sigma_{x_j}} \quad (51)$$

An eigendecomposition of the $\Lambda(x_i, x_j)$ matrix gives the eigenvector P and the diagonal matrix D whose elements are the eigenvalues of $\Lambda(x_i, x_j)$:

$$\Lambda(x_i, x_j) = P D P^{-1} \quad (52)$$

Any negative eigenvalues in D are replaced by a very small positive number. In MATLAB, the “floating-point relative accuracy” parameter (eps) which is equal to 2^{-52} is used in NUSS for this purpose. A new $\tilde{\Lambda}(x_i, x_j)$ is created with the original eigenvectors P and the modified \tilde{D} :

$$\tilde{\Lambda}(x_i, x_j) = P \tilde{D} P^{-1} \quad (53)$$

The decision to adjust correlation matrix in SHARKX as opposed to fixing the covariance matrix directly is because correlation values are between -1 to 1 whereas those in covariance matrix can vary in much greater extent in terms of order of magnitude. The absolute nuclear data variances are also unchanged. The new covariance matrix is positive semidefinite:

$$\tilde{C}(x_i, x_j) = \tilde{\Lambda}(x_i, x_j) \cdot \sigma_{x_i} \sigma_{x_j} \quad (54)$$

which can be used to generate multivariate normal random numbers.

A5 Covariance of Samples from Simple Random Sampling

The recipe of obtaining samples which have the desired multivariate normal distributions involves three steps:

1. Decomposition of the $[K \times K]$ covariance matrix \mathbf{M} such that $\mathbf{M} = \mathbf{A}\mathbf{A}^T$, where K is the number of inputs. It can be accomplished by Cholesky or eigendecomposition algorithms as explained in Appendix A4.
2. Let matrix \mathbf{Z} be with the dimension $[K \times N]$:

$$\mathbf{Z} = \begin{pmatrix} \vec{Z}_1 \\ \vec{Z}_2 \\ \vdots \\ \vec{Z}_K \end{pmatrix} = \begin{pmatrix} z_{1,1} & z_{1,2} & \cdots & z_{1,N} \\ z_{2,1} & z_{2,2} & \cdots & z_{2,N} \\ \vdots & \vdots & \ddots & \vdots \\ z_{K,1} & z_{K,2} & \cdots & z_{K,N} \end{pmatrix} \quad (55)$$

where all row vectors \vec{Z} are independent and identically distributed (i.i.d.) random

variables, meaning they have the same probability distribution and are mutually independent. Specifically, the probability distribution is standard normal (mean=0 and standard deviation=1) and N is the size of the samples.

3. The matrix containing the new samples are calculated as:

$$\mathbf{X}' = \mathbf{A} \cdot \mathbf{Z} + \mathbf{X}_0 \quad \text{where} \quad \mathbf{X}_0 = \begin{pmatrix} \mu_1 & \mu_1 & \cdots & \mu_1 \\ \mu_2 & \mu_2 & \cdots & \mu_2 \\ \mu_3 & \mu_3 & \cdots & \mu_3 \\ \vdots & \vdots & \ddots & \vdots \\ \mu_K & \mu_K & \cdots & \mu_K \end{pmatrix} \quad (56)$$

has the identical column vectors of nominal mean values.

Eqn(56) can be viewed as a linear transformation of \mathbf{Z} by some constant matrices \mathbf{X}_0 and \mathbf{A} . The expectation and covariance of \mathbf{X}' are respectively:

$$E[\mathbf{X}'] = E[\mathbf{A} \cdot \mathbf{Z} + \mathbf{X}_0] = \mathbf{A} \cdot E[\mathbf{Z}] + \mathbf{X}_0 \quad (57)$$

$$\begin{aligned} \text{cov}(\mathbf{X}') &= E \left[(\mathbf{X}' - E[\mathbf{X}']) (\mathbf{X}' - E[\mathbf{X}'])^T \right] \\ &= E \left[(\mathbf{A} \cdot \mathbf{Z} + \mathbf{X}_0 - \mathbf{A} \cdot E[\mathbf{Z}] - \mathbf{X}_0) (\mathbf{A} \cdot \mathbf{Z} + \mathbf{X}_0 - \mathbf{A} \cdot E[\mathbf{Z}] - \mathbf{X}_0)^T \right] \\ &= \mathbf{A} \cdot E \left[(\mathbf{Z} - E[\mathbf{Z}]) (\mathbf{Z} - E[\mathbf{Z}])^T \right] \cdot \mathbf{A}^T \\ &= \mathbf{A} \cdot \text{cov}(\mathbf{Z}) \cdot \mathbf{A}^T \end{aligned} \quad (58)$$

As sample size increases, $\text{cov}(\mathbf{Z})$ which is the covariance of \mathbf{Z} is approximately the $[K \times K]$ identity matrix \mathbf{I} because \mathbf{Z} consists of vectors which are normally distributed and independent, resulting in zero covariances and the variances along the diagonal of $\text{cov}(\mathbf{Z})$ to approach the theoretical value of 1 for the imposed standard normal distribution. Therefore,

$$\text{cov}(\mathbf{X}') = \mathbf{A} \cdot \text{cov}(\mathbf{Z}) \cdot \mathbf{A}^T \approx \mathbf{A} \cdot \mathbf{I} \cdot \mathbf{A}^T = \mathbf{A} \mathbf{A}^T = \mathbf{M}$$

Similarly, $E[\mathbf{X}']$ approximates \mathbf{X}_0 because $E[\mathbf{Z}] \rightarrow 0$ as $N \rightarrow \infty$.

A6 Nuclear Data Variances in Different Energy Groups

In Fig.3.19, the relative standard deviation ($\Delta\alpha/\alpha$) of $^{239}\text{Pu}(\bar{\nu})$ cross section (from ENDF/B-VII.1 evaluation) is plotted in terms of 30, 44 and 80-group structures. Counter-intuitively, the values of $\Delta\alpha/\alpha$ seem to fluctuate around different average values below 10^6 eV, and this has raised question about whether the NJOY-processed multigroup $\Delta\alpha/\alpha$ values are correct. As these data are generated by applying the same flux shape weighting function, the difference lies in the energy group boundaries (i.e. width of the energy “bins”). For example, the 80-group structure consists of many narrow “bins” and 44-group has wider “bins”, especially

Appendix . Appendix

below 10^6 eV. Hence, the uncertainty given by a wide bin affects more pointwise cross section points than a narrow bin does. This is seen also in terms of multigroup sensitivity coefficients. Fig.A1 shows the sensitivity coefficients (S_k) in 30, 44 and 80 groups, which are obtained from Eqn.(3.8) with the SCALE6's default 238-group S_k . Note that the 30- and 80-group structures are not exactly the same as those in Fig.3.19 because they are given by NJOY and misalign with the boundary values in SCALE6. But they illustrate the same idea of grouping energies. More commonly, the representation of S_k is in "per unit lethargy" as shown in Fig.A2. The normalization is done in order to take into account the varying width of energy bins in different group structures. The larger the energy bin, the more pointwise data are perturbed, hence the larger the Δk and S_k values. But the unit lethargy is also bigger for large energy bins, so the normalized sensitivity coefficients are on average the same.

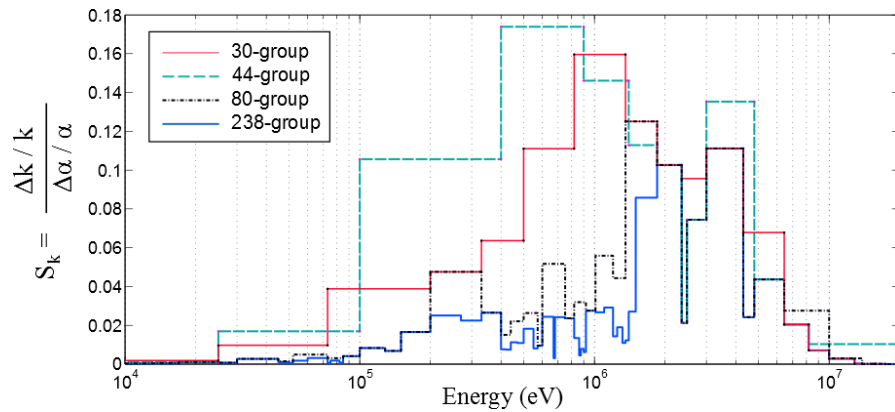


Figure A1: k_{eff} sensitivity coefficients (S_k) to $^{239}\text{Pu}(\bar{\nu})$ in Jezebel. TSUNAMI-3D generates the 238-group S_k which are added by energy groups to obtain S_k in 30, 44 and 80-group structures.

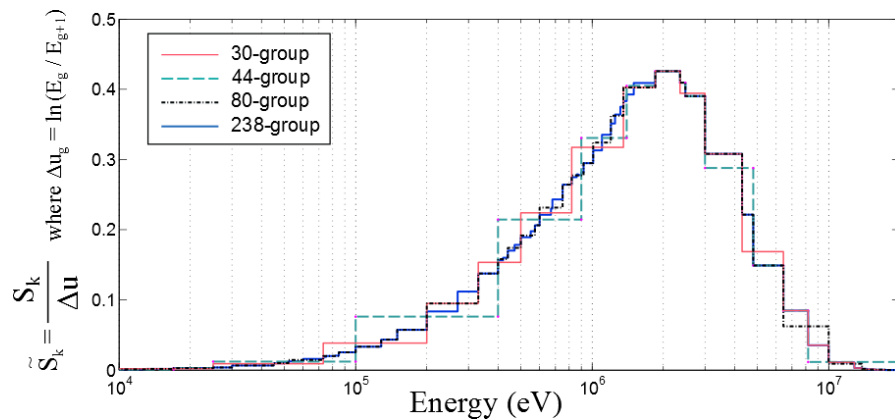


Figure A2: k_{eff} sensitivity coefficient per unit lethargy (\tilde{S}_k) to $^{239}\text{Pu}(\bar{\nu})$ in Jezebel.

Since the overall cross section uncertainty should be the same regardless of the width of the bins, the Sandwich Rule would combine a larger S_k with a smaller cross section uncertainty from a wide energy bin, and a smaller S_k with a larger cross section uncertainty from a narrow energy bin. As shown in Fig.3.19 already, the NUSS-calculated k_{eff} uncertainties (sum of

variance and covariance terms in Sandwich Rule) are practically the same when 30, 44 or 80-group uncertainties are used.

A7 Derivation of Squared of Pearson Correlation Coefficient

The Pearson coefficient between two variables X and Y is defined as:

$$r_p = \frac{\sum_i^N (X_i - \bar{X})(Y_i - \bar{Y})}{\sqrt{\sum_i^N (X_i - \bar{X})^2} \sqrt{\sum_i^N (Y_i - \bar{Y})^2}} = \frac{\text{COV}(X, Y)}{\sqrt{\text{VAR}(X)} \sqrt{\text{VAR}(Y)}} \quad (59)$$

The squared value of r_p is therefore:

$$r_p^2 = \left(\frac{\sum_i^N (X_i - \bar{X})(Y_i - \bar{Y})}{\sqrt{\sum_i^N (X_i - \bar{X})^2} \sqrt{\sum_i^N (Y_i - \bar{Y})^2}} \right)^2 = \left(\frac{\text{COV}(X, Y)}{\sqrt{\text{VAR}(X)} \sqrt{\text{VAR}(Y)}} \right)^2 = \frac{\text{COV}(X, Y)}{\text{VAR}(X)} \frac{\text{COV}(X, Y)}{\text{VAR}(Y)} \quad (60)$$

If there is strong evidence that variables X and Y are linearly correlated, $Y' = aX + b$ is used as an approximation of Y in the calculation of r_p^2 :

$$\begin{aligned} r_p^2 &= \frac{\text{COV}(X, Y)}{\text{VAR}(X)} \frac{\text{COV}(X, Y)}{\text{VAR}(Y)} \approx \frac{\text{COV}(X, aX + b)}{\text{VAR}(X)} \frac{\text{COV}(X, aX + b)}{\text{VAR}(Y)} \quad (61) \\ &= \frac{a \cdot \text{COV}(X, X)}{\text{VAR}(X)} \frac{a \cdot \text{COV}(X, X)}{\text{VAR}(Y)} \\ &= a^2 \cdot \frac{\text{VAR}(X)}{\text{VAR}(X)} \frac{\text{VAR}(X)}{\text{VAR}(Y)} \\ &= \frac{a^2 \cdot \text{VAR}(X)}{\text{VAR}(Y)} \quad (62) \end{aligned}$$

A8 Fourier Transform and Parseval's Theorem

The orthogonality relations and integrals of trigonometry functions are given below without proof:

$$\frac{1}{L} \int_{-L}^L \sin\left(\frac{n\pi s}{L}\right) \sin\left(\frac{m\pi s}{L}\right) ds = \begin{cases} 1 & n = m \neq 0 \\ 0 & n \neq m \end{cases} \quad (63)$$

$$\frac{1}{L} \int_{-L}^L \cos\left(\frac{n\pi s}{L}\right) \cos\left(\frac{m\pi s}{L}\right) ds = \begin{cases} 1 & n = m \neq 0 \\ 0 & n \neq m \\ 2 & n = m = 0 \end{cases} \quad (64)$$

$$\frac{1}{L} \int_{-L}^L \sin\left(\frac{n\pi s}{L}\right) \cos\left(\frac{m\pi s}{L}\right) ds = 0 \quad (65)$$

$$\int \sin(ax) dx = \cos(ax) + C \quad \text{and} \quad \int \cos(ax) dx = -\sin(ax) + C \quad (66)$$

The Fourier series expansion of a continuous function $f(s)$ using orthogonal basis sin and cos is:

$$f(s) = \sum_{\omega=-\infty}^{\infty} (A_{\omega} \cos(\omega s) + B_{\omega} \sin(\omega s)) = A_o + 2 \sum_{\omega=1}^{\infty} (A_{\omega} \cos(\omega s) + B_{\omega} \sin(\omega s)) \quad (67)$$

For Eqn.(4.9):

$$\begin{aligned} \frac{1}{2\pi} \int_{-\pi}^{\pi} f(s) ds &= \frac{1}{2\pi} \int_{-\pi}^{\pi} A_o ds + \frac{1}{2\pi} \int_{-\pi}^{\pi} 2 \sum_{\omega=1}^{\infty} (A_{\omega} \cos(\omega s) + B_{\omega} \sin(\omega s)) ds \\ &= \frac{A_o}{2\pi} \int_{-\pi}^{\pi} ds + \frac{2}{2\pi} \sum_{\omega=1}^{\infty} \int_{-\pi}^{\pi} A_{\omega} \cos(\omega s) ds + \frac{2}{2\pi} \sum_{\omega=1}^{\infty} \int_{-\pi}^{\pi} B_{\omega} \sin(\omega s) ds \\ &= A_o + \frac{1}{\pi} \sum_{\omega=1}^{\infty} A_{\omega} (-\sin(\omega\pi) - (-\sin(-\omega\pi))) + \frac{1}{\pi} \sum_{\omega=1}^{\infty} B_{\omega} (\cos(\omega\pi) - \cos(-\omega\pi)) \\ &= A_o + \frac{1}{\pi} \sum_{\omega=1}^{\infty} A_{\omega} (0 - 0) + \frac{1}{\pi} \sum_{\omega=1}^{\infty} B_{\omega} \cdot 0 \\ &= A_o \end{aligned} \quad (68)$$

For Eqn.(4.10):

$$\begin{aligned} &\frac{1}{2\pi} \int_{-\pi}^{\pi} f(s)^2 ds \\ &= \frac{1}{2\pi} \int_{-\pi}^{\pi} \left(A_o + 2 \sum_{\omega=1}^{\infty} (A_{\omega} \cos(\omega s) + B_{\omega} \sin(\omega s)) \right) \times \left(A_o + 2 \sum_{\omega'=1}^{\infty} (A_{\omega'} \cos(\omega' s) + B_{\omega'} \sin(\omega' s)) \right) ds \\ &= \frac{1}{2\pi} \int_{-\pi}^{\pi} A_o^2 ds + \frac{4}{2\pi} \sum_{\omega=1}^{\infty} \sum_{\omega'=1}^{\infty} \int_{-\pi}^{\pi} (A_{\omega} \cos(\omega s) + B_{\omega} \sin(\omega s)) (A_{\omega'} \cos(\omega' s) + B_{\omega'} \sin(\omega' s)) ds \\ &\quad + \frac{2A_o}{2\pi} \sum_{\omega'=1}^{\infty} \int_{-\pi}^{\pi} (A_{\omega'} \cos(\omega' s) + B_{\omega'} \sin(\omega' s)) ds + \frac{2A_o}{2\pi} \sum_{\omega=1}^{\infty} \int_{-\pi}^{\pi} (A_{\omega} \cos(\omega s) + B_{\omega} \sin(\omega s)) ds \\ &= A_o^2 + \frac{4}{2\pi} \sum_{\omega=1}^{\infty} \sum_{\omega'=1}^{\infty} \left\{ \int_{-\pi}^{\pi} A_{\omega} \cos(\omega s) A_{\omega'} \cos(\omega' s) ds \right. \\ &\quad \left. + \int_{-\pi}^{\pi} A_{\omega} \cos(\omega s) B_{\omega'} \sin(\omega' s) ds + \int_{-\pi}^{\pi} B_{\omega} \sin(\omega s) A_{\omega'} \cos(\omega' s) ds \right. \\ &\quad \left. + \int_{-\pi}^{\pi} B_{\omega} \sin(\omega s) B_{\omega'} \sin(\omega' s) ds \right\} + 0 + 0 \\ &= A_o^2 + \frac{2}{\pi} \sum_{\omega=1}^{\infty} \sum_{\omega'=1}^{\infty} (A_{\omega} A_{\omega'} \pi \delta(\omega\omega') + 0 + 0 + B_{\omega} B_{\omega'} \pi \delta(\omega\omega')) \\ &= A_o^2 + 2 \sum_{\omega=1}^{\infty} (A_{\omega}^2 + B_{\omega}^2) \quad \text{known as the Parseval's theorem} \end{aligned} \quad (69)$$

Combining Eqn.(68) and Eqn.(69):

$$V_{f(s)} = \frac{1}{2\pi} \int_{-\pi}^{\pi} f(s)^2 ds - \left(\frac{1}{2\pi} \int_{-\pi}^{\pi} f(s) ds \right)^2 = 2 \sum_{\omega=1}^{\infty} (A_{\omega}^2 + B_{\omega}^2) \quad \text{Q.E.D.} \quad (70)$$

A9 Power Spectrum and Variance Calculation in MATLAB

As derived in Appendix A8, Eqn.(70), the summation of the power spectrum components (Λ_{ω}) gives the variance of $f(s)$:

$$V_{f(s)} = 2 \sum_{\omega=1}^{\infty} \Lambda_{\omega} \quad \text{where} \quad \Lambda_{\omega} = A_{\omega}^2 + B_{\omega}^2 \quad (71)$$

To calculate it in practice, the steps shown in Fig.5.3 are specific to MATLAB since it is the mathematical tool for NUSS-RF. For example, vector indexing in MATLAB starts with 1, whereas in C programming, it starts with 0. Such differences are important to take into account when coding mathematical equations in various programs.

NUSS-RF uses MATABLB function `fft.m` to perform discrete Fourier transform on $f(s) = \{y_s | s = 1 \cdots N\}$, a vector of length N which is the number of data points. The `fft.m` output is a vector $Y = \{Y_k | k = 1 \cdots N\}$ with each element equal to:

$$Y_k = \sum_{n=1}^N \left(y_n \times e^{-\frac{2\pi j}{N}(n-1)(k-1)} \right) \quad \text{with } j^2 = -1 \quad \text{from } Y = \text{fft}(y) \quad (72)$$

Note that the indexing for n and k both start from 1 not 0. More importantly, the first element (ie. for $k = 1$) is:

$$Y_1 = \sum_{n=1}^N y_n \cdot 1 = N \bar{y} \quad \text{where } \bar{y} \text{ denotes the mean value of } y \quad (73)$$

The output of `fft.m` is normalized by N :

$$Y = \text{fft}(y) / N \quad \text{such that} \quad Y_1 = \frac{1}{N} \sum_{n=1}^N y_n = \bar{y} \quad (74)$$

The rest of the Y outputs are complex numbers consisting of the amplitude and phase of the signal in the frequency space: $Y_k = A_k + B_k \cdot j$ with $j^2 = -1$.

The power spectrum of Y is by definition the absolute magnitude of Y_k squared, and in MATLAB it is performed in the following, with the consideration of the normalization of Eqn.(74):

$$Pi = (\text{abs}(\text{fft}(y)/N)).^2 \quad \text{with elements } Pi_k = A_k^2 + B_k^2 = \Lambda_k \quad (75)$$

Fig.A3 shows a generic example of the result of Eqn.(75), in which the first data point cor-

Appendix . Appendix

responds to $(\bar{y})^2$, and the rest of the data points are mirrored as a result of MATLAB's `fft` algorithm for the positive and negative frequency components. The number of unique frequency points is determined by the Nyquist criterion that the maximum resolved frequency is no larger than half of the sampling frequency.

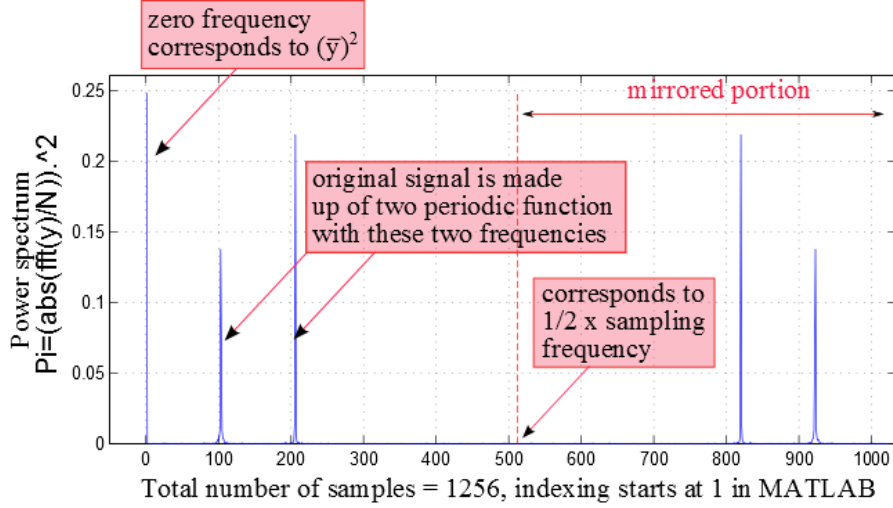


Figure A3: Output of Eqn.(75) is plotted for an example function $(y=\sin(2\pi\omega t) + \cos(\pi\omega t)+\text{random noise})$. The maximum frequency (ω_{\max}) which can be resolved from `fft.m` is half of the sampling frequency.

By summing the power spectrum components, Eqn.(71) is effectively computed:

$$V_s = \text{sum}(P_i(2:N)) \quad \text{for} \quad V_{f(s)} = 2 \sum_{\omega=1}^{\omega_{\max}} \Lambda_{\omega} \quad (76)$$

In Chapter 4.3 Eqn.(4.11) showed that the variance of $f(\bar{x})$ could be estimated by $V_{f(s)}$:

$$f^2(\bar{x})d\bar{x} - \left(\int f(\bar{x})d\bar{x} \right)^2 \approx \frac{1}{2\pi} \int_{-\pi}^{\pi} f(s)^2 ds - \left(\frac{1}{2\pi} \int_{-\pi}^{\pi} f(s) ds \right)^2 = V_{f(s)} \quad (77)$$

which is modified below for discrete data points (ie. $f(\bar{x})=k_{\text{eff}}$ samples denoted by k_n):

$$\int f^2(\bar{x})d\bar{x} - \left(\int f(\bar{x})d\bar{x} \right)^2 \xrightarrow{\text{discrete}} \sum_{n=1}^N (k_n^2/N) - \left(\sum_{n=1}^N (k_n/N) \right)^2 \quad (78)$$

$$\begin{aligned} &= \left(\frac{1}{N} \sum_{n=1}^N k_n^2 \right) - \bar{k}^2 \\ &= \frac{1}{N} \left(\sum_{n=1}^N k_n^2 - 2N\bar{k}\bar{k} + N\bar{k}^2 \right) \\ &= \frac{1}{N} \sum_{n=1}^N (k_n - \bar{k})^2 \quad (79) \end{aligned}$$

The sample variance is by definition:

$$\frac{1}{N-1} \sum_{n=1}^N (k_n - \bar{k})^2 = \frac{1}{N-1} N \times V_{f(s)} = \frac{N}{N-1} 2 \sum_{\omega=1}^{\omega_N} \Lambda_{\omega} \quad (80)$$

or in MATLAB:

$$Vt = \text{sum}(Pi(2:end)) * N / (N-1) \quad (81)$$

Note that the value of Vt does not vary with the different ordering of k_{eff} samples. However, the re-ordering is necessary for the retrieval of individual input contribution to the total variance. The components are determined by the assigned frequency (ω) and the maximum order of harmonics (h) during the transformation of \vec{x} into $x(s, \omega)$:

$$\text{components} = (1:h) * \omega \quad \text{i.e. components} = \{\omega, 2\omega, 3\omega, \dots\} \quad (82)$$

The power spectrum of the re-ordered k_{eff} samples for the i^{th} input is denoted by Pi and its variance contribution (SI_i) is calculated as:

$$Vi = \text{sum}(Pi(\text{components}+1)) * N / (N-1) \quad \text{and} \quad SI_i = Vi / Vt \quad (83)$$

where $\text{components}+1$ is to account for the zero frequency as the first data point.

A10 Additive Model with Multivariate Normal Distribution

The general formulas for conditional mean, conditional covariance matrix and conditional distribution of multivariate normal inputs are given here. Suppose the entire input set is partitioned into subsets s and t . Their mean values and covariance matrix are also partitioned as:

$$\vec{\mu} = \begin{pmatrix} \mu_s \\ \mu_t \end{pmatrix} \quad \text{and} \quad M = \begin{pmatrix} M_s & M_{st} \\ M_{ts} & M_t \end{pmatrix} \quad (84)$$

The multivariate normal density distribution function is the following with $\vec{\mu}$ and M , and n is the number of inputs in \vec{x} :

$$\Phi(\vec{x}) = \frac{1}{(2\pi)^{n/2} \sqrt{|M|}} \exp \left\{ -\frac{1}{2} (\vec{x} - \vec{\mu})^T M^{-1} (\vec{x} - \vec{\mu}) \right\} \quad (85)$$

The marginal density distribution of s is:

$$\hat{\Phi}_s = \frac{1}{\sqrt{2\pi\sigma_s}} \exp \left\{ -\frac{(x_s - \mu_s)^2}{2\sigma_s^2} \right\} \quad (86)$$

Appendix . Appendix

The conditional density distribution of t given s is:

$$\tilde{\Phi}_t(s, t|s) = \frac{1}{(2\pi)^{(n_t)/2} \sqrt{|\tilde{M}_t|}} \exp \left\{ -\frac{1}{2} (t - \tilde{\mu}_t) \tilde{M}_t^{-1} (t - \tilde{\mu}_t) \right\} \quad (87)$$

where n_t is the dimension of subset t , $\tilde{\mu}_t$ and \tilde{M}_t are the conditional mean and conditional covariance matrix respectively (proof in [92]):

$$\tilde{\mu}_t = \mu_t + M_{ts} M_s^{-1} [s - \mu_s] \quad (88)$$

$$\tilde{M}_t = M_t - M_{ts} M_s^{-1} M_{st} \quad (89)$$

For our current 3-input model $f(x_1, x_2, x_3) = x_1 + x_2 + x_3$, the inputs are normally distributed with zero mean values, so that the model mean is zero ($f_o = 0$). The input covariance matrix is:

$$M = \begin{pmatrix} \sigma_1^2 & 0 & 0 \\ 0 & \sigma_2^2 & \rho\sigma_2\sigma_3 \\ 0 & \rho\sigma_2\sigma_3 & \sigma_3^2 \end{pmatrix} = \begin{pmatrix} 1^2 & 0 & 0 \\ 0 & 1^2 & 2\rho \\ 0 & 2\rho & 2^2 \end{pmatrix} \quad (90)$$

Following Eqn.(84), the covariance and mean values are partitioned in the following:

$$M = \begin{pmatrix} \sigma_1^2 & \begin{bmatrix} 0 & 0 \end{bmatrix} \\ \begin{bmatrix} 0 \\ 0 \end{bmatrix} & \begin{bmatrix} \sigma_2^2 & \sigma_2\sigma_3\rho \\ \sigma_3\sigma_2\rho & \sigma_3^2 \end{bmatrix} \end{pmatrix} \quad \text{and} \quad \mu = \begin{pmatrix} \mu_1 \\ \mu_2 \\ \mu_3 \end{pmatrix} \quad (91)$$

Substituting $\mu_s = \mu_1$ and $\mu_t = [\mu_2 \quad \mu_3]^T$ into Eqn.(88) and Eqn.(89):

$$\tilde{\mu}_{23} = \begin{bmatrix} \mu_2 \\ \mu_3 \end{bmatrix} + \begin{bmatrix} 0 \\ 0 \end{bmatrix} \begin{bmatrix} \frac{1}{\sigma_2^2\sigma_3^2(1-\rho^2)} & \frac{-\rho}{\sigma_2^2\sigma_3^2(1-\rho^2)} \\ \frac{-\rho}{\sigma_2^2\sigma_3^2(1-\rho^2)} & \frac{1}{\sigma_3^2(1-\rho^2)} \end{bmatrix} (x_1 - \mu_1) = \begin{bmatrix} \mu_2 \\ \mu_3 \end{bmatrix} \quad (92)$$

$$\tilde{M}_{23} = \begin{bmatrix} \sigma_2^2 & \sigma_2\sigma_3\rho \\ \sigma_3\sigma_2\rho & \sigma_3^2 \end{bmatrix} - \begin{bmatrix} 0 \\ 0 \end{bmatrix} \begin{bmatrix} \frac{1}{\sigma_2^2\sigma_3^2(1-\rho^2)} & \frac{-\rho}{\sigma_2^2\sigma_3^2(1-\rho^2)} \\ \frac{-\rho}{\sigma_2^2\sigma_3^2(1-\rho^2)} & \frac{1}{\sigma_3^2(1-\rho^2)} \end{bmatrix} \begin{bmatrix} 0 & 0 \end{bmatrix} = \begin{bmatrix} \sigma_2^2 & \sigma_2\sigma_3\rho \\ \sigma_3\sigma_2\rho & \sigma_3^2 \end{bmatrix} \quad (93)$$

Using Eqn(87), the conditional distribution of y given x_1 is obtained:

$$\begin{aligned}
 & \tilde{\Phi}_{23}(x_1, x_2, x_3|x_1) \\
 &= \frac{1}{(2\pi)^{1/2}\sqrt{|\tilde{M}_{23}|}} \exp\left\{-\frac{1}{2}(\tilde{x}_{23} - \tilde{\mu}_{23})\tilde{M}_{23}^{-1}(\tilde{x}_{23} - \tilde{\mu}_{23})\right\} \\
 &= \frac{1}{2\pi\sqrt{(1-\rho^2)}\sigma_2\sigma_3} \exp\left\{-\frac{1}{2}\begin{bmatrix} x_2 - \mu_2 \\ x_3 - \mu_3 \end{bmatrix}^T \begin{bmatrix} \frac{1}{\sigma_2^2\sigma_3^2(1-\rho^2)} & \frac{-\rho}{\sigma_2^2\sigma_3^2(1-\rho^2)} \\ \frac{-\rho}{\sigma_2^2\sigma_3^2(1-\rho^2)} & \frac{1}{\sigma_3^2(1-\rho^2)} \end{bmatrix} \begin{bmatrix} x_2 - \mu_2 \\ x_3 - \mu_3 \end{bmatrix}\right\} \\
 &= \frac{1}{2\pi\sqrt{(1-\rho^2)}\sigma_2\sigma_3} \exp\left\{-\frac{1}{2(1-\rho^2)}\left\{\frac{(x_2 - \mu_2)^2}{\sigma_2^2} + \frac{(x_3 - \mu_3)^2}{\sigma_3^2} - \frac{2\rho(x_2 - \mu_2)(x_3 - \mu_3)}{\sigma_2\sigma_3}\right\}\right\} \\
 & \tag{94}
 \end{aligned}$$

which is also the formula for the joint probability density of a bivariate normal distribution and gives the following:

$$\int \tilde{\Phi}_{23} dx_2 dx_3 = 1 \quad \text{and} \quad \int (x_2 + x_3)\tilde{\Phi}_{23} dx_2 dx_3 = \mu_2 + \mu_3 \tag{96}$$

The variance contribution of x_1 is calculated as:

$$\begin{aligned}
 V_{x_1} &= \int \left(\int f(x_1, x_2, x_3)\tilde{\Phi}_{23} dx_2 dx_3 \right)^2 \hat{\Phi}_1 dx_1 - f_o^2 \\
 &= \int \left(\int x_1 \tilde{\Phi}_{23} dx_2 dx_3 + \int (x_2 + x_3)\tilde{\Phi}_{23} dx_2 dx_3 \right)^2 \hat{\Phi}_1 dx_1 - 0 \\
 &= \int (x_1 + (\mu_2 + \mu_3))^2 \hat{\Phi}_1 dx_1 \quad \text{with} \quad \mu_2 + \mu_3 = 0 \\
 &= \int x_1^2 \frac{1}{\sqrt{2\pi}\sigma_1} \exp\left\{-\frac{(x_1 - \mu_1)^2}{2\sigma_1^2}\right\} dx_1 \\
 &= \sigma_1^2
 \end{aligned} \tag{97}$$

Of course, this results is expected since x_1 is not correlated with x_2 and x_3 . Its variance contribution in the model y is exactly its variance.

Next, we will show that the variance contribution of x_3 is its own variance in addition to the variance contributed by its correlated “partner” x_2 :

$$V_{x_3} = (\sigma_3 + \sigma_2\rho)^2 \tag{98}$$

Let $s = x_3$ and $t = (x_1, x_2)$ so that Eqn.(88) and (89) become:

$$\tilde{\mu}_{12} = \begin{bmatrix} \mu_1 \\ \mu_2 \end{bmatrix} + \begin{bmatrix} 0 \\ \sigma_2 \sigma_3 \rho \end{bmatrix} \frac{1}{\sigma_3^2} (x_3 - \mu_3) = \begin{bmatrix} \mu_1 \\ \mu_2 + \frac{\sigma_2}{\sigma_3} \rho (x_3 - \mu_3) \end{bmatrix} \quad (99)$$

$$\tilde{M}_{12} = \begin{bmatrix} \sigma_1^2 & 0 \\ 0 & \sigma_2^2 \end{bmatrix} - \begin{bmatrix} 0 \\ \sigma_2 \sigma_3 \rho \end{bmatrix} \frac{1}{\sigma_3^2} \begin{bmatrix} 0 & \sigma_2 \sigma_3 \rho \end{bmatrix} = \begin{bmatrix} \sigma_1^2 & 0 \\ 0 & \sigma_2^2 (1 - \rho^2) \end{bmatrix} \quad (100)$$

The conditional distribution of (x_1, x_2) given x_3 is

$$\begin{aligned} & \tilde{\Phi}_{12}(x_1, x_2, x_3 | x_3) \\ &= \frac{1}{2\pi\sigma_1\sigma_2\sqrt{1-\rho^2}} \exp \left\{ -\frac{1}{2(1-\rho^2)} \left(\frac{x_2 - \mu_2}{\sigma_2} - \frac{\rho(x_3 - \mu_3)}{\sigma_3} \right)^2 - \frac{(x_1 - \mu_1)^2}{2\sigma_1^2} \right\} \\ &= \frac{1}{2\pi\sigma_1\sigma_2\sqrt{1-\rho^2}} \exp \left\{ -\frac{1}{2(1-\rho^2)} \left(\left(\frac{x_2}{\sigma_2} - \frac{\rho x_3}{\sigma_3} \right) - \left(\frac{\mu_2}{\sigma_2} - \frac{\rho \mu_3}{\sigma_3} \right) \right)^2 - \frac{(x_1 - \mu_1)^2}{2\sigma_1^2} \right\} \\ &= \left(\frac{1}{2\pi\sigma_1} \exp \left\{ -\frac{(x_1 - \mu_1)^2}{2\sigma_1^2} \right\} \right) \left(\frac{1}{\sqrt{2\pi}\sigma_z\sigma_2} \exp \left\{ -\frac{(z - \mu_z)^2}{2\sigma_z^2} \right\} \right) \\ &= \phi(x_1)\phi(z)/\sigma_2 \end{aligned} \quad (101)$$

where substitutions have been used by:

$$z = \frac{x_2}{\sigma_2} - \frac{\rho x_3}{\sigma_3} \quad \text{and} \quad \mu_z = \frac{\mu_2}{\sigma_2} - \frac{\rho \mu_3}{\sigma_3} \quad \text{and} \quad \sigma_z = \sqrt{1 - \rho^2} \quad (102)$$

Furthermore,

$$\frac{dz}{dx_2} = \frac{1}{\sigma_2} \quad \text{and} \quad x_2 + x_3 = \sigma_2 z + \frac{\sigma_2 \rho}{\sigma_3} x_3 + x_3 \quad (103)$$

The variance contribution from x_3 is determined:

$$\begin{aligned} V_{x_3} &= \int \left[\int (x_1 + x_2 + x_3) \tilde{\Phi}_{12} dx_1 dx_2 \right]^2 \hat{\Phi}_3 dx_3 - f_o^2 \quad (104) \\ &= \int \left[\int x_1 \phi(x_1) dx_1 \int \phi(z)/\sigma_2 dx_2 + \int \phi(x_1) dx_1 \int (x_2 + x_3) \phi(z)/\sigma_2 dx_2 \right]^2 \hat{\Phi}_3 dx_3 \\ &= \int \left[\mu_1 \cdot \int \phi(z) dz + 1 \cdot \int \left(\sigma_2 z + \left(\frac{\sigma_2 \rho}{\sigma_3} + 1 \right) x_3 \right) \phi(z) dz \right]^2 \hat{\Phi}_3 dx_3 \\ &= \int \left[0 + \sigma_2 \mu_z + \left(\frac{\sigma_2 \rho}{\sigma_3} + 1 \right) x_3 \right]^2 \hat{\Phi}_3 dx_3 \\ &= \left(\frac{\sigma_2 \rho}{\sigma_3} + 1 \right)^2 \int x_3^2 \hat{\Phi}_3 dx_3 \\ &= \left(\frac{\sigma_2 \rho}{\sigma_3} + 1 \right)^2 \sigma_3^2 \\ &= (\sigma_2 \rho + \sigma_3)^2 \end{aligned} \quad (105)$$

The same procedures from Eqn.(99) to Eqn.(104) applied by setting $s = x_2$ and $t = (x_1, x_3)$ result in the variance contribution from x_2 :

$$V_{x_2} = (\sigma_3\rho + \sigma_2)^2 \quad (106)$$

In summary, the individual variance contributions for the additive model $y = x_1 + x_2 + x_3$ are:

$$V_{x_1} = \sigma_1^2 = 1 \quad (107)$$

$$V_{x_2} = (\sigma_2 + \rho\sigma_3)^2 = (1 + \rho\sigma)^2 \quad (108)$$

$$V_{x_3} = (\sigma_3 + \rho\sigma_2)^2 = (\sigma + \rho)^2 \quad (109)$$

A11 Higher-Order Sensitivity Coefficient and Variance

The model $y = x_1x_3 + x_2x_4$ can be written in two parts:

$$H = x_1x_3 \quad \text{and} \quad G = x_2x_4 \quad (110)$$

For the first term H :

$$\frac{\partial H}{\partial x_1} = x_3 \quad \frac{\partial H}{\partial x_3} = x_1 \quad (111)$$

$$\frac{\partial}{\partial x_3} \frac{\partial H}{\partial x_1} = \frac{\partial}{\partial x_1} \frac{\partial H}{\partial x_3} = 1 \quad \frac{\partial}{\partial x_1} \frac{\partial H}{\partial x_1} = \frac{\partial}{\partial x_3} \frac{\partial H}{\partial x_3} = 0 \quad (112)$$

They are applied in the Taylor expansion of H up to 2nd order:

$$\begin{aligned} H - H_0 &= \frac{\partial H}{\partial x_1} \delta x_1 + \frac{\partial H}{\partial x_3} \delta x_3 + \frac{1}{2} \frac{\partial^2 H}{\partial x_1 \partial x_1} \delta x_1 \delta x_1 + \frac{1}{2} \frac{\partial^2 H}{\partial x_3 \partial x_3} \delta x_3 \delta x_3 \\ &\quad + \frac{1}{2} \frac{\partial^2 H}{\partial x_1 \partial x_3} \delta x_1 \delta x_3 + \frac{1}{2} \frac{\partial^2 H}{\partial x_3 \partial x_1} \delta x_3 \delta x_1 \end{aligned} \quad (113)$$

$$= x_3 \delta x_1 + x_1 \delta x_3 + \delta x_3 \delta x_1 = \mu_3 \delta x_1 + \mu_1 \delta x_3 + \delta x_3 \delta x_1 \quad (114)$$

$$= \mu_3 \delta x_1 + \delta x_3 \delta x_1 \quad (115)$$

as evaluated at the nominal input $(\mu_1, \mu_2, \mu_3, \mu_4) = (0, 0, \mu_3, \mu_4)$. Analogously:

$$G - G_0 = x_4 \delta x_2 + x_2 \delta x_4 + \delta x_2 \delta x_4 = \mu_4 \delta x_2 + \delta x_2 \delta x_4 \quad (116)$$

The second moment of $y = H + G$ is then calculated as:

$$\mu_2[(H + G) - (H_o + G_o)] \quad (117)$$

$$= \int (\mu_3 \delta x_1 + \mu_4 \delta x_2 + \delta x_3 \delta x_1 + \delta x_2 \delta x_4)^2 p(x_1, x_2) p(x_3, x_4) d\vec{x} \quad (118)$$

$$\begin{aligned} &= \int \mu_3^2 \delta x_1^2 p(x_1, x_2) p(x_3, x_4) d\vec{x} \\ &\quad + 2 \int (\mu_3 \mu_4 \delta x_1 \delta x_2 + \mu_3 \delta x_1 \delta x_3 \delta x_1 + \mu_3 \delta x_1 \delta x_4 \delta x_2) p(x_1, x_2) p(x_3, x_4) d\vec{x} \\ &\quad + \int \mu_4^2 \delta x_2^2 p(x_1, x_2) p(x_3, x_4) d\vec{x} \\ &\quad + 2 (\mu_4 \delta x_2 \delta x_3 \delta x_1 + \mu_4 \delta x_2 \delta x_4 \delta x_2) p(x_1, x_2) p(x_3, x_4) d\vec{x} \\ &\quad + \int (\delta x_3 \delta x_1)^2 p(x_1, x_2) p(x_3, x_4) d\vec{x} \\ &\quad + 2 \int (\delta x_3 \delta x_1 \delta x_4 \delta x_2) p(x_1, x_2) p(x_3, x_4) d\vec{x} + \int (\delta x_4 \delta x_2)^2 p(x_1, x_2) p(x_3, x_4) d\vec{x} \quad (119) \end{aligned}$$

$$= \mu_3^2 \sigma_1^2 + 2\mu_3 \mu_4 \sigma_{12} + \mu_4^2 \sigma_2^2 + \sigma_1^2 \sigma_3^2 + 2\sigma_{12} \sigma_{34} + \sigma_2^2 \sigma_4^2 \quad (120)$$

B Supplementary Tables and Figures

B1 xsdir File

Fig.B.1 shows an excerpt of the generic `xsdir` file which contains information on ZAID, atomic weight ratio, the name of the individual ACE continuous-energy nuclear data files, some information of the ACE file such as its length and the incident neutron energy implied in the corresponding ACE file. More specifically, the general form of the ZAID is `ZZZAAA.nnX` where `ZZZ` is the atomic number, `AAA` the atomic weight, `nn` the nuclear data evaluation identifier and `X` for the class of data (`D` for discrete and default is `C` for continuous). As the unit convention of temperature (`T`) in MCNPX is MeV, the conversion between energy and temperature is through

$$E \text{ (in MeV)} = 8.617 \times 10^{-11} T \quad \text{(in degrees K)}$$

$$E \text{ (in MeV)} = 8.617 \times 10^{-11} (T + 273.15) \quad \text{(in degrees C)}$$

For example, $2.530E-08$ MeV is equivalent to 293.6 K, the default room temperature in MCNPX.

B2 Explanation of NXS and JXS Arrays

NXS and JXS arrays are the first portion of the ACE-formatted data file. For the example shown in Fig. 2.3, specific numbers such as the expected length of data points, the number of reactions, and locations of these reactions and so forth are identified in Table B1 with explanations.

ZAID	Atomic weight ratio	ACE file name	Table length	Incident neutron energy in MeV
42100.00c	99.049000	4249	0 1 1	192467
4009.00c	8.934780	425	0 1 1	580783
50112.00c	110.944000	5025	0 1 1	123746
50114.00c	112.925000	5031	0 1 1	127709
50115.00c	113.916000	5034	0 1 1	92335
50116.00c	114.906000	5037	0 1 1	262672
50117.00c	115.899000	5040	0 1 1	146502
50118.00c	116.889000	5043	0 1 1	71594
50119.00c	117.882000	5046	0 1 1	123307
50120.00c	118.872000	5049	0 1 1	233595
50122.00c	120.856000	5055	0 1 1	360443
50124.00c	122.841000	5061	0 1 1	237923
5010.00c	9.926921	525	0 1 1	54514
5011.00c	10.914700	528	0 1 1	150161
6000.00c	11.898000	600	0 1 1	79690
7014.00c	13.882780	725	0 1 1	145364
82204.00c	202.220800	8225	0 1 1	613556
82206.00c	204.205000	8231	0 1 1	1205531
82207.00c	205.197900	8234	0 1 1	551210
82208.00c	206.190000	8237	0 1 1	484977
8016.00c	15.857510	825	0 1 1	409202
92234.00c	232.030400	9225	0 1 1	424576
92235.00c	233.024800	9228	0 1 1	837937
92236.00c	234.017800	9231	0 1 1	357476
92238.00c	236.005800	9237	0 1 1	1637607
94238.00c	236.004600	9434	0 1 1	330734
94239.00c	236.998600	9437	0 1 1	813270
94240.00c	237.991600	9440	0 1 1	782842
94241.00c	238.978000	9443	0 1 1	193800
94242.00c	239.979000	9446	0 1 1	382018
95241.00c	238.986000	9543	0 1 1	278466

Figure B.1: xsdир file contains directory information for MCNPX to access the ACE-formatted files for materials requested in the MCNPX input file. For example, when 92235.00c is used, ACE file named 9228 is accessed by MCNPX.

B3 NJOY Input File Example

Fig.B.2 shows an example NJOY input file to prepare the 30-group covariance data for isotope ^{238}U .

B4 Energy Boundaries for SCALE 238-group and 44-group

Fig.B.3 shows the upper and lower boundaries of the 238- and 44-group structures defined in SCALE6 manual Chapter M04[52]. The upper boundary for thermal energy range is at 3.0000E+00eV. The lower boundary for both 238-group and 44-group is at 1.0000E-05eV..

Appendix . Appendix

element	definition	in example
NXS(1)	length of data block	17969 values
NXS(2)	$ZA=1000 \times Z+A$	1001 for ^1H
NXS(3)	number of energies	590 energy points
NXS(4)	number of reactions excluding elastic	3
NXS(5)	number of reaction with 2 nd excluding elastic	0
NXS(6)	number of photon production reactions	1
NXS(7)-NXS(14)	allocated for future expansion	-
NXS(15)	number of PIKMT reactions (photon-production bias)	0
NXS(16)	photon production flag	0 = normal
JXS(1)	location of energy table	1
JXS(2)	location of ν data	0, no ν data
JXS(3)	location of list of MT	2951
JXS(4)	location of Q-value array	2954
JXS(5)	location of reaction type array	2957
JXS(6)	location of XS table locators	2960
JXS(7)	location of cross sections (XS)	2963
JXS(8)-JXS(32)	locations of locators and respective data	

Table B1: Explanation of NXS and JXS arrays in the ACE-formatted file for ^1H in Fig.2.3. Values in JXS table are with respect to XSS table which is right after the JXS table.

input file	Explanation
moder	change the mode of an endf/b tape
20 -21 /	from ASCII tape 20 to binary tape -21
reconr	reconstruct pointwise cross sections
-21 -22 /	
'MAT=9237 ENDFB7.1 zhu_t'	
9237 0 0	9237 is the material ID for 238U
/	fractional reconstruction tolerance
0.001 /	
0 /	
broadr	doppler broaden and thin neutron point cross sections
-21 -22 -23 /	
9237 1 0 0 0 /	
0.001 /	fractional tolerance for thinning
300. /	final temperatures (Kelvin)
0 /	
groupr	compute self-shielded group-averaged cross sections
-21 -23 0 91 /	
9237 3 0 9 1 1 1 0 /	3 is the option for 30-group structure, 9 is the "claw weight function"
'test'	
300. /	temperature (Kelvin)
1.0e10 /	background sigma zero value
3 /	MF3 file to be processed
3 251 'mubar' /	
3 252 'xi' /	
3 452 'nu' /	
3 455 'nu' /	
3 456 'nu' /	
5 18 'xi' /	
/	
0 /	
0 /	
--	
-- process mf31	
errorr	produce cross section covariances
-21 0 91 25 0 0 /	
9237 3 9 1 1 /	for MF31 file
0 31 1 1 -1 /	
--	
-- process mf32 and 33	
errorr	produce cross section covariances
-21 0 91 26 0 0 /	
9237 3 9 1 1 /	for MF33 file
0 33 1 1 -1 /	
--	
-- make mf31 plot file	
covr	plot covariance data from errorr
25 0 355 /	
1 /	
/	
/	
9237 /	
--	
-- make mf33 plot file.	
covr	plot covariance data from errorr
26 0 36	
/	
1 /	
/	
/	
9237 /	
--	
-- make mf31 postscript file.	
viewr	view plots generated by "covr" module
355 45 /	
--	
-- make mf33 postscript file.	
viewr	view plots generated by "covr" module
36 46 /	
stop	

Figure B.2: Example of NJOY input file.

Appendix . Appendix

238 Group	44 Group	Upper Energy (eV)	238 Group	44 Group	Upper Energy (eV)	238 Group	44 Group	Upper Energy (eV)	238 Group	44 Group	Upper Energy (eV)
1	1	2.0000E+07	61		3.9000E+03	121		2.0000E+01	181		1.0900E+00
2		1.7333E+07	62		3.7400E+03	122		1.9000E+01	182		1.0800E+00
3		1.5683E+07	63	15	3.0000E+03	123		1.8500E+01	183		1.0700E+00
4		1.4550E+07	64		2.5800E+03	124		1.7000E+01	184		1.0600E+00
5		1.3840E+07	65		2.2900E+03	125		1.6000E+01	185		1.0500E+00
6		1.2840E+07	66		2.2000E+03	126		1.5100E+01	186		1.0400E+00
7		1.0000E+07	67		1.8000E+03	127		1.4400E+01	187		1.0300E+00
8	2	8.1873E+06	68		1.5500E+03	128		1.3750E+01	188		1.0200E+00
9	3	6.4340E+06	69		1.5000E+03	129		1.2900E+01	189		1.0100E+00
10	4	4.8000E+06	70		1.1500E+03	130		1.1900E+01	190	25	1.0000E+00
11		4.3040E+06	71		9.5000E+02	131		1.1500E+01	191		9.7500E-01
12	5	3.0000E+06	72		6.8300E+02	132	19	1.0000E+01	192		9.5000E-01
13	6	2.4790E+06	73		6.7000E+02	133		9.1000E+00	193		9.2500E-01
14	7	2.3540E+06	74	16	5.5000E+02	134	20	8.1000E+00	194		9.0000E-01
15	8	1.8500E+06	75		3.0500E+02	135		7.1500E+00	195		8.5000E-01
16		1.5000E+06	76		2.8500E+02	136		7.0000E+00	196		8.0000E-01
17	9	1.4000E+06	77		2.4000E+02	137		6.7500E+00	197		7.5000E-01
18		1.3560E+06	78		2.1000E+02	138		6.5000E+00	198		7.0000E-01
19		1.3170E+06	79		2.0750E+02	139		6.2500E+00	199		6.5000E-01
20		1.2500E+06	80		1.9250E+02	140	21	6.0000E+00	200	26	6.2500E-01
21		1.2000E+06	81		1.8600E+02	141		5.4000E+00	201		6.0000E-01
22		1.1000E+06	82		1.2200E+02	142		5.0000E+00	202		5.5000E-01
23		1.0100E+06	83		1.1900E+02	143	22	4.7500E+00	203		5.0000E-01
24		9.2000E+05	84		1.1500E+02	144		4.0000E+00	204		4.5000E-01
25	10	9.0000E+05	85		1.0800E+02	145		3.7300E+00	205	27	4.0000E-01
26		8.7500E+05	86	17	1.0000E+02	146		3.5000E+00	206	28	3.7500E-01
27		8.6110E+05	87		9.0000E+01	147		3.1500E+00	207	29	3.5000E-01
28		8.2000E+05	88		8.2000E+01	148		3.0500E+00	208	30	3.2500E-01
29		7.5000E+05	89		8.0000E+01	149	23	3.0000E+00	209		3.0000E-01
30		6.7900E+05	90		7.6000E+01	150		2.9700E+00	210	31	2.7500E-01
31		6.7000E+05	91		7.2000E+01	151		2.8700E+00	211	32	2.5000E-01
32		6.0000E+05	92		6.7500E+01	152		2.7700E+00	212	33	2.2500E-01
33		5.7300E+05	93		6.5000E+01	153		2.6700E+00	213	34	2.0000E-01
34		5.5000E+05	94		6.1000E+01	154		2.5700E+00	214		1.7500E-01
35		4.9952E+05	95		5.9000E+01	155		2.4700E+00	215	35	1.5000E-01
36		4.7000E+05	96		5.3400E+01	156		2.3800E+00	216		1.2500E-01
37		4.4000E+05	97		5.2000E+01	157		2.3000E+00	217	36	1.0000E-01
38		4.2000E+05	98		5.0600E+01	158		2.2100E+00	218		9.0000E-02
39	11	4.0000E+05	99		4.9200E+01	159		2.1200E+00	219		8.0000E-02
40		3.3000E+05	100		4.8300E+01	160		2.0000E+00	220	37	7.0000E-02
41		2.7000E+05	101		4.7000E+01	161		1.9400E+00	221		6.0000E-02
42		2.0000E+05	102		4.5200E+01	162		1.8600E+00	222	38	5.0000E-02
43		1.5000E+05	103		4.4000E+01	163	24	1.7700E+00	223	39	4.0000E-02
44		1.2830E+05	104		4.2400E+01	164		1.6800E+00	224	40	3.0000E-02
45	12	1.0000E+05	105		4.1000E+01	165		1.5900E+00	225	41	2.5300E-02
46		8.5000E+04	106		3.9600E+01	166		1.5000E+00	226	42	1.0000E-02
47		8.2000E+04	107		3.9100E+01	167		1.4500E+00	227	43	7.5000E-03
48		7.5000E+04	108		3.8000E+01	168		1.4000E+00	228		5.0000E-03
49		7.3000E+04	109		3.7000E+01	169		1.3500E+00	229		4.0000E-03
50		6.0000E+04	110		3.5500E+01	170		1.3000E+00	230	44	3.0000E-03
51		5.2000E+04	111		3.4600E+01	171		1.2500E+00	231		2.5000E-03
52		5.0000E+04	112		3.3750E+01	172		1.2250E+00	232		2.0000E-03
53		4.5000E+04	113		3.3250E+01	173		1.2000E+00	233		1.5000E-03
54		3.0000E+04	114		3.1750E+01	174		1.1750E+00	234		1.2000E-03
55	13	2.5000E+04	115		3.1250E+01	175		1.1500E+00	235		1.0000E-03
56	14	1.7000E+04	116	18	3.0000E+01	176		1.1400E+00	236		7.5000E-04
57		1.3000E+04	117		2.7500E+01	177		1.1300E+00	237		5.0000E-04
58		9.5000E+03	118		2.5000E+01	178		1.1200E+00	238		1.0000E-04
59		8.0300E+03	119		2.2500E+01	179		1.1100E+00	---	---	1.0000E-05
60		6.0000E+03	120		2.1000E+01	180		1.1000E+00			

Figure B.3: Energy boundaries for the SCALE 238-group and 44-group structures.

Bibliography

- [1] ANS, “ANSI/ANS-8.17-2004: American National Standard Criticality Safety Criteria for the Handling, Storage, and Transportation of LWR Fuel Outside Reactors’,” tech. rep., American Nuclear Society, 555 North Kensington Ave., La Grange Park, IL 60525, 2004.
- [2] OECD/NEA, “Overview of Approaches Used to Determine Calculational Bias in Criticality Safety Assessment, State-of-the-Art Report (Part 1),” tech. rep., OECD/NEA/Nuclear Science, October 2013.
- [3] R. Macian, M. Zimmermann, and R. Chawla, “Statistical Uncertainty Analysis Applied to Fuel Depletion Calculations,” *Journal of Nuclear Science and Technology*, vol. 44, pp. 875–885, June 2007.
- [4] W. Wieselquist, A. Vasiliev, and H. Ferroukhi, “Nuclear Data Uncertainty Propagation in a Lattice Physics Code Using Stochastic Sampling,” in *PHYSOR2012*, (Knoxville, USA), pp. 1–16, 2012.
- [5] “Compilation of experimental nuclear reaction data (EXFOR/CSISRS).” Available at <http://www.nndc.bnl.gov/exfor>.
- [6] “Computer Index of Nuclear Reaction Data (CINDA).” Available at <https://www-nds.iaea.org/exfor/cinda.htm>.
- [7] N. M. Larson, L. C. Leal, H. Derrien, G. Arbanas, R. O. Sayer, and D. Wiarda, “A Systematic Description of the Generation of Covariance Matrices,” in *PHYSOR2006*, (Vancouver, BC, Canada), 2006.
- [8] M. Herman and A. Trkov, eds., *ENDF-6 Formats Manual*. Upton, USA: National Nuclear Data Center/Brookhaven National Laboratory, 2009.
- [9] “NEA Nuclear Data High Priority Request List.” Available at= <http://www.oecd-nea.org/dbdata/hprl/>.
- [10] R. MacFarlane, D. Muir, R. Boicourt, and A. Kahler, *The NJOY Nuclear Data Processing System, Version 2012*. Los Alamos National Security LLC, 2012.

Bibliography

- [11] L. B. Levitt, "The Probability Table Method for Treating Unresolved Neutron Resonances in Monte Carlo Calculations," *Nuclear Science and Engineering*, vol. 49, pp. 450–457, Dec. 1972.
- [12] E. Lewis and J. Miller, *Computational Methods of Neutron Transport*. New York, NY, USA.: John Wiley & Sons, 1984.
- [13] N. M. Larson, *Updated Users' Guide for SAMMY: Multi-level R-matrix Fits to Neutron Data Using Bayes' Equation*. Oak Ridge National Laboratory, 2008.
- [14] D. L. Smith, "Evaluated Nuclear Data Covariances: The Journey From ENDF/B-VII.0 to ENDF/B-VII.1," *Nuclear Data Sheets*, vol. 112, pp. 3037–3053, Dec. 2011.
- [15] D. L. Smith, "Nuclear Data Uncertainties in 2004: A Perspective," *AIP Conference Proceedings*, vol. 769, pp. 320–325, 2005.
- [16] I. Kodeli, "Multidimensional Deterministic Nuclear Data Sensitivity and Uncertainty Code System: Method and Application," *Nuclear Science and Engineering*, vol. 138, pp. 45–66, May 2001.
- [17] G. Rimpault, D. Plisson, J. Tommasi, R. Jacqmin, J.-M. Rieunier, D. Verrier, and D. Biron, "The ERANOS Code and Data System for Fast Reactor Neutronic Analyses," in *PHYSOR2002*, (Seoul, Korea), 2002.
- [18] H. Rief, "Generalized Monte Carlo Perturbation Algorithms for Correlated Sampling and a Second-order Taylor Series Approach," *Annals of Nuclear Energy*, vol. 11, no. 9, pp. 455–476, 1984.
- [19] T. E. Booth, "A Sample Problem for Variance Reduction in MCNP," Tech. Rep. LA-10363-MS, Los Alamos National Laboratory, Los Alamos, USA, 1985.
- [20] T. He and B. Su, "Simulating Small Changes in System Response by MCNP," in *International Conference on Mathematics, Computational Methods and Reactor Physics (M&C 2009)*, (LaGrange Park, IL, USA), pp. 1–12, American Nuclear Society, 2009.
- [21] J. A. Favorite, "On the Accuracy of the Differential Operator Monte Carlo Perturbation Method for Eigenvalue Problems," in *American Nuclear Society Winter Meeting*, vol. 836, (Washington DC, USA), American Nuclear Society, 2009.
- [22] B. Broadhead, B. Rearden, and C. Hopper, "Sensitivity-and uncertainty-based criticality safety validation techniques," *Nuclear science and Engineering*, no. 146, pp. 340–366, 2004.
- [23] H. J. Shim and C. H. Kim, "Adjoint Sensitivity and Uncertainty Analyses in Monte Carlo Forward Calculations," *Journal of Nuclear Science and Technology*, vol. 48, no. 12, pp. 1453–1461, 2011.

- [24] B. C. Kiedrowski and F. B. Brown, "Adjoint-Based k-Eigenvalue Sensitivity Coefficients to Nuclear Data Using Continuous-Energy Monte Carlo," *Nuclear science and Engineering*, vol. 174, pp. 227–244, 2013.
- [25] M. A. Jessee, M. L. Williams, and M. D. Dehart, "Development of Generalized Perturbation Theory Capability within the SCALE Code Package," in *International Conference on Mathematics, Computational Methods, and Reactor Physics (M&C2009)*, 2009.
- [26] Y. Nagaya and F. B. Brown, "Estimation of Change in k-effective Due To Perturbation Fission Source Distribution in MCNP," in *American Nuclear Society Topical Meeting in Mathematics and Computations*, vol. 836, (Gatlinburg, USA), American Nuclear Society, 2003.
- [27] A. Blyskavka, K. Raskach, and A. Tsiboulia, "Algorithm of calculation of Keff sensitivities to group cross sections using Monte Carlo method and features of its implementation in the MMKKENO code," in *International Conference on Mathematics, Computational Methods and Reactor Physics (M&C 2005)*, (Palais des Papes, Avignon, France), 2005.
- [28] M. Pusa, "Perturbation-Theory-Based Sensitivity and Uncertainty Analysis with CASMO-4," *Science and Technology of Nuclear Installations*, vol. 2012, pp. 1–11, 2012.
- [29] A. Bidaud, G. Marleau, and E. Noblat, "Nuclear Data Uncertainty Analysis using the coupling of DRAGON with SUS3D," in *International Conference on Mathematics, Computational Methods & Reactor Physics (M&C2009)*, (Saratoga Springs, USA), 2009.
- [30] T. Takeda and T. Umamo, "Burnup Sensitivity Analysis in a Fast Breeder Reactor - Part I: Sensitivity Calculation Method with Generalized Perturbation Theory," *Nuclear Science and Engineering*, vol. 91, pp. 1–10, Sept. 1985.
- [31] M. D. McKay, R. J. Beckman, and W. J. Conover, "A Comparison of Three Methods for Selecting Values of Input Variables in the Analysis of Output from a Computer Code," *Technometrics*, vol. 42, no. Special 40th Anniversary Issue, pp. 55–61, 2000.
- [32] S. Mughabghab, *Atlas of Neutron Resonances: Resonance Parameters and Thermal Cross sections, Z=1-100*. Amsterdam, The Netherlands: Elsevier Publishers, 2006.
- [33] A. J. Koning, M. C. Duijvestijn, S. van Der Marck, R. Klein Meulekamp, and A. Hogenbirk, "New Nuclear Data Libraries for Lead and Bismuth and Their Impact on Accelerator-Driven Systems Design," *Nuclear Science and Engineering*, vol. 156, pp. 357–390, 2007.
- [34] D. Rochman, W. Zwermann, S. C. van der Marck, a. J. Koning, H. Sjöstrand, P. Helgesson, and B. Krzykacz-Hausmann, "Efficient Use of Monte Carlo: Uncertainty Propagation," *Nuclear Science and Engineering*, vol. 177, pp. 337–349, July 2014.
- [35] D. Rochman, a.J. Koning, and S. van der Marck, "Uncertainties for Criticality-Safety Benchmarks and Distributions," *Annals of Nuclear Energy*, vol. 36, pp. 810–831, June 2009.

Bibliography

- [36] C. Díez, O. Cabellos, D. Rochman, a.J. Koning, and J. Martínez, “Monte Carlo uncertainty propagation approaches in ADS burn-up calculations,” *Annals of Nuclear Energy*, vol. 54, pp. 27–35, Apr. 2013.
- [37] N. García-Herranz, O. Cabellos, J. Sanz, J. Juan, and J. C. Kuijper, “Propagation of statistical and nuclear data uncertainties in Monte Carlo burn-up calculations,” *Annals of Nuclear Energy*, vol. 35, pp. 714–730, Apr. 2008.
- [38] D. Rochman, A. Koning, S. van der Marck, A. Hogenbirk, and C. Sciolla, “Nuclear data uncertainty propagation: Perturbation vs. Monte Carlo,” *Annals of Nuclear Energy*, vol. 38, pp. 942–952, May 2011.
- [39] O. Buss, A. Hoefler, and J. C. Neuber, “NUDUNA - Nuclear Data Uncertainty Analysis,” in *International Conference on Nuclear Criticality*, (Edinburgh, Scotland), pp. 1–13, 2011.
- [40] D. Wiarda and M. E. Dunn, “PUFF-IV : A Code for Processing ENDF Uncertainty Data into Multigroup Covariance Matrices,” tech. rep., Oak Ridge National Laboratory, 2006.
- [41] W. Zwermann, L. Gallner, M. Klein, I. Pasichnyk, A. Pautz, and K. Velkov, “Status of XSUSA for Sampling Based Nuclear Data Uncertainty and Sensitivity Analysis,” in *WONDER-2012 , 3rd International Workshop On Nuclear Data Evaluation for Reactor applications* (O. Serot, C. De Saint Jean, O. Litaize, and G. Noguere, eds.), vol. 03003, (Aix-en-Provence, France), EDP Sciences, 2013.
- [42] L. Gallner, B. Krzykacz-Hausmann, A. Pautz, M. Wagner, and W. Zwermann, “Influence of Nuclear Data Uncertainties on Depletion Chain,” in *Annual Meeting on Nuclear Technology (Jahrestagung Kerntechnik)*, (Berlin, Germany), p. 870, 2011.
- [43] M. L. Williams, G. Ilas, M. A. Jessee, B. Rearden, D. Wiarda, W. Zwermann, L. Gallner, M. Klein, B. Krzykacz-Hausmann, and A. Pautz, “A Statistical Sampling Method for Uncertainty Analysis with SCALE and XSUSA,” *Nuclear Technology*, vol. 183, 2012.
- [44] W. Wieselquist, T. Zhu, A. Vasiliev, and H. Ferroukhi, “PSI Methodologies for Nuclear Data Uncertainty Propagation with CASMO-5M and MCNPX : Results for OECD / NEA UAM Benchmark Phase I,” *Science and Technology of Nuclear Installations*, vol. 2013, p. 15, 2013.
- [45] C. Mattoon, D. Brown, and J. Elliott, “Covariance Applications with Kiwi,” in *2nd Workshop on Neutron Cross Section Covariances*, vol. 27, EDP Sciences, May 2012.
- [46] O. Cabellos, “Presentation and Discussion of the UAM/Exercise I-1b: "Pin-Cell Burn-Up Benchmark" with the Hybrid Method,” *Science and Technology of Nuclear Installations*, vol. 2013, pp. 1–12, 2013.
- [47] R. O’Dell, R. W. Brewer, and C. A. Atkinson, “Bare Sphere of Plutonium-239 Metal,” in *International Handbook of Evaluated Criticality Safety Benchmark Experiments, Volume I*, OECD/NEA, 2002.

- [48] W. Zwermann, B. Krzykacz-Hausmann, L. Gallner, M. Klein, A. Pautz, and K. Velkov, "Aleatoric and Epistemic Uncertainties in Sampling Based Nuclear Data Uncertainty and Sensitivity Analyses," in *PHYSOR2012*, (Knoxville, USA), American Nuclear Society, 2012.
- [49] F. A. Alpan, L. C. Leal, and A. Courcelle, "Effect of Energy Self-Shielding Methods on ^{238}U for Criticality Safety Problems," in *PHYSOR2004*, (LaGrange Park, USA), American Nuclear Society, 2004.
- [50] G. Chiba, M. Tsuji, and T. Narabayashi, "Resonance Self-Shielding Effect in Uncertainty Quantification of Fission Reactor Neutronics Parameters," *Nuclear Engineering and Technology*, vol. 46, no. 3, 2014.
- [51] OECD/NEA, "ZZ-SCALE6.0/COVA-44G, a 44-group cross section covariance matrix library retrieved from the SCALE 6.0 package," 2011.
- [52] S. Bowman and M. Dunn, "SCALE Cross-section Libraries," in *SCALE: A Modular Code System for Performing Standardized Computer Analyses for Licensing Evaluation*, vol. III, ch. M04, 6th ed., 2009.
- [53] G. Žerovnik, A. Trkov, and L. C. Leal, "Challenges and solutions for random sampling of parameters with extremely large uncertainties and analysis of the ^{232}Th resonance covariances," *Nuclear Instruments and Methods in Physics Research Section A: Accelerators, Spectrometers, Detectors and Associated Equipment*, vol. 743, pp. 39–43, Apr. 2014.
- [54] W. Wieselquist, "CASMO-5MX: Tools for Sensitivity Analysis and Uncertainty Quantification with Respect to Nuclear Data in CASMO-5M," tech. rep., Paul Scherrer Institute, Villigen, Switzerland, 2012.
- [55] E. Cho and M. J. Cho, "Variance of the With-Replacement Sample Variance," in *Section on Survey Research Methods - Joint Statistical Meetings*, pp. 1291–1293, American Statistical Association, 2008. Available at <http://www.amstat.org/sections/srms/proceedings/y2008/Files/300992.pdf>.
- [56] J. A. Favorite, "An Alternative Implementation of the Differential Operator (Taylor Series) Perturbation Method for Monte Carlo Criticality Problems," *Nuclear Science and Technology Engineering*, vol. 142, pp. 327–341, 2002.
- [57] D. Rochman and A. J. Koning, "Pb and Bi neutron data libraries with full covariance evaluation and improved integral tests," *Nuclear Instruments and Methods in Physics Research Section A: Accelerators, Spectrometers, Detectors and Associated Equipment*, vol. 589, pp. 85–108, Apr. 2008.
- [58] T. Zhu, D. Rochman, a. Vasiliev, H. Ferroukhi, W. Wieselquist, and a. Pautz, "Comparison of Two Approaches for Nuclear Data Uncertainty Propagation in MCNPX for Selected Fast Spectrum Critical Benchmarks," *Nuclear Data Sheets*, vol. 118, pp. 388–391, Apr. 2014.
- [59] 2012. Private Communication with Dimitri Rochman.

Bibliography

- [60] A. Koning, D. Rochman, S. van der Marck, J. Kopecky, J. Sublet, S. Pomp, H. Sjostrand, and R. Forrest, "TENDL-2014: TALYS-based evaluated nuclear data library," 2014. Available at <ftp://ftp.nrg.eu/pub/www/talys/tendl2014/tendl2014.html>.
- [61] K. Ivanov, M. Avramova, S. Kamerow, I. Kodeli, and E. Sartori, *Benchmark for Uncertainty Analysis in Modeling (UAM) for Design, Operation and Safety Analysis of LWRs, Vol I: Specification and Support Data for the Neutronics Case (Phase I)*. OECD/NEA, 2012.
- [62] M. Chadwick, M. Herman, P. Obložinský, M. Dunn, Y. Danon, a.C. Kahler, D. Smith, B. Pritychenko, G. Arbanas, R. Arcilla, R. Brewer, D. Brown, R. Capote, a.D. Carlson, Y. Cho, H. Derrien, K. Guber, G. Hale, S. Hoblit, S. Holloway, T. Johnson, T. Kawano, B. Kiedrowski, H. Kim, S. Kunieda, N. Larson, L. Leal, J. Lestone, R. Little, E. McCutchan, R. MacFarlane, M. MacInnes, C. Mattoon, R. McKnight, S. Mughabghab, G. Nobre, G. Palmiotti, a. Palumbo, M. Pigni, V. Pronyaev, R. Sayer, a.a. Sonzogni, N. Summers, P. Talou, I. Thompson, a. Trkov, R. Vogt, S. van der Marck, a. Wallner, M. White, D. Wiarda, and P. Young, "ENDF/B-VII.1 Nuclear Data for Science and Technology: Cross Sections, Covariances, Fission Product Yields and Decay Data," *Nuclear Data Sheets*, vol. 112, pp. 2887–2996, Dec. 2011.
- [63] T. Ivanova, F. Fernex, E. Kolbe, A. Vasiliev, G. S. Lee, S. W. Woo, D. Mennerdahl, B. Rearden, D. Mueller, Y. Rugama, O. Nea, A. Santamarina, and C. Venard, "OECD / NEA Expert Group on Uncertainty Analysis for Criticality Safety Assessment: Current Activities," in *PHYSOR2010*, (Pittsburgh, USA), American Nuclear Society, 2010.
- [64] A. Vasiliev, E. Kolbe, M. A. Zimmermann, and H. Ferroukhi, "PSI contributions to the OECD / NEA WPNCS / EG UACSA State of the Art Report on Uncertainty Analysis Methods for Criticality Safety Assessment and to the Benchmark Exercises of Phase I: Comparison of Uncertainty Analysis Methods for Criticality Safety Assessment," tech. rep., Paul Scherrer Institut, Villigen PSI, 2009.
- [65] J. Dean and R. Tayloe Jr., "Guide for Validation of Nuclear Criticality Safety Computational Methodology," tech. rep., Regulatory, U. S. Nuclear Commission, Office of Nuclear Material Safety and Safeguards, Washington DC, USA, 2001.
- [66] T. Zhu, A. Vasiliev, H. Ferroukhi, and A. Pautz, "Application of the PSI-NUSS Tool for the Estimation of Nuclear Data Related keff Uncertainties for the OECD/NEA WPNCS UACSA Phase I Benchmark," *Nuclear Data Sheets*, vol. 118, pp. 453–455, Apr. 2014.
- [67] B. Rearden and D. Mueller, "TSUNAMI Results for Phase I Benchmarks," 2008. Presentation at OECD / NEA WPNCS / EG UACSA Meeting.
- [68] R. I. Cukier, C. M. Fortuin, and K. E. Shuler, "Study of the sensitivity of coupled reaction systems to uncertainties in rate coefficients. I Theory," *Journal of Chemical Physics*, vol. 59, no. 8, pp. 3873–3878, 1973.

- [69] Y. Lu and S. Mohanty, "Sensitivity analysis of a complex, proposed geologic waste disposal system using the Fourier Amplitude Sensitivity Test method," *Reliability Engineering & System Safety*, vol. 72, pp. 275–291, June 2001.
- [70] A. Francos, F. J. Elorza, F. Bouraoui, G. Bidoglio, and L. Galbiati, "Sensitivity analysis of distributed environmental simulation models : understanding the model behaviour in hydrological studies at the catchment scale," *Reliability Engineering & System Safety*, vol. 79, pp. 205–218, 2003.
- [71] H. Weyl, "Mean Motion," *American Journal of Mathematics*, vol. 60, no. 4, pp. 889–896, 1938.
- [72] A. Saltelli and R. Bolado, "An alternative way to compute Fourier amplitude sensitivity test (FAST)," *Computational Statistics & Data Analysis*, vol. 26, pp. 445–460, 1998.
- [73] S. Tarantola, D. Gatelli, and T. Mara, "Random balance designs for the estimation of first order global sensitivity indices," *Reliability Engineering & System Safety*, vol. 91, pp. 717–727, June 2006.
- [74] C. Xu and G. Z. Gertner, "A general first-order global sensitivity analysis method," *Reliability Engineering & System Safety*, vol. 93, pp. 1060–1071, July 2008.
- [75] R. Iman and W. Conover, "A distribution-free approach to induce rank correlation among input variables," *Communication in Statistics- Simulation and Computation*, vol. 11, no. 3, pp. 311–334, 1982.
- [76] S. Kucherenko, S. Tarantola, and P. Annoni, "Estimation of global sensitivity indices for models with dependent variables," *Computer Physics Communications*, vol. 183, pp. 937–946, Apr. 2012.
- [77] I. Sobol, "Global sensitivity indices for nonlinear mathematical models and their Monte Carlo estimates," *Mathematics and Computers in Simulation*, vol. 55, pp. 271–280, Feb. 2001.
- [78] T. A. Mara, "Extension of the RBD-FAST method to the computation of global sensitivity indices," *Reliability Engineering & System Safety*, vol. 94, pp. 1274–1281, Aug. 2009.
- [79] D. Rochman and A. J. Koning, "Random Adjustment of the H in H₂O Neutron Thermal Scattering Data," *Nuclear Science and Engineering Engineering*, vol. 172, pp. 287–299, 2012.
- [80] J. Holmes and A. Hawari, "Generation of an $S(\alpha, \beta)$ Covariance Matrix by Monte Carlo Sampling of the Phonon Frequency Spectrum," *Nuclear Data Sheets*, vol. 118, pp. 392–395, Apr. 2014.
- [81] G. Žerovnik, R. Capote, and A. Trkov, "On random sampling of correlated resonance parameters with large uncertainties," *Nuclear Instruments and Methods in Physics Research Section A: Accelerators, Spectrometers, Detectors and Associated Equipment*, May 2013.

Bibliography

- [82] D. Wiarda, G. Arbanas, L. Leal, and M. Dunn, "Recent Advances with the AMPX Covariance Processing Capabilities in PUFF-IV," *Nuclear Data Sheets*, vol. 109, pp. 2791–2795, Dec. 2008.
- [83] H. J. Park, H. J. Shim, and C. H. Kim, "Uncertainty Propagation Analysis for PWR Burnup Pin-Cell Benchmark by Monte Carlo Code McCARD," *Science and Technology of Nuclear Installations*, vol. 2012, pp. 1–6, 2012.
- [84] E. Kolbe, P. Grimm, A. Vasiliev, and H. Ferroukhi, "Assessment of MCNPX/CINDER for burnup calculations," in *International Conference on Nuclear Criticality ICNC*, (Edinburgh, Scotland), pp. 1–10, 2011.
- [85] D. Rochman and C. M. Sciolla, "Total Monte Carlo Uncertainty propagation applied to the Phase I-1 burnup calculation," tech. rep., Nuclear Research and Consultancy Group NRG, Petten, The Netherlands, 2012.
- [86] M. Pecchia, A. Vasiliev, O. Leray, H. Ferroukhi, and A. Pautz, "New PSI Methodology for Manufacturing and Technological Uncertainty Quantification," in *PHYSOR2014*, pp. 1–14, 2014.
- [87] D. G. Cacuci, *Sensitivity and Uncertainty Analysis Theory, Volume I*. Chapman & Hall/CRC, 2003.
- [88] J. Densmore, G. McKinney, and J. Hendricks, "Correction to the MCNP Perturbation Feature for Cross-Section Dependent Tallies," Tech. Rep. LA-13374 UC-2000, Los Alamos National Laboratory, Los Alamos, USA, 1997.
- [89] G. W. Mckinney and J. L. Iverson, "Verification of the Monte Carlo Differential Operator Technique for MCNPTM," tech. rep., Los Alamos National Lab, 1996.
- [90] C. M. Perfetti, *Advanced Monte Carlo Methods for Eigenvalue Sensitivity Coefficient Calculations*. PhD thesis, University of Michigan, 2012.
- [91] H. Hurwitz, "Naval Reactors," in *Naval Reactor Physics Handbook* (A. Radkowsky, ed.), p. 864, U.S. Atomic Energy Commission, 1st ed., 1964.
- [92] "Marginal and conditional distributions of multivariate normal distribution." Available at <http://fourier.eng.hmc.edu/e161/lectures/gaussianprocess/node7.html>.

Curriculum Vitae

Ting Zhu

Contact:	reach.ting@gmail.com	Date of birth:	26.03.1987
Web:	linkedin.com/in/zhuting	Nationality:	Canadian
Home address:	908 – 18 Hillcrest Ave Toronto, Canada M2N6T5	Languages:	Chinese/English (fluent) French/German (B1)

Education

PhD in Energy		2011 – 2015
École Polytechnique Fédérale de Lausanne (EPFL), Lausanne, Switzerland		
Supervisors: Prof. Andreas Pautz, Dr. Alexander Vasiliev		
Master of Applied Science in Engineering Physics (Nuclear)		2009 – 2011
McMaster University, Hamilton, Canada		
Supervisor: Prof. Adriaan Buijs		
Bachelor of Applied Science in Engineering Science (Physics)		2005 – 2009
University of Toronto, Toronto, Canada		

Research Experience

PhD Student at Paul Scherrer Institute (PSI), Villigen, Switzerland	2011 – Present
--	-----------------------

Completing PhD studies in the Laboratory for Reactor Physics and Systems Behavior

- **Nuclear data:** prepared multigroup nuclear data covariance in NJOY and modified ACE-formatted nuclear data libraries with MATLAB and Bash programs for nuclear data uncertainty propagation.
- **Uncertainty analysis:** implemented random sampling methods to perturb nuclear data and analyzed k_{eff} uncertainty due to nuclear data uncertainties.
- **Sensitivity analysis:** proposed and implemented a Fourier-based global sensitivity approach to identify top nuclear data uncertainty contributors in terms of variance fractions.
- **OECD/NEA working parties:** updated PSI's contribution in UACSA-Phase 1 to include nuclear data uncertainties in observed k_{eff} bias; submitted report on technological parameter uncertainties in criticality safety assessment to UACSA-Phase 2 Expert Group; presented PSI's nuclear data uncertainty quantification methodology at UAM-6 Expert Group meeting.
- **Criticality safety:** performed MCNPX calculations including nuclear data uncertainties for the suite of ICSBEP benchmarks selected for PSI's criticality safety assessment methodology to determine k_{eff} upper subcriticality limit.
- **Collaboration:** completed studies and co-authored conference papers with Dr. D. Rochman (NRG) and Dr. S. Tarantola (EU JRC, Ispra).

Master's Student at McMaster University, Hamilton, Canada	2009 – 2011
--	--------------------

- **Benchmark modeling:** created SCALE6 KENO-3D models for criticality experiments in the ZED-2 zero power reactor with (Th,Pu)O₂ fuel.
- **Sensitivity/Uncertainty analysis:** performed SCALE6 TSUNAMI-3D, TSUNAMI-IP, TSAR, TSURFER calculations to obtain nuclear data uncertainty contributions for (Th,Pu)O₂ fuel bundle in ZED-2 and sensitivity profiles for similarity studies.

Teaching Experience

Instructor for a 1-week course titled “Nuclear Engineering and Energy Policy” for senior high school students at the DEEP Summer Academy, University of Toronto (Canada). Designed course curriculum covering topics of radiation, reactor designs and technologies, nuclear accidents etc. **July 2011**

Teaching Assistant for experimental courses at CROCUS zero-power reactor (EPFL Switzerland) and at McMaster Nuclear Reactor (Canada). Supervised university students during experiments such as neutron radiography, neutron moderation, approach to reactor criticality etc. **Fall semesters 2009 – 2011**

Awards

Best Summary at International Youth Nuclear Congress, Burgos, Spain **July 2014**

2nd Year Best Presentation at PhD Day of Energy & Safety Department, PSI **May 2013**

1st Year Best Poster at PhD Day of Energy & Safety Department, PSI **June 2012**

3rd Prize for Best Student Paper and Presentation at PHYSOR Conference, USA **April 2012**

Scientific Contributions

Journal

- **T. Zhu**, S. Tarantola, A. Vasiliev, H. Ferroukhi, A. Pautz, “NUSS-RF: Stochastic Sampling-Based Tool for Nuclear Data Sensitivity and Uncertainty Quantification”, *Journal of Nuclear Science and Technology* (submitted).
- **T. Zhu**, A. Vasiliev, H. Ferroukhi, A. Pautz, “Comparison between Deterministic Approach and Sampling-based NUSS-RF for the Decomposition of Total k_{eff} Uncertainty into Individual Nuclear Data Uncertainty Contribution”, *Nuclear Science and Engineering* (submitted).
- **T. Zhu**, A. Vasiliev, H. Ferroukhi, A. Pautz, “NUSS: A Tool for Propagating Multigroup Nuclear Data Covariances in Pointwise ACE-Formatted Nuclear Data Using Stochastic Sampling Method”, *Annals of Nuclear Energy* (75), January 2015, P. 713–722.
- **T. Zhu**, D. Rochman, A. Vasiliev, H. Ferroukhi, W. Wieselquist, A. Pautz, “Comparison of Two Approaches for Nuclear Data Uncertainty Propagation in MCNP(X) for Selected Fast Spectrum Critical Benchmarks”, *Nuclear Data Sheets* (118), April 2014.
- **T. Zhu**, A. Vasiliev, H. Ferroukhi, A. Pautz, “Application of the PSI-NUSS Tool for the Estimation of Nuclear Data Related k_{eff} Uncertainties for the OECD/NEA WPNGS UACSA Phase I Benchmark”, *Nuclear Data Sheets* (118), April 2014.

Presentation

PHYSOR2014 Conference, Kyoto, Japan **September 2014**

International Youth Nuclear Congress, Burgos, Spain **July 2014**

European Nuclear Education Network PhD Event, Burgos, Spain **July 2014**

International Conference of Nuclear Data, New York, USA **March 2013**

6th Uncertainty Analysis in Modeling Meeting, Karlsruhe, Germany **May 2012**

PHYSOR2012 Conference, Knoxville, USA **April 2012**

Technical Meeting on Low-Power Critical Facilities and Small Reactors, Ottawa, Canada **October 2010**